The physiological relevance of ADAM17 in colon cancer development

Dissertation

zur Erlangung des Doktorgrades

der Mathematisch-Naturwissenschaftlichen Fakultät

der Christian-Albrechts-Universität zu Kiel

vorgelegt von

Daniela Stefanie Schmidt

Kiel, 2017

Erster Gutachter:	Prof. Dr. Stefan Rose-John
Zweiter Gutachter:	Prof. Dr. Thomas Roeder
Tag der mündlichen Prüfung:	17. November 2017
Zum Druck genehmigt:	17. November 2017

Der Dekan

TABLE OF CONTENTS

ERKLÄRUNG

Hiermit erkläre ich an Eides statt, dass die vorliegende Dissertation nach den Regeln der guten wissenschaftlichen Praxis der Deutschen Forschungsgemeinschaft selbstständig und nur unter Verwendung der angegebenen Hilfsmittel und Quellen sowie Anleitung meiner akademischen Lehrer angefertigt wurde. Des Weiteren erkläre ich, dass noch kein Promotionsversuch unternommen wurde und diese Dissertation an keiner anderen Fakultät vorgelegt wurde.

Kiel, den 17. Juli 2017

_____

Stefanie Schmidt

ZUSAMMENFASSUNG

ADAM17 gehört zur Familie der ADAM (*A Disintegrin And Metalloprotease*) Metalloproteasen und wurde ursprünglich als die verantwortliche Protease identifiziert, welche membrangebundenes TNF-α (*tumor necrosis factor alpha*) via proteolytischer Prozessierung, dem sog. *ectodomain shedding*, in die lösliche Form überführt. ADAM17 ist ein Typ I Transmembranprotein und wird ubiquitär in allen Organen exprimiert. Deutliche Expression von ADAM17 findet sich unter physiologischen Bedingungen vor allem im Darm.

Die physiologische Bedeutung von ADAM17 besteht in der irreversiblen proteolytischen Regulation von wichtigen Signalwegen wie dem EGFR (*epidermal growth factor receptor*)-Signalweg, wobei ADAM17 für die proteolytische Freisetzung von löslichen ErbB (*erythroblastosis oncogene B*)-Liganden wie Amphiregulin (AREG) verantwortlich ist. Lösliche EGFR-Liganden binden an Rezeptoren der ErbB-Rezeptor-Tyrosinkinasefamilie, woraufhin sich Homo- oder Heterodimere der ErbB-Rezeptoren bilden, welche durch Phosphorylierung aktiviert werden und intrazellulär u.a. Proliferationssignale weiterleiten. Die Expression von ADAM17, AREG und EGFR ist in Tumoren erhöht, was sich physiologisch durch signifikant verstärkte proteolytische Freisetzung von AREG auf intestinalen Epithelzellen äußert. Im Verlauf dieser Arbeit ließ sich dies *in vitro* bei humanen Kolorektalzelllinien, *ex vivo* in murinen 3D Organoidzellkulturen und *in vivo* in Gewebelysaten und Kolonkulturen von ADAM17-defizienten hypomorphen ADAM17$^{ex/ex}$ Mäusen zeigen.

Um die pathophysiologische Relevanz von ADAM17 während der Darmkarzinogenese zu bestimmen, wurde im Rahmen dieser Arbeit zum einen ein entzündungsbasiertes Kolitis-assoziiertes Darmkrebsmodell (CAC; *colitis-associated cancer*) und zum anderen ein genetisch prädispositioniertes Modell mit hypomorphen Apc$^{Min/+}$ ADAM17$^{ex/ex}$ Mäusen etabliert und analysiert. Die Mutation im Adenomatous polyposis coli (*Apc*) Gen hat eine Dysregulation des Wnt-Signalwegs zur Folge, was zur spontanen Entwicklung einer Vielzahl intestinaler Neoplasien (Min; *multiple intestinal neoplasia*) führt.

Zusammenfassend konnte in dieser Arbeit gezeigt werden, dass die ADAM17-Defizienz im CAC Mausmodell zu einer signifikant erhöhten Ausbildung von Karzinomen, assoziiert mit verstärkten Entzündungsmerkmalen, im Kolon führt. Bemerkenswerterweise zeigen die genetisch prädispositionierten Apc$^{Min/+}$ Mäuse bei ADAM17-Defizienz eine signifikant reduzierte Tumoranzahl und verminderte Zellproliferation, die einheitlich geringgradigen Dysplasien entsprechen.

ABSTRACT

As a member of the ADAM (A Disintegrin And Metalloproteinase) family of metalloproteases, ADAM17 was originally identified as the protease responsible for the ectodomain shedding of the membrane-bound precursor of TNF-α (tumor necrosis factor alpha). ADAM17 is a type I transmembrane protein and is ubiquitously expressed in all tissues, with high expression levels in the intestine.

One of the physiological roles of ADAM17 is the proteolytic regulation of important pathways like the EGFR (epidermal growth factor receptor) pathway. ADAM17 cleaves membrane bound ErbB (erythroblastosis oncogene B) ligands such as Amphiregulin (AREG). The soluble ligands bind to receptors of the ErbB receptor tyrosine kinase family and trigger phosphorylation of both homo- or heterodimers of the ErbB receptors. Phosphorylation of ErbB receptors has been shown to activate intracellular signals such as proliferation. Expression and activation of ADAM17, AREG and EGFR is highly upregulated during tumorigenesis, which leads to increased shedding of AREG on intestinal epithelial cells as presented in this thesis. This effect was shown *in vitro* using human colorectal cancer cells, *ex vivo* in an established 3D murine organoid culture system and *in vivo* using tissue lysates and colon cultures from ADAM17-deficent hypomorphic $ADAM17^{ex/ex}$ mice.

To identify the pathophysiological relevance of the previous results, the effect of ADAM17-deficiency on tumor formation was investigated *in vivo* in murine colitis-associated cancer (CAC) as a model for inflammation-associated colorectal cancer. Further a genetically predisposed colorectal cancer model was chosen, whereby $Apc^{Min/+}$ mice crossbred with hypomorphic $ADAM17^{ex/ex}$ mice were generated and evaluated in this work. The mutated Adenomatous polyposis coli (*Apc*) gene results in dysregulation of the Wnt signaling pathway, which leads to a spontaneous development of multiple intestinal neoplasia (Min) in this mouse model.

In summary, tumor formation is altered in ADAM17-deficiency CAC mouse model and hypomorphic $ADAM17^{ex/ex}$ mice developed higher numbers of carcinoma coupled with increased intestinal inflammation. Remarkably, the genetically predisposed $Apc^{Min/+}$ mice deficient for ADAM17 showed a significantly reduced tumor number, diminished cell proliferation and low grade dysplasia.

LIST OF ABBREVIATIONS AND SYMBOLS

ADAM	A Disintegrin And Metalloproteinase
AOM	Azoxymethane
APC/Apc	Adenomatous polyposis coli
APS	Ammonium persulfate
AREG	Amphiregulin
BCM	Basal culture medium
BMP	Bone morphogenetic protein
bp	base pair
BSA	Bovine serum albumin
BTC	Betacellulin
CAC	Colitis associated cancer
CD	Crohn´s disease
cDNA	complementary DNA
CK1α	casein kinase 1 alpha
CRC	Colorectal cancer
DAB	3,3'-Diaminobenzidine
DCC	Deleted in colorectal cancer
DMEM	Dubelco´s Modified Eagle Medium
DMSO	Dimethyl sulfoxide
DNA	Deoxyribonucleic acid
dNTP	Deoxynucleoside triphosphate
Dsh	Dishevelled
DSS	Dextran sulfate sodium
DTT	Dithiothreitol
EDTA	Ethylene diamine tetraacetat

EGF	Epidermal growth factor
EGFR	Epidermal growth factor receptor
ELISA	Enzyme linked immunosorbent assay
ErbB	Erythroblastosis oncogene B
EREG	Epiregulin
EtOH	Ethanol
FAP	Familial adenomatous polyposis
FCS	Fetal calf serum
FFPE	Formalin-fixed paraffin-embedded
g	relative centrifugal force
gDNA	genomic DNA
GFR	Growth Factor Reduced
GI	GI254023X; ADAM10 Inhibitor
GSK3ß	Glycogen synthase kinase 3 beta
GW	GW280264X; ADAM10 and ADAM17 Inhibitor
h	hour
HE	Haematoxylin and Eosin
HER	Human epidermal growth factor receptor
Het	heterozygous
HRP	Horseradish peroxidase
i.p.	intra-peritoneal
IBD	Inflammatory bowel disease
IEC	Intestinal epithelial cells
IHC	Immunohistochemistry
IL	Interleukin
IVC	individual ventilated cages

JAK	Janus kinasen
kDa	kilodalton
KEGG	Kyoto Encyclopedia of Genes and Genomes
LOH	Loss of heterozygosity
min	minute
Min	Multiple intestinal neoplasia
ml	milliliter
mM	millimol
MM	Marimastat
MMP	Matrix-Metalloproteinase
NAC	N-Acetyl-L-cysteine
NRG	Neuregulin
PAS	Periodic acid-Schiff
PBS	Phosphate-buffered saline
PCR	Polymerase chain reaction
Pen/Strep	Penicilin/Streptomycin
PFA	Paraformaldehyde
PVDF	Polyvinylidenfluorid
qRT-PCR	quantitative real time PCR
RNA	Ribonucleic acid
Rsp-1	R-Spondin-1
RTK	receptor tyrosine kinase
RT-PCR	reverse transcriptase PCR

sAREG	soluble AREG
SDS	Sodium dodecyl sulfate
SDS-PAGE	SDS polyacrylamide gel electrophoresis
sec	second
SI	small intestine
TA	Transit amplifying
TACE	Tumor necrosis factor alpha converting enzyme
TBS	Tris-buffered sline
TEMED	Tetramethylethylenediamine
TGF-α	Transforming growth factor alpha
TNF	Tumor necrosis factor
UC	Ulcerative colitis
µl	microliter
UPL	Universal probe library
V	Volt
v/v	Volume per volume
Wnt	wingless type MMTV integration site
wt	Wildtype
w/v	weight per volume
°C	degree Celsius

CHAPTER ONE: INTRODUCTION

1.1 ANATOMY OF THE INTESTINE

Both the small intestine and large intestine, also known as colon, are parts of the gastrointestinal system. The small intestine consists of sections named duodenum, jejunum and ileum and is followed by the cecum and colon.

The intestine has two main functions: First, the intestine is responsible for digestion and absorption of nutrients and water. Second, the intestine contains a variety of immune cells and plays an important role in the immune system. In order to complete these functions, the intestine has a unique structure. Two muscle layers, namely inner circular muscle and outer longitudinal muscle layer, shape the outer part of the intestine. These layers are necessary for periodic muscle contraction called intestinal peristalsis to move the digestive content distally. The two muscle layers are surrounded by irregular connective tissue including nerves, blood and lymphatic vessels. The mucosa is located next to the submucosa and consists of three sections: muscularis mucosae, lamina propria and intestinal epithelium. The muscularis mucosa, a thin muscle layer, separates the submucosa from the mucosa. The lamina propria consists of loose connective tissue and harbors a variety of immune cells. To form a spatial boundary to the inner intestinal lumen, a single cell layered barrier named intestinal epithelium, is placed above the lamina propria. The intestinal epithelium consists of different specialized cell types such as enterocytes, goblet cells, enteroendocrine cells, Tuft cells and Paneth cells which are characteristic for the small intestine (Fig. 1) (van der Flier and Clevers, 2009, Clevers, 2013).

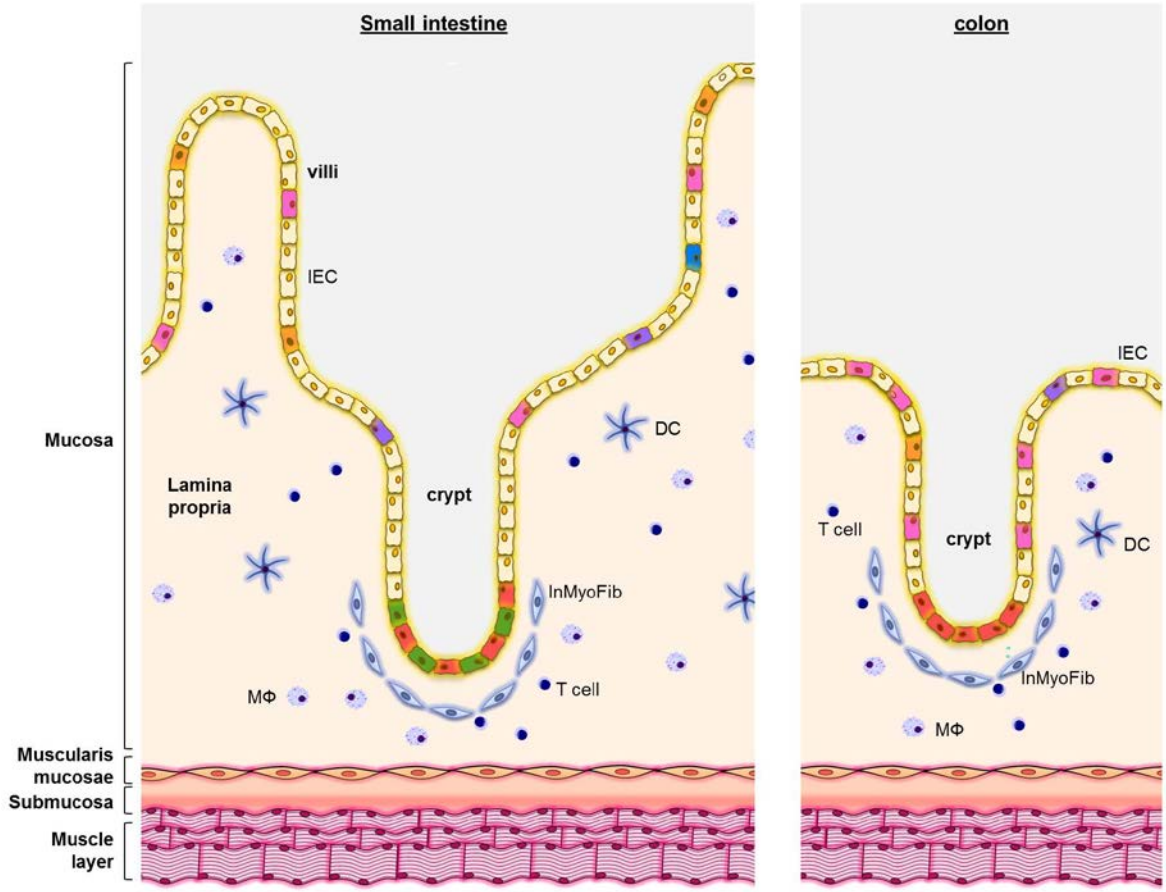

Fig. 1: Illustration of the small intestine and the colon

Graphical representation of the small intestine and colon. The small intestine consists of crypt-villus-units with specialized epithelial cell types such as goblet cells (pink), Tuft cells (blue), enterocytes (orange), enteroendocrine cells (purple), Paneth cells (green) and stem cells (red). The lamina propria contain immune cells and is a central part of the villus-unit. Characteristic for the colon are a large number of goblet cells, a rare number of Paneth cells and lacking villi structures. IEC=intestinal epithelial cells; InMyoFib=intestinal Myofibroblasts; DC=dendritic cell; MΦ=macrophages. Adapted from (Mowat and Agace, 2014).

The small intestine and colon can be identified by characteristic structures of the mucosa. In Fig. 2 a typical crypt-villus-unit of the small intestine is depicted. The mucosa of the small intestine forms bulges to increase the intestinal surface area, named villus. This is physiological important, because the absorption of nutrients takes place within the small intestine. Invagination of the mucosa within the small intestine and the colon are named crypt of Lieberkühn, in the following referred to as crypt (Reya and Clevers, 2005). The crypt domain harbors the stem cell zone at the bottom and the transit amplifying (TA) compartment above, which are physiological important to provide new intestinal epithelial cells (IECs) to replenish differentiated IECs along the crypt-villus-unit. The intestinal epithelium in mammals is the most regenerative tissue and is renewed every 3-5 days (Brittan and Wright, 2004, Radtke and Clevers, 2005, Heath, 1996). It was shown that two types of stem cells, namely crypt-based columnar cells and +4 position stem cells, are located at the crypt domain of the

intestine (Cheng and Leblond, 1974). Crypt-based columnar cells are active cycling stem cells that are highly proliferative and divide daily. Crypt-based columnar cells express the marker proteins Lgr5 (Leu-rich repeat-containing G protein-coupled receptor 5) and Ascl2 (Achaete scute homolog 2) (Li and Clevers, 2010, Barker et al., 2007, van der Flier and Clevers, 2009). Position +4 stem cells are located four cells above the crypt bottom and are negative for Lgr5, Ascl2 as well as the nuclear proliferation marker Ki-67 and perform only few cycling events. These cells are also termed quiescent stem cells and are thought to serve as a backup system during severe intestinal epithelial damage (Li and Clevers, 2010, Barker et al., 2007, Scoville et al., 2008, van der Flier and Clevers, 2009). Stem cells at the crypt bottom divide daily and become new intestinal epithelia cells of the TA compartment, while cells of the TA compartment divide nearly four times a day to refill the intestinal epithelium before they undergo cell cycle arrest and migrate to the apical crypt site (van der Flier and Clevers, 2009, Marshman et al., 2002). Taken together, the crypt domain is maintained by multipotent stem cells, is monoclonal and mainly proliferative whereas the villus domain is polyclonal due to composition of differentiated cells from multiple crypts (Wright, 2000).

The maintenance of the entire stem cell niche is controlled by Wnt, Notch, ErbB and BMP1 signaling pathways. The differentiation process of newly arisen IECs into one of the four specialized intestinal epithelial cell types is mainly regulated by Wnt and Notch signaling (Jones et al., 2015). Absorptive enterocytes are responsible for nutrient and water uptake and comprise nearly 80 % of the intestinal epithelium (van der Flier and Clevers, 2009). Goblet cells belong to the secretory cell types and appear second most frequent within the intestinal epithelium. The main task of goblet cells is to secrete mucins, which are highly glycosylated proteins required to build up the mucus layer. The mucus layer protects the intestinal epithelium from direct contact with intestinal content and bacteria (McGuckin et al., 2009). The second group of secretory cells within the small intestine and colon are the enteroendocrine cells, which secrete peptide hormones to regulate intestinal peristalsis and secretion of digestive juice (Clevers, 2013). During differentiation, enterocytes, goblet cells and enteroendocrine cells move towards the tip of the villus domain before they undergo anoikis, a special kind of cell death induced by detachment from the basal membrane (Gilmore, 2005, Reya and Clevers, 2005). Paneth cells complete the group of secretory cells within the small intestine. This cell type secretes antimicrobial peptides and defensins to control the physiological bacterial load in the intestinal lumen. After differentiation, Paneth cells migrate towards the crypt bottom where they are located within the small intestine (Reya and Clevers, 2005, Wehkamp and Stange, 2006, Bjerknes and Cheng, 1981).

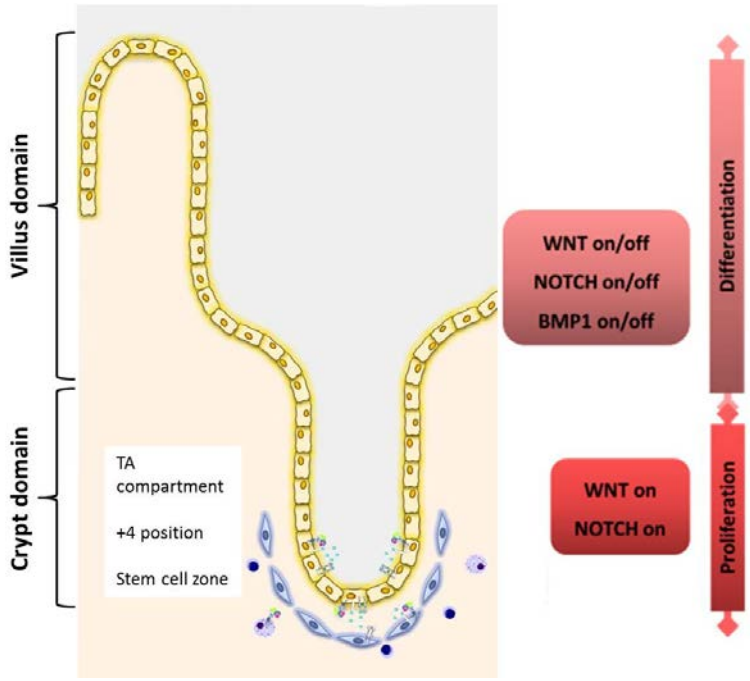

Fig. 2: Illustration of the crypt-villus-unit.

Model of the cell arrangement within the crypt-villus-unit. The stem cell zone including Paneth cells is located at the crypt bottom. In the crypt domain, the +4 position stem cells and their progeny cells are located in the transit amplifying (TA) compartment. The cell proliferation in the crypt domain is regulated by a gradient of Wnt, Notch and BMP1 signaling. The differentiation of intestinal epithelial cells takes place in the villus domain.

The barrier integrity of the intestinal epithelium is physiologically important, because it prevents a direct contact of intestinal content and commensal bacteria with the immune cells from the lamina propria. If the barrier is disturbed, intestinal immune homeostasis is impaired by direct contact and crosstalk of lamina propria immune cells and immune reactive intestinal content. This leads to inflammatory responses and is well described in patients who suffers from inflammatory bowel diseases (IBD) like Crohn´s disease (CD) or Ulcerative colitis (UC) (McGuckin et al., 2009, Roda et al., 2010). This may result in chronic inflammation of the intestine and predisposition of colon cancer development (Itzkowitz and Yio, 2004, Itzkowitz and Harpaz, 2004).

1.2 VOGELSTEIN-MODEL OF COLORECTAL CARCINOGENESIS

According to the world health organization, colorectal cancer is one of the most commonly diagnosed cancers and a leading cause of cancer-related death in both men and women. The number of colorectal cancer-related cases of death could be diminished by extended knowledge about colorectal cancer initiation, progression, treatment and prevention.

Tumorigenesis is characterized by uncontrolled cell proliferation and tumor formation. Colorectal cancer in humans can develop very slowly over 10 to 20 years. Colon cancer progression comprises several well described steps accompanied by defined genetic mutations and is until now known as “adenoma to carcinoma sequence” (Fearon and Vogelstein, 1990).

In accordance with the model of colorectal carcinogenesis proposed by Fearon and Vogelstein in 1990, accumulation of certain driver mutations in proto-oncogenes or tumor suppressor genes are necessary to support the transformation from healthy tissue with normal differentiated intestinal epithelial cells towards tumor tissue with undifferentiated intestinal epithelial cells and potentially metastasizing cells (Fig. 3). Mutations which lead to activation of *KRAS* (Kirsten rat sarcoma viral oncogene homolog), inactivation of *APC* (Adenomatous polyposis coli), *DCC* (Deleted in colorectal cancer) or *P53* are termed driver mutations because they drive tumor progression and tumor unresponsiveness to apoptosis or cell cycle regulation forward. An accumulation of driver mutations was shown to enhance polyp growth, malignancy and finally metastasis in intestinal tissue (Yamada and Mori, 2006, Vogelstein and Kinzler, 1993).

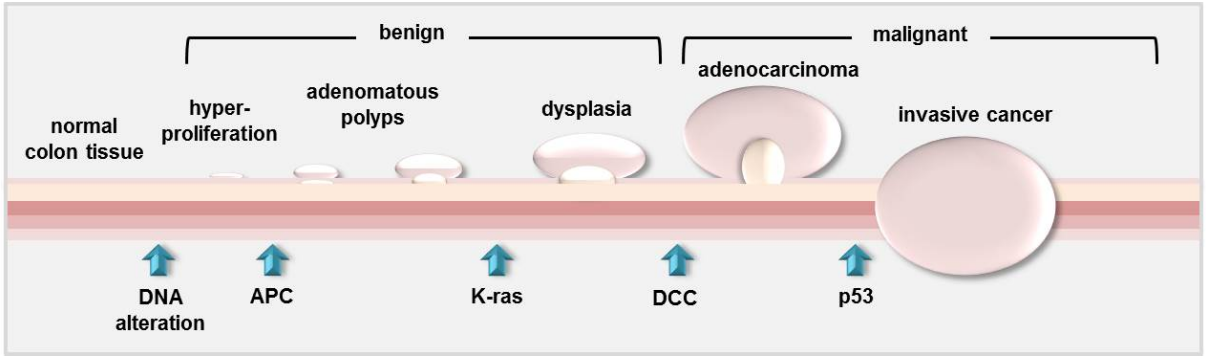

Fig. 3: The Vogelstein adenoma to carcinoma sequence.

The outline of the adenoma to carcinoma sequence shows the development from normal colon tissue to benign polyps and dysplasia up to malignant adenocarcinoma and invasive cancer by accumulation of certain mutations. Adapted from (Fearon and Vogelstein, 1990).

While tumor initiation is mostly induced by mutations within the Wnt signaling pathway, tumor progression, tumor invasion and tumor metastasis are mainly related to mutations of *KRAS*, *DCC* and *P53*. The first key event during colon cancer development is the loss of function of the tumor suppressor gene *APC* which is an important modulator within the Wnt pathway. The loss of *APC* and dysregulation of the Wnt pathway leads to alterations in the balance between proliferation and apoptosis resulting in hyperproliferation and the formation of

adenomatous polyps in the intestinal epithelium (van de Wetering et al., 2002). Gain of function mutations of the *KRAS* proto-oncogene promote cell survival of intestinal epithelial cells due to constitutive activated downstream signaling (Bos, 1989). Moreover, mutations in the tumor suppressor genes *DCC* and *P53* lead additionally to an imbalanced interplay between proliferation and apoptosis which results in the progression of colon cancer into a malignant phenotype (Fearon and Vogelstein, 1990, May and May, 1999, Fearon et al., 1990).

Although colon cancer is very heterogeneous, colon cancer development is similar in mice, rats and humans. It was shown in murine models and human clinical data that c-Myc plays a key role in colon cancer development by linking Wnt-dependent and Wnt-independent pathways (Hanada et al., 2006, Rigby et al., 2007, Sansom et al., 2007, Kaiser et al., 2007, Amos-Landgraf et al., 2007). EGFR is overexpressed in 60-80 % of colorectal cancers and is associated with bad prognosis and shortened survival rate (Zlobec et al., 2007).

1.3 WNT SIGNALING PATHWAY AND APC

It is well established that the Wnt pathway is involved in cell differentiation and proliferation and subsequently in the development and tissue homeostasis of the intestine as well as in the development of colon cancer (Arias et al., 1999, Funayama et al., 1995, Polakis, 2000, Willert and Nusse, 1998).

The physiological proliferation of intestinal epithelial cells and the proper differentiation of specialized intestinal epithelial cell types along the crypt-villus-unit depend on correctly regulated Wnt signaling. Beyond that, precise Wnt signaling is necessary to maintain the intestinal stem cell niche (Fevr et al., 2007, Korinek et al., 1998, Batlle et al., 2002).

If the canonical Wnt pathway is inactive, a regulatory multiprotein complex, called destruction complex, containing the scaffolding proteins APC (adenomatous polyposis coli) and Axin-2/Conduction, the kinase GSK3ß (glycogen synthase kinase 3 beta) and the serine/threonine casein kinase 1 alpha (CK1α) is formed and bound to ß-Catenin in the cytoplasm (Kimelman and Xu, 2006). Consequently, ß-Catenin becomes N-terminally phosphorylated by GSK3ß and CK1α leading to ubiquitinylation and finally to proteasomal degradation of ß-Catenin (Bienz and Clevers, 2000). This Wnt ligand absent state is characterized by a low amount of ß-Catenin in the cytoplasm and a gene expression signature for less proliferation and high differentiation of cells (Fodde et al., 2001b) (Fig. 4A).

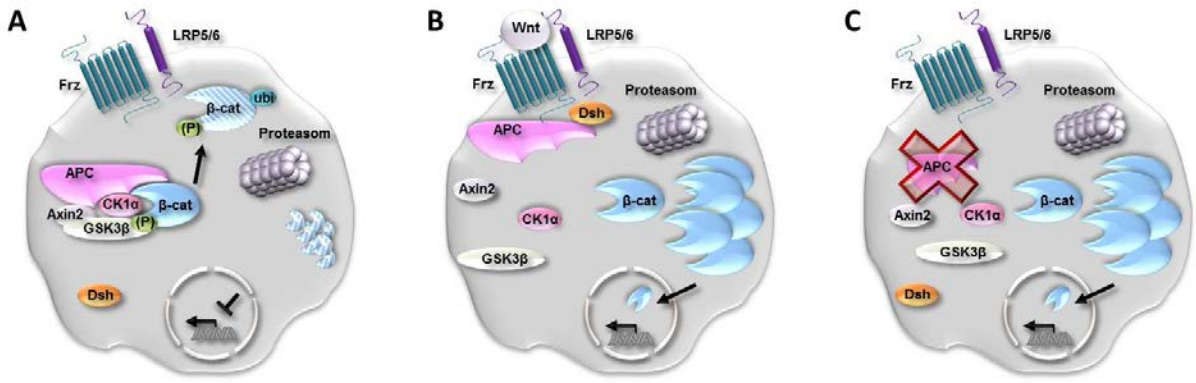

Fig. 4: Outline of the Wnt signaling pathway.

Outline of the canonical Wnt signaling pathway. (A) In absence of the Wnt ligand, cytosolic ß-Catenin is bound by a multiprotein destruction complex that includes APC, Axin-2, GSK3ß and CK1α. ß-Catenin becomes phosphorylated, ubiquitinylated and degraded by the proteasome. (B) In the presence of the Wnt ligand, Dsh and APC are recruited to the cell membrane. The multiprotein destruction complex is restructured and is not able to bind ß-Catenin anymore. Thereupon, ß-Catenin accumulates in they cytoplasm, translocates to the nucleus and activates Wnt-dependent target genes. (C) Truncation or loss of APC impede the formation of the destruction complex on which ß-Catenin accumulates in the cytoplasm. Although the Wnt ligand is absent, a constitutive active Wnt signal is mimicked and Wnt-dependent target genes are expressed.

In the presence of Wnt ligands, a receptor complex consisting of the seven-transmembrane receptor Frizzled (Frz) and the LRP5/6 (low-density lipoprotein receptor-related protein 5/6) coreceptor is activated. This leads to relocalization of the proteins Dishevelled (Dsh) and Axin-2 to the receptor complex at the cell membrane and further to a restructuring of the destruction complex. Due to the restructuration of the destruction complex, GSK3ß and CK1α lose their ability to phosphorylate ß-Catenin to target it for proteasomal degradation (Lee et al., 1999). Thus, ß-Catenin accumulates in the cytoplasm and translocates to the nucleus where it forms heterodimers with transcription factors from the T cell factor (TCF)/ lymphocyte-enhancer factor (LEF) family (Clevers, 2006, Morin et al., 1997, Ben-Ze'ev and Geiger, 1998) (Fig. 4B). This leads to a changed gene expression signature with downstream targets for pro-mitotic genes like c-Myc. (Fodde, 2002) (Tab. 1).

Tab. 1: Selection of target genes relevant to colon cancer.

Wnt/ ß-catenin signaling	Reference	STAT3 signaling	Reference
c-Myc	(He et al., 1998)	c-Myc	(Kiuchi et al., 1999)
MMP7	(Brabletz et al., 1999)	Cyclin-D1	(Leslie et al., 2006)
Axin-2	(Yan et al., 2001)	TGF-ß	(Kinjyo et al., 2006)
Survivin	(Zhang et al., 2001)	TNF-α	(Chappell et al., 2000)
Met	(Boon et al., 2002)	Survivin	(Gritsko et al., 2006)
Claudin-1	(Miwa et al., 2001)	HGF	(Hung and Elliott, 2001)
Jagged	(Rodilla et al., 2009)	IL-6	(Wang et al., 2004)
Sox9	(Blache et al., 2004)	Bcl-2	(Choi and Han, 2012)
Sox17	(Du et al., 2009)	MMP2	(Xie et al., 2004)
MMP13	(Huang et al., 2010)	MMP9	(Song et al., 2008)

Alongside the crypt-villus-unit of the intestinal epithelium, a gradient Wnt signaling occurs. Near the crypt bottom, Wnt signaling is highest and decreases along the crypt-villus-unit to the villus tip. This effect is revealed by ß-Catenin translocation from nucleus to cytoplasm and decreased Wnt target gene expression in IECs during migration along the crypt-villus-unit (Scoville et al., 2008).

Based on the influence of ß-Catenin target genes on differentiation and proliferation within the intestinal epithelium, it is obvious that a dysregulation of the Wnt signaling pathway has serious consequences for intestinal homeostasis and carcinogenesis. In fact, mutations leading to constitutive activation of the Wnt signaling pathway frequently affect APC.

APC TUMOR SUPPRESSOR GENE

APC (adenomatous polyposis coli) plays an important role during Wnt signaling, because APC inhibits mitosis by indirectly mediating proteasomal degradation of cytoplasmic ß-Catenin (Näthke, 2004). If APC is mutated and fails to build up the destruction complex for

proteasomal ß-Catenin degradation, ß-Catenin levels increase within the cytoplasm and nucleus. This in turn leads to dysregulated Wnt target gene expression and enhanced cell proliferation (Fig. 4C).

Most tissue alterations begin with enhanced cell proliferation due to DNA alterations followed by formation of adenomatous polyps caused by mutations in the tumor suppressor gene *APC*. The aberrant crypt foci (ACF) are characterized by elevated levels of ß-Catenin in both, the nucleus and cytoplasm, and during chromosomal degradation during mitosis (Yamada et al., 2002, Fodde et al., 2001a, Powell et al., 1992). APC is involved in the Wnt pathway by regulation of the ß-Catenin levels and plays a role in cell adhesion, migration and apoptosis (Su et al., 1992, Fodde et al., 2001b). In addition to dysregulated mitosis, the proliferative zone of intestinal epithelial cells is enlarged, migration along the crypt-villus-unit is retarded and cell differentiation diminished (Fodde et al., 2001b, Sansom et al., 2004).

Cancer-related *APC* mutations usually lead to truncated APC proteins which are incapable to bind ß-Catenin in the regulatory complex composed of APC, Axin-2, GSK3ß and CK1α (Fodde, 2002). The majority of colon cancers are accompanied by mutations in the *APC* gene which is located on chromosome 5q21 (Fodde, 2002, Heyer et al., 1999). Lost portions of chromosome 5q21 were found in hereditary colon cancer, such as familial adenomatous polyposis (FAP) and spontaneous colon cancer (Kinzler 1991). FAP originates from germline mutation in one *APC* allele followed by spontaneous mutation of the wildtype allele later in life. Somatic mutations where both *APC* alleles are eliminated lead to sporadic colon cancer.

Mutations within the *APC* gene occur frequently with 80-95 % in hereditary cancers such as spontaneous intestinal cancer and familial adenomatous polyposis (FAP) (Laken et al., 1999). In humans, a mutation within the *APC* gene results predominantly in colonic polyps. In the murine system, approximately 10 to 100 neoplasia occur within the small intestine while in the colon only a low number of polyps occur (Groden et al., 1991).

The classification of *APC* as a tumor suppressor gene was established when genetically engineered mice carrying a mutated *Apc* allele or mice depleted of *Apc* developed spontaneous intestinal cancer (Fodde et al., 2001b, Bjerknes and Cheng, 1981).

Tab. 2: Selection of genetically engineered Apc mice.

Mouse strain	APC modification	Reference
$Apc^{\Delta 474/+}$	Neomycin insertion in exon 9, duplication of exon 7, 8, 9, 10 and frameshift at codon 474	(Sasai et al., 2000)
$Apc^{\Delta 14}$	Frameshift at codon 580	(Colnot et al., 2004)
Apc^{580D}	Exon 14 flanked by loxp sites, adenovirus cre exposure and frameshift at codon 580	(Shibata et al., 1997)
$Apc^{\Delta 716/+}$	Neomycin insertion in exon 15 and protein truncation at codon 716	(Oshima et al., 1995)
$Apc^{Min/+}$	Protein truncation at codon 850	(Moser et al., 1990)
$Apc^{1309/+}$	Frameshift at codon 1309	(Quesada et al., 1998)
$Apc^{1638N/+}$	Antisense Neomycin insertion in exon 15 and protein truncation at codon 1638	(Fodde et al., 1994)
$Apc^{\Delta 14/+}$	Exon 14 flanked by loxp sites	(Shibata et al., 1997)
$Apc^{\Delta 15/+}$	Exon 15 flanked by loxp sites	(Robanus-Maandag et al., 2010)
Apc^{tm1Tyj}	Exon 1-15 flanked by loxp sites	(Cheung et al., 2009)

Of the many commercially available mouse models with different *Apc* mutations, the $Apc^{Min/+}$ mouse is the most frequently used model to study spontaneous colon cancer development (Tab. 2).

1.4 EGFR SIGNALING PATHWAY AND AMPHIREGULIN

ErbB RECEPTOR FAMILY

In 1962, a growth factor was discovered and named by its effect: epidermal growth factor (EGF). A few years later the corresponding receptor, namely epidermal growth factor receptor (EGFR), was determined and represented the first identified receptor tyrosine kinase (Cohen, 1962, King et al., 1980). Sequencing of the complete human receptor revealed high homology to the avian erythroblastosis virus v-erbB oncogene and is therefore also called ErbB (Ullrich et al., 1984, Downward et al., 1984).

EGFR (also known as ErbB1) is a member of the membrane spanning ErbB (erythroblastosis oncogene B) receptor tyrosine kinase (RTK) family (Fig. 5), which also includes ErbB2 (also

known as HER2/Neu), ErbB3 (also known as HER3) and ErbB4 (also known as HER4). The EGFR signaling pathway is complex and responsible for a variety of cellular signals such as proliferation, migration, adhesion, survival and differentiation (Yarden and Sliwkowski, 2001, Zaczek et al., 2005).

All four members of the receptor tyrosine kinase family are transmembrane proteins with a basic structure containing an extracellular domain including ligand-binding regions and cysteine-rich regions, a single membrane-spanning transmembrane domain and an intracellular domain with an intrinsic tyrosine kinase domain as well as several tyrosine residues (Olayioye et al., 2000, Ullrich et al., 1984). Dimerization and phosphorylation of the involved receptors of the ErbB receptor family are essential for signal transduction. Upon ligand binding, ErbB receptors form dimers, either homo- or heterodimers, which triggers activation of the intrinsic tyrosine kinase activity and triggers trans-phosphorylation of tyrosine residues throughout the intracellular C-terminal region of the receptors (Weiss and Schlessinger, 1998, Hubbard et al., 1998).

Each ErbB receptor shows a distinct phosphorylation pattern on different tyrosine (Y) residues which serves as binding sites for specific adapter proteins containing SH2 (Src Homology 2) or PTB (phosphotyrosine binding) domains to forward intracellular signals (Pawson and Gish, 1992). The EGFR contain specific tyrosine residues in the kinase domain and tyrosine sites which are identified as autophosphorylation sites within the C-terminal domain (Y992, Y1045, Y1068, Y1086, Y1101; Y1148 and Y1193). These phosphorylated tyrosine residues provide docking sites for specific adaptor proteins such as PLC-gamma (phospholipase c gamma) via its SH2 domain to Y992 or Y1173 and GRB2 (growth factor receptor-bound protein 2) via its SH2 domain to Y1068 or Y1086, to induce different downstream signaling events (Jorissen et al., 2003, Olayioye et al., 2000, Batzer et al., 1994, Rotin et al., 1992).

However, the ErbB3 receptor is an exception since it lacks tyrosine kinase activity. As a consequence, the ErbB3 receptor has to form a heterodimer with one of the other ErbB receptor tyrosine kinase family members to forward signal transduction (Guy et al., 1994, Plowman et al., 1990b).

ErbB DOWNSTREAM SIGNALING

To ensure that extracellular signals are correctly transferred into downstream signals, intracellular adapter proteins bound to the phosphorylated ErbB receptors are important key players for signal transduction. Due to the individual C-terminal tyrosine phosphorylation

patterns of each ErbB receptor family member and the resulting distinct adapter protein binding, the number of activated downstream pathways is extensive.

One of the most crucial downstream pathways in the ErbB signaling network is the RAS-RAF-MEK-MAPK pathway. Phosphorylated tyrosine residues of the EGFR recruit adapter proteins like GRB2, which can either interact directly with EGFR at Y1086 and Y1068 or indirectly via Y1173 through the adapter molecule Shc. GRB2 in turn, binds to SOS (son of sevenless), a guanosine nucleotide exchange factor, to activate RAS by exchange of GDP with GTP. Activated RAS then activates the serine/threonine protein kinase RAF. The following mitogen-activated protein kinase (MAPK) pathway, accompanied by a highly conserved downstream kinase cascade and activation of nuclear transcription factors, is involved in cell proliferation, in particular the shift from G1 to S phase during cell cycle progression (Marshall, 1994, Suhardja and Hoffman, 2003).

Additional downstream pathways after ErbB activation are PI3K/AKT signaling and STAT signaling as well as indirect crosstalk with G-protein coupled receptors (GPCR) (Olayioye et al., 2000).

Upon activation of GPCRs an intracellular signaling cascade through kinases like PKC (protein kinase C) or ions like Ca^{2+} lead to ADAM (A Disintegrin And Metalloproteinase) protease activation. This in turn leads to enhanced cleavage of membrane bound EGFR ligands by ADAM proteases, also known as ectodomain shedding, and thereupon to increased EGFR signaling (Ohtsu et al., 2006, Prenzel et al., 1999).

Moreover, phosphorylated EGFR can interact either directly with signal transducers and activators of transcription (STAT) proteins through their SH2 domain or indirectly through SRC proteins (David et al., 1996). The STAT family is comprised of seven members, whereby only selected STAT proteins are related to cancer, for instance STAT3 and STAT5a/b. The STAT pathway can either be activated by cytokine signaling mediated through Janus kinases (JAK) or via EGFR signaling independent of Janus kinases (Andl et al., 2004, Darnell et al., 1994). It is known that Amphiregulin-dependent activation of the EGFR signaling pathway leads to induction of STAT1, STAT3 and STAT5, whereby Amphiregulin activates STAT signaling independent of JAKs (David et al., 1996). Thereby, EGFR activation leads to STAT phosphorylation and dimerization followed by translocation to the nucleus to activate transcription of target genes which are involved in proliferation, cell cycle progression and angiogenesis. Further, STAT3 contributes to intestinal epithelial cell survival and regeneration (Grivennikov et al., 2009). Due to these effects, dysregulated STAT signaling contributes to tumor development in cancer-related cells (Silva, 2004).

The phosphatidylinositol 3 kinase (PI3K)/ AKT signaling pathway is also activated by ErbB3 or ErbB4 upstream signaling. Upon ligand binding and phosphorylation of ErbB3 or ErbB4, the PI3K regulatory subunit p85α interacts with various phosphorylated tyrosine residues of the ErbB receptors via its SH2 domain. The regulatory subunit p85α exists in a heterodimer formation with the PI3K catalytic subunit p110α which is crucial for AKT (also known as protein kinase B) recruitment mediated by PIP3 (phosphatidylinositol-3,4,5-triphosphate) production. Activated AKT enhances cell survival through inhibition of the pro-apoptotic proteins BAD and Caspase-9 (Stover et al., 1995, Franke et al., 1997, Datta et al., 1997). Enhanced cell survival and prevention of apoptosis mediated by ErbB downstream pathways due to upregulation of anti-apoptotic proteins (e.g. BCL-2) or downregulation of pro-apoptotic proteins (e.g. BAK, BAD and BAX) to block cytochrome c release are the main challenges of clinical chemotherapy and radiation during cancer treatment (Danielsen and Maihle, 2002).

Two types of inhibitors are available for therapeutical approaches against EGFR-related cancers: antibodies (e.g. Cetuximab, Trastuzumab, Panitumumab) or small molecule tyrosine kinase inhibitors (e.g. Lapatinib, Gefitinib, Erlotinib) (Arteaga and Engelman, 2014).

The characteristics of EGFR as a proto-oncogene are underlined by its role in regular development and homeostasis together with fatal effects in alterations of EGFR signaling. The homeostasis of EGFR signaling pathways is crucial for physiological functions and developmental processes because ErbB receptors are broadly expressed in several tissues. Indeed, the importance of the EGFR signaling pathway was shown *in vivo* by using genetically modified mice with null mutations of each individual ErbB receptor. The complete knockout of EGFR leads to placental defects, organ malformation and pre- or perinatal lethality (Threadgill et al., 1995, Sibilia and Wagner, 1995, Miettinen et al., 1995). Loss of ErbB2 in all tissues resulted in abnormal heart development and embryonic lethality (Lee et al., 1995). Equally, knockout mice for ErbB3 or ErbB4 were embryonically lethal due to heart malformation and neuronal defects (Gassmann et al., 1995, Erickson et al., 1997). The generation of several conditional ErbB knockout mice allows to investigate the role of EGFR signaling *in vivo*.

ErbB mutations, overexpression or enhanced ErbB ligand expression and release is often associated with various types of cancer because dysregulated EGFR pathways can trigger self-sufficient proliferation and survival by evading apoptosis thereby supporting cancer cells to comply with the “hallmarks of cancer” (Hanahan and Weinberg, 2011, Sebastian et al., 2006).

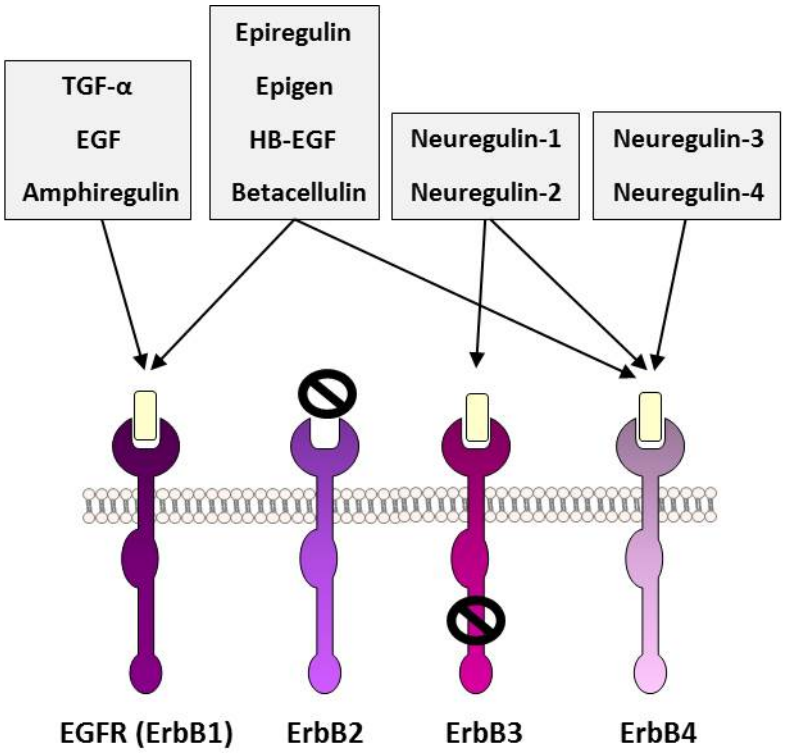

Fig. 5: Overview of the ErbB receptor family and corresponding ErbB ligands.

Depiction of the ErbB ligand binding specificity to the ErbB receptor tyrosine kinase family divided into four groups. Transforming growth factor-alpha (TGF-α), Epidermal growth factor (EGF) and Amphiregulin (AREG) bind to EGFR (also known as ErbB1). Epiregulin (EREG), Epigen (EPG), Heparin-binding epidermal growth factor (HB-EGF) and Betacellulin (BTC) bind to EGFR (also known as ErbB1) and ErbB4. Neuregulin-1 (NRG-1) and Neuregulin-2 (NRG-2) bind to ErbB3 and ErbB4. Neuregulin-3 (NRG-3) and Neuregulin-4 (NRG-4) bind to ErbB4. Adapted from (Olayioye et al., 2000).

ErbB LIGANDS

Various ligands have been identified to activate the different ErbB receptors, however, ErbB2 remains an orphan receptor without any recognized ligands (Zaczek et al., 2005). The conformation of the ErbB2 receptor resembles a ligand-activated state which makes it the prevalent dimerization partner for other ErbB family members (Graus-Porta et al., 1997, Garrett et al., 2003).

As depicted in Fig. 5, ErbB ligands belonging to the EGF-like ligands namely Epidermal growth factor (EGF), Amphiregulin (AREG) and Transforming growth factor-alpha (TGF-α) bind to EGFR. Subsequently Betacellulin (BTC), Epiregulin (EREG), Epigen (EPG) and Heparin-binding epidermal growth factor (HB-EGF) also bind to EGFR and further to ErbB4. The receptors ErbB3 and ErbB4 are activated by binding Neuregulins (NRG) as ErbB ligands. In this particular case, Neuregulin-1 (NRG-1) and Neuregulin-2 (NRG-2) bind to ErbB3 and ErbB4, but Neuregulin-3 (NRG-3) and Neuregulin-4 (NRG-4) only bind to ErbB4 (Riese and Stern, 1998, Zhang et al., 1997, Harari et al., 1999, Harris et al., 2003).

All EGF-like ligands have an EGF-like domain in their extracellular region, which includes six conserved cysteine residues to form three intramolecular disulfide bonds and which is essential to bind to ErbB receptors (Guy et al., 1994, Harris et al., 2003). EGF itself harbors nine EGF-like domains, whereas the other EGF-like ligands contain only one single EGF-like domain (Singh and Coffey, 2014). EGF-like ligands are type I transmembrane proteins, which are shed by ADAM proteases to convert from membrane bound to mature soluble ErbB receptor binding forms (Blobel, 2005, Singh and Coffey, 2014).

Three well-known mechanisms for ErbB receptor and ErbB ligand interaction are described: autocrine, paracrine and juxtacrine (Singh and Coffey, 2014). If a soluble ErbB ligand stimulates the ErbB receptor on the cell which it produced, it is named autocrine signaling. Paracrine signaling occurs when the soluble ErbB ligand is shed from a cell independent of the cell of which it activates the ErbB receptor. Whenever a membrane bound ErbB ligand interacts with an ErbB receptor from a nearby cell, it is referred to as juxtacrine signaling. However, recently a novel mechanism for ErbB receptor and ErbB ligand interaction was discovered *in vitro*: Exosomal targeted receptor activation (ExTRAcrine). During ExTRAcrine signaling ErbB ligands are packed and released by exosomes. The advantage of exosomally packed ErbB ligands are prolonged activity at local or distant sites and protection from degradation (Higginbotham et al., 2011).

AMPHIREGULIN

In 1988, Amphiregulin was discovered as an EGFR ligand in a human breast adenocarinoma cell line after phorbol 12-myristate 13-acetate (PMA) treatment (Shoyab et al., 1988).

Amphiregulin precursor proteins are synthesized as type I transmembrane proteins, undergo posttranslational modifications such as glycosylation and are finally proteolytically processed on the cell surface (Brown et al., 1998). Mature Amphiregulin contains a heparin-binding domain proximal to the EGF-like domain through which can interact with heparin sulfate proteoglycan to trigger Amphiregulin-induced EGFR activation (Brown et al., 1998, Johnson and Wong, 1994).

Amphiregulin is a widely expressed protein and can be detected in pancreas, heart, ovarian, testis, placenta, spleen, colon, lung and kidney (Stern, 2003, Plowman et al., 1990a). During developmental processes in mice, Amphiregulin plays an important role in mammary gland formation and ductal elongation (Luetteke et al., 1999). Expression levels of Amphiregulin in healthy intestinal tissue are moderate. In colon cancer, however, Amphiregulin is overexpressed (Cook et al., 1992).

It was shown in polarizing human colorectal cancer cells such as HCA-7 or Caco2 that Amphiregulin is the most highly expressed EGFR ligand on the basolateral cell surface (Brown et al., 1998). In these cells, Amphiregulin is transported to the basolateral surface where it is processed via ectodomain shedding. Proteolytic processing is catalyzed by ADAM17 and is an essential step to release Amphiregulin as soluble EGFR ligand to induce EGFR activation (Singh and Coffey, 2014). Kenny and Bissell showed that ADAM17 inhibition blocks Amphiregulin-induced EGFR activation (Kenny and Bissell, 2007).

When Amphiregulin binds to the EGFR, a mitogenic signal is induced (Wong et al., 1999). Further it was shown that Amphiregulin-induced EGFR activation increases MMP2 and -9, whereby the extracellular matrix was altered to promote cell invasion (Kondapaka et al., 1997).

1.5 PROTEOLYSIS AND ADAM17

Physiological processes such as homeostasis and development as well as pathophysiological processes like inflammation and cancer are often regulated by proteolytic enzymes. So far, 567 human proteolytic enzymes are identified and categorized into groups related to their catalytically active site: metallo-, threonine-, serine-, cysteine- and aspartic proteases (López-Otín and Matrisian, 2007). These groups are divided in several subgroups such as the metzincin superfamily of metalloproteinases. This metzincin superfamily includes i.a. the adamlysin subfamily which in turn contains SVMPs (Snake Venom Metalloproteases), ADAMTSs (A Disintegrin and Metalloproteinases with thrombospondin motifs) and ADAMs (A Disintegrin and Metalloproteinases) (Rivera et al., 2010, Stöcker et al., 1995, Edwards et al., 2008).

ADAM proteases belong to multidomain type I transmembrane proteins and are involved in ectodomain shedding, during which extracellular parts of membrane bound proteins are cleaved and released into the extracellular environment (Jones et al., 2015). In contrast to other posttranslational modifications such as phosphorylation and proteolysis, ectodomain shedding is a completely irreversible mechanism and serve as a key regulator of signal transduction (Blobel, 2005, Reiss and Saftig, 2009). Here, shed proteins interact in their soluble form via autocrine or paracrine signaling with a variety of receptors (Hooper et al., 1997). So far, 21 human ADAM proteases have been identified, but only 13 ADAM proteins are proteolytic active enzymes. The proteolytic inactive enzymes evolutionary lack the zinc ion binding site (Rivera et al., 2010). The best characterized members of the ADAM proteases are the closely related ADAMs ADAM17 and ADAM10. Some studies revealed

redundant and compensatory mechanisms between ADAM10 and ADAM17 (Folgosa et al., 2013).

ADAM17 (A DISINTEGRIN AND METALLOPROTEINASE)

Like all ADAM proteases ADAM17 is expressed as zymogen with an N-terminal signal sequence, an extracellular domain, a transmembrane domain, and an intracellular domain. The extracellular domain of ADAM proteases contains a regulatory prodomain, a catalytic domain, a disintegrin domain, an EGF-like domain and a cysteine-rich domain. ADAM17 harbors an additional membrane-proximal domain (MPD) which plays a role in substrate recognition (Takeda, 2009, Lorenzen et al., 2012). The catalytic domain contains a conserved histidine motif (HEXXHXXGXXH) for correct coordination of a zinc ion within the catalytic center (Roghani et al., 1999). To gain full activity, the prodomain of immature ADAM proteases has to be removed first. For ADAM17, this maturation occurs during the secretory pathway in the Golgi complex by furin-like convertases (Endres et al., 2003). It was described that the prodomain acts as a chaperon and contributes to accurate protein folding of ADAM proteases (Roghani et al., 1999).

ADAM17 was discovered as the enzyme that cleaves membrane bound TNF-α and that is why ADAM17 is also named Tumor Necrosis Factor (TNF) alpha converting enzyme (TACE) (Moss et al., 1997, Black et al., 1997). Apart from this, ADAM17 is involved in the proteolytic processing of numerous type I and type II transmembrane proteins. Amongst ADAM17 substrates are cytokines, cell adhesion molecules, receptors, growth factors like TNF-α and both of its receptors TNFRI and TNFRII, as well as the membrane bound ErbB ligands TGF-α, HB-EGF, Epigen and Amphiregulin (Peschon et al., 1998, Hinkle et al., 2004, Sahin and Blobel, 2007, Scheller et al., 2011) (Fig. 6).

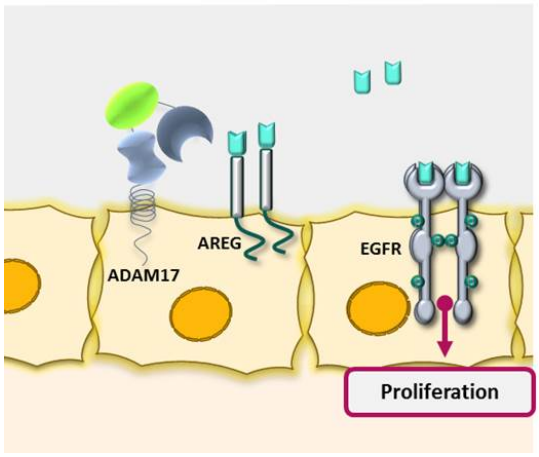

Fig. 6: Outline of the ADAM17-mediated ectodomain shedding of Amphiregulin.

ADAM17 (A Disintegrin And Metalloproteinase) localized on the cell surface is able to convert the membrane bound precursor form of Amphiregulin (AREG) via ectodomain shedding into a mature soluble form. Soluble AREG binds as a ligand to the EGFR (epidermal growth factor receptor; also known as ErbB1) which leads upon activation and phosphorylation of the receptor to several downstream signals which support cell proliferation.

As a consequence of this broad substrate spectrum, ADAM17 is involved in different physiological and pathophysiological processes such as regeneration, immune response, inflammation and cancer. The regulation of the TNF signaling pathway due to ADAM17-mediated shedding of TNF-α, TNFRI and TNFRII is a model example for the dual role of ADAM17 in pro- and anti-inflammatory responses. On the one hand, ADAM17 can activate the TNF signaling pathway by shedding the ligand TNF-α. On the other hand, ADAM17 is able to diminish TNF signaling by shedding TNF receptors, which then become soluble and bind TNF-α thereby blocking its activity (Scheller et al., 2011).

The important role of ADAM17 becomes apparent in *in vivo* studies, because ADAM17 is ubiquitously expressed and a deletion of ADAM17 in mice leads to severe phenotypes such as heart defects, epithelial abnormalities, hair defects, open eyelids, defects in mammary gland development and perinatal lethality (Black et al., 1997, Peschon et al., 1998). The broad substrate spectrum of ADAM17 is supported by the comparison of ADAM17$^{-/-}$ knockout mice with EGFR$^{-/-}$ knockout mice as well as HB-EGF$^{-/-}$ knockout mice, TGF-α$^{-/-}$ knockout mice and AREG$^{-/-}$ knockout mice because all these mice have severe developmental defects with similar epithelial structure impairments (Peschon et al., 1998, Jackson et al., 2003, Luetteke et al., 1999). Combined studies of ADAM17-deficient mice and hypomorphic EGFR mice confirm that ADAM17 acts as an upstream regulator of EGFR signaling via ectodomain shedding of EGFR ligands (Blobel et al., 2009, Sunnarborg et al., 2002). Moreover, a dextran sodium sulfate (dextran)-induced colonic inflammation mouse model showed that ADAM17

activity is essential for TGF-α shedding to induce EGFR signaling for anti-inflammatory response to heal colonic inflammation (Chalaris et al., 2010, Brandl et al., 2010).

To study ADAM17 *in vivo*, several conditional knockout mice were generated. The hypomorphic ADAM17$^{ex/ex}$ mice from Chalaris et al. are particularly important due to drastically reduced ADAM17 protein expression in all tissues accompanied by impaired shedding of ADAM17 substrates while ADAM17 residual activity is sufficient to generate viable mice (Chalaris et al., 2010).

The regulation of ADAM17 activity takes place during transcription or by posttranslational modifications such as the removal of the inhibitory prodomain or phosphorylation (Scheller et al., 2011, Schlondorff et al., 2000). Two amino acids (T735 and S974) within the intracellular domain of ADAM17 are involved in regulation due to novel interaction partners, namely Polo-like kinase 2 (PLK2) and inactive rhomboid protease 2 (iRhom2). This protein-protein modification and interaction accomplish different functions in ADAM17 biology. The inactive rhomboid protease 2 has a promoting effect on ADAM17 maturation by iRhom2-mediated transportation during the secretory pathway. Whereas PLK2-mediated phosphorylation contributes to ADAM17 activity on the cell surface (Yoda et al., 2013, Soond et al., 2005, Schwarz et al., 2014, Adrain et al., 2012). Endogenous inhibition of ADAMs is mediated by tissue inhibitor of metalloproteinases (TIMPs) and TIMP3 is a natural ADAM17 inhibitor (Brew and Nagase, 2010, Khokha et al., 2013). The development of synthetic ADAM inhibitors is limited because of low specificity and severe toxicity (Murumkar et al., 2010).

The intestinal microbiome had an influence on ADAM17 activity in a direct or indirect manner via for instance LPS (lipopolysaccharide) which is important for host-microbe crosstalk (Yan et al., 2016, Brandl et al., 2010). Thereby enhanced ADAM17 activity and signal crosstalk between the basolateral surface of IECs and microbes is needed to resolve inflammation or injury of the epithelial lining of the intestine by epithelial regeneration. However, long-term chronic inflammation can be observed in inflammatory bowel disease (IBD) and enhanced proteolytic activity by established host-microbe crosstalk increases the risk of inflammation-associated cancer (Itzkowitz and Harpaz, 2004, Itzkowitz and Yio, 2004).

ADAM17 is ubiquitously expressed on the basolateral surface of polarized epithelial cells throughout the small intestine and colon (Merchant et al., 2008). It was shown that ADAM17 mRNA is upregulated in various cancers i.a. colon cancer and breast cancer (Blanchot-Jossic et al., 2005, McGowan et al., 2008, Nakagawa et al., 2009). Overexpression of ADAM17 within the tumor microenvironment is often correlated with tumor progression, tumor invasiveness and poor clinical prediction based on the number of affected ADAM17

signaling pathways such as ErbB, IL-6, Notch or STAT3 pathway (Murphy, 2008, Duffy et al., 2009).

1.6 RESEARCH OBJECTIVES

Mice lacking functional ADAM17 are not viable. The unique hypomorphic ADAM17$^{ex/ex}$ mice used in my study are viable and characterized by a negligible minimal expression of ADAM17 in all tissues (Chalaris et al., 2010). Using these mice allowed investigating the physiological relevance of ADAM17 within the murine system.

I investigated whether ADAM17 had an impact of tumor initiation and tumor development in a colitis-associated cancer (CAC) model as well as in a genetically predisposed colorectal cancer (CRC) mouse model. For this purpose, a novel mouse model with deficiency in ADAM17 expression and mutation in the *Apc* tumor suppressor gene was established to determine the effect of ADAM17 on genetically predisposed CRC. Furthermore, I examined which ADAM17-regulated signaling pathway is involved in the development of colon cancer. Thus, I focused on the proteolytic function of ADAM17 as a metalloprotease in irreversible ectodomain shedding of membrane bound substrates for regulation of signaling pathways. To investigate whether EGFR signaling related proteins have an impact on colon cancer development, I analyzed mRNA levels, protein expression and ectodomain shedding in human colorectal cancer cells as well as in murine CRC 3D organoids and CRC tissue.

CHAPTER TWO: MATERIAL & METHODS

Unless otherwise indicated, all chemicals, consumables and cell culture material were purchased by Sigma-Aldrich (Taufkirchen, D), Roth (Karlsruhe, D), Sarstedt (Nümbrecht, D) Biozym (Hess. Oldenburg, D), Millipore (Darmstadt, D) and Thermo Fisher Scientific, Life Technologies GmbH including Gibco™ (Darmstadt, D). All buffers and solutions were prepared with ddH_2O.

2.1 MICE

All mice were kept under barrier conditions in individually ventilated cages (IVC) in species-appropriate husbandry at the Victor-Hensen-Haus (VHH, University of Kiel) in a 12 h light-dark-cycle under standard conditions. The mice were pathogen-free and checked periodically by microbiologic screenings. All experiments involving mice were permitted by national law in context of project proposal #524 „Funktionelle Charakterisierung der Metalloprotease ADAM17 als Regulator von chronisch entzündlichen Darmerkrankungen und kolorektaler Karzinogenese“ (Aktenzeichen V 312-72241.121-3 (74-6/11)) and #853 „Etablierung von hypomorphen ADAM17 Darmkrebszelllinien aus der Maus für $ADAM17^{ex/ex}/APC^{+/-}$ “.

For genotyping mouse tail biopsies from 3-week-old mice were lysed overnight in 200 µl DirectPCR® Lysis Reagent Tail Kit from Peqlab/VWR (Erlangen, D), supplemented with 2 µl Proteinase K at 55 °C followed by heat inactivation at 85 °C for 45 min to stop enzymatic activity. Samples were centrifuged for 10 min at 12,000 x g to separate genomic DNA from insoluble parts. Supernatants were used for individual genotyping PCR.

2.1.1 HYPOMORPHIC $ADAM17^{ex/ex}$ MICE

ADAM17-deficent hypomorphic $ADAM17^{ex/ex}$ mice were generated by a novel gene target strategy named exon induced translational stop (EXITS). The *Adam17* gene of hypomorphic $ADAM17^{ex/ex}$ mice contains an additional in frame translational stop codon and as a result homozygous mice harbored 95 % mRNA coding for ADAM17 with a premature stop codon (Chalaris et al., 2010). This premature stop codon leads to drastically reduced ADAM17 protein expression in all tissues. Hypomorphic $ADAM17^{ex/ex}$ mice are viable albeit with hair,

skin, heart and epithelial abnormalities, open eye lids and limitations in their fertility. Hypomorphic ADAM17$^{ex/ex}$ mice showed high susceptibility to DSS-induced colitis with insufficient regeneration of the gut epithelium (Chalaris et al., 2010). The hypomorphic ADAM17$^{ex/ex}$ mice used in this work were on a mixed B6;129 background.

Tail biopsies from ADAM17$^{ex/ex}$ mice were lysed (see section 2.1) and used for the PCR protocol described in Tab. 3.

Tab. 3: Layout ADAM17$^{ex/ex}$ mice Genotyping-PCR.

1x mix ADAM17$^{ex/ex}$ PCR	
10x Puffer DreamTaq	2.5 µl
$MgCl_2$ [25 mM]	2.0 µl
dNTP-Mix [10 mM]	1.0 µl
Primer exex_up [1:10]	1.0 µl
Primer exex_dn [1:10]	1.0 µl
DreamTaq Polymerase	0.1 µl
H_2O	15.4 µl
gDNA	2.0 µl
	25.0 µl

temperature [°C]	**time [sec]**	**cycles**
95	300	1 x
95	60	40 x
52	60	
72	60	
72	600	1 x
4	∞	

Primer A17exex_up: 5´-TAT GTG ATA GGT GTA ATG-3´
Primer A17exex_dn: 5´-CTT ATT ATT CTC GTG GTC ACC-3´

The ADAM17 wildtype allele was characterized via agarose gel electrophoresis detected as a PCR product of 380 bp while the hypomorphic ADAM17$^{ex/ex}$ allele including the additional exon was determined by a PCR product of 550 bp (Fig. 7).

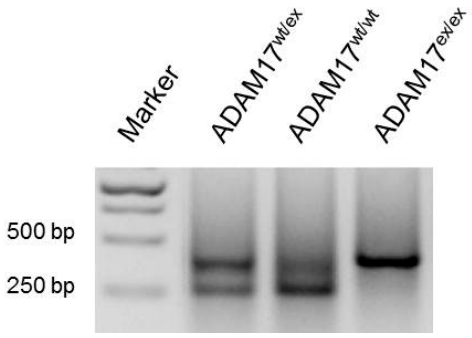

Fig. 7: Genotyping-PCR for ADAM17$^{ex/ex}$ mice.

Genomic DNA extracted from tail biopsies were used for PCR. 6x DNA loading dye was added to the samples. Up next, separation via agarose gel electrophoresis with 2.0 % (w/v) agarose in 0.5 % TBE buffer including 0.002 % (v/v) ethidium bromide was performed. The detected PCR products were located at 380 bp for ADAM17$^{wt/wt}$ mice and at 550 bp for hypomorphic ADAM17$^{ex/ex}$ mice. In case of ADAM17$^{wt/ex}$ mice, both products were present.

2.1.2 APC$^{MIN/+}$ADAM17$^{ex/ex}$ MICE

C57BL/6J-Apc$^{Min/+}$/J mice were purchased by Jackson Laboratory (#002020). These mice are highly susceptible to spontaneous intestinal adenoma formation due to a mutation in the tumor suppressor gene *Apc* and loss of heterozygosity (LOH) at the APC locus. Apc$^{Min/+}$ mice develop multiple intestinal neoplasia like intestinal polyposis in FAP patients. Homozygous mice are embryonically lethal. Within the scope of this doctoral thesis, C57BL/6J-Apc$^{Min/+}$ mice were crossbred with homozygous hypomorphic ADAM17$^{ex/ex}$ mice on a mixed B6;129 background or wildtype ADAM17$^{wt/wt}$ mice on a mixed B6;129 background to receive mice termed Apc$^{Min/+}$ADAM17$^{ex/ex}$ or Apc$^{Min/+}$ADAM17$^{wt/wt}$ on a mixed B6;129 background. Tail biopsies from Apc$^{Min/+}$ADAM17$^{ex/ex}$ mice and Apc$^{Min/+}$ADAM17$^{wt/wt}$ mice were lysed (see section 2.1) and used for the PCR protocol described in Tab. 4.

Tab. 4: Layout $Apc^{Min/+}$ mice Genotyping-PCR.

1x mix $Apc^{Min/+}$ PCR	
10x Puffer DreamTaq	2.0 µl
$MgCl_2$ [25mM]	2.5 µl
dNTP-Mix [10 mM]	1.0 µl
Primer 33 [1:10]	3.0 µl
Primer 34 [1:10]	3.0 µl
Primer 35 [1:10]	2.4 µl
DreamTaq Polymerase	0.1 µl
H_2O	4.0 µl
gDNA	2.0 µl
	20.0 µl

temperature [°C]	time [sec]	cycles
94	180	1 x
94	30	35 x
55	30	
72	60	
72	600	1 x
4	∞	

Primer APC_33: 5´-GCC ATC CCT TCA CGT TAG-3´(wildtype)
Primer APC_34: 5´-TTC CAC TTT GGC ATA AGG C-3´(common)
Primer APC_35: 5´-TTC TGA GAA AGA CAG AAG TTA-3´(mutant)

The Apc wildtype allele was detected via agarose gel electrophoresis by a PCR product of 600 bp while the heterozygous $Apc^{Min/+}$ allele was determined by PCR products of 340 bp and 600 bp (Fig. 8). The $Apc^{Min/+}$ Genotyping-PCR can not distinguish homozygous (embryonic lethal) from heterozygous mice.

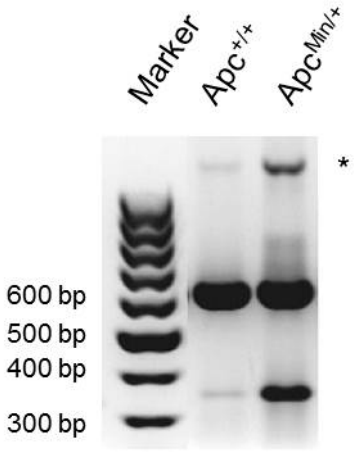

Fig. 8: Genotyping-PCR for $Apc^{Min/+}$ mice.

DNA extracted from tail biopsies were used for PCR. 6x DNA loading dye was added to the samples. Up next, separation via agarose gel electrophoresis with 1.0 % (w/v) agarose in 0.5 % TBE buffer including 0.002 % (v/v) ethidium bromide was performed. The PCR product from wildtype $Apc^{+/+}$ mice has a size of 600 bp. The PCR from $Apc^{Min/+}$ mice shows a result at a size of 340 bp and 600 bp. * unspecific signal.

2.2 MOUSE MODELS

To investigate the role of ADAM17 during the development of colon cancer, a chemically inducible inflammation-associated AOM/DSS mouse model and the genetically predisposed $Apc^{Min/+}$ mouse model were used.

2.2.1 AOM/DSS MOUSE MODEL

AOM/DSS is a well-established mouse model to investigate colon cancer development coupled with chronic mucosal inflammation which is observed in inflammatory bowel disease (IBD) patients (Wirtz et al., 2007).

To induce tumor formation, mice were injected i.p. with azoxymethane (AOM) at two different time points accompanied by three cycles of dextran sulfate sodium (DSS) via drinking water *ad libitum* to promote chronic inflammation within the colon (Fig. 9).

AOM was purchased by Sigma-Aldrich (Taufkirchen, D) and prepared in sterile H_2O up to a final concentration of 10 mg/ml stock solution. For the working solution, solved AOM was diluted in sterile 1x PBS up to a final concentration of 1 mg/ml. All experiments were performed with AOM from the same lot number. To start the experimental procedure, a dose of 10 mg/kg body weight AOM was administered on day 0. A second dose of 5 mg/kg body weight followed at day 21.

DSS was purchased from MPBiomedicals (Eschwege, D) and prepared freshly for each cycle in normal drinking water up to a final concentration of 1.5 % (w/v) for the first cycle from

day 7-14. During the following treatment from day 28-35 and day 49-56 the concentration was reduced to 1.0 % (w/v) DSS. All experiments were performed with DSS (molecular weight of 36,000-50,000) from the same lot number to exclude variances regarding sulfur content.

Mice used throughout the AOM/DSS experiment were 8-week-old male hypomorphic ADAM17$^{ex/ex}$ and ADAM17$^{wt/wt}$ mice.

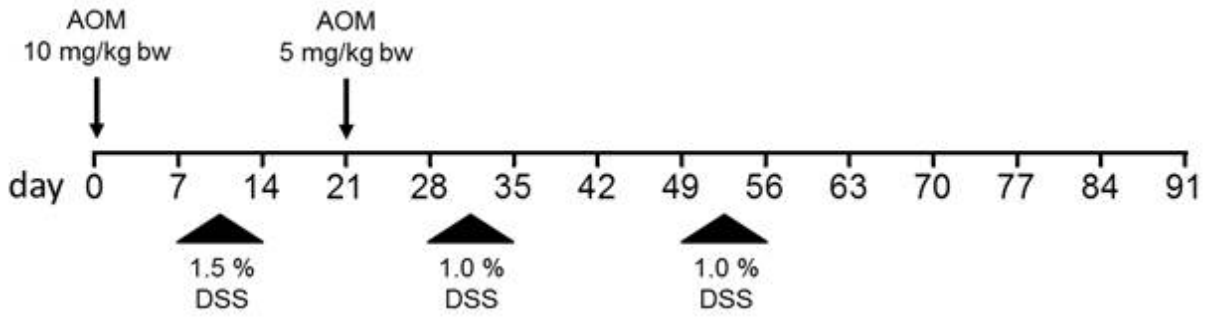

Fig. 9: Experimental timeline for AOM/DSS-induced CAC and analysis.

Schematic representation of the colitis-associated colorectal cancer (CAC) model used in this study. Mice were treated with two i.p. injections of azoxymethane (AOM) as directed followed by repeated administration of dextran sulfate sodium (DSS) provided in the drinking water for one week. The formation of colonic tumors was monitored after 90 days.

According to the permitted project proposal #524, all mice were monitored during AOM/DSS-treatment. Daily weight check during DSS-treatment and the following seven days were mandatory because weight loss of more than 25 % was a legally defined termination criterion. Additionally, feces were controlled for consistency and occult blood by Guaiac-based Haemoccult® test from Beckman Coulter (USA) before and after each DSS cycle.

2.2.2 APC$^{MIN/+}$ MOUSE MODEL

Apc$^{Min/+}$ mice are genetically predisposed to spontaneous intestinal adenoma formation which leads to the Min (Multiple intestinal neoplasia) phenotype upon loss of the *Apc* wildtype allele (Luongo et al., 1994). This phenotype is based on a single germline mutation where the tumor suppressor gene *Apc* was initially chemically mutated using N-ethyl-N-nitrosourea (ENU) leading to a T to A transversion of nucleotide 2549 resulting in a L850* nonsense

mutation (Moser et al., 1990, Hursting et al., 1999). The premature stop codon at amino acid 850 leads to a truncated APC protein of 95 kDa. This truncated APC protein lacks the ß-Catenin binding sequence (Su et al., 1992). As a consequence, the Wnt pathway is constitutively activated in $Apc^{Min/+}$ mice and ß-Catenin accumulates and translocates to the nucleus where it interacts with transcription factors of the TCF/LEF family.

Mice used throughout the analysis were six-month-old. During this time, loss of heterozygosity (LOH) at the APC locus in the $Apc^{Min/+}$ mouse takes place. LOH describes a mutation in which the entire allele is lost (Bienz and Clevers, 2000). LOH is an initial event, because *Apc* is a recessive tumor suppressor gene and inactivation of both alleles is necessary for spontaneous tumor formation because the remaining *Apc* wildtype allele can compensate for the mutated allele (Yamada and Mori, 2006). This finding was first postulated in the currently accepted Knudson´s two-hit hypothesis, which describes that an additional mutation in the second allele is essential to lose both alleles and the associated function of a tumor suppressor gene (Knudson et al., 1975).

2.2.3 SACRIFICE OF MICE

All mice were sacrificed by cervical dislocation according to animal welfare guidelines. After sacrifice, small intestine and colon were removed and flushed with ice-cold PBS to remove feces, opened longitudinally and prepared for further experiments and analysis as indicated.

2.3 ORGANOID CULTURE

Organoid cultures make it possible to investigate intestinal epithelial cells *ex vivo* without influence of the microenvironment.

The following protocols were initially adapted from Sato et al. (Sato et al., 2009), provided by our cooperation partner Assoc. Prof. Dr. Peter J. Dempsey from the University of Colorado Medical School, Aurora, Colorado, USA and modified during the present work by myself.

2.3.1 CRYPT ISOLATION

Mice were euthanized, dissected and the small intestine was collected and stored in ice-cold PBS. For *ex vivo* organoid culture the following steps were performed under sterile conditions. The small intestine was opened longitudinally, rinsed three times with ice-cold 1x PBS and cut into small pieces (~5 mm). Tissue pieces were transferred into a 50 ml tube and washed with 10 ml ice-cold 1x PBS to reduce bacterial levels and mucin content until the supernatant was clear. Thereupon, the tissue pieces were incubated with 10 ml freshly prepared 2 mM EDTA and 0.5 mM DTT in 1x PBS on ice to loosen villus fragments and crypts. The EDTA/DTT buffer was gently removed after 30 min and replaced by 10 ml 1x PBS without Ca^{2+} and Mg^{2+}. The 50 ml tube was vigorously shaken to resuspend tissue pieces and to release crypts. The tissue pieces were allowed to settle under normal gravity for up to 5 min. The supernatant including released crypts was passed through a 100 µm cell strainer to remove residual villus material. 100 µl from the filtrate was transferred to a 96 well plate to check for well-preserved crypts by microscopic analysis. The resuspension-sedimentation step was repeated 2-4 times, and each single step was microscopically monitored for well-preserved crypts. The supernatants without crypts or bad crypt-debris ratio were discarded. Supernatants containing well-preserved crypts were combined and gently pelleted by centrifugation at 500 x g for 4 min at RT to separate crypts from single cells. Crypt pellets were resuspended in 3-5 ml EDTA/DTT buffer, transferred to a 15 ml tube and centrifuged at 500 x g for 4 min at RT. As a last step, the crypts were mixed with up to 500 µl Corning® Matrigel® Basement Membrane Matrix Growth Factor Reduced (GFR) from Corning (USA), plated in 24 well plates with 50 µl Matrigel® GFR drops per well plus 500 µl individual medium and cultured until they reached the state of mature organoids (Fig. 10). Further information about organoid culture conditions is described in the following subchapter 2.3.2.

2.3.2 ORGANOID CULTURE CONDITIONS

Corning® Matrigel® Basement Membrane Matrix Growth Factor Reduced (GFR) from Corning (USA) is a solubilized basement membrane extracted from the Engelbreth-Holm-Swarm mouse sarcoma and supported the laminin and collagen IV-rich crypt base under *ex vivo* cell culture conditions. Hardened Matrigel® GFR drops allowed to grow cells or organoids within a three-dimensional matrix. Matrigel® GFR must be stored at -20 °C, thawed on ice in a 4 °C refrigerator overnight and kept on ice until usage, because Matrigel® GFR hardened above 10 °C.

Pelleted crypts from chapter 2.3.1 or mature organoids were gently mixed with up to 500 µl Matrigel® GFR in a 1:2 ratio with Gibco™ Advanced DMEM/F12 containing 1x GlutaMAX and 50 U/ml Pen/Strep. Organoids were seeded in a 24 well plate with 50 µl Matrigel® GFR drops per well. Plates remained at 37 °C for 5-15 min until Matrigel® GFR hardened. Each drop was covered with 500 µl individual medium per well. The entire culture medium was changed every second day and organoids were passaged twice a week in a 1:5 ratio.

For passaging, the culture medium was replaced with fresh Gibco™ Advanced DMEM/F12 containing 1x GlutaMAX and 50 U/ml Pen/Strep as washing medium. Organoids and Corning® Matrigel® GFR were mechanically disrupted by using a 1,000 µl pipette and transferred into a 15 ml tube. Further mechanical disruption was achieved by using a 21G x 4¾" needle. Dissociated organoids were washed with up to 3 ml wash medium and centrifuged at 800 x g for 4 min. The supernatant was discarded and the pellet was resuspended in a 1:2 ratio of Matrigel® GFR and washing medium. Organoids were seeded as described above.

For cryopreservation, Matrigel® GFR spots including well proliferating organoids were thoroughly disrupted mechanically by pipetting with wash medium, transferred into a 15 ml tube and centrifuged at 800 x g for 4 min. The supernatant was discarded and the pellet resuspended in freezing medium containing 90 % (v/v) FCS and 10 % (v/v) DMSO. For long-term storage, cryo tubes were kept at -160 °C.

2.3.3 BCM ORGANOIDS

To maintain organoid cultures from ADAM17$^{wt/wt}$ and ADAM17$^{ex/ex}$ mice, basal culture medium (BCM) was freshly prepared every 10-14 days as indicated in Tab. 5 and Tab. 6.

To generate conditioned media, L cells expressing Wnt3a and HEK293 cells expressing R-Spondin-1 were kindly provided by our cooperation partner Assoc. Prof. Dr. Peter J. Dempsey from the University of Colorado Medical School, Aurora, Colorado, USA. Both cell lines were cultured in Gibco™ Advanced DMEM/F12 containing 10 % FCS, 10 mM HEPES, 1x GlutaMAX and 50 U/ml Pen/Strep. To select Wnt3a expressing L cells, 0.4 mg/ml G418 were added to the cell culture medium. R-Spondin-1 expressing HEK293 cells were selected by adding 0.6 mg/ml Zeocin to the cell culture medium. To generate conditioned media, the cells were grown in 10 cm dishes in media containing antibiotics until near confluency. The cells were passaged in 1:10 ratio in 10 cm dishes into 10 ml cell culture medium without antibiotics. After 4 days, the conditioned media were collected, stored at

4 °C and fresh media without antibiotics were added for additional 4 days. Conditioned media were passed through a 0.2 µm filter for sterilization and aliquoted for storage at -20 °C. It is recommended to test each new batch of conditioned media on organoids to determine the concentration of Wnt3a and R-Spondin-1 due to their necessity to maintain Wnt signaling and crypt proliferation in organoid cultures.

Depending on the origin of isolated crypts, BCM for small intestine or BCM for colon were chosen depending on the physiological distribution of Paneth cells in the intestine and the required amount of conditioned media. Since Paneth cells secrete Wnt3a, conditioned media from L cells is not required in BCM for small intestine.

Tab. 5: Basal culture medium for colon organoids.

BCM colon	final conc.	source of supply
R-Spondin-1	15 ml	cond. medium HEK_Rsp-1
Wnt3a	15 ml	cond. medium L cells_Wnt3a
B27 [50x]	1x	Life technologies
N2 [100x]	1x	Life technologies
Pen/Strep [100x]	1x	Life technologies
GlutaMax [100x]	1x	Life technologies
HEPES [1 M]	10 mM	Life technologies
NAC [1 M]	1 mM	Sigma
Noggin [25 µg/ml]	25 ng/ml	Peprotech
Gentamycin [50 mg/ml]	50 µg/ml	Life technologies
Primocyn [50 mg/ml]	0.5 mg/ml	Invivogen
EGF [120 µg/ml]	40 ng/ml	Peprotech

Tab. 6: Basal culture medium for small intestinal organoids.

BCM small intestine	final conc.	source of supply
R-Spondin-1	12 ml	cond. medium HEK_Rsp-1
Wnt3a	/	cond. medium L cells_Wnt3a
B27 [50x]	1x	Life technologies
N2 [100x]	1x	Life technologies
Pen/Strep [100x]	1x	Life technologies
GlutaMax [100x]	1x	Life technologies
HEPES [1 M]	10 mM	Life technologies
NAC [1 M]	1 mM	Sigma
Noggin [25 µg/ml]	25 ng/ml	Peprotech
Gentamycin [50 mg/ml]	50 µg/ml	Life technologies
Primocyn [50 mg/ml]	0.5 mg/ml	Invivogen
EGF [120 µg/ml]	40 ng/ml	Peprotech

Freshly prepared medium was passed through a 0.2 µm filter for sterilization and stored at -20 °C.

As shown in the flow diagram in Fig. 10, organoids generated from ADAM17$^{wt/wt}$ mice and ADAM17$^{ex/ex}$ mice cultured in basal culture medium retain crypt- and villus-domains in organoid cultures.

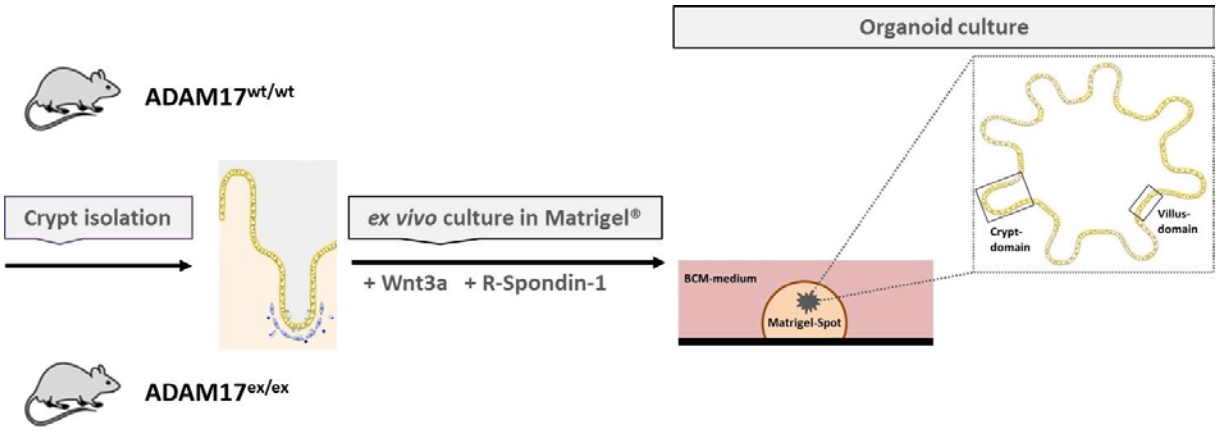

Fig. 10: Flow diagram showing the generation of murine organoids cultured in basal culture medium (BCM).

Murine intestinal crypts from ADAM17$^{wt/wt}$ mice and hypomorphic ADAM17$^{ex/ex}$ mice were isolated and cultured *ex vivo* in Matrigel® GFR with specific niche factors as well as Wnt3a and R-Spondin-1 to form murine organoids. Organoids cultured in basal culture medium (BCM) showed characteristic budded structures which retain villus- and crypt-domains as well as an intestinal lumen-like cavity. BCM supplements led to directed differentiation of Lgr5^{+} stem cells into intestinal epithelial cells. Adapted from (Barker, 2014, Schuijers and Clevers, 2012).

2.3.4 APC ORGANOIDS

To maintain organoid cultures from Apc$^{Min/+}$ADAM17$^{ex/ex}$ mice and Apc$^{Min/+}$ADAM17$^{wt/wt}$ mice, APC tumor medium was freshly prepared every 10-14 days as indicated in Tab. 7.

Due to the fact that Wnt signaling is constitutively active in Apc$^{Min/+}$ mice, Apc$^{Min/+}$ organoids grow without Wnt supplements. Therefore, the admixture of conditioned media from L cells expressing Wnt3a and HEK293 cells expressing R-Spondin-1 to the APC medium was not necessary.

Tab. 7: APC tumor medium for $Apc^{Min/+}$ organoids.

APC tumor	final conc.	source of supply
B27 minus insulin [50x]	1x	Life technologies
N2 [100x]	1x	Life technologies
Pen/Strep [100x]	1x	Life technologies
GlutaMax [100x]	1x	Life technologies
HEPES [1 M]	10 mM	Life technologies
NAC [1 M]	1 mM	Sigma
Noggin [25 µg/ml]	25 ng/ml	Peprotech
Gentamycin [50 mg/ml]	50 µg/ml	Life technologies
Primocyn [50 mg/ml]	0.5 mg/ml	Invivogen
EGF [120 µg/ml]	40 ng/ml	Peprotech

Freshly prepared medium was passed through a 0.2 µm filter for sterilization and stored at -20 °C.

2.3.5 TREATMENT OF ORGANOIDS

For experiments, organoids were seeded in 24 well plates as described in subchapter 2.3.2. Inhibitors or recombinant proteins were added as indicated (Tab. 8) in APC tumor medium and organoids were incubated at 37 °C for 72 h. For ELISA analysis (see subchapter 2.5.5), organoid supernatants were harvested, centrifuged at 1,000 x g for 5 min, transferred into a new tube and stored at -20 °C until usage. Each well was microscopically evaluated and photographed with the Nikon AZ100 microscope and NIS-Elements D 4.12.01 software to assess the number and size of every organoid.

Tab. 8: Inhibitors and recombinant proteins used for organoid treatment.

chemicals	final conc.
GI254023X	30 µM
GW280264	30 µM
Marimastat	100 µM
IL-6	100 ng/ml
Hyper IL-6	100 ng/ml
sgp130Fc	100 ng/ml

2.3.6 CELL VIABILITY ASSAY

To assess the number of viable and proliferating cells in organoid cultures, a cell viability assay (Promega, D) was performed. For this, a normal cultured well of a 24 well plate from each organoid line was split into 48 wells of a 96 well plate and evenly distributed in 15 µl Matrigel® GFR per well. APC tumor medium with or without EGF was mixed up with IL-6, Hyper IL-6 or sgp130Fc as indicated in Tab. 8. Minimum six wells per condition were analyzed in three independent experiments and pure Matrigel® GFR spots without organoids served as negative control. Each well was filled up with 150 µl APC tumor medium and incubated at 37 °C for 72 h. After incubation, 20 µl CellTiter-Blue® were added directly onto each well and cell viability was measured due to conversion of the dye resazurin via redox reaction into resorufin, a fluorescent dye. Only proliferating cells are able to convert resazurin into resorufin due to metabolic activity whereby the fluorescence intensity was measured as an indirect indicator for proliferation. After measurement, a photo from each well was taken to count for number of organoids per well to normalize each value to number of organoids per well.

2.3.7 CRYOSECTIONING OF ORGANOIDS

To maintain organoid morphology, it was necessary to remove the medium gently without washing and pre-fixing organoids with 4 % PFA for 10 min. After removal of PFA, the organoids were carefully washed with 1x PBS containing Ca^{2+} and Mg^{2+} ions. The organoids were collected in a 15 ml tube with double volume of 1x PBS to dilute Matrigel® GFR residues. Following this, organoids were pelleted by centrifugation at 200 x g for 3 min at RT and the supernatant was discarded. Organoids were resuspended in 1 ml 1x PBS,

transferred to a 1.5 ml tube and centrifuged at 200 x g for 3 min. Subsequently the organoid pellet was gently resuspended in 100-400 µl chilled 2 % agarose in 1x PBS. After hardening, the agarose plug was transferred to 4 % PFA for 1 h and stored overnight in 30 % sucrose in 1x PBS at 4 °C. Finally, the agarose plug was embedded in the center of Tissue-Tek® Cryomold® (Sakura, D) with Tissue-Tek® O.C.T.™ compound (Sakura, D) on dry ice in methylbutane. The frozen block was stored at -80 °C until usage.

For cryosectioning, the frozen block was allowed to equilibrate in the cryostat chamber for approximately 15 min before usage after manufacturers's specifications. The specimen was prepared in slices of 7 µm and stored at -80 °C until staining.

2.4 RNA ANALYSIS

2.4.1 RNA-ISOLATION FROM TISSUE OR CELLS

Right at the start of RNA isolation all equipment was cleaned with RNase-ExitusPlus™ (AppliChem, D) and gloves were worn during the whole procedure.

To isolate total RNA from animal tissue for RNA sequencing, the RNeasy Mini Kit from Qiagen (Hilden, D) was used according to manufacturers instructions including QIAshredder column from Qiagen. To ensure a complete homogenization, the tissue was freshly ground in liquid nitrogen before use.

TRIzol® reagent from Thermo Fisher Scientific, Life Technologies GmbH (Darmstadt, D) was used to isolate RNA from animal tissue for cDNA synthesis and qRT-PCR according to manufacturers instructions.

RNA isolation of samples obtained from laser microdissection (see subchapter 2.6.6) was conducted using the innuPREP RNA Kit from Analytik Jena (Jena, D) according to manufacturers instructions.

All RNA samples were stored at -80 °C. Purity and concentration of isolated RNA was determined spectroscopically by NanoDrop® ND-1000 (Peqlab, D) before usage.

2.4.2 RNA-SEQUENCING

RNA-sequencing and transcriptome analysis were performed in cooperation with Dr. Robert Häsler from the Institute of Clinical Molecular Biology (IKMB) in Kiel using Illumina HiSeq technology. Quality, purity and concentration of isolated RNA was determined via TapeStation (Agilent technologies, USA) and RNA integrity number equivalent (RINe) of total RNA degradation analysis.

2.4.3 cDNA SYNTHESIS

For cDNA synthesis, the RevertAid H Minus Reverse Transcriptase from Thermo Fisher Scientific, Life Technologies GmbH (Darmstadt, D) was used as recommended. The resulting cDNA was diluted 1:4 with ddH_2O and stored at -20 °C. To assess a successful cDNA synthesis, a RT-PCR for β-Actin was performed as followed:

Tab. 9: Layout β-Actin RT-PCR.

1x mix β-Actin	
cDNA	2.0 µl
10x DreamTaq Puffer	2.5 µl
$MgCl_2$ [25 mM]	2.0 µl
dNTP-Mix [10 mM]	1.0 µl
β- Actin Primer up [1:10]	1.0 µl
β- Actin Primer dn [1:10]	1.0 µl
DreamTaq Polymerase	0.1 µl
H_2O	15.4 µl
	25.0 µl

temperature [°C]	**time [sec]**	**cycles**
95	300	1 x
95	30	35 x
52	30	
72	60	
72	600	1 x
4	∞	

Primer β- Actin up: 5´-GATGGTGGGAATGGGTCA-3´
Primer β- Actin dn: 5´-CACGCACGACGATTTCCCTCT-3´

The β-Actin PCR product with a size of 500 bp was detected via agarose gel electrophoresis.

2.4.4 QUANTITATIVE REAL TIME PCR

For gene expression analysis, 1 µg RNA was reversely transcribed (see subchapter 2.4.3). The cDNA was used as a template in a quantitative real-time PCR (qRT-PCR) assay by using LightCycler® 480 system from Roche Applied System (Prenzberg, D) according to manufacturers´s instructions. All contents were purchased by Roche Applied System (Prenzberg, D) except the Primer for 20x Assay Universal ProbeLibrary (UPL)-Probes. Primer were designed by using Roche Universal ProbeLibrary Assay Design Center. Used Primer are listed below in Tab. 11 and Tab. 12. Preparations of 20x Assay UPL-Probe for gene of interest and 20x Assay GAPDH for housekeeping control were done with dimmed light to protect fluorophore-coupled UPL-Probes. 1x mix for each specimen was purpose-built as indicated in Tab. 10.

Tab. 10: Layout 20x Assays for qRT-PCR LightCycler® 480.

20x Assay UPL Probe #	
Primer up [100 pM/µl]	1.2 µl
Primer down [100 pM/µl]	1.2 µl
UPL Probe #	4.0 µl
H_2O	13.6 µl

20x Assay GAPDH	
Primer Mix	1.2 µl
Probe	4.0 µl
H_2O	14.8 µl

1x mix qRT-PCR	
20x Assay	0.5 µl
2x MasterMix	5.0 µl
H_2O	2.5 µl
cDNA	2.0 µl
	→ 10 µl/ well

10 µl of 1x mix were added to each well of a 384 well plate. All samples were run in triplicates. Quantification of relative changes in gene expression pattern was determined by the LightCycler® 480 Software 1.5.0 (Roche Diagnostics, CH). The relative mRNA levels were assessed by the $2^{-\Delta\Delta Ct}$ method. The ΔCt rates were calculated for each sample by normalization to the housekeeping gene glyceraldehyde-3-phosphate dehydrogenase (GAPDH).

2.4.5 PRIMER

Primer design was conducted by using UPL Assay Design Centre by Roche. All oligonucleotides were synthesized by Metabion International AG (München, D).

Tab. 11: Primer for human qRT-PCR target genes.

Target	UPL-Probe	Sequence	Primer
Notch-1	# 85	ACGCACAAGGTGTCTTCCA	hNotch-1_up_#85
		AGGATCAGTGGCGTCGTG	hNotch-1_dn_#85
Hes-1	# 60	GAAGCACCTCCGGAACCT	hHes-1_up_#60
		GTCACCTCGTTCATGCACTC	hHes-1_dn_#60
Hey-1	# 29	CATACGGCAGGAGGGAAAG	hHey-1_up_#29
		GCATCTAGTCCTTCAATGATGCT	hHey-1_up_#29
ADAM17	# 77	CGTTTTTCACAAAATTTCAAGGT	hADAM17_up_#77
		CCCTAGAGTCAGGCTCACCA	hADAM17_dn_#77
EGFR	# 25	CAGAGTGATGTCTGGAGCTACG	hEGFR_up_#25
		GGGAGGCGTTCTCCTTTCT	hEGFR_dn_#25
ErbB2	# 16	GCCATGAGCAGTGTGCTG	hERBB-2_up_#16
		ACAGATGCCACTGTGGTTGA	hERBB-2_dn_#16
ErbB3	# 25	CAATCCCCACACCAAGTATCA	hERBB-3_up_#25
		GATGTTTGATCCACCACAAAGTT	hERBB-3_dn_#25
ErbB4	# 25	GCGAGACAAACCCAAACAAG	hERBB-4_up_#25
		CAATGCTTGAAGGTCTCCATT	hERBB-4_dn_#25
BTC	# 49	ACTGCATCAAAGGGAGATGC	hBTC_up_#49
		TCTCACACCTTGCTCCAATG	hBTC_dn_#49
EGF	# 77	CGCAGGAAATGGGAATTCTA	hEGF_up_#77
		CCATGATCACTGAGACACCAG	hEGF_dn_#77
AREG	# 38	CGGAGAATGCAAATATATAGAGCAC	hAREG_up_#38
		CACCGAAATATTCTTGCTGACA	hAREG_dn_#38
EREG	# 13	AGGAGGATGGAGATGCTCTG	hEREG_up_#13
		GAGGACTGCCTGTAGAAGATGG	hEREG_dn_#13
TGFα	# 38	CCCAGATTCCCACACTCAG	hTGFa_up_#38
		ACGTACCCAGAATGGCAGAC	hTGFa_dn_#38
NRG-2	# 38	TGTGGTGGCCTACTGCAA	hNRG-2_up_#38
		ACATGTTCTGCCGGAGGT	hNRG-2_dn_#38
ADAM10	# 53	GCCAGCAGAGAGATATATTAAAGACC	hADAM10_up_#53
		GGACCGTATTTATGGGGATAGTT	hADAM10_dn_#53
IL-6	# 68	GCCCAGCTATGAACTCCTTCT	hIL-6_up_#68
		CTTCTCCTGGGGGTACTGG	hIL-6_dn_#68
IL-6R	# 38	GGACTGTGCACTTGCTGGT	hIL-6R_up_#38
		ATTGCTGAGGGGGCTCTT	hIL-6R_dn_#38

Tab. 12: Primer for murine qRT-PCR target genes.

Target	UPL-Probe	Sequence	Primer
EGFR	# 10	TGTGCAAAGGAATTACGACCT	mEGFR_up_#10
		GTTGAGGGCAATGAGGACA	mEGFR_dn_#10
ErbB2	# 25	TTTGCCGGAGAGCTTTGAT	mErbB2_up_#25
		TCTGGCCATGCTGAAATGTA	mErbB2_dn_#25
ErbB3	# 99	AAGTACAACCGGCCTCTGG	mErbB3_up_#99
		CGACAAGACAAGCACTGACC	mErbB3_dn_#99
ErbB4	# 75	TGGAGAAAGGAGAGCGTCTG	mErbB4_up_#75
		CAGCATCGATCATCCAACA	mErbB4_dn_#75
BTC	# 68	CGGGTAGCAGTGTCAGCTC	mBTC_up_#68
		ACAGTGGAGAATTGCAAGACC	mBTC_dn_#68
EGF	# 38	GGGATGTGGGGGACTTACTAC	mEGF_up_#38
		TGGCTCATCACAAGGGTTC	mEGF_dn_#38
EREG	# 96	TTGACGCTGCTTTGTCTAGG	mEREG_up_#96
		GGATCACGGTTGTGCTGAT	mEREG_dn_#96
TGFα	# 77	CAGAAGAAGCAAGCCATCACT	mTGFa_up_#77
		CAGTGTTTGCGGAGCTGAC	mTGFa_dn_#77
AREG	# 53	TCCAAGATTGCAGTAGTAGCTGTC	mAREG_up_#53
		CCCTGAAGTATCGTTTCCAAAG	mAREG_dn_#53
c-Met	# 82	CACCACCAAGTCAGATGTGTG	mc-Met_up_#82
		AGGGGCTCCTCTCGTCAT	mc-Met_dn_#82
HGF	# 100	CACCCCTTGGGAGTATTGTG	mHGF_up_#100
		GGGACATCAGTCTCATTCACAG	mHGF_dn_#100
Notch-1	# 85	TGGACGACAATCAGAACGAG	mNotch-1_up_#85
		GGAGAACTACTGGCTCCTCAAA	mNotch-1_dn_#85
Hes-1	# 99	ACACCGGACAAACCAAAGAC	mHes-1_up_#99
		CGCCTCTTCTCCATGATAGG	mHes-1_dn_#99
Hes-5	# 22	CCAAGGAGAAAAACCGACTG	mHes-5_up_#22
		TGCTCTATGCTGCTGTTGATG	mHes-5_dn_#22
Hey-1	# 17	CATGAAGAGAGCTCACCCAGA	mHey-1_up_#17
		CGCCGAACTCAAGTTTCC	mHey-1_dn_#17
Hey-2	# 104	GTGGGGAGCGAGAACAATTA	mHey-2_up_#104
		GTTGTCGGTGAATTGGACCT	mHey-2_dn_#104
ß-Catenin	# 77	CTTGGATATCGCCAGGATGA	mb-Cat_up_#77
		CCCATCAACTGGATAGTCAGC	mb-Cat_dn_#77
ADAM17	# 77	CCGAACGCTTTTCACAAAAC	mADAM17_up_#77
		AACCCTAGAGTCAGGCTCACC	mADAM17_dn_#77
Sox17	# 53	CACAACGCAGAGCTAAGCAA	mSox17_up_#53
		ACTTGTAGTTGGGGTGGTCCT	mSox17_dn_#53
Sox9	# 25	CAGCAAGACTCTGGGCAAG	mSox9_up_#25
		ATCGGGGTGGTCTTTCTTGT	mSox9_dn_#25
LGR5	# 60	GACTTTAACTGGAGCAAAGATCTCA	mLGR5_up_#60
		CGAGTAGGTTGTAAGACAAATCTAGC	mLGR5_dn_#60

Claudin-1	# 68	CTTGACCCCCATCAATGC	mClaudin1_up_#68
		GTGGTGTTGGGTAAGAGGTTG	mClaudin1_dn_#68
Axin-2	# 68	GAGGATGCTGAAGGCTCAAA	mAxin2_up_#68
		TCGCCTTCTTGAAATAATACCTG	mAxin2_dn_#68
MMP7	# 94	TAATTGGCTTCGCAAGGAGA	mMMP7_up_#94
		AAGGCATGACCTAGAGTGTTCC	mMMP7_dn_#94
MMP13	# 89	GCCAGAACTTCCCAACCAT	mMMP13_up_#89
		TCAGAGCCCAGAATTTTCTCC	mMMP13_dn_#89
Muc2	# 85	CCTTGTCTTCTGCTGGAAGG	mMuc2_up_#85
		TCACCAAAGGAACTGATCTGC	mMuc2_dn_#85
Lysozym-1	# 46	GGCAAAACCCCAAGATCTAA	mLyso1_up_#46
		TCTCTCACCACCCTCTTTGC	mLyso1_dn_#46
Lysozym-2	# 64	GAATGGAATGGCTGGCTACT	mLyso2_up_#64
		CGTGCTGAGCTAAACACACC	mLyso2_dn_#64
Olfm4	# 102	CTCCGGGAGGCACTTCTT	mOlfm4_up_#102
		CTGTCCACAGACCCAGTGAA	mOlfm4_dn_#102
IL-6	# 6	GCTACCAAACTGGATATAATCAGGA	mIL-6_up_#6
		CCAGGTAGCTATGGTACTCCAGAA	mIL-6_dn_#6
IL-6R	# 53	ATCCTCTGGAACCCCACAC	mIL6R_left_#53
		GAACTTTCGTACTGATCCTCGTG	mIL6R_right_#53
IL6ST	# 85	AGGACCAAAGATGCCTCAAC	mIL6ST_up_#85
		TGAAGGAAGTTCGAGGAGACA	mIL6ST_dn_#85
BIRC5	# 71	CCCGATGACAACCCGATA	mBIRC5_up_#71
		CATCTGCTTCTTGACAGTGAGG	mBIRC5_dn_#71
LATS1	# 95	GCTGTCCAGAAGCCTCACC	mLATS1 _up_#95
		TTCTGAGCCAAGGTGAAAGG	mLATS1 _dn_#95
Ctgf	# 85	CTGCAGACTGGAGAAGCAGA	mCtgf_up_#85
		GCTTGGCGATTTTAGGTGTC	mCtgf_dn_#85
Cyr61	# 70	CGTCACCCTTCTCCACTTG	mCyr61_up_#70
		CACTTGGGTGCCTCCAGA	mCyr61_dn_#70
YAP-1	# 99	TTCCGATCCCTTTCTTAACAGT	mYAP1_up_#99
		GAGGGATGCTGTAGCTGCTC	mYAP1_dn_#99
DCC	# 25	CACTGGAAGTGGTTAACTCAAGG	mDCC(EC)_up_#25
		GCCAGTAATAAATCCATTTTGTGTT	mDCC(EC)_dn_#25
c-Myc	#77	CCTAGTGCTGCATGAGGAGA	mcMyc_up_#77
		TCCACAGACACCACATCAATTT	mcMyc_dn_#77

2.5 PROTEIN ANALYSIS

2.5.1 PREPARATION OF PROTEIN LYSATES FROM TISSUE OR CELLS

To extract proteins, cells were resuspended in 50-150 µl ice-cold lysis buffer (50 mM Tris; 150 mM NaCl; 2 mM EDTA; 1 % (v/v) NP-40; 1 % (v/v) Triton X-100; two complete-protease inhibitor cocktail tablets (Roche) per 50 ml) by pipetting. In order to ensure a complete lysis, the samples were incubated on ice for 60 min. Afterwards, the samples were centrifuged at 13,000 x g for 15 min to harvest the protein-containing supernatant. Protein lysates were stored at -20 °C until usage.

Animal tissues were mechanically disrupted by using the Precellys® (Peqlab, D) homogenizer according to manufacturers instructions. The tissue was mixed with RIPA (Radioimmunoprecipitation assay) lysis buffer (50 mM Tris; 150 mM NaCl; 0.1 % (v/v) SDS; 1 % (v/v) Triton X-100; 0.5 % (w/v) sodium deoxycholate) and ceramic beads for homogenization. After homogenization, samples were incubated on ice for 60 min and centrifuged at 13,000 x g for 15 min to collect the protein-containing supernatant.

To inhibit phosphatases, sodium orthovanadate (final conc. 1 mM) was added to the appropriate lysis buffer if necessary.

The protein concentration of the samples was determined by Bichinonic acid protein assay from Pierce™ (Thermo Fisher Scientific, Life Technologies GmbH, D) in relation to a BSA standard curve. The extinctions were measured at a wavelength of 568 nm in a microtiter plate reader from Tecan (Männedorf, CH).

To enrich glycosylated proteins from supernatant or cell lysate, a Concanavalin A precipitation was performed. 1 mg protein was refilled with 1x PBS up to 1 ml and 30 µl of Concanavalin A buffered aqueous suspension (#C9017 Sigma-Aldrich, D) was added. The sample was wheeled at 4 °C overnight. To remove non-bound proteins, the sample was centrifuged at 5,000 x g for 5 min and the supernatant was discarded. Precipitated Concanavalin A with bound glycosylated proteins was washed with ice-cold 1x PBS and centrifuged again at 5,000 x g for 5 min. Afterwards, 50-150 µl 5x Laemmli buffer (250 mM Tris-HCl (pH 6.8); 50 % (v/v) Glycerol; 0.01 % Bromphenolblue (w/v); 10 % (v/v) ß-Mercaptoethanol; 10 % (w/v) SDS) was added and samples were boiled at 95 °C for 10 min.

2.5.2 INTESTINAL CULTURE

Colon culture assays were performed to assess the amount of released soluble proteins from mouse tissue via enzyme-linked immunosorbent assay (ELISA) (Fig. 11).

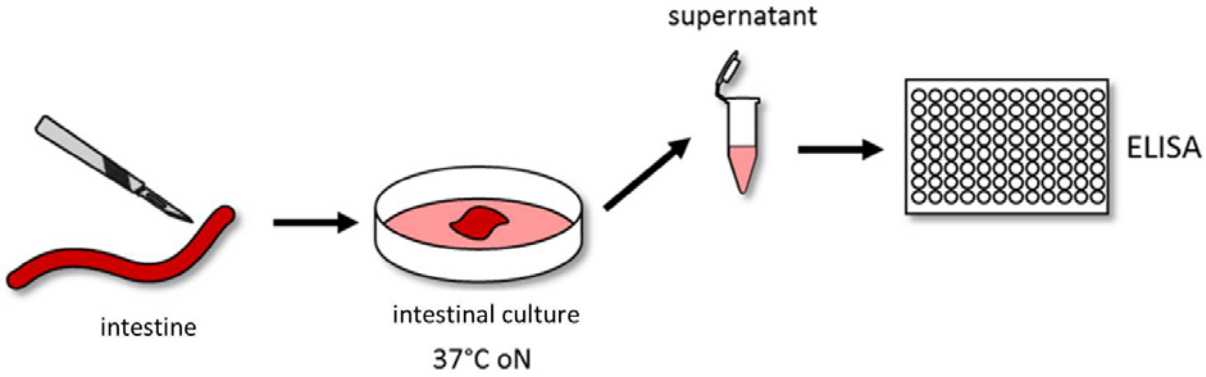

Fig. 11: Layout of an intestinal culture experiment.

To study soluble proteins and released cytokines selected tissue pieces were cultured overnight in DMEM medium and afterwards the supernatant was analyzed via ELISA.

Selected tissue pieces (1 cm) were washed thoroughly in 1x PBS mixed with 2x Pen/Strep for up to 5 min and incubated overnight in 1 ml Gibco™ DMEM with 2x Pen/Strep at 37 °C. Subsequently the supernatant was harvested, centrifuged at 1,000 x g for 5 min, transferred to a new tube and stored until usage at -20 °C. The weights of the tissue pieces were used to normalize ELISA results.

2.5.3 WESTERN BLOT ANALYSIS

Depending on the mass of the proteins to be analyzed, adequate SDS-polyacrylamide gels with a different polyacrylamide concentration were made (Tab. 13).

Tab. 13: Polyacrylamide gel for SDS-PAGE

7.5 - 15 % Running Gel	
ddH_2O	2.25-4.8 ml
1.5 M Tris/HCl pH 8.8	2.255 ml
10 % SDS	100.0 µl
10 % APS	100.0 µl
TEMED	10.0 µl
Polyacrylamide	2.4-4.95 ml
Total volume	9.96 ml

*Volume for one 1.5 mm Gel

4 % Stacking Gel	
ddH_2O	1.863 ml
0.5 M Tris/HCl pH 6.8	313.0 µl
10 % SDS	25.0 µl
10 % APS	25.0 µl
TEMED	3.0 µl
Polyacrylamide	335.0 µl
Total volume	2.563 ml

*Volume for one 1.5 mm Gel

Equal amounts of total protein supplemented with 5x Laemmli buffer (250 mM Tris-HCl (pH 6.8); 50 % (v/v) Glycerol; 0.01 % Bromphenolblue (w/v); 10 % (v/v) ß-Mercaptoethanol; 10 % (w/v) SDS) were boiled at 95 °C for 5 min, briefly centrifuged and loaded on the gel.

The discontinuous SDS-PAGE was started by applying a voltage in the range of approx. 120-160 V in 1x SDS running buffer in SDS-PAGE Mini Protean III system from Bio-Rad (München, D).

The protein gel transfer was performed by Tank-Blot System Mini Transblot from Bio-Rad (München, D) onto a PVDF membrane (Thermo Fisher Scientific, Life Technologies GmbH, D) in 1x Tank-Blot buffer at voltage of 90 V for 120 min (Tab. 14). The PVDF membrane was previously activated in methanol for 30 sec.

Tab. 14: Buffer for Western blot analysis.

10x SDS running buffer	
Glycerol	144 g
Tris	30 g
SDS	10 g
	add 1 L ddH_2O

1x SDS running buffer	
10x SDS running buffer	100 ml
	add 1 L ddH_2O

10x Tank-Blot buffer	
Glycine	144.1 g
Tris	30.3 g
	add 1 L ddH_2O

1x Tank-Blot buffer	
10x Tank-Blot buffer	100 ml
Methanol	200 ml
	add 1 L ddH_2O

10x TBS buffer	
Sodium chloride	87.6 g
Tris	12.1 g
	add 1 L ddH_2O

1x TBST	
10x TBS buffer	100 ml
Tween-20	500 µl
	add 1 L ddH_2O

After transfer, the PVDF membrane was incubated in 6 % (w/v) dry non-fat milk in TBST for 30 min at room temperature to avoid unspecific binding of antibodies. For detection of phosphorylated proteins, the PVDF membrane was washed with TBST before the primary antibody in 5 % (w/v) BSA in TBST was added. For all other applications, the primary antibody was applied in 6 % (w/v) dry non-fat milk in TBST. The incubation took place at 4 °C overnight. After three times of washing with TBST, HRP-labeled secondary antibody in 6 % (w/v) dry non-fat milk in TBST, or 5 % (w/v) BSA in TBST, was added at room temperature for 2 h. Subsequently, the PVDF membrane was washed again three times in TBST before detection of immunoreactive proteins via Pierce™ SuperSignal West Pico or Pierce™ SuperSignal West Femto enhanced chemiluminescence (ECL) solution by chemiluminescense camera system LAS-1000 (Fujifilm, USA).

2.5.4 ANTIBODIES

Tab. 15: Primary antibodies used for Western blot analysis.

specificity	host	dilution	clone / company
α-mouse ADAM17 (18.2)	rabbit	1:1,000	polyclonal / Pineda (D)
α-mouse ADAM17 (10.1)	rabbit	1:1,000	polyclonal / Pineda (D)
α-human ADAM17	rabbit	1:1,000	#3976 / Cell Signaling (USA)
α-human EGFR	rabbit	1:1,000	D38B1 #4267 / Cell Signaling (USA)
α-human EGFR	rabbit	1:10,000	EP38Y #528949 / Abcam (UK)
α-human pEGFR	rabbit	1:1,000	D7A5 #3777 / Cell Signaling (USA)
α-human STAT3	mouse	1:1,000	124H6 #9137 / Cell Signaling (USA)
α-mouse pSTAT3	rabbit	1:2,000	D3A7 #9145 / Cell Signaling (USA)
α-mouse Actin	mouse	1:10,000	Ac-15 #A5441 / Sigma-Aldrich (D)

Tab. 16: HRP-labeled secondary antibodies for Western blot analysis.

specificity	host	dilution	clone / company
α-rabbit-IgG-POD	goat	1:20,000	polyclonal / Dianova (D)
α-mouse-IgG-POD	sheep	1:20,000	polyclonal / Dianova (D)

Tab. 17: Primary antibodies used for IHC.

specificity	host	dilution	clone / company
α-MMP7	rat	1:400	Vanderbilt Antibody Resource
α-Ki-67	rabbit	1:400	D3B5#12202 / Cell signaling (USA)
α-ß-Catenin	mouse	1:200	610154 / BD (D)
α-human Muc2	rabbit	1:400	H300#sc-15334/ Santa Cruz (USA)
α-human Lysozyme	rabbit	1:200	A 0099 / Dako
α-human STAT3	rabbit	1:150	H190#sc-7179 / Santa Cruz (USA)
α-mouse pSTAT3	rabbit	1:80	D3A7 #9145 / Cell Signaling (USA)

Tab. 18: Fluorochrome-conjugated secondary antibodies for IHC.

specificity	host	conjugate	dilution	clone / company
α-rabbit-FITC	donkey	FITC	1:100	polyclonal / Dianova (D)
α-rat-FITC	donkey	FITC	1:100	polyclonal / Dianova (D)
α-rat-Cy3	donkey	Cy3	1:400	polyclonal / Dianova (D)
α-rabbit-Cy3	donkey	Cy3	1:400	polyclonal / Dianova (D)

HRP-labeled secondary antibodies for IHC were purchased from Empire Genomics (USA) by IDetect™ Universal mouse Kit-HRP* 400 Slide Kit.

2.5.5 ELISA

ELISA DuoSet Kits were purchased from R&D Systems (Wiesbaden, D) and Ready-SET-GO!® Kits were purchased from eBioscience (USA). All ELISA Kits were used according to manufacturers instructions.

Tab. 19: ELISA kits

ELISA	company
mouse Amphiregulin	DY989 / R&D (USA)
mouse IL-6	88-7064 / eBioscience (D)
mouse IL-6R	DY1830 / R&D (USA)
mouse TNFRI	DY425 / R&D (USA)
mouse TNF alpha	88-7324 / eBioscience (D)
human Amphiregulin	DY262 / R&D (USA)

2.6 HISTOLOGY

For histological analysis, it is important to maintain intestinal morphology and crypt-villus architecture. Therefore, it is necessary to dissect the intestine quickly and gently and store it in a petri dish with ice-cold 1x PBS on ice. The junction between stomach and duodenum, and the junction between ileum and cecum were cut to get the whole small intestine. Afterwards, the junction between cecum and colon was cut to get the whole colon. The small intestine and colon were repeatedly flushed with ice-cold 1x PBS to remove digestive

enzymes and feces. Finally, pancreas, mesentery, blood vessels and fat on the surface of the intestine were removed.

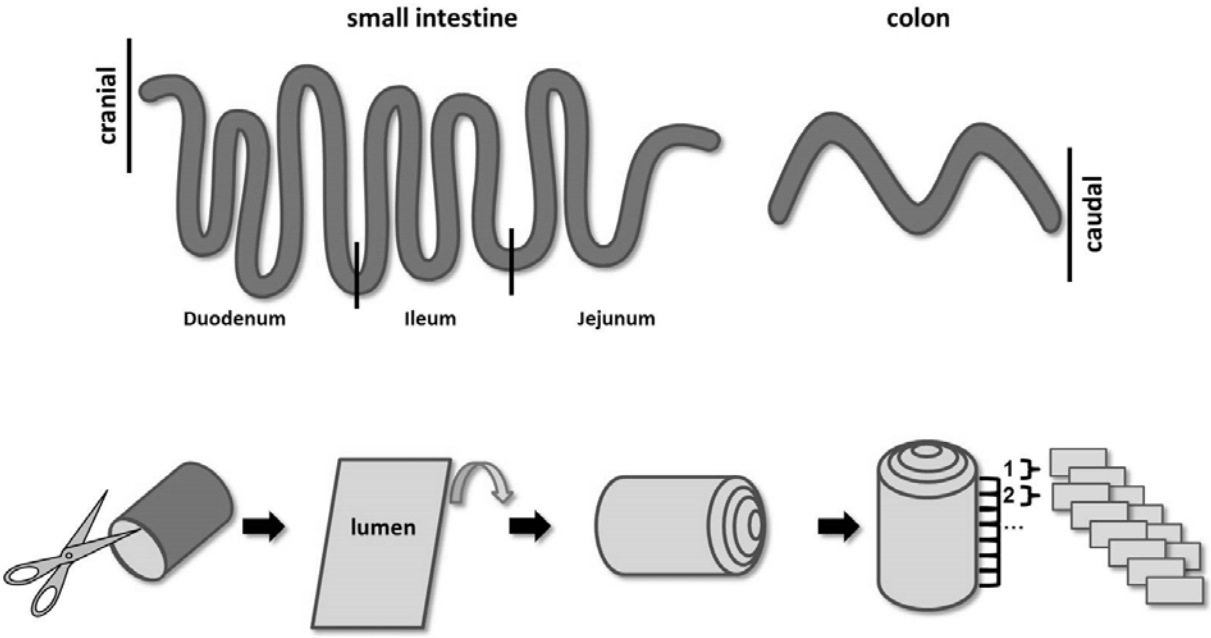

Fig. 12: Layout "Swiss role" preparation.

The intestine was opened longitudinally, rolled up to a "Swiss role", fixed and cut into sections.

To examine the entire length of the small intestine or colon, the complete segment was opened longitudinally by using fine scissors (Fig. 12). Remaining feces were removed carefully by wet cotton sticks. To asses macroscopically the tumor number and distribution, the intestine was photographed with the Nikon AZ100 microscope and evaluated with the NIS-Elements D 4.12.01 software. Following this, the cleaned intestine was rolled up with forceps from cranial to caudal part to a "Swiss role" (Moolenbeek and Ruitenberg, 1981) and prepared as indicated in subchapter 2.6.1 or 2.6.4.

2.6.1 FORMALIN-FIXED PARAFFIN-EMBEDDED TISSUE

The small intestine and colon were gently flushed from the proximal end with ice-cold 1x PBS. The intestine was opened longitudinally, rolled up with forceps to a "Swiss role" (Moolenbeek and Ruitenberg, 1981) and placed into an embedding cassette (Roth, D). The coiled tissue was fixed in 4 % PFA overnight, washed in H_2O for 24 h and was dehydrated by

ascending alcohol series and Xylene incubation for paraffin-embedded sections as listed below (Tab. 20).

Tab. 20: Ascending alcohol series for FFPE-tissue slides.

Alcohol series	time
4 % PFA	24 h
H_2O	oN
50 % Ethanol	60 min
70 % Ethanol	60 min
96 % Ethanol I	30 min
96 % Ethanol II	60 min
100 % Ethanol I	90 min
100 % Ethanol II	120 min
Xylene I	90 min
Xylene II	90 min
Paraffin I	30 min
Paraffin II	oN
Paraffin III	60 min
Paraffin-embedding	

Formalin-fixed Paraffin-embedded (FFPE)-tissue blocks were stored at RT until usage. Intestinal tissue was sectioned with a microtome at 3-7 µm thickness and stained after deparaffinization (see subchapter 2.6.2) as indicated.

2.6.2 HISTOLOGICAL STAINS OF FFPE-TISSUE

To visualize cellular structures, FFPE-tissue were stained with Haematoxylin and Eosin (HE), Azan or Periodic acid-Schiff (PAS). At first, Formalin-fixed Paraffin-embedded (FFPE) sections had to be deparaffinized as listed below (Tab. 21).

Tab. 21: Layout for deparaffinization of FFPE-tissue slides.

Deparaffinization	time
3x in Xylene	5 min each
2x in 100 % Ethanol	10 min each
1x in 95 % Ethanol	10 min
1x in 70 % Ethanol	10 min
1x in 50 % Ethanol	10 min
1x in 30 % Ethanol	10 min
2x in ddH_2O	5 min each

Haematoxylin as a basic dye stained acidic structures such as DNA in the nucleus or RNA in ribosomes purple. Vice versa, Eosin as an acidic dye stained acidophilic structures such as basic proteins in the cytoplasm pink. After deparaffinization and rehydration, FFPE-tissue slides were placed into commercially available Haematoxylin staining solution for 6 min. The slides were washed one time in ddH_2O with 0.5 % (v/v) glacial acetic acid and one time in ddH_2O for 10 sec each. After being kept in water for 6 min, the slides were placed in commercially available Eosin staining solution for 8 sec and excessive staining was removed by washing several times in ddH_2O and ascending alcohol series (70 % Ethanol, 96 % Ethanol) for 8 sec. each before Xylene treatment. Finally, the slides were covered with Eukitt®.

Azan staining was performed to stain epithelium and connective tissue. Collagen, basement membranes and mucin were stained blue, nuclei were stained red and muscle as well as red blood cells were stained orange. FFPE-tissue slides were deparaffinized and rehydrated as described above and incubated in 0.1 % anilin-ethanol for 5 min. Subsequently, slides were washed first in Ethanol with 1.0 % (v/v) glacial acetic acid and afterwards in ddH_2O. In the following 60 min the slides were incubated in 5 % phosphotungstic acid and washed in ddH_2O. Subsequently, the slides were incubated in 1:3 diluted aniline blue orange G acetic acid for 60 min, washed in ddH_2O and differentiated in 96 % Ethanol before being covered with Eukitt®.

Periodic acid-Schiff (PAS) staining was utilized to identify carbohydrate macromolecules in tissue. The magenta stained structures are equivalent to goblet cells which produce mucin within the intestine. FFPE-tissue slides were oxidized in 0.8 % periodic acid solution for 15 min and washed in ddH_2O. Afterwards, slides were placed in commercially available Schiff reagent for 15 min and washed in ddH_2O for 5 min to remove excessive staining. Counterstaining in commercially available Haematoxylin staining solution for 1 min was

performed. Slides were washed in ddH_2O, dehydrated in ascending alcohol series and covered with Eukitt®.

2.6.3 IMMUNOSTAINING OF FFPE-TISSUE

For immunostaining, FFPE-tissue slides were deparaffinized as described in subchapter 2.6.2. For antigen unmasking in form of heat induced epitope retrieval, two different protocols were used depending on primary antibody datasheet (Tab. 22). If necessary, endogenous peroxidase activity was quenched by short incubation of FFPE-tissue slides in 3 % hydrogen peroxide.

Tab. 22: Antigen retrieval buffer.

Citrate buffer	EDTA buffer
10 mM sodium citrate buffer pH 6.0	1 mM EDTA pH 8.0
boil slides for 10 min	boil slides for 15 min
cool slides at RT for 30 min	no cooling necessary

To limit the following volumes, the area of interest was encircled with a delimiting hydrophobic Dako Pen from DAKO (Agilent Technologies, USA). If permeabilization was desired, slides were incubated with 0.1 % (v/v) Triton X-100 in 1x PBS for 5 min. Specimen were blocked in 100 µl serum free protein block from DAKO (Agilent Technologies, USA). While blocking, primary antibody (Tab. 17) was diluted as indicated in antibody dilution solution from Invitrogen™ (Thermo Fisher Scientific, D) and incubated at 4 °C overnight. After three washing steps in 1x PBS for 5 min each, the fluorochrome-conjugated secondary antibody (Tab. 18), diluted as indicated in antibody dilution solution from Invitrogen™ (Thermo Fisher Scientific, D), was added in the dark for 2 h at RT. Sections were washed again three times in 1x PBS in the dark for 5 min each and rinsed briefly in deionized water before being mounted in ProLong® Gold antifade reagent with DAPI (Thermo Fisher Scientific, D). Slides were stored in the dark at RT until usage.

If the protein of interest was targeted by a HRP-labeled secondary antibody, a DAB-Substrate-Solution (0.05 % 3,3'-diaminobenzidine, 0.015 % H_2O_2, 0.01 M PBS, pH 7.2)

was used to visualize labeled proteins by a brown precipitate. FFPE-tissue slides were covered with DAB-Substrate-Solution and incubated at RT for 1-3 min. During this time, the DAB substrate was oxidized in the presence of HRP and H_2O_2 which led to an alcohol-xylene-insoluble brown precipitate at the enzymatically active site of the HRP-labeled secondary antibody. Slides were rinsed in ddH_2O, drained and covered with mounting medium.

Further formalin-fixed paraffin-embedded (FFPE) tissues were stained in cooperation with the pathologist Prof. Dr. Lukas Kenner and the laboratory animal pathologist Dr. med. vet. Simone Roos at the University of Veterinary Medicine Vienna.

2.6.4 CRYOSECTIONING TISSUE

The small intestine and colon were gently flushed from the proximal end with cold 4 % PFA in PBS. The intestine was prepared to a “Swiss role” (see section 2.6), wrapped with wet Kimwipe™ and fixed in cold 4 % PFA for 3 h at 4 °C. After removal of the Kimwipe™, the tissue was transferred to 30 % sucrose in 1x PBS overnight at 4 °C. Half of the 30 % sucrose was removed and replaced with Tissue-Tek® O.C.T.™ compound (Sakura, D) and incubated for 3 h at 4 °C. Before embedding, the intestine was spread on a glass plate, Tissue-Tek® O.C.T.™ compound (Sakura, D) was added on the tissue surface to act as glue and to prevent water crystallization. Subsequently, the intestine was rolled up with forceps from cranial to caudal to form a “Swiss role” (Moolenbeek and Ruitenberg, 1981) again and placed in the center of Tissue-Tek® Cryomold® (Sakura, D) with Tissue-Tek® O.C.T.™ compound (Sakura, D) on dry ice in methylbutane until Tissue-Tek® O.C.T.™ compound and tissue were frozen. The frozen blocks were stored at -80 °C until sectioning.

2.6.5 IMMUNOSTAINING OF CRYOSECTIONING TISSUE

Cryoblocks were sectioned with a cryotome at 5-7 µm thickness. Cryosection slides had to equilibrate at RT for 15-30 min. To limit the following volumes, the area of interest was encircled with a delimiting hydrophobic Dako Pen from DAKO (Agilent Technologies, USA). Optionally, sections were permeabilized for 30 min at RT in 100 µl 0.1 % (v/v) Triton X-100 in 1x PBS. Slides were blocked for 1 h at RT in 100 µl 5 % (v/v) normal donkey serum (Dianova, D) in 0.1 % Triton X-100 in 1x PBS. Afterwards the sections were incubated with

primary antibody (Tab. 17) diluted in blocking buffer containing 5 % (v/v) donkey serum in 0.1 % (v/v) Triton X-100 in 1x PBS overnight at 4 °C. After three washing steps in 0.1 % Triton X-100/PBS for 10 min each, the sections were incubated with fluorochrome-conjugated secondary antibody (Tab. 18) diluted in blocking buffer containing 5 % (v/v) donkey serum in 0.1 % Triton X-100/PBS in the dark for 1 h at RT. Sections were washed again three times in 0.1 % Triton X-100/PBS in the dark for 10 min each and rinsed briefly in deionized water before being mounted in ProLong® Gold antifade reagent with DAPI (Thermo Fisher Scientific, D). Slides were stored in the dark at RT until usage.

2.6.6 LASER MICRODISSECTION

In cooperation with Prof. Dr. med. Jürgen Westermann from the University of Lübeck laser microdissection experiments were performed. This method allowed to isolate specific areas or cells of interest from microscopic slides with the help of a laser to get pure enriched tissue of interest or cell populations.

In preparation for laser microdissection, mice were sacrificed and the intestines were removed quickly following thorough washing with ice-cold 1x PBS on ice to remove feces. Thereupon, the intestine was opened longitudinally, spread on a glass plate and Tissue-Tek® O.C.T.™ compound (Sakura, D) was added on the tissue surface. The intestine was rolled up with forceps to a “Swiss role” (Moolenbeek and Ruitenberg, 1981) and directly placed in the center of Tissue-Tek® Cryomold® (Sakura, D) with Tissue-Tek® O.C.T.™ compound (Sakura, D) on dry ice in methylbutane until Tissue-Tek® O.C.T.™ compound and tissue were completely frozen. Cryoblocks were stored at -80 °C until cryosectioning. Freshly prepared cryosections (12 µm thick) were placed on special glass membrane slides and stained with Toluidine blue. A laser coupled microscope was used to cut out the tissue area of interest. The dissected tissue area was collected and directly lysed in innuPREP RNA Kit lysis buffer (see subchapter 2.4.1).

2.6.7 TUMOR STAGING

Tumor staging was performed in cooperation with the pathologist Prof. Dr. Lukas Kenner and the laboratory animal pathologist Dr. med. vet. Simone Roos at the University of Veterinary Medicine Vienna. Required stainings were also implemented at the University of Veterinary Medicine Vienna.

2.7 CELL CULTURE

Cells were cultured in individual Dulbecco Modified Eagle Medium (DMEM), high glucose (4.5 g/l), supplemented with 10 % (v/v) FCS and 50 U/ml Pen/Strep in a 37 °C incubator at 5 % CO_2 air content and 90 % relative humidity. All cells were subcultivated at a ratio of 1:10 twice a week. Adherent cells were detached by medium removal and incubation with Trypsin/EDTA solution for 5 min at 37 °C. Detached cells were transferred to new 10 cm dishes with fresh 10 ml culture medium.

2.7.1 HUMAN COLORECTAL CANCER CELLS

All human colorectal cancer cells used in this work were cultured in Iscove´s Modified Dulbecco´s Medium (IMEM), supplemented with 10 % (v/v) FCS, 1 % (v/v) sodium pyruvate, 50 U/ml Pen/Strep in a 37 °C incubator at 5 % CO_2 air content and 90 % relative humidity.

Tab. 23: List of human colorectal cancer cells.

cell line	cell type	note
HCA-7	epithelial	kindly provided by Prof. Dr. Stephan Michael Feller *
HDC-8	epithelial	kindly provided by Prof. Dr. Stephan Michael Feller *
HDC-9	epithelial	kindly provided by Prof. Dr. Stephan Michael Feller *
HDC-111	epithelial	kindly provided by Prof. Dr. Stephan Michael Feller *
HDC-135	epithelial	kindly provided by Prof. Dr. Stephan Michael Feller *
HT-29	epithelial	ATCC®, HTB-38™ (USA)
Caco2	epithelial	ATCC®, HTB-37 ™ (USA)

* PMID18950493

2.7.2 TREATMENT OF HUMAN COLORECTAL CANCER CELLS

For experiments 3.0 x 10^6 cells were seeded in a 5 cm dish with 2.5 ml medium and allowed to adhere overnight. For inhibitor experiments, cells were washed three times with 1x PBS and inhibitors were added as indicated in Tab. 24 in serum free medium for 24 h. EGF stimulation in serum free medium took place 10 min before harvesting. For ELISA analysis, cell supernatants were collected, centrifuged at 1,000 x g for 5 min, transferred to a new tube

and stored at -20 °C until usage. Adherent cells were washed with 1x PBS, scraped off and lysed in lysis buffer including sodium orthovanadate at 4 °C for 4 h. To enrich glycosylated proteins, a Concanavalin A precipitation was optionally implemented.

Tab. 24: Chemicals used for hCRC cell treatment.

chemicals	final conc.
GI254023X	3 µM
GW280264	3 µM
Marimastat	10 µM
AG1478	10 µM
EGF	100 ng/ml

2.8 STATISTICS

Histological evaluation was done by using the Nikon AZ100 microscope and NIS-Elements D 4.12.01 software. Tumor staging was carried out in a blinded fashion by pathologists. Results were represented including their standard deviation. Significances were calculated by Student´s unpaired t-test with Welch´s correction, Mann Whitney test or two data sets and ANOVA followed by Tukey post hoc tests or Bonferroni posttest for multiple data sets by using GraphPad Prism 6 software. Differences were considered significant if $p \leq 0.05$ (*), $p \leq 0.01$ (**), $p \leq 0.001$ (***).

CHAPTER THREE: RESULTS

3.1 THE ROLE OF ADAM17 IN HUMAN COLORECTAL CANCER CELLS

In order to analyze the role of ADAM17 in intestinal epithelial cells (IEC) during tumorigenesis, seven epithelial human colorectal cancer (CRC) cell lines were investigated (Tab. 23).

3.1.1 mRNA CODING FOR EGFR AND AMPHIREGULIN ARE UPREGULATED IN HUMAN CRC

RNA was isolated from human colorectal cancer (CRC) cells and analyzed separately. First, genes related to the ErbB receptor tyrosine kinase family and ErbB ligands were studied. The mRNA levels of ErbB1, also known as EGFR, were found to be markedly increased in all tested human colorectal cancer cells. The other members of the ErbB receptor tyrosine kinase family named ErbB2, ErbB3 and ErbB4 showed no comparable upregulation of mRNA transcripts in the analyzed human colorectal cancer cells (Fig. 13).

Moreover, mRNA levels of the ErbB ligands Amphiregulin (AREG) and Epiregulin (EREG) were elevated in human CRC. However, ErbB ligands like Betacellulin (BTC), Epidermal growth factor (EGF), Transforming growth factor alpha (TGF-α) and Neuregulin-2 (NRG-2) showed no increased mRNA levels (Fig. 13).

There was no significant difference between the epithelial human colorectal cancer cell lines, meaning that all tested cell lines had comparable mRNA signatures regarding ErbB receptor tyrosine kinase family and ErbB ligand transcription.

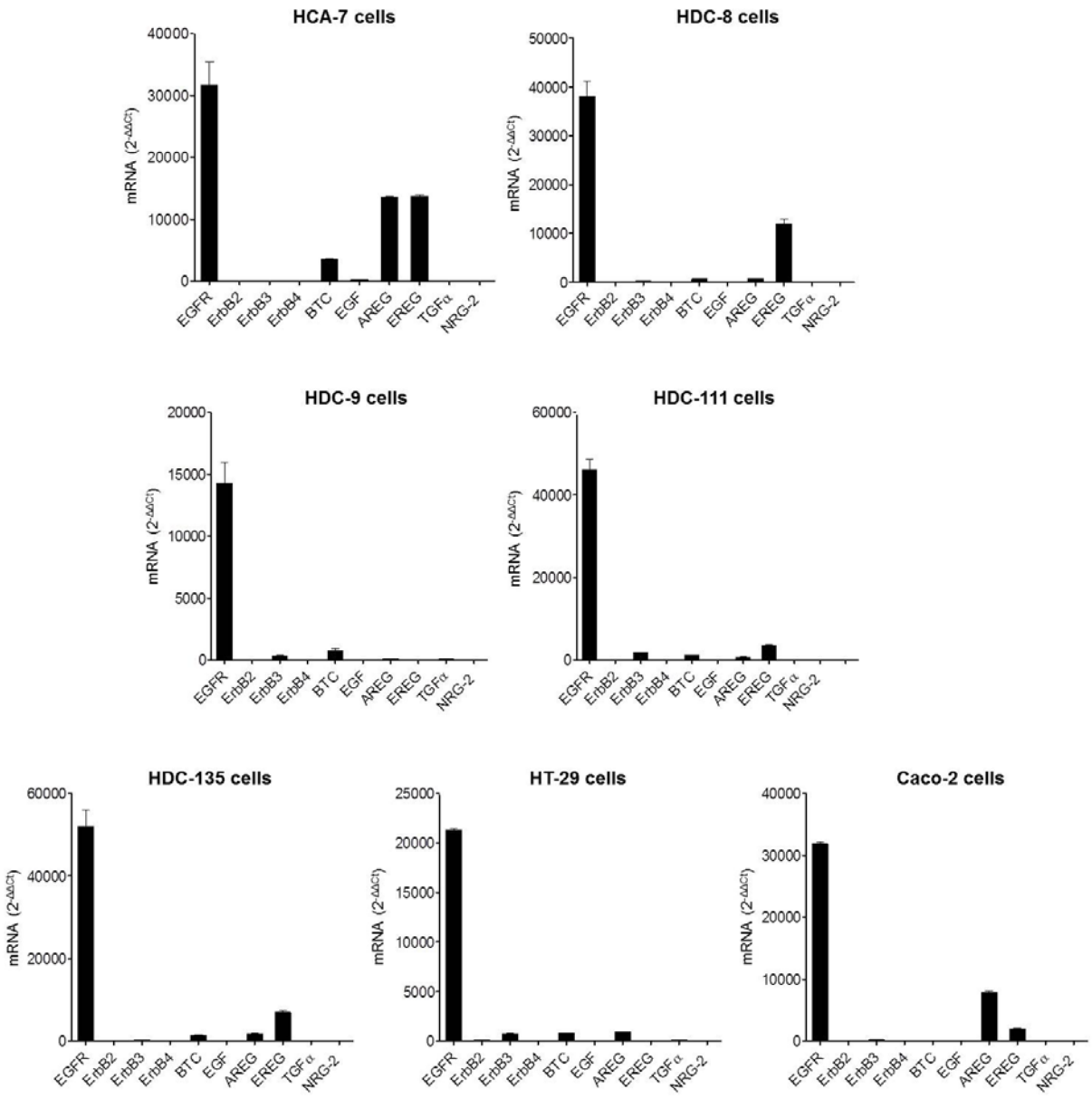

Fig. 13: qRT-PCR analysis of epidermal growth factor receptors and corresponding ligands in human CRC cells.

Quantitative real-time PCR showed increased mRNA levels of a subset of ErbB receptor tyrosine kinases (EGFR-ErbB4) and ErbB ligands (BTC, Betacellulin; EGF, Epidermal growth factor; AREG, Amphiregulin; EREG, Epiregulin; TGF-α, Transforming growth factor alpha; NRG-2, Neuregulin-2) in indicated human colorectal cancer cells. qRT-PCR data were normalized to GAPDH.

Additionally, as shown in Fig. 14, ADAM17 mRNA levels were elevated in human colorectal cancer cells. HCA-7 cells, HDC-8 cells, HDC-135 cells and Caco2 cells revealed higher ADAM17 mRNA levels than ADAM10 mRNA level. In HDC-9 cells and HDC-111 cells a vice versa ratio was detected. Only in HT-29 cells the ADAM17-ADAM10 mRNA ratio was balanced.

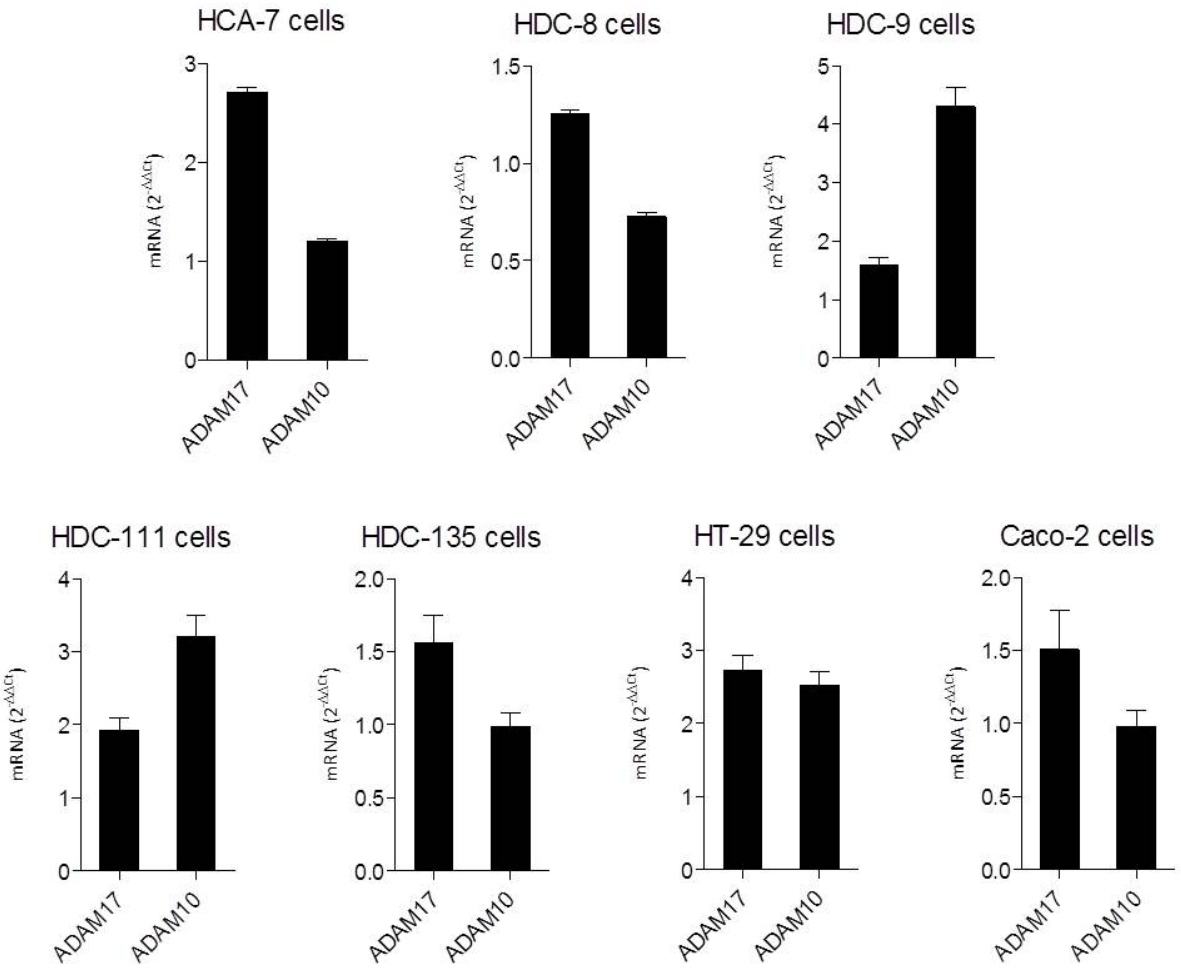

Fig. 14: qRT-PCR analysis of ADAM17 and ADAM10 in human CRC cells.

qRT-PCR analysis revealed elevated amounts of ADAM17 and ADAM10 in indicated human colorectal cancer cells. qRT-PCR data were normalized to GAPDH.

To further validate the quantitative real-time PCR results, the protein expression of selected genes of interest was analyzed.

3.1.2 Protein expression of ADAM17 and EGFR in Human CRC is verifiable

The increase in ADAM17 mRNA levels in human CRC cells should lead to higher ADAM17 protein expression in these cells. If this is indeed the case, ADAM17 protein expression was assessed by Western blot analysis. As shown in Fig. 15, the human CRC cells showed a varying intensity of ADAM17 protein expression. As expected, ADAM17 protein expression levels in HCA-7 cells and HDC-135 cells were higher than in HDC-9 cells. Surprisingly, HT-29 cells and HDC-111 cells showed very low amounts of ADAM17 protein expression

despite increased mRNA levels detected by qRT-PCR result. However, ADAM17 protein expression in HDC-8 cells was increased compared to expression levels in Caco2 cells and HDC-9 cells.

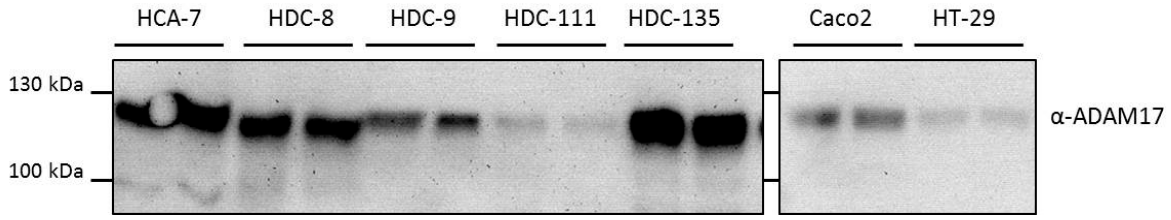

Fig. 15: ADAM17 protein expression in human CRC cells.

Indicated human CRC cells were lysed and 1 mg of total protein was concentrated by Concanavalin A precipitation. ADAM17 protein expression was assessed by Western blot analysis using an anti-ADAM17 antibody (#3976).

Additionally, protein expression of the EGFR was assessed in human CRC cells (Fig. 16). In line with the detected mRNA levels shown in Fig. 13, EGFR protein expression could be verified in all human CRC cell lines. HDC-8 cells and HDC-135 cells show the highest EGFR protein expression within the tested cell lines and these findings match with the previously assessed mRNA levels. Protein expression of EGFR in HDC-111 cells and Caco2 cells was lower than expected after mRNA analysis. However, the EGFR protein expression in HCA-7 cells, HDC-9 cells and HT-29 cells was increased compared to the lower mRNA levels.

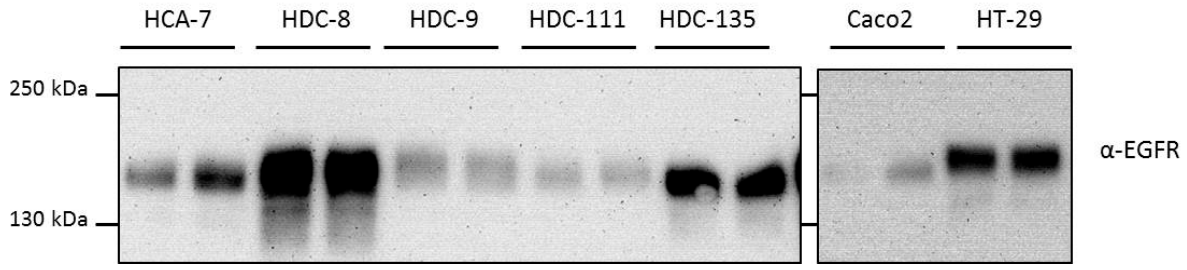

Fig. 16: EGFR protein expression in human CRC cells.

Indicated human CRC cells were lysed and 50 µg of total protein were analyzed. EGFR protein expression was assessed by Western blot analysis using an anti-EGFR antibody (#4267).

To validate a connection between ADAM17 protein expression and a possible activation of the EGFR, the level and the role of the EGFR ligand Amphiregulin and ADAM17-mediated shedding was evaluated.

3.1.3 Inhibition of ADAM17 suppresses EGFR phosphorylation in human CRC cells

In the following experimental setup, selected human CRC cells, namely HCA-7 cells, were treated with metalloprotease inhibitors (Tab. 24) and stimulated with EGF as positive control to assess the influence of ADAM17-mediated Amphiregulin shedding on EGFR activation. EGFR protein expression was confirmed by Western blot analysis (Fig. 17 A lower panel). In addition, the activation of the EGFR was verified by detection of phosphorylated Tyrosine (Y) at the position 1068 via Western blot analysis (Fig. 17 A upper panel).

The EGFR inhibitor AG1478 lead to reduced protein levels of phosphorylated EGFR and serves as negative control. Conversely, stimulation with EGF activated the EGFR and an increase of phosphorylated Tyrosine Y1068 was detectable in HCA-7 cells.

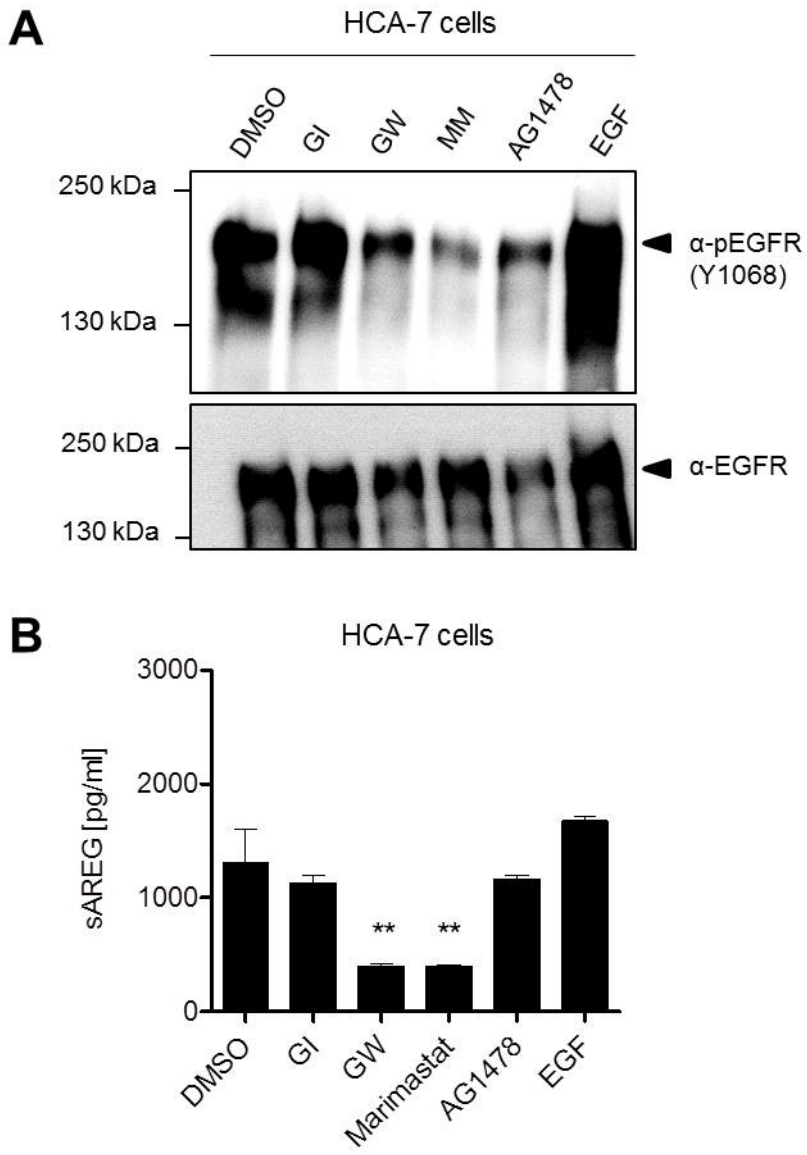

Fig. 17: Inhibition of ADAM17 leads to decreased Amphiregulin shedding.

HCA-7 cells were seeded at a density of 3.0 x 10^6 cells and starved for 24 h in presence or absence of the pan-metalloprotease inhibitor MM (Marimastat, 10 µM), the metalloprotease inhibitors GI (GI254023X, ADAM10-selective, 3 µM) and GW (GW280264X, ADAM10- and ADAM17-selective, 3 µM) or the EGFR and ErbB2 kinase inhibitor AG1478 (10 µM). EGF (100 ng/ml) stimulated cells served as positive control. (A) Tyrosine-phosphorylated EGFR was assessed by Western blot analysis using a monoclonal anti-pEGFR Tyr1068 (#3777) antibody and EGFR was assessed by Western blot analysis using a anti-EGFR (#4267) antibody. (B) Soluble Amphiregulin was measured by ELISA in the conditioned media of indicated cell lines. 1way ANOVA with Tukey´s multiple comparison test.

To investigate the dependence of Amphiregulin shedding on ADAM17 inhibition, HCA-7 cells were treated with a broad-spectrum matrix metalloprotease inhibitor (Marimastat) and selective inhibitors for ADAM10 (GI) or ADAM10 and ADAM17 (GW). To determine the amount of soluble Amphiregulin, the cell supernatant was harvested and measured by ELISA

(Fig. 17 B). The amount of soluble Amphiregulin was not drastically affected by GI treatment and the resulting ADAM10 inhibition.

Conversely, if ADAM17 was inhibited by Marimastat and GW treatment, the amount of soluble Amphiregulin was markedly decreased. In line with these observations, EGFR phosphorylation at Tyrosine Y1068 was clearly diminished after Marimastat and GW treatment in HCA-7 cells.

In line with Tyrosine Y1068 phosphorylation of EGFR as well as accumulation of soluble AREG in the cell supernatant, the results confirmed that ADAM17-AREG-EGFR-axis is dependent on ADAM17-activity.

3.2 THE ROLE OF ADAM17 IN INFLAMMATION ASSOCIATED COLORECTAL CANCER

The *in vitro* human colorectal cancer cell experiments (see section 3.1) demonstrated the link between ADAM17-regulated Amphiregulin shedding on intestinal epithelial cells and diminished activation of the EGFR after ADAM17 inhibition. This knowledge, however, may not lead to improved cancer patient treatment without further *in vivo* studies. The usage of genetically engineered mouse models has made the examination and understanding of *in vivo* processes possible.

For that reason, the hypomorphic ADAM17$^{ex/ex}$ mice (see subchapter 2.1.1) were generated by Chalaris et al. to obtain a mouse with markedly reduced ADAM17 protein expression in all tissues. The hypomorphic ADAM17$^{ex/ex}$ mice were utilized to elucidate whether minimized ADAM17 protein expression influences tumor formation in the colon after AOM/DSS-treatment *in vivo*.

In order to assess ADAM17 mRNA levels in different organs, RNA from ADAM17$^{wt/wt}$ control mice was isolated and measured by quantitative real-time PCR (Fig. 18).

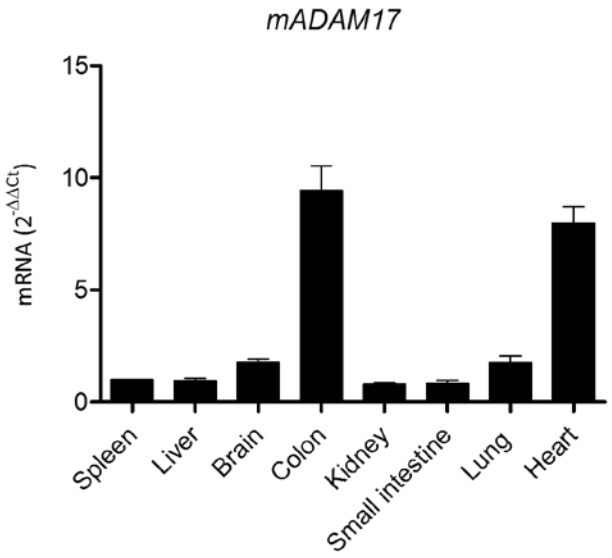

Fig. 18: mRNA levels of ADAM17 in different mouse tissues.

qRT-PCR analysis revealed different amounts of ADAM17 in indicated organs of ADAM17$^{wt/wt}$ mice. qRT-PCR data were normalized to the housekeeping gene GAPDH.

ADAM17 mRNA was identified in all examined organs such as in the kidney, liver, spleen and small intestine. The mRNA levels of ADAM17 in the brain and lung were slightly

increased, but markedly enhanced in the heart and colon. These results were the reason to investigate the role of ADAM17 in the intestine during colitis-associated colorectal cancer.

3.2.1 LOSS OF ADAM17 ENHANCES INFLAMMATION IN COLITIS-ASSOCIATED CANCER

In order to analyze the physiological role of ADAM17 during colitis-associated colorectal cancer, hypomorphic ADAM17$^{ex/ex}$ mice and ADAM17$^{wt/wt}$ control mice were exposed to AOM/DSS-treatment as explained in subchapter 2.2.1.

As required, all mice were monitored during AOM/DSS-treatment because more than 25 % weight loss was a legally defined termination criterion. The body weight of each mouse was documented daily during DSS-administration and the following seven days as well as during AOM-administration at day 0 and 21 (Fig. 19).

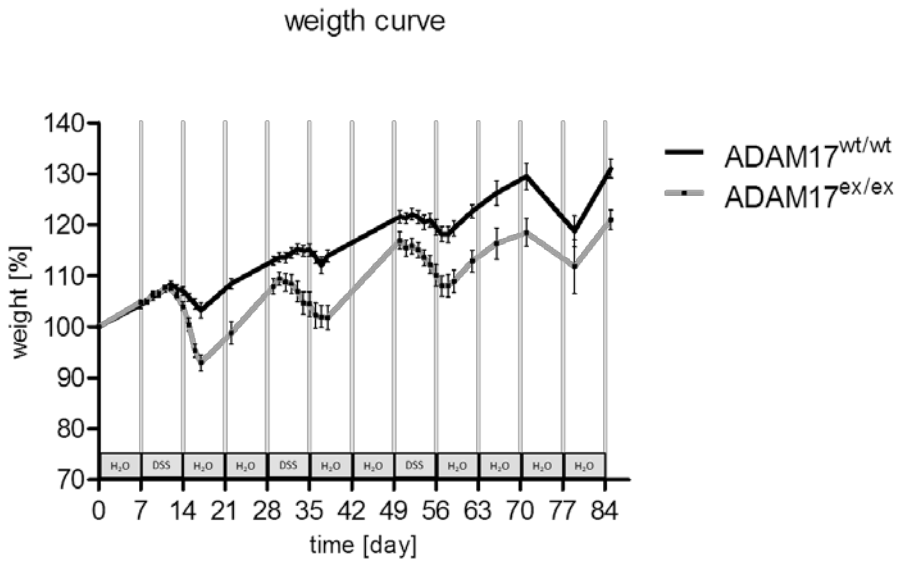

Fig. 19: Weight curve of AOM/DSS-treated hypomorphic ADAM17$^{ex/ex}$ mice.

Body weight was assessed during AOM/DSS-treatment for each mouse and converted in percentage terms referred to day 0. ADAM17$^{wt/wt}$ mice (n=26) and ADAM17$^{ex/ex}$ mice (n=28).

Approximately four to five days after the start of DSS-administration the mice lost body weight. This effect was enhanced in hypomorphic ADAM17$^{ex/ex}$ mice compared to ADAM17$^{wt/wt}$ control mice in each DSS-cycle. Upon DSS-administration the intestinal

epithelium started to regenerate and four to five days after DSS-administration the mice gained body weight again.

The observed weight loss was accompanied by pathologically altered stool character and occult blood. One day before DSS-treatment, feces from each mouse were analyzed for occult blood by Guaiac-based Haemoccult® test and rated for scoring. Feces samples from each mouse on the last day of DSS-treatment were analyzed in the same way.

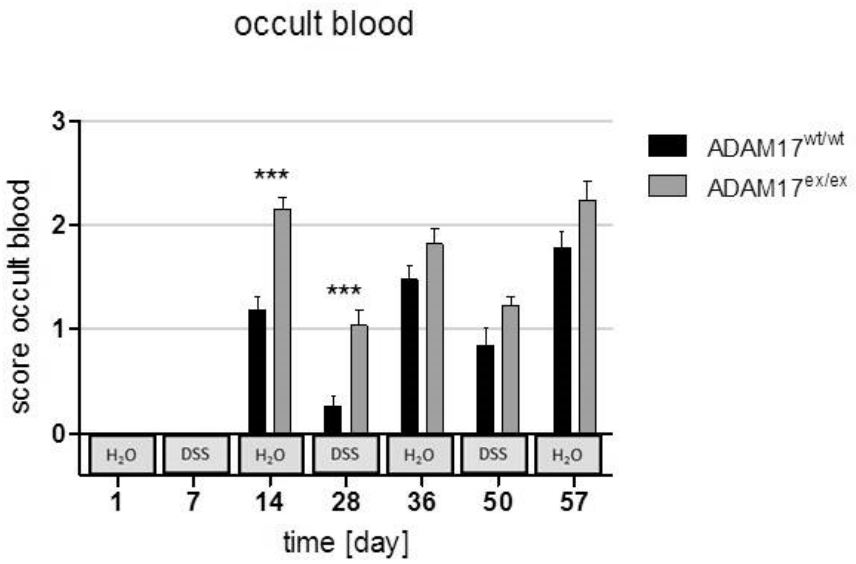

Fig. 20: Occult blood score of AOM/DSS-treated hypomorphic ADAM17$^{ex/ex}$ mice.

Occult blood was measured by Haemoccult® test. Test was done during AOM/DSS-treatment for each mouse. Occult blood was scored as follows: [0, negative Haemoccult®; 1, positive Haemoccult®; 2, macroscopic visible traces of blood; 3, rectal bleeding]. ADAM17$^{wt/wt}$ mice (n=26) and ADAM17$^{ex/ex}$ mice (n=28). 2way ANOVA with Bonferroni posttest.

Scoring for occult blood shown in Fig. 20 revealed an increased score in hypomorphic ADAM17$^{ex/ex}$ mice, while ADAM17$^{wt/wt}$ control mice were protected from rectal bleeding in response to AOM/DSS-treatment. After the first DSS-cycle, hypomorphic ADAM17$^{ex/ex}$ mice never reached a negative Haemuccult® score again, whereas ADAM17$^{wt/wt}$ control mice regained a score lower than 1. ADAM17$^{wt/wt}$ control mice showed a basal positive Haemuccult® score starting at the third DSS-cycle.

The delay in regeneration of the inflamed intestinal epithelium was demonstrated by the presence of diarrhea only in hypomorphic ADAM17$^{ex/ex}$ mice after DSS-treatment, whereas ADAM17$^{wt/wt}$ control mice had soft but well-formed feces (Fig. 21).

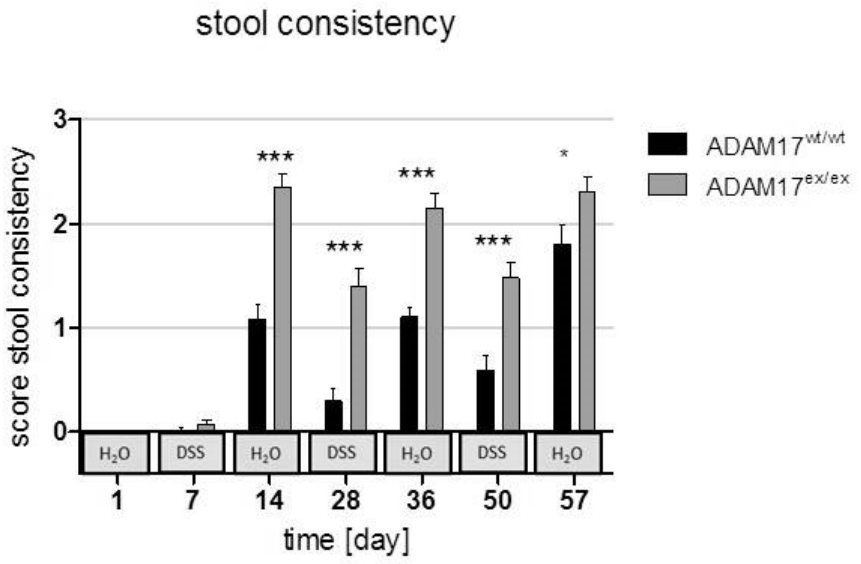

Fig. 21: Stool consistency score of AOM/DSS-treated hypomorphic ADAM17$^{ex/ex}$ mice.

Stool character is scored as follows: [0, normal; 1, soft with well-formed pellets; 2, soft without pellets; 3, diarrhea]. Test was done during AOM/DSS-treatment for each mouse. ADAM17$^{wt/wt}$ mice (n=26) and ADAM17$^{ex/ex}$ mice (n=28).

In response to DSS-challenge, hypomorphic ADAM17$^{ex/ex}$ mice showed severe hallmarks for inflammation like diarrhea or rectal bleeding accompanied by enhanced weight loss, while ADAM17$^{wt/wt}$ control mice showed little signs of inflammation indicated by moderate weight loss, soft stool and positive Haemoccult® test.

DSS-induced inflammation leads to a disruption of the intestinal epithelial barrier and thereby to the initiation of an inflammatory response. All three clinical signs of inflammation like weight loss, occult blood and stool consistency were rated for each mouse and Fig.d up to a clinical activity score for the classification of colitis activity (Fig. 22). A significant increase in the clinical activity score of hypomorphic ADAM17$^{ex/ex}$ mice could be observed in comparison to ADAM17$^{wt/wt}$ control mice after the first cycle of DSS-treatment. In the course of the second and third cycle of DSS-treatment, the clinical activity score of ADAM17$^{wt/wt}$ control mice approached the clinical activity score of hypomorphic ADAM17$^{ex/ex}$ mice at around 5.

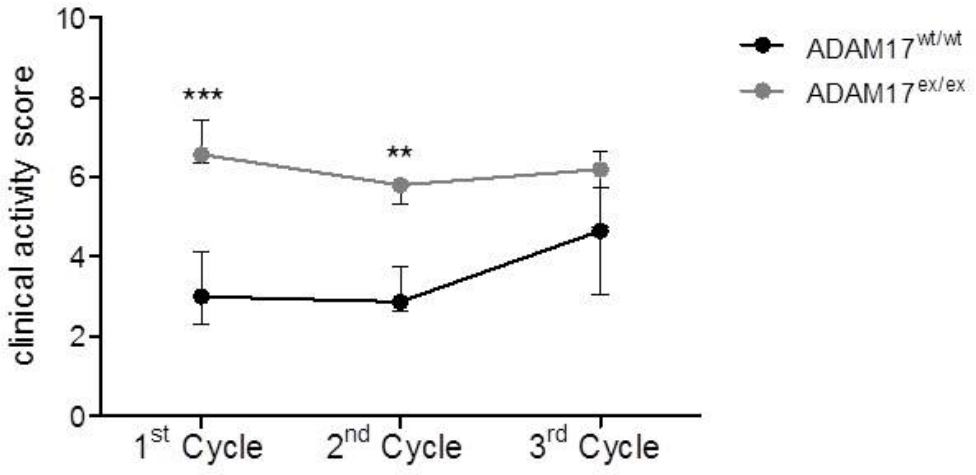

Fig. 22: Clinical activity score of AOM/DSS-treated hypomorphic ADAM17$^{ex/ex}$ mice.

Assessment of body weight loss, stool consistency and the presence of occult blood by Haemoccult® test. Test was done during AOM/DSS-treatment for each mouse. Body weight change is scored as follows: [0, no change; 1, 1 %-5 % weight loss; 2,5 %-10 % weight loss; 3, 10 %-20 % weight loss; 4, > 20 % weight loss]. Stool character is scored as follows: [0, normal; 1, soft with well-formed pellets; 2, soft without pellets; 3, diarrhea]. Occult blood was scored as follows: [0, negative Haemoccult®; 1, positive Haemoccult®; 2, macroscopic visible traces of blood; 3, rectal bleeding]. These scores were added to generate a clinical activity score ranging from 0 to 10. ADAM17$^{wt/wt}$ mice (n=26) and ADAM17$^{ex/ex}$ mice (n=28). 2way ANOVA with Bonferroni posttest.

To investigate if the lack of ADAM17 has an impact on the survival of AOM/DSS-treated hypomorphic ADAM17$^{ex/ex}$ mice and ADAM17$^{wt/wt}$ control mice, all challenged mice were assessed according to their survival until the end of the experiment (Fig. 23). Because of weight loss, rectal bleeding or bowel prolapse induced by tumors, 30 % of the ADAM17$^{ex/ex}$ mice were sacrificed earlier than 90 days. Only 5 % of the ADAM17$^{wt/wt}$ control mice became moribund during AOM/DSS-treatment.

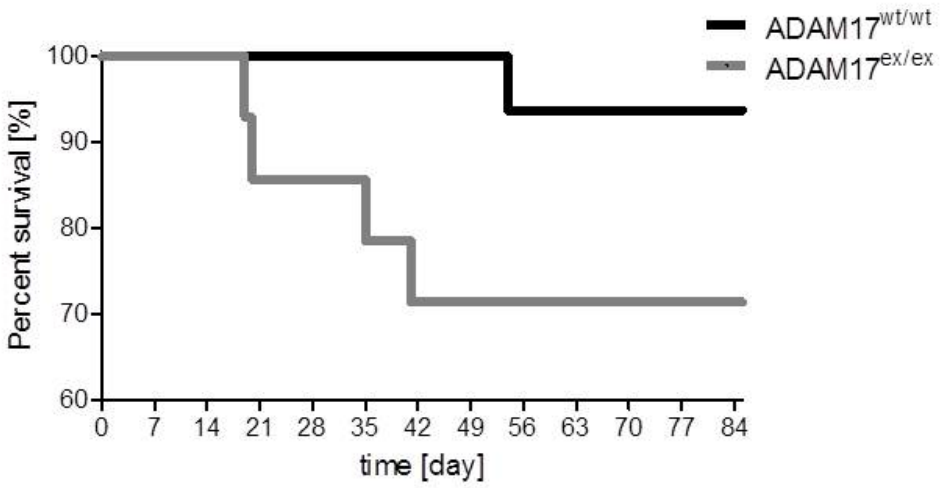

Fig. 23: Kaplan-Meier survival curve for hypomorphic ADAM17$^{ex/ex}$ mice during AOM/DSS-treatment.

Mice which become moribund during AOM/DSS-treatment due to weight loss, enhanced rectal bleeding, diarrhea and/or bowel prolapse were sacrificed earlier than 90 days. ADAM17$^{wt/wt}$ mice (n=26) and ADAM17$^{ex/ex}$ mice (n=28). Gehan-Breslow-Wilcoxon Test (*) p = 0.0377.

In accordance with the clinical activity score (Fig. 22) observed in hypomorphic ADAM17$^{ex/ex}$ mice, the colon tissue of hypomorphic ADAM17$^{ex/ex}$ mice was thicker and tighter than colon tissue from less inflamed ADAM17$^{wt/wt}$ mice (Fig. 24 B). Furthermore, the colon length was significantly shorter compared to ADAM17$^{wt/wt}$ mice, which was a strong indication for intestinal inflammation (Fig. 24 A).

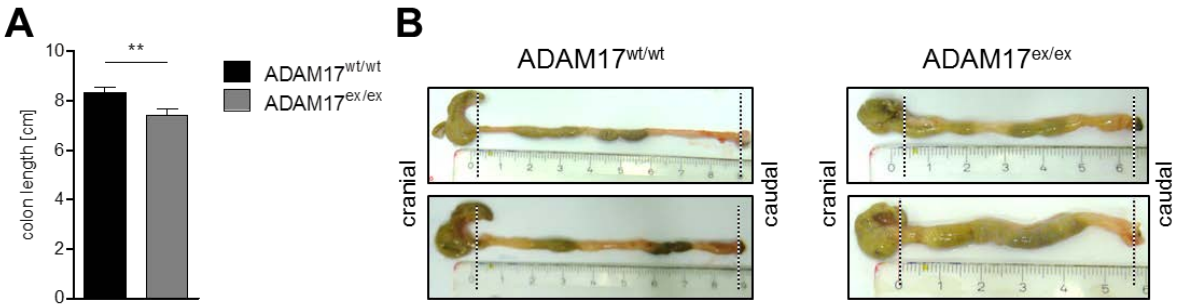

Fig. 24: Colon length from hypomorphic ADAM17$^{ex/ex}$ mice after AOM/DSS-treatment.

Entire length of removed colon from each mouse was assessed and (A) quantified after necropsy at day 90 of the CAC model. (B) Representative images of removed colons after AOM/DSS-treatment are shown. ADAM17$^{wt/wt}$ mice (n=26) and ADAM17$^{ex/ex}$ mice (n=28). Unpaired t test with Welch´s correction.

DSS-induced inflammation leads to disruption of the intestinal barrier function and thereby to infiltration of commensal bacteria and subsequently immune cells into the lamina propria (Suzuki et al., 2006). HE stained tissue sections of AOM/DSS-treated mice were examined for frequency of infiltrated inflammation-related immune cells (Fig. 25 B). Severe inflammatory infiltration described by inflammation score 3 was dominantly detected in AOM/DSS-treated hypomorphic ADAM17$^{ex/ex}$ mice. AOM/DSS-treated ADAM17$^{wt/wt}$ control mice harbored an inflammation score between 0-1, which stands for no up to mild inflammatory infiltrate and matched with the results of the previous tests for inflammation parameters (Fig. 25 A).

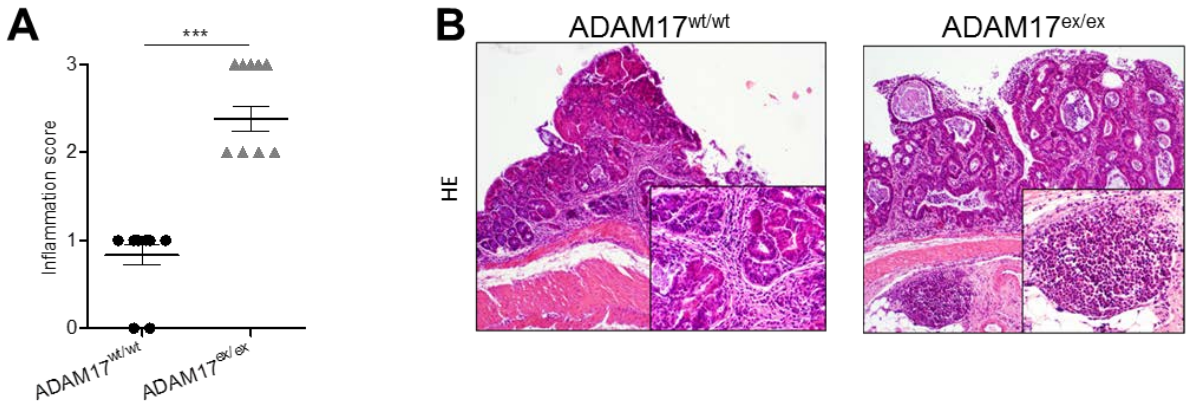

Fig. 25: Inflammation score of AOM/DSS-treated hypomorphic ADAM17$^{ex/ex}$ mice.

(A) Grading of inflammatory infiltrate in colon tissue [0, no infiltrate; 1, mild infiltrate; 2, moderate infiltrate; 3, severe infiltrate] and (B) representative images. ADAM17$^{wt/wt}$ mice (n=10) and ADAM17$^{ex/ex}$ mice (n=8). Unpaired t test.

The hypomorphic ADAM17$^{ex/ex}$ mice, with markedly reduced ADAM17 protein expression in all tissues, suffered from more severe intestinal inflammation accompanied by increased tissue damage and less survival in response to AOM/DSS-treatment.

Correlating with significantly increased signs of inflammation in hypomorphic ADAM17$^{ex/ex}$ mice, inflammatory cells were recruited to the tumor tissue. In contrast, immune cells in ADAM17$^{wt/wt}$ tumor tissue were more evenly distributed.

3.2.2 GENETIC ADAM17 INACTIVATION AFFECTS TUMOR INCIDENCE IN THE AOM/DSS MODEL

Carcinogen-induced colon cancer in mice is a reliable model to mimic human tumor initiation and tumor progression. Azoxymethane (AOM) is an indirectly acting pro-carcinogen which requires metabolic activation by enzymatic conversion mediated through commensal bacteria. If AOM is enzymatically converted into the reactive metabolite methylazoxymethanol (MAM), the activated carcinogen alters DNA molecules by alkylation or methylation leading to DNA mispairing. As a result, AOM is able to induce DNA damage specific within the intestinal epithelium of the colon. (Delker et al., 1998, Rosenberg et al., 2009, Tanaka et al., 2003, Neufert et al., 2007).

AOM/DSS-treated mice were sacrificed after 90 days and the colon tissue was analyzed for tumor burden. Examples for macroscopic analysis by incident light and transmitted light as well as microscopic analysis of Azan stained tissue sections showed that AOM/DSS-treated mice mostly developed distal colonic tumors (Fig. 26). Separated tumors from AOM/DSS-treated ADAM17$^{wt/wt}$ control mice showed distinct boundaries and indication of vascularization. The surrounding non-tumor tissue was thin and sheer and looked healthy. In hypomorphic ADAM17$^{ex/ex}$ mice, thickened colon tissue without distinct boundaries was observed in proximity to extensive tumor areas.

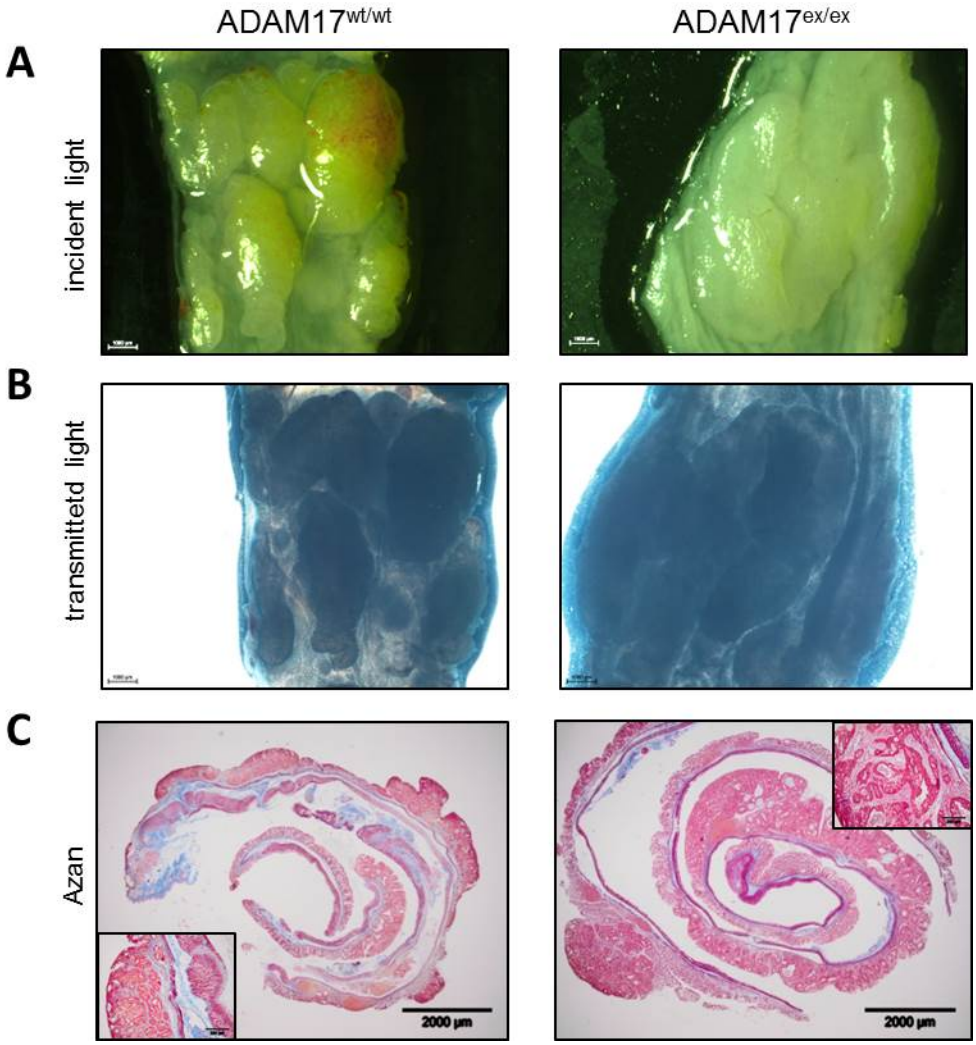

Fig. 26: Representative images of the colon from AOM/DSS-treated hypomorphic ADAM17$^{ex/ex}$ mice.

Representative images of (A) incident light, (B) transmitted light unstained tissue from colon of AOM/DSS-treated mice. (C) Representative Azan trichrome-stained distal colonic sections at day 90 after AOM/DSS-treatment. ADAM17$^{wt/wt}$ mice (n=26) and ADAM17$^{ex/ex}$ mice (n=28).

Furthermore, Azan stained tissue sections of hypomorphic ADAM17$^{ex/ex}$ mice revealed different tumor morphology compared with ADAM17$^{wt/wt}$ control mice.

The different tumor morphology was investigated in more detail by microscopic histopathological analysis in cooperation with the pathologists Prof. Dr. Lukas Kenner and Dr. med. vet. Simone Roos from University of Veterinary Medicine Vienna. For that reason, FFPE-tissue was HE stained and evaluated for tumor staging (Fig. 27).

Microscopic histopathological analysis showed that AOM/DSS-treatment initiates the formation of flat low grade dysplasia in colonic epithelial cells. The number of low grade dysplasia in AOM/DSS-treated hypomorphic ADAM17$^{ex/ex}$ mice and ADAM17$^{wt/wt}$ control mice was similar with a mean of four low grade dysplasia per mice. However, hypomorphic

ADAM17$^{ex/ex}$ mice showed a significantly higher number of high grade dysplasia with a mean of five per mouse than ADAM17$^{wt/wt}$ control mice with a mean of one high grade dysplasia per mouse. The difference in carcinoma tumor stages between hypomorphic ADAM17$^{ex/ex}$ mice and ADAM17$^{wt/wt}$ control mice was even more pronounced as only hypomorphic ADAM17$^{ex/ex}$ mice showed carcinoma formation within the colon after AOM/DSS-treatment. The different tumor stages were defined by elongated and branched crypts with comparative reduced stroma and preserved cell polarity in low grade dysplasia, irregular glands and nuclear membranes associated with non-existent cell polarity in high grade dysplasia plus penetration of the lamina muscularis mucosae in carcinoma tumor stage (Boivin et al., 2003).

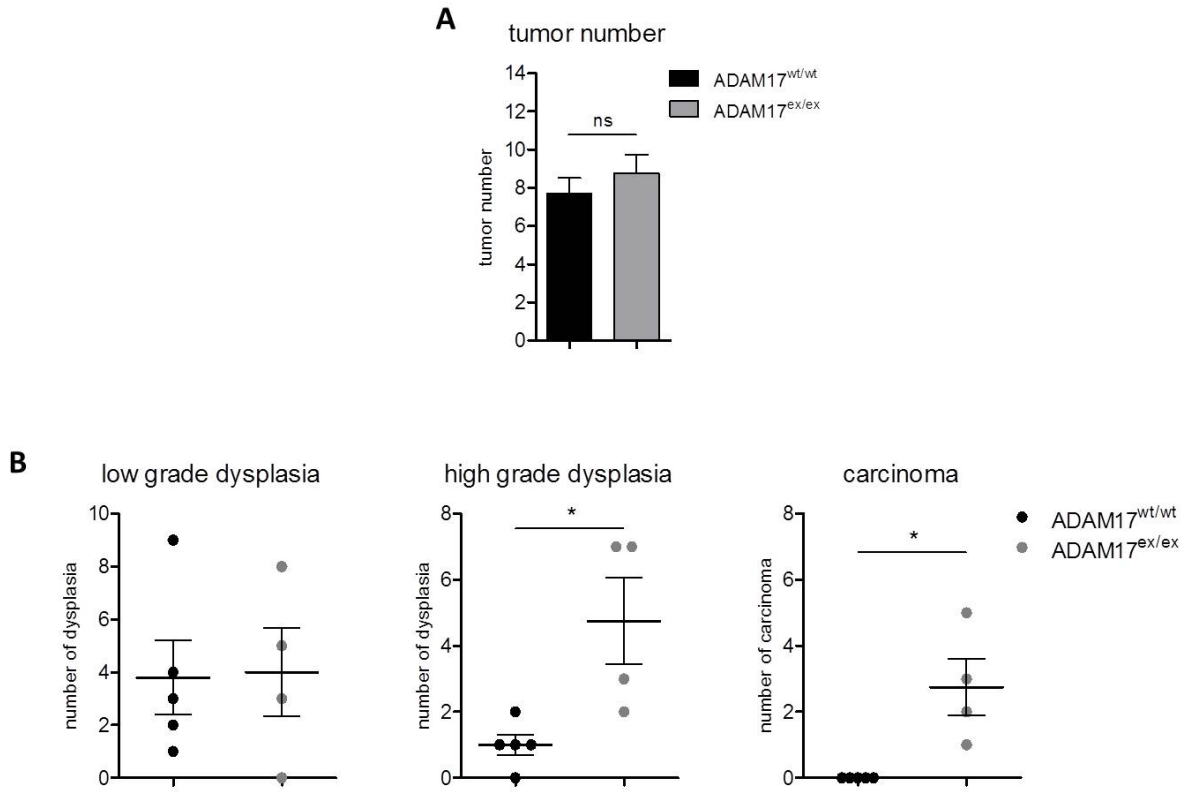

Fig. 27: Tumor number and staging from AOM/DSS-treated hypomorphic ADAM17$^{ex/ex}$ mice.

(A) Number of neoplasia of ADAM17$^{wt/wt}$ mice (n=26) and ADAM17$^{ex/ex}$ mice (n=28) and (B) tumor staging from lesions of ADAM17$^{wt/wt}$ mice (n=5) and ADAM17$^{ex/ex}$ mice (n=4) after necropsy at day 90 of the CAC model. Mann Whitney test.

In accordance with the macroscopic observations from Fig. 26 the microscopically measured tumor sizes in hypomorphic ADAM17$^{ex/ex}$ mice was increased 2-3-fold compared to ADAM17$^{wt/wt}$ control mice (Fig. 28).

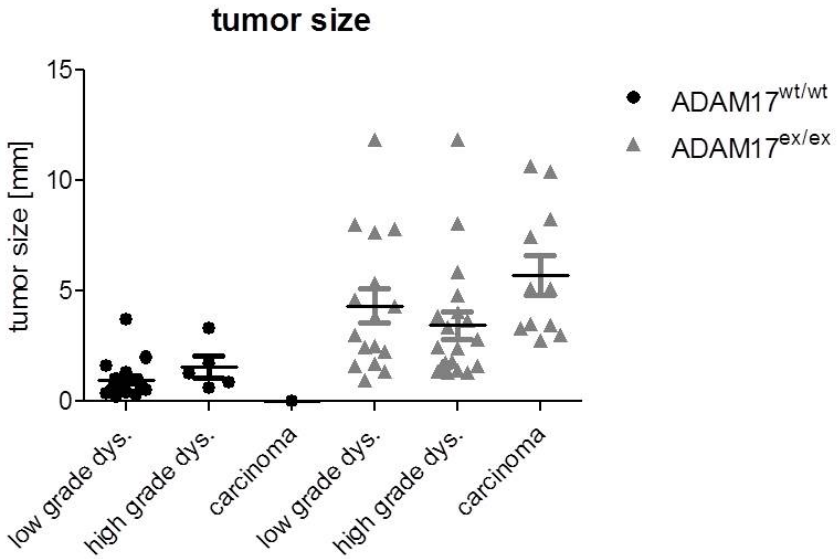

Fig. 28: Tumor number and size from AOM/DSS-treated hypomorphic ADAM17$^{ex/ex}$ mice.

Size of low grade dysplasia, high grade dysplasia and carcinoma of mice after necropsy at day 90 of the CAC model. Mann Whitney test.

3.3 THE ROLE OF ADAM17 IN THE GENETICALLY PREDISPOSED $APC^{Min/+}$ INTESTINAL CANCER MODEL

The results from experiments with human colorectal cancer cells *in vitro* (chapter 3.1.) and hypomorphic $ADAM17^{ex/ex}$ mice *in vivo* (chapter 3.2.) reveal the influential role of ADAM17 in colorectal cancer. In order to assess the influence of ADAM17 on colon cancer development without association to inflammation and chronic colitis, the genetically predisposed $Apc^{Min/+}$ mouse model was analyzed. The $Apc^{Min/+}$ mouse is an established model of human colorectal cancer without inflammation-related onset.

3.3.1 ESTABLISHMENT OF THE $APC^{Min/+}ADAM17^{ex/ex}$ MOUSE MODEL

For generation of the genetically predisposed $Apc^{Min/+}ADAM17^{ex/ex}$ colon cancer mouse model, $Apc^{Min/+}$ mice were crossbred with hypomorphic $ADAM17^{ex/ex}$ mice or $ADAM17^{wt/wt}$ mice as control. The F1 littermates $Apc^{Min/+}ADAM17^{wt/ex}$ and $Apc^{Min/+}ADAM17^{wt/wt}$ were crossbred again with $ADAM17^{ex/ex}$ mice or $ADAM17^{wt/wt}$ mice. The following genotypes were obtained: $Apc^{Min/+}ADAM17^{ex/ex}$ and $Apc^{Min/+}ADAM17^{wt/wt}$ as well as corresponding $Apc^{+/+}$ wildtype mice. In consequence of the hypomorphic $ADAM17^{ex/ex}$ mice phenotype, the $Apc^{Min/+}ADAM17^{ex/ex}$ mice show hair, skin, heart and epithelial abnormalities, open eye lids and limitations in their fertility (Chalaris et al., 2010).

These newly bred mice reveal whether lack of ADAM17 influences tumor development in the intestine of the $Apc^{Min/+}$ mouse model. To determine the exact genotype, each mouse was controlled by Genotype-PCR (Tab. 3 and Tab. 4). In addition to that, small intestinal tissue lysates of the generated $Apc^{Min/+}ADAM17^{ex/ex}$ and $Apc^{Min/+}ADAM17^{wt/wt}$ mice were examined for their endogenous ADAM17 protein expression.

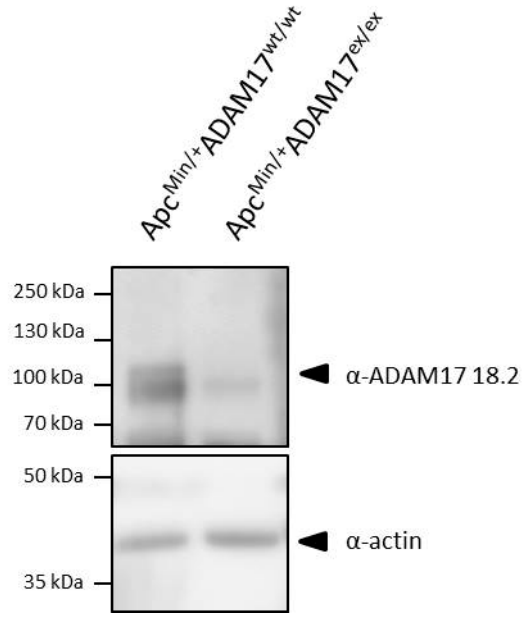

Fig. 29: ADAM17 protein expression in the small intestine from Apc$^{Min/+}$ADAM17$^{wt/wt}$ mice and hypomorphic Apc$^{Min/+}$ADAM17$^{ex/ex}$ mice.

Small intestinal tissue from indicated mice was lysed and 50 µg of total protein were analyzed. ADAM17 protein expression was assessed by Western blot analysis using a polyclonal anti-ADAM17 antibody (18.2).

The Western blot analysis from intestinal tissue lysates verified the lack of ADAM17 protein expression in Apc$^{Min/+}$ADAM17$^{ex/ex}$ mice (Fig. 29), whereas endogenous ADAM17 protein expression within the small intestine of Apc$^{Min/+}$ADAM17$^{wt/wt}$ mice was verifiable.

3.3.2 Reduced initiation of sporadic intestinal tumorigenesis in Apc$^{Min/+}$ADAM17$^{ex/ex}$ mice

Tumorigenesis in Apc$^{Min/+}$ mice occurs when the remaining wildtype *Apc* allele is lost by chance via LOH over time (Hursting et al., 1999). It was described previously that impaired EGFR signaling in Apc$^{Min/+}$ mice reduces the number of neoplasia in the small intestine (Roberts et al., 2002).

The obtained Apc$^{Min/+}$ADAM17$^{ex/ex}$ and Apc$^{Min/+}$ADAM17$^{wt/wt}$ mice indeed developed colorectal cancer and were first analyzed by macroscopic observations. The mice were sacrificed at the age of six months. After necropsy, the intestine was removed, washed thoroughly, opened longitudinally and placed mucosa surface side up for transmitted light microscopy (Fig. 30 A). The number of neoplasia as well as the size of neoplasia were determined and evaluated

with the Nikon AZ100 microscope and NIS-Elements D 4.12.01 software. The number of neoplasia was found to be already significantly reduced in $Apc^{Min/+}ADAM17^{ex/ex}$ mice compared to $Apc^{Min/+}ADAM17^{wt/wt}$ control mice (Fig. 30 B). Nevertheless, the size of neoplasia in $Apc^{Min/+}ADAM17^{ex/ex}$ mice was not altered when compared with $Apc^{Min/+}ADAM17^{wt/wt}$ control mice (Fig. 30 C).

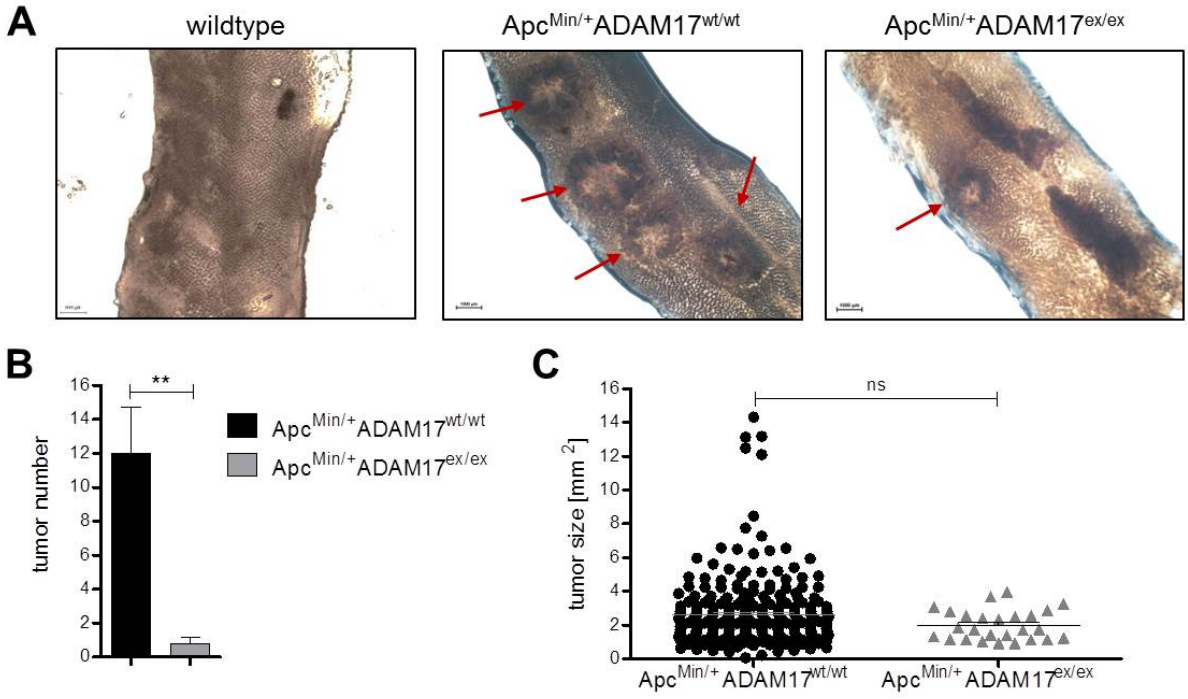

Fig. 30: Gross pathology of neoplasia in the small intestine from $Apc^{Min/+}ADAM17^{wt/wt}$ mice and hypomorphic $Apc^{Min/+}ADAM17^{ex/ex}$ mice.

(A) Neoplasia number was determined macroscopically in the small intestine. (B) Quantification of tumor number and (C) size of neoplasia throughout the small intestine. $Apc^{Min/+}ADAM17^{wt/wt}$ mice (n=15) and $Apc^{Min/+}ADAM17^{ex/ex}$ mice (n=14) six months of age. Mann Whitney test.

Furthermore, the distribution of neoplasia in the intestine of $Apc^{Min/+}ADAM17^{ex/ex}$ mice and $Apc^{Min/+}ADAM17^{wt/wt}$ control mice was assessed. For both genotypes, no significant difference regarding neoplasia distribution between duodenum, jejunum or ileum were measurable. In some cases, neoplasia in the colon were detected as well as in the small intestine of $Apc^{Min/+}ADAM17^{ex/ex}$ mice and $Apc^{Min/+}ADAM17^{wt/wt}$ control mice (Fig. 31). However, there was no significant difference in the number or size of neoplasia in the colon in both genotypes (data not shown).

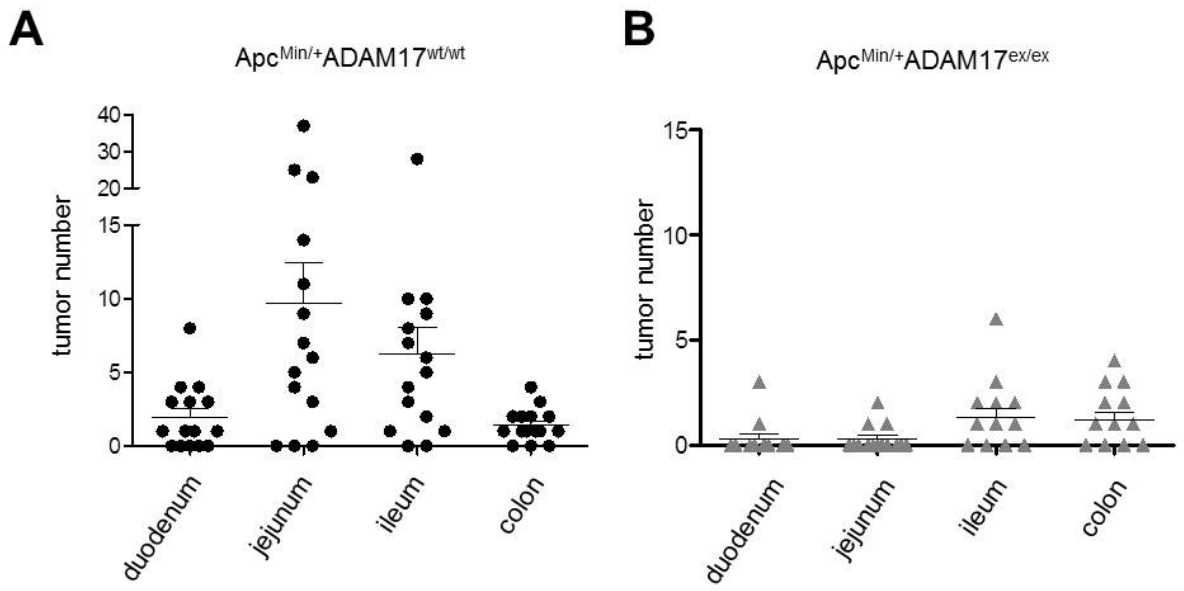

Fig. 31: Distribution of neoplasia within the small intestine from Apc$^{Min/+}$ADAM17$^{wt/wt}$ mice and hypomorphic Apc$^{Min/+}$ADAM17$^{ex/ex}$ mice.

The number of neoplasia was determined macroscopically within the small intestine (duodenum, jejunum, ileum) and colon of (A) Apc$^{Min/+}$ADAM17$^{wt/wt}$ mice (n=15) and (B) Apc$^{Min/+}$ADAM17$^{ex/ex}$ mice (n=14).

Efficient reduction of neoplasia formation in Apc$^{Min/+}$ADAM17$^{ex/ex}$ mice compared with Apc$^{Min/+}$ADAM17$^{wt/wt}$ control mice was microscopically confirmed by HE (Fig. 32 A) staining as well as Azan staining (Fig. 32 B). The morphological shape of neoplasia in Apc$^{Min/+}$ADAM17$^{ex/ex}$ mice was different compared to Apc$^{Min/+}$ADAM17$^{wt/wt}$ control mice.

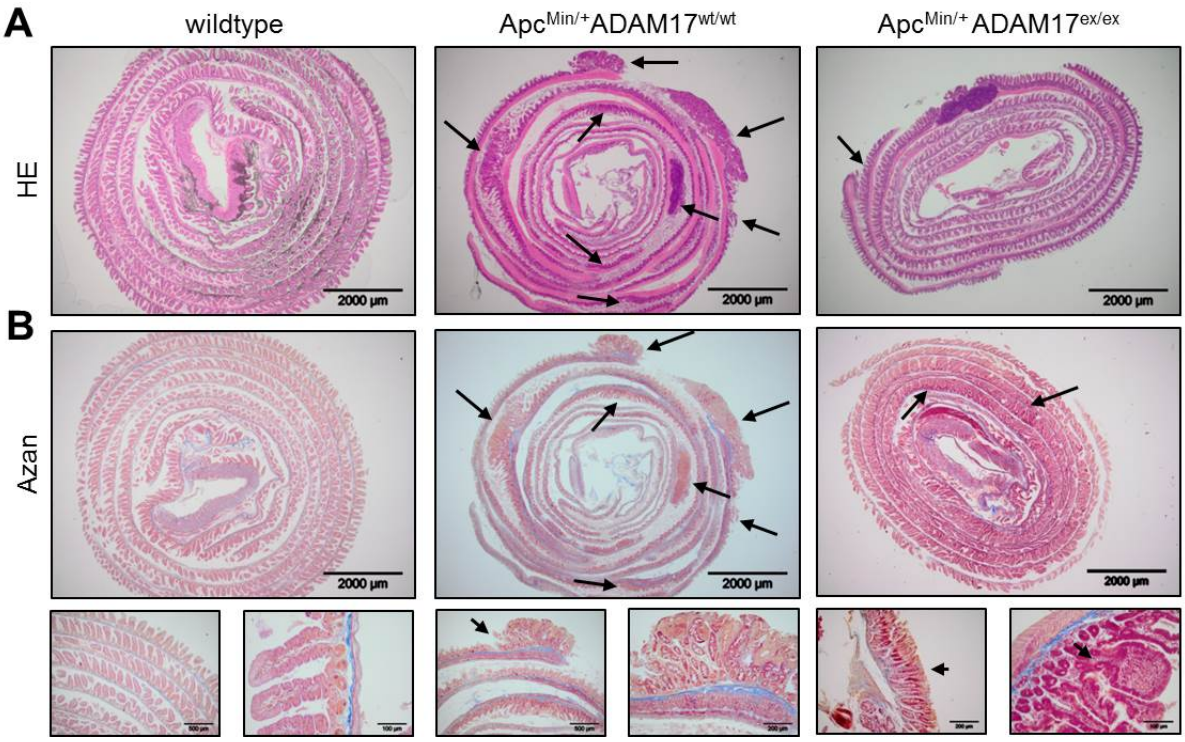

Fig. 32: Representative images of small intestinal tissue from Apc$^{Min/+}$ADAM17$^{wt/wt}$ mice and hypomorphic Apc$^{Min/+}$ADAM17$^{ex/ex}$ mice.

(A) Haematoxylin and eosin (HE) stained and (B) Azan trichrome-stained small intestines demonstrate distribution of neoplasia in Apc$^{Min/+}$ADAM17$^{wt/wt}$ mice and Apc$^{Min/+}$ADAM17$^{ex/ex}$ mice. Apc$^{Min/+}$ADAM17$^{wt/wt}$ mice (n=15) and Apc$^{Min/+}$ADAM17$^{ex/ex}$ mice (n=14).

In order to analyze the establishment of an inflammatory microenvironment in Apc$^{Min/+}$ADAM17$^{ex/ex}$ mice and Apc$^{Min/+}$ADAM17$^{wt/wt}$ mice, histological sections of neoplasia were analyzed for infiltration of macrophages, neutrophils and granulocytes (Fig. 33).

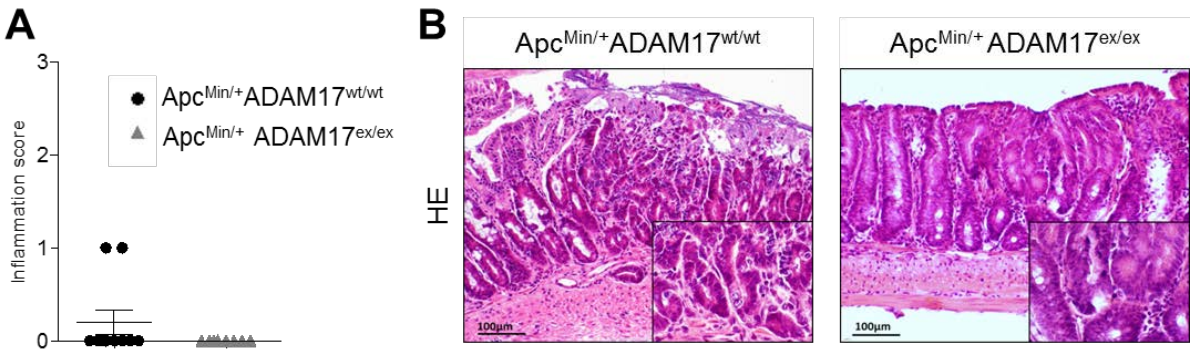

Fig. 33: Grading of inflammatory infiltrate in neoplasia from Apc$^{Min/+}$ADAM17$^{wt/wt}$ mice and hypomorphic Apc$^{Min/+}$ADAM17$^{ex/ex}$ mice.

(A) Inflammatory scoring (0, no infiltrate; 1, mild infiltrate; 2, moderate infiltrate; 3, severe infiltrate). (B) Representative images of haematoxylin and eosin (HE) stained tissue. Apc$^{Min/+}$ADAM17$^{wt/wt}$ mice (n=10) and Apc$^{Min/+}$ADAM17$^{ex/ex}$ mice (n=8). Unpaired t test.

Enhanced recruitment of infiltrating immune cells was neither observed in neoplasia of Apc$^{Min/+}$ADAM17$^{ex/ex}$ mice nor in neoplasia of Apc$^{Min/+}$ADAM17$^{wt/wt}$ control mice. Only two Apc$^{Min/+}$ADAM17$^{wt/wt}$ control mice showed a mild infiltration of immune cells within neoplasia tissue.

3.3.3 Loss of ADAM17 prevents carcinoma formation in Apc$^{Min/+}$ADAM17$^{ex/ex}$ mice

In order to determine whether the difference in shape of neoplasia is pathologically important, tumor staging (see subchapter 2.6.7) from histological sections of Apc$^{Min/+}$ADAM17$^{ex/ex}$ mice and Apc$^{Min/+}$ADAM17$^{wt/wt}$ control mice was performed. To assess the tumor stage of neoplasia, HE stained intestinal sections of both genotypes were screened for altered cell morphology and aberrant tissue structure.

The incidence of low grade dysplasia in hypomorphic Apc$^{Min/+}$ADAM17$^{ex/ex}$ mice was comparable to the incidence in Apc$^{Min/+}$ADAM17$^{wt/wt}$ control mice with a mean of three low grade dysplasia per mouse. (Fig. 34 A). Characteristics of low grade dysplasia are elongated and branched crypts accompanied by moderately reduced stroma, maintained cell polarity and regular nuclear membranes (Boivin et al., 2003). However, low grade dysplasia from Apc$^{Min/+}$ADAM17$^{ex/ex}$ mice exhibited a more organized structure while low grade dysplasia from Apc$^{Min/+}$ADAM17$^{wt/wt}$ mice were less differentiated with additional branched crypts as shown in Fig. 34 D.

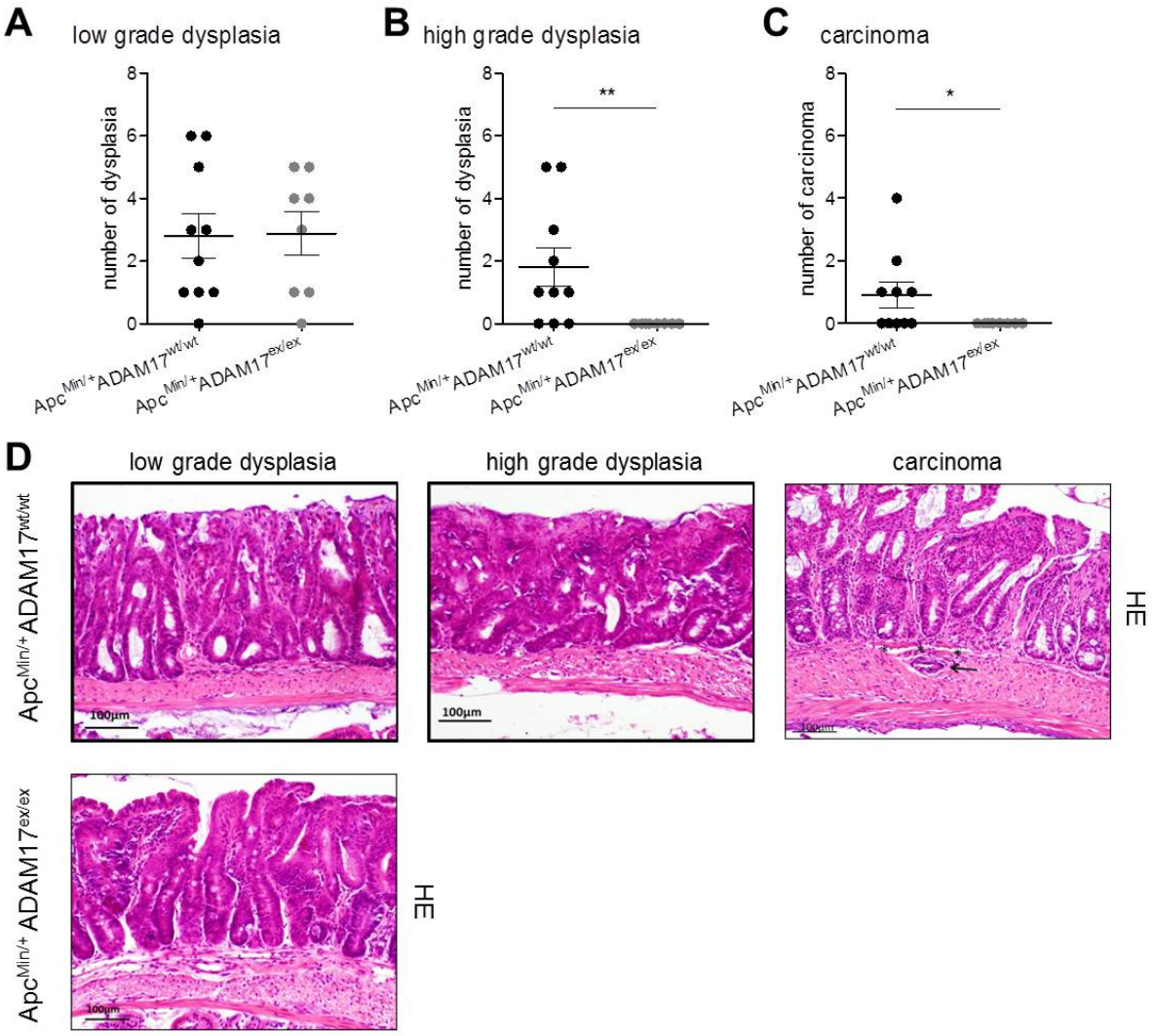

Fig. 34: Tumor staging of neoplasia from $Apc^{Min/+}ADAM17^{wt/wt}$ mice and hypomorphic $Apc^{Min/+}ADAM17^{ex/ex}$ mice.

Number of (A) low grade dysplasia, (B) high grade dysplasia and (C) carcinoma from $Apc^{Min/+}ADAM17^{wt/wt}$ mice (n=10) and $Apc^{Min/+}ADAM17^{ex/ex}$ mice (n=8) at the age of six months and (D) representative images of haematoxylin and eosin (HE) stained tissue. Arrow indicates the lamina muscularis mucosae, which is penetrated by the carcinoma. Mann Whitney test.

In addition to low grade dysplasia, $Apc^{Min/+}ADAM17^{wt/wt}$ mice frequently developed high grade dysplasia as well as carcinoma (Fig. 34 B and C). Apart from less organized crypt structures, high grade dysplasia were further characterized by irregular glands, lost cell polarity, irregular nuclear membranes and marked reduction of stroma. Additional penetration of the lamina muscularis mucosae are a typical hallmark of carcinoma formation (Boivin et al., 2003). The mean number of high grade dysplasia was two per $Apc^{Min/+}ADAM17^{wt/wt}$ mouse. The number of carcinoma was decreased with a mean of one per $Apc^{Min/+}ADAM17^{wt/wt}$ mouse. Interestingly, neither high grade dysplasia nor carcinoma occurred in hypomorphic $Apc^{Min/+}ADAM17^{ex/ex}$ mice.

The microscopically sized low grade dysplasia with a mean of 1.3 mm^2 in $Apc^{Min/+}ADAM17^{wt/wt}$ mice were significantly enlarged compared to low grade dysplasia in $Apc^{Min/+}ADAM17^{ex/ex}$ mice with a mean of 0.9 mm^2. Only in $Apc^{Min/+}ADAM17^{wt/wt}$ mice neoplasia with a tumor stage belonging to high grade dysplasia or carcinoma were detectable. As expected, the mean size of high grade dysplasia and carcinoma showed no significant differences and was determined with a size of 1.5-1.7 mm^2 (Fig. 35).

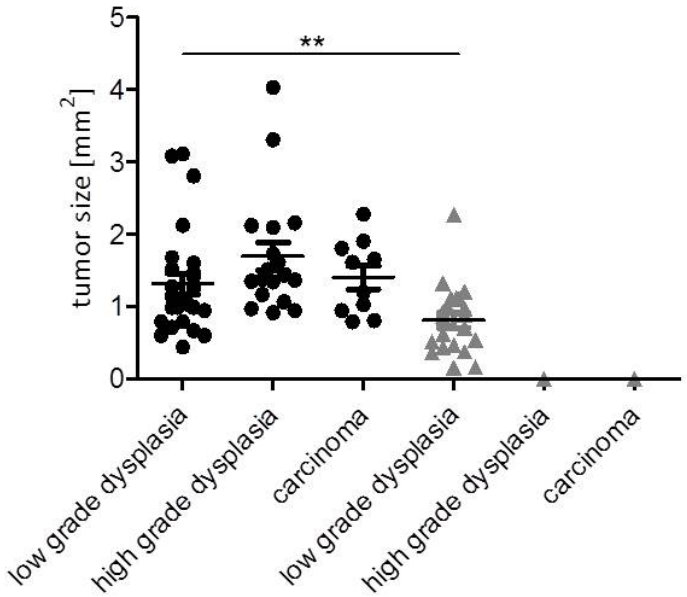

Fig. 35: Tumor size of neoplasia from $Apc^{Min/+}ADAM17^{wt/wt}$ mice and hypomorphic $Apc^{Min/+}ADAM17^{ex/ex}$ mice.

Size of low grade dysplasia, high grade dysplasia and carcinoma of $Apc^{Min/+}ADAM17^{wt/wt}$ mice (n=10) and $Apc^{Min/+}ADAM17^{ex/ex}$ mice (n=8) at the age of six months after necropsy. Mann Whitney test.

In accordance with Fig. 30, the microscopic evaluation of HE stained intestinal tissue of $Apc^{Min/+}ADAM17^{wt/wt}$ mice confirmed the significantly increased tumor incidence coupled with advanced tumor stages in comparison to $Apc^{Min/+}ADAM17^{ex/ex}$ mice, while the low grade dysplasia size differ significantly between both genotypes (Fig. 34 and 35).

3.3.4 INTESTINAL CELLULAR DIFFERENTIATION AND PROLIFERATION IN $APC^{MIN/+}ADAM17^{ex/ex}$ MICE

The influence of ADAM17 on colon cancer development was initially analyzed by a basic characterization of the small intestine and colon of healthy unchallenged hypomorphic $ADAM17^{ex/ex}$ mice and $ADAM17^{wt/wt}$ mice (Fig. 66; additional results). To receive a basic impression of the intestinal cell morphology, immunohistochemical staining for MMP7 (Matrix metalloproteinase 7) and Muc2 (Mucin 2) was performed. Positive MMP7 staining was a signature for Paneth cells, which are present within the small intestine at the stem cell region near the bottom of the crypts. Positive MMP7 staining is non-existent in the colon (Fig. 66 A; additional results). Goblet cells were identified by positive Muc2 staining within the small intestine and the colon and were spread along the crypt-villus-unit (Fig. 66 B; additional results).

The hypomorphic $ADAM17^{ex/ex}$ mice showed no differences in intestinal development assessed by number and differentiation of cells compared to $ADAM17^{wt/wt}$ mice. The equal differentiation and cell number of Paneth cells in the small intestine of hypomorphic $ADAM17^{ex/ex}$ mice and $ADAM17^{wt/wt}$ mice was shown here by MMP7 as a marker for the presence of Paneth cells. Regular differentiation of goblet cells in the small intestine and colon of hypomorphic $ADAM17^{ex/ex}$ mice and $ADAM17^{wt/wt}$ mice was shown by Muc2 staining.

Variances in intestinal cell morphology of healthy unchallenged hypomorphic $ADAM17^{ex/ex}$ mice and $ADAM17^{wt/wt}$ mice were not observed.

In order to assess the morphological alterations within the neoplasia of hypomorphic $Apc^{Min/+}ADAM17^{ex/ex}$ mice and $Apc^{Min/+}ADAM17^{wt/wt}$ control mice, further histological and immunohistochemical (IHC) staining experiments were performed. Categorization of tumor stages from stained tissue slides was conducted in cooperation with pathologist from the University of Veterinary Medicine Vienna (see subchapter 2.6.7).

To study the distribution of differentiated cell types within the small intestine of both $Apc^{Min/+}$ mouse strains, the existence of goblet cells and Paneth cells was investigated.

To visualize the occurrence of goblet cells, Periodic acid-Schiff (PAS) staining was utilized. Mucin, a glycoprotein, produced and secreted by goblet cells, was stained by a reaction with Schiff reagent.

Unaffected small intestinal tissue of hypomorphic $Apc^{Min/+}ADAM17^{ex/ex}$ mice and $Apc^{Min/+}ADAM17^{wt/wt}$ control mice showed a normal physiological occurrence and distribution of goblet cells (Fig. 36). Goblet cells could not be detected in dysplasia of both $Apc^{Min/+}$ genotypes. Carcinoma of $Apc^{Min/+}ADAM17^{wt/wt}$ mice also showed a loss of goblet cells in line with a negative PAS staining.

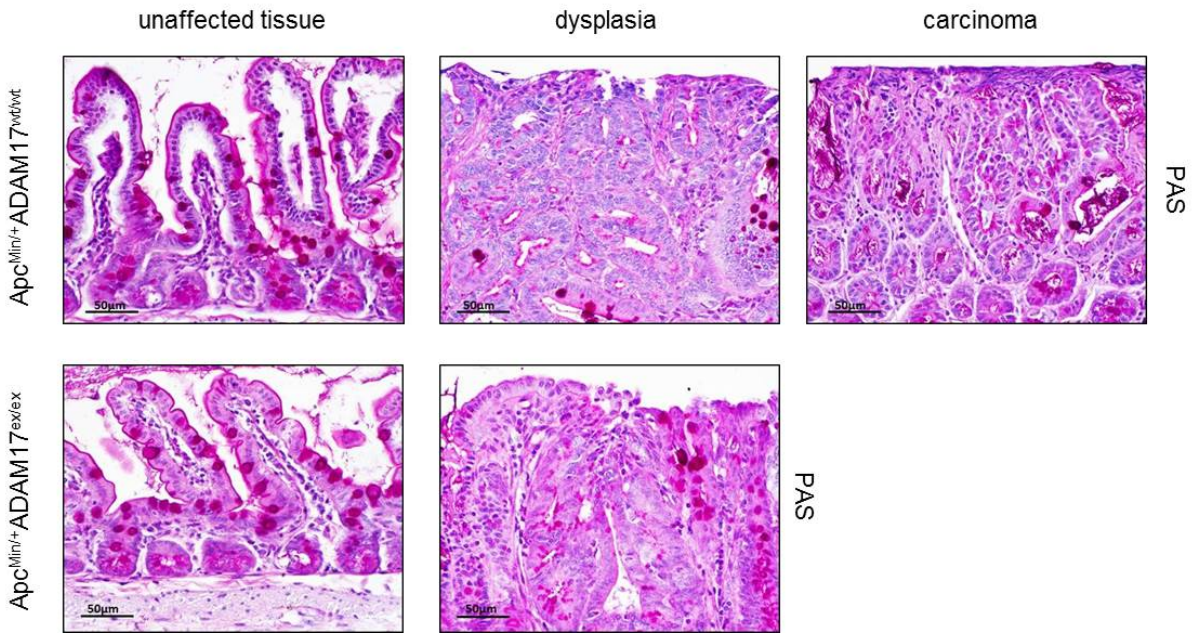

Fig. 36: Representative images of PAS-stained tissue from hypomorphic $Apc^{Min/+}ADAM17^{wt/wt}$ mice and $Apc^{Min/+}ADAM17^{ex/ex}$ mice.

Small intestine from 24-week-old $Apc^{Min/+}ADAM17^{wt/wt}$ mice and $Apc^{Min/+}ADAM17^{ex/ex}$ mice was used for PAS staining to visualize mucin produced by goblet cells in purple. $Apc^{Min/+}ADAM17^{wt/wt}$ mice (n=8) and $Apc^{Min/+}ADAM17^{ex/ex}$ mice (n=6).

Lysozyme, a well-known marker for Paneth cells, was used for IHC-DAB staining to identify differentiated Paneth cells (Fig. 37).

Both $Apc^{Min/+}$ genotypes showed an equal expression of Paneth cells in unaffected small intestinal tissue at the bottom of the crypts. Dysplasia in hypomorphic $Apc^{Min/+}ADAM17^{ex/ex}$ mice and $Apc^{Min/+}ADAM17^{wt/wt}$ control mice showed patchy abnormal arrangement of Paneth cells within irregular branched crypts. Additionally, Paneth cells were not restricted to the crypt bottom. Paneth cells were absent in carcinoma of $Apc^{Min/+}ADAM17^{wt/wt}$ mice.

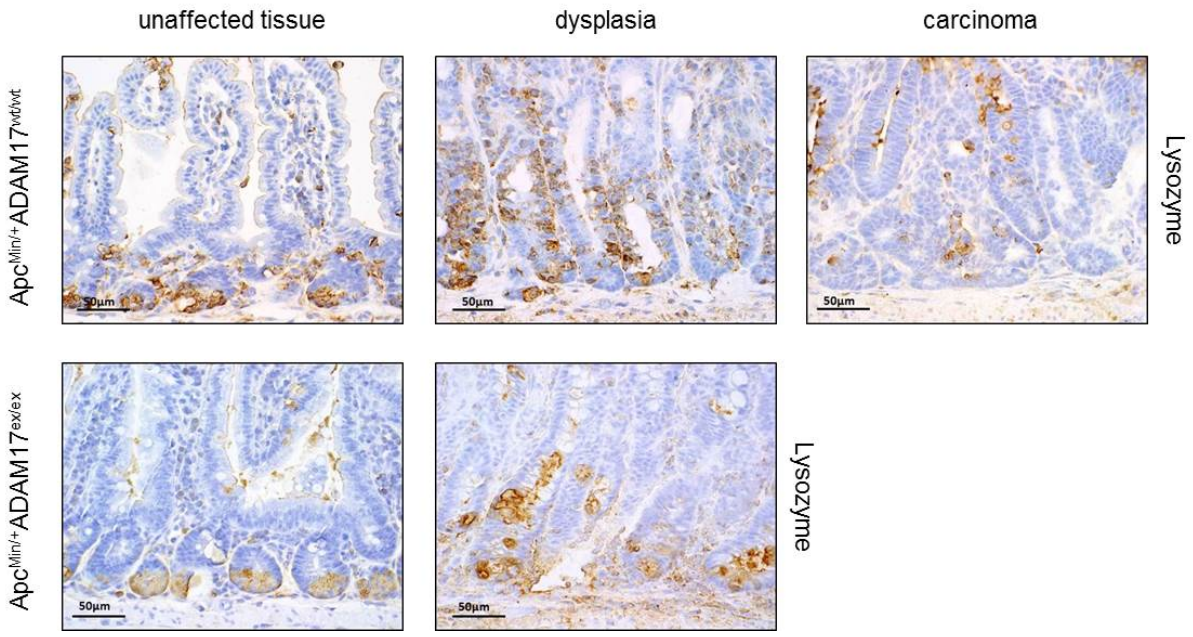

Fig. 37: Representative images of tissue from hypomorphic $Apc^{Min/+}ADAM17^{wt/wt}$ mice and $Apc^{Min/+}ADAM17^{ex/ex}$ mice stained for lysozyme.

Small intestine from 24-week-old $Apc^{Min/+}ADAM17^{wt/wt}$ mice and $Apc^{Min/+}ADAM17^{ex/ex}$ mice was used for IHC analysis to visualize lysozyme secreted by Paneth cells in brown. $Apc^{Min/+}ADAM17^{wt/wt}$ mice (n=8) and $Apc^{Min/+}ADAM17^{ex/ex}$ mice (n=6).

The expression pattern of selected proteins of interest within the small intestine of hypomorphic $Apc^{Min/+}ADAM17^{ex/ex}$ mice and $Apc^{Min/+}ADAM17^{wt/wt}$ control mice was specified by IHC staining experiments.

First, the expression pattern of ß-Catenin was examined as high staining levels of ß-Catenin confirm active Wnt signaling.

In unaffected small intestinal tissue, both $Apc^{Min/+}$ genotypes showed ß-Catenin expression at the cell membrane as well as sparse ß-Catenin expression within the cytoplasm (Fig. 38). The amount of cytoplasmic ß-Catenin expression was increased in dysplasia in hypomorphic $Apc^{Min/+}ADAM17^{ex/ex}$ mice and $Apc^{Min/+}ADAM17^{wt/wt}$ control mice, while levels of ß-Catenin located to the cell membrane were maintained. A similar signature was detected in carcinoma of $Apc^{Min/+}ADAM17^{wt/wt}$ mice. Overall, at similar tumor stage, no obvious differences in intestinal localization for ß-Catenin were observed between $ADAM17^{wt/wt}$ mice and hypomorphic $ADAM17^{ex/ex}$ mice.

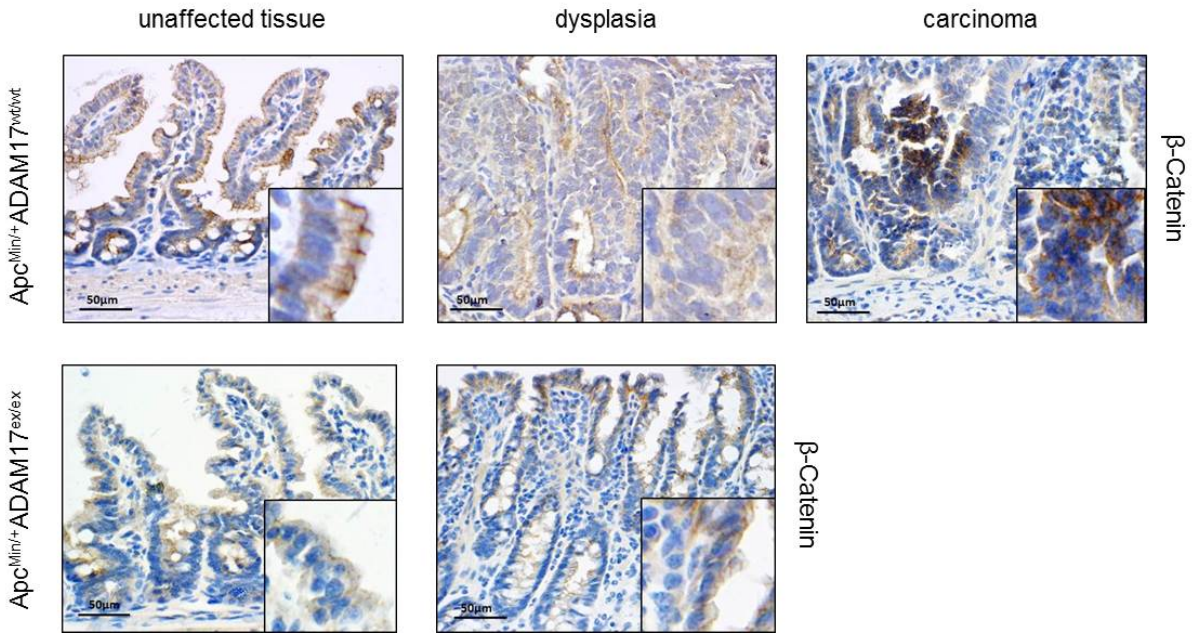

Fig. 38: Representative images of tissue from hypomorphic $Apc^{Min/+}ADAM17^{wt/wt}$ mice and $Apc^{Min/+}ADAM17^{ex/ex}$ mice stained for ß-Catenin.

Small intestine from 24-week-old $Apc^{Min/+}ADAM17^{wt/wt}$ mice and $Apc^{Min/+}ADAM17^{ex/ex}$ mice was used for IHC analysis to visualize ß-Catenin in brown. $Apc^{Min/+}ADAM17^{wt/wt}$ mice (n=8) and $Apc^{Min/+}ADAM17^{ex/ex}$ mice (n=6).

To assess the activation of the signal transducer and activator of transcription 3 (STAT3) in hypomorphic $Apc^{Min/+}ADAM17^{ex/ex}$ mice and $Apc^{Min/+}ADAM17^{wt/wt}$ mice, immunohistochemistry (IHC) staining for STAT3 and phosphorylated STAT3 (pSTAT3) was performed.

The IHC experiments confirmed activation of STAT3 by translocation from the cytoplasm to the nucleus. $Apc^{Min/+}ADAM17^{wt/wt}$ mice showed areas of nuclear STAT3 staining in unaffected intestinal tissue. Additionally, the translocation of STAT3 inside the nucleus was positive in neoplasia of $Apc^{Min/+}ADAM17^{wt/wt}$ mice. In some dysplasia and carcinoma of $Apc^{Min/+}ADAM17^{wt/wt}$ mice a patchy nuclear staining for STAT3 was detectable. However, no positive staining for STAT3 in hypomorphic $Apc^{Min/+}ADAM17^{ex/ex}$ mice was quantifiable in unaffected intestinal tissue and in dysplasia (Fig. 39).

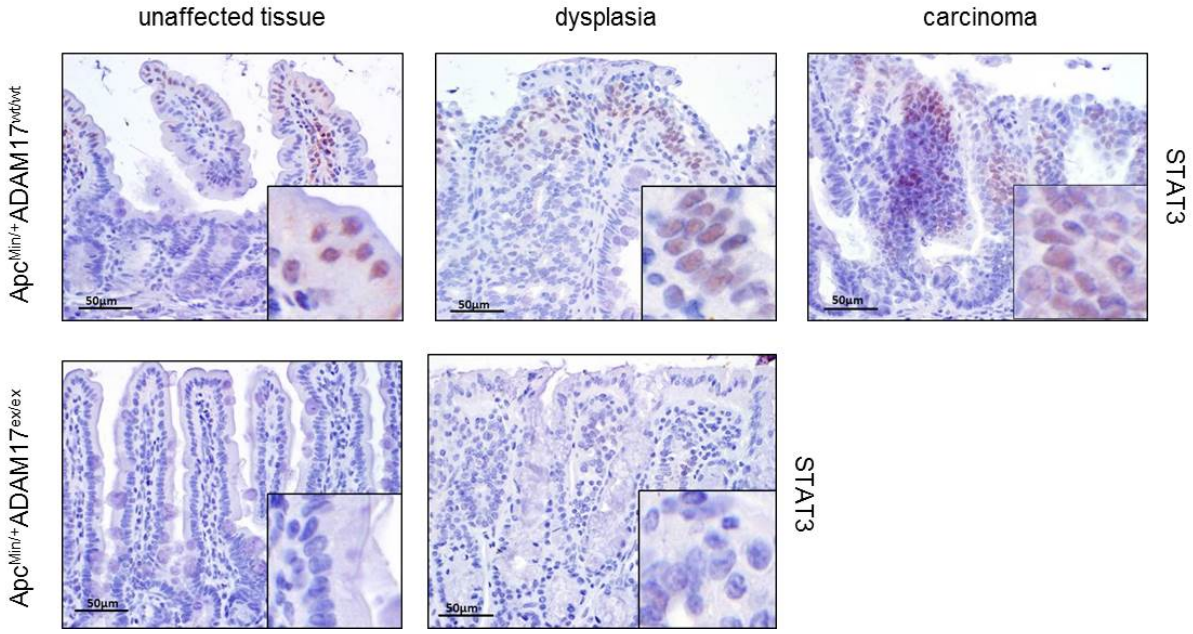

Fig. 39: Representative images of tissue from hypomorphic $Apc^{Min/+}ADAM17^{wt/wt}$ mice and $Apc^{Min/+}ADAM17^{ex/ex}$ mice stained for STAT3.

Small intestine from 24-week-old $Apc^{Min/+}ADAM17^{wt/wt}$ mice and $Apc^{Min/+}ADAM17^{ex/ex}$ mice was used for IHC analysis to visualize STAT3 in brown. $Apc^{Min/+}ADAM17^{wt/wt}$ mice (n=8) and $Apc^{Min/+}ADAM17^{ex/ex}$ mice (n=6).

Nevertheless, phosphorylation of STAT3 was occasionally detectable in unaffected intestinal tissue or neoplasia of $Apc^{Min/+}ADAM17^{wt/wt}$ mice (Fig. 40). Only a few leucocytes within the lamina propria of $Apc^{Min/+}ADAM17^{wt/wt}$ mice showed positive staining for pSTAT3. Subsequently, no differences between genotypes or histological lesions were measurable in epithelial pSTAT3 staining.

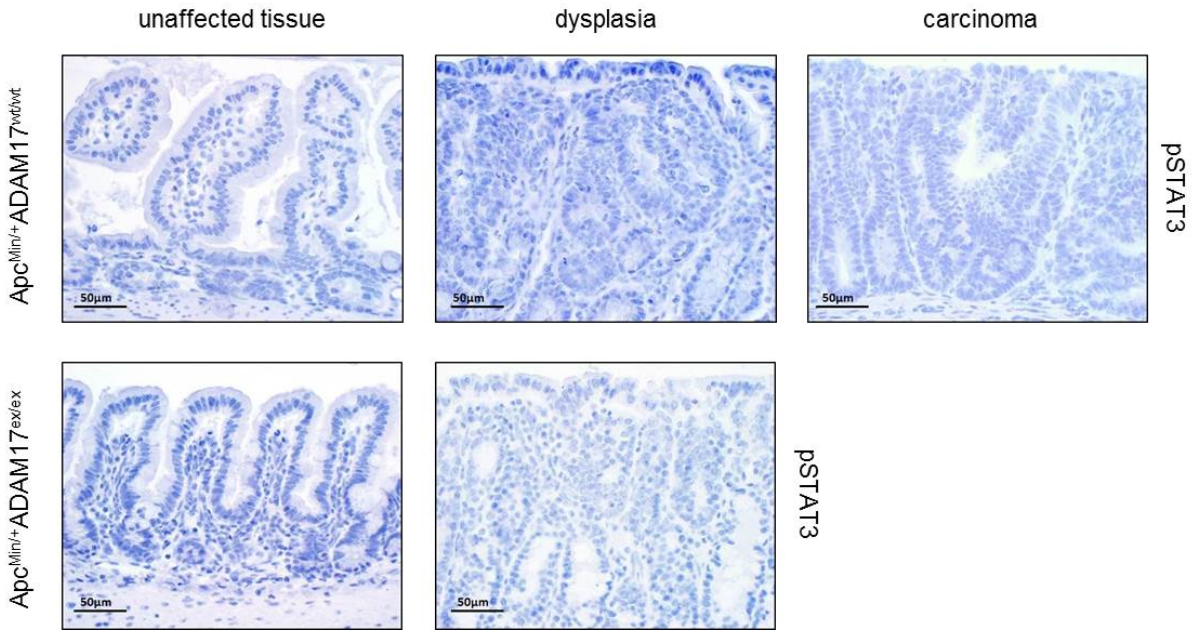

Fig. 40: Representative images of tissue from hypomorphic $Apc^{Min/+}ADAM17^{wt/wt}$ mice and $Apc^{Min/+}ADAM17^{ex/ex}$ mice stained for pSTAT3.

Small intestine from 24-week-old $Apc^{Min/+}ADAM17^{wt/wt}$ mice and $Apc^{Min/+}ADAM17^{ex/ex}$ mice was used for IHC analysis to visualize pSTAT3. $Apc^{Min/+}ADAM17^{wt/wt}$ mice (n=8) and $Apc^{Min/+}ADAM17^{ex/ex}$ mice (n=6).

To assess tumor cell proliferation in neoplasia of hypomorphic $Apc^{Min/+}ADAM17^{ex/ex}$ mice and $Apc^{Min/+}ADAM17^{wt/wt}$ mice, IHC analysis for Ki-67, a specific nuclear marker for cell proliferation, was performed (Fig. 41).

Unaffected intestinal tissue of both genotypes showed an equal Ki-67 signal at the bottom of the crypts, which is known as physiological proliferating zone within the crypt-villus-unit. An increased signal for Ki-67 was observed in dysplasia and carcinoma and goes in line with tumor progression. However, hypomorphic $Apc^{Min/+}ADAM17^{ex/ex}$ mice showed a decreased signal for Ki-67 in dysplasia compared to $Apc^{Min/+}ADAM17^{wt/wt}$ mice.

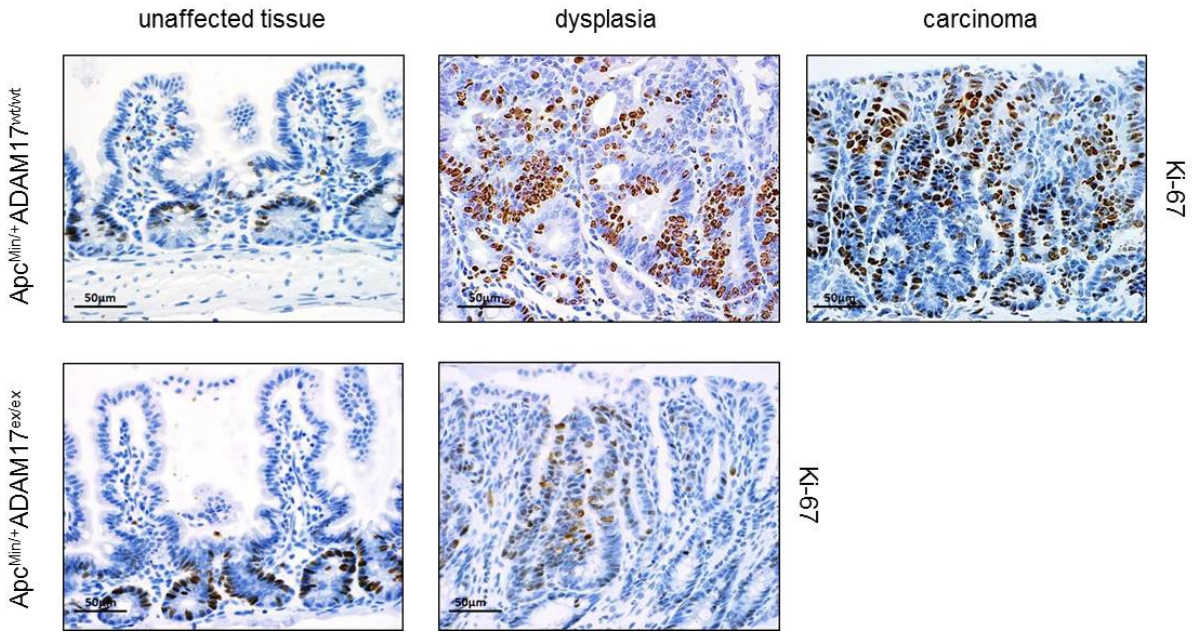

Fig. 41: Representative images of tissue from hypomorphic $Apc^{Min/+}ADAM17^{wt/wt}$ mice and $Apc^{Min/+}ADAM17^{ex/ex}$ mice stained for Ki-67.

Small intestine from 24week-old $Apc^{Min/+}ADAM17^{wt/wt}$ mice and $Apc^{Min/+}ADAM17^{ex/ex}$ mice was used for IHC analysis to visualize Ki-67 as a marker for cell proliferation in brown. $Apc^{Min/+}ADAM17^{wt/wt}$ mice (n=8) and $Apc^{Min/+}ADAM17^{ex/ex}$ mice (n=6).

Quantification of the Ki-67 stained tissue slides revealed significant differences in proliferation in dysplasia between hypomorphic $Apc^{Min/+}ADAM17^{ex/ex}$ mice and $Apc^{Min/+}ADAM17^{wt/wt}$ mice (Fig. 42). Dysplasia of hypomorphic $Apc^{Min/+}ADAM17^{ex/ex}$ mice contained 0.5 % Ki-67 positive cells compared to 13 % Ki-67 positive cells in dysplasia of $Apc^{Min/+}ADAM17^{wt/wt}$ mice.

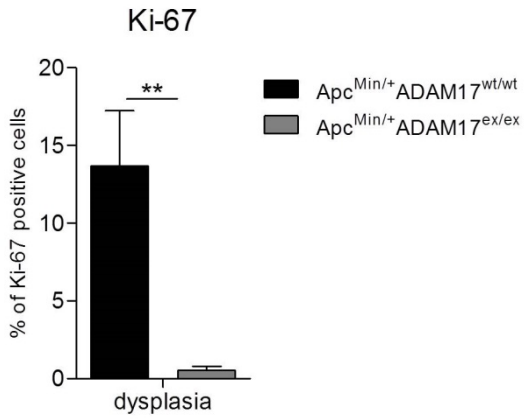

Fig. 42: Quantification of Ki-67 stained tissue from hypomorphic $Apc^{Min/+}ADAM17^{wt/wt}$ mice and $Apc^{Min/+}ADAM17^{ex/ex}$ mice.

Small intestine from 24-week-old $Apc^{Min/+}ADAM17^{wt/wt}$ mice and $Apc^{Min/+}ADAM17^{ex/ex}$ mice was used in IHC for analysis of Ki-67 positive cell proliferation. Quantification of Ki-67 positive signals by ImageJ. $Apc^{Min/+}ADAM17^{wt/wt}$ mice (n=8) and $Apc^{Min/+}ADAM17^{ex/ex}$ mice (n=6). Mann-Whitney test.

3.3.5 EGFR AND AMPHIREGULIN mRNA EXPRESSION IS UPREGULATED IN TUMOR TISSUE

To address the question if loss of heterozygosity and neoplasia formation in the analyzed $Apc^{Min/+}$ mouse strains was accompanied by other dysregulated genes, comprehensive quantitative real-time PCR analysis from murine tissue samples was performed.

Based on the results of chapter 3.1 and the resulting link between ADAM17-regulated Amphiregulin shedding on intestinal epithelial cells and adjusted activation of the epidermal growth factor receptor (EGFR), non-tumor tissue and tumor tissue from $Apc^{Min/+}ADAM17^{wt/wt}$ mice were screened for aberrant expression of the ErbB receptor tyrosine kinases family and corresponding EGFR ligands. Tumor tissues from $Apc^{Min/+}ADAM17^{wt/wt}$ mice showed increased mRNA levels for EGFR compared to non-tumor tissue (Fig. 43). mRNA transcripts for ErbB receptor tyrosine kinases ErbB2, ErbB3 and ErbB4 were not altered in tumor tissue. Additionally, mRNA coding for the EGFR ligands Amphiregulin (AREG), Betacellulin (BTC) and Epiregulin (EREG) was significantly elevated in tumor tissue compared to non-tumor tissue in $Apc^{Min/+}ADAM17^{wt/wt}$ mice.

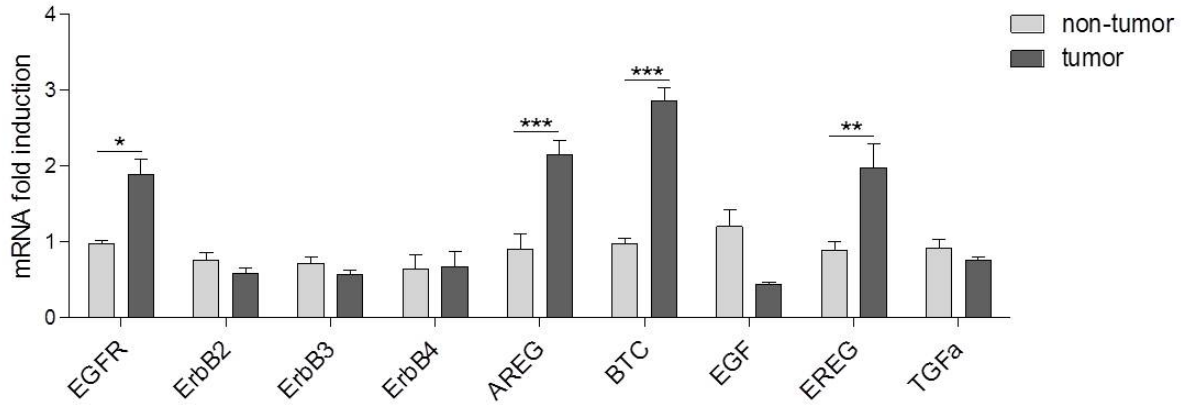

Fig. 43: qRT-PCR analysis of epidermal growth factor receptors and EGFR ligands from $Apc^{Min/+}ADAM17^{wt/wt}$ mice tissue.

18 tumors and 5 non-tumor tissue samples obtained from $Apc^{Min/+}ADAM17^{wt/wt}$ mice (n=3) were analyzed for the expression of epidermal growth factor receptors and EGFR ligands. (EGFR–ErbB4, ErbB receptor tyrosine kinase family; AREG, Amphiregulin; BTC, Betacellulin; EGF, Epidermal growth factor; EREG, Epiregulin; TGF-α, Transforming growth factor alpha). 2way ANOVA with Bonferroni posttest.

In order to verify the observed mRNA signature from Fig. 43, laser microdissection experiments were perfomed (see subchapter 2.6.6). Neoplasia of $Apc^{Min/+}ADAM17^{ex/ex}$ mice and $Apc^{Min/+}ADAM17^{wt/wt}$ mice as well as healthy crypt-villus-units from $ADAM17^{wt/wt}$ mice

were analyzed. Due to the fact that the amount of dissected tissue material was limited, only selected genes of interest were measured. Significantly elevated mRNA levels for EGFR and AREG compared to healthy wildtype tissue were detected in neoplasia from $Apc^{Min/+}ADAM17^{ex/ex}$ mice and $Apc^{Min/+}ADAM17^{wt/wt}$ mice (Fig. 44).

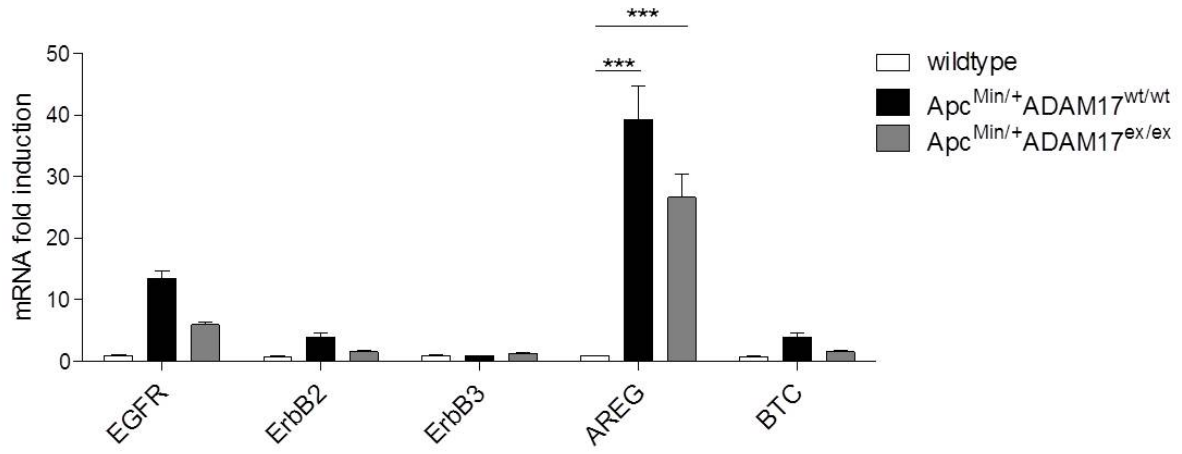

Fig. 44: Laser microdissection and qRT-PCR analysis of ErbB receptors and EGFR ligands from neoplasia of $Apc^{Min/+}ADAM17^{wt/wt}$ mice and hypomorphic $Apc^{Min/+}ADAM17^{ex/ex}$ mice.

Real-time data were normalized to GAPDH. Tissue samples from six neoplasia from $Apc^{Min/+}ADAM17^{wt/wt}$ mice (n=3) and four neoplasia from $Apc^{Min/+}ADAM17^{ex/ex}$ mice (n=2) were collected via Laser microdissection and compared to wildtype tissue (n=1). (EGFR–ErbB3, ErbB receptor tyrosine kinase family; AREG, Amphiregulin; BTC, Betacellulin). 2way ANOVA with Bonferroni posttest.

To identify additional participating signaling pathways to benefit colon cancer development in the $Apc^{Min/+}ADAM17^{ex/ex}$ model, the Notch signaling pathway was investigated. It is well known that the Notch signaling pathway plays a key role in developmental processes and proliferation as well as differentiation during intestinal epithelial turnover (Barker, 2014, VanDussen et al., 2012). Apart from this, it is assumed that ADAM17 is also involved in ligand-independent Notch signaling under pathophysiological conditions (Bozkulak and Weinmaster, 2009, Brou et al., 2000, Murthy et al., 2012).

The mRNA levels of presumed Notch-regulated target genes such as *Hes-1*, *Hey-2* and *Hey-1* seemed to be slightly downregulated in $Apc^{Min/+}ADAM17^{ex/ex}$ mice compared to $Apc^{Min/+}ADAM17^{wt/wt}$ mice. Nevertheless, *Hey2* and *Hey-1* were significantly upregulated in both $Apc^{Min/+}$ strains as opposed to $ADAM17^{wt/wt}$ mice (Fig. 45 B and C). *Hes-1* mRNA is equally transcribed in $ADAM17^{wt/wt}$ mice and $Apc^{Min/+}ADAM17^{ex/ex}$ mice or $Apc^{Min/+}ADAM17^{wt/wt}$ mice (Fig. 45 A).

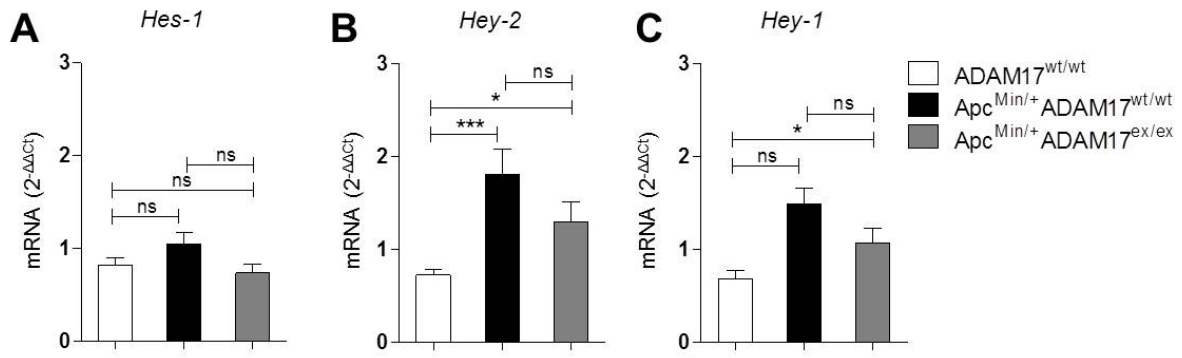

Fig. 45: qRT-PCR analysis of Notch target genes from Apc$^{Min/+}$ADAM17$^{wt/wt}$ mice and hypomorphic Apc$^{Min/+}$ADAM17$^{ex/ex}$ mice tissue.

10 tumor samples obtained from Apc$^{Min/+}$ADAM17$^{wt/wt}$ mice (n=5) and 5 tumor samples obtained from Apc$^{Min/+}$ADAM17$^{ex/ex}$ mice (n=2) were compared to three tissue samples from wildtype (n=1). Unpaired t test with Welch´s correction.

To address the question whether the altered number of neoplasia in Apc$^{Min/+}$ADAM17$^{ex/ex}$ mice was mediated by other receptor tyrosine kinases, the transcript levels of mRNA coding for *c-Met* (Fig. 46 A) and the corresponding ligand hepatocyte growth factor (HGF) were measured (Fig. 46 B). It was documented that upregulation of the proto-oncogene *c-Met* is correlated with colon cancer progression (Di Renzo et al., 1995). No significant amplification of *c-Met* transcripts was detectable in neither Apc$^{Min/+}$ADAM17$^{ex/ex}$ mice nor in Apc$^{Min/+}$ADAM17$^{wt/wt}$ mice when compared to ADAM17$^{wt/wt}$ mice. The transcript levels of mRNA coding for *HGF* was elevated similarly in both Apc$^{Min/+}$ strains.

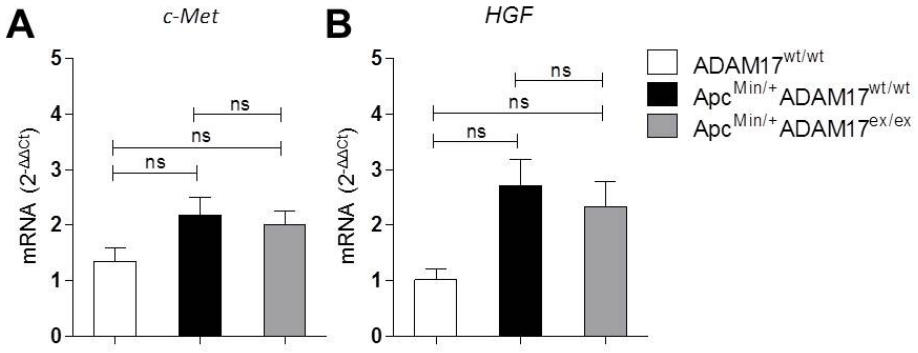

Fig. 46: qRT-PCR analysis of c-Met pathway from Apc$^{Min/+}$ADAM17$^{wt/wt}$ mice and hypomorphic Apc$^{Min/+}$ADAM17$^{ex/ex}$ mice tissue.

10 tumor samples obtained from Apc$^{Min/+}$ADAM17$^{wt/wt}$ mice (n=5) and 5 tumor samples obtained from Apc$^{Min/+}$ADAM17$^{ex/ex}$ mice (n=2) were compared to three tissue samples from wildtype (n=1). Unpaired t test with Welch´s correction.

Consistent with the constitutively activated Wnt pathway in $Apc^{Min/+}$ mice, both mouse strains $Apc^{Min/+}ADAM17^{ex/ex}$ and $Apc^{Min/+}ADAM17^{wt/wt}$ revealed increased mRNA levels encoding for Wnt target genes such as *c-Myc*, *Claudin-1*, *Axin-2*, *Sox17* and *Sox9* in comparison to $ADAM17^{wt/wt}$ mice, while *MMP13* levels were indistinguishable in both $Apc^{Min/+}$ strains compared to $ADAM17^{wt/wt}$ mice (Fig. 47 A-G). Only mRNA encoding *c-Myc* showed a significant downregulation in hypomorphic $Apc^{Min/+}ADAM17^{ex/ex}$ compared to $Apc^{Min/+}ADAM17^{wt/wt}$ mice (Fig. 47 A). However, mRNA encoding for *Sox9* showed a significant upregulation in hypomorphic $Apc^{Min/+}ADAM17^{ex/ex}$ compared to $Apc^{Min/+}ADAM17^{wt/wt}$ mice (Fig. 47 F).

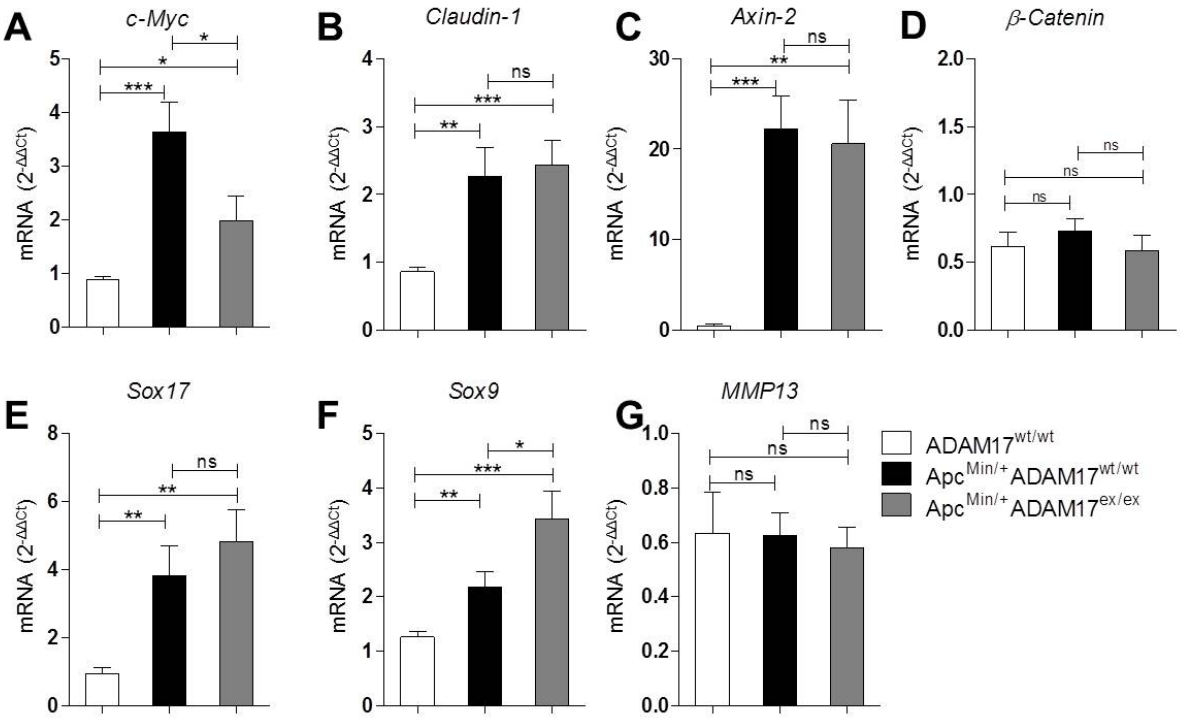

Fig. 47: qRT-PCR analysis of Wnt target genes from $Apc^{Min/+}ADAM17^{wt/wt}$ mice and hypomorphic $Apc^{Min/+}ADAM17^{ex/ex}$ mice tissue.

10 tumor samples obtained from $Apc^{Min/+}ADAM17^{wt/wt}$ mice (n=5) and 5 tumor samples obtained from $Apc^{Min/+}ADAM17^{ex/ex}$ mice (n=2) were compared to three tissue samples from wildtype (n=1). Unpaired t test with Welch´s correction.

To analyze target genes involved in the formation of neoplasia in $Apc^{Min/+}ADAM17^{ex/ex}$ mice and $Apc^{Min/+}ADAM17^{wt/wt}$ mice, further quantitative real-time PCR analysis focusing on the expression of mRNAs involved in IL-6 signaling was performed (Fig. 48 A-D). A marked increase in mRNA levels of *IL-6* and *IL-6R* in both $Apc^{Min/+}$ strains were observed compared to $ADAM17^{wt/wt}$ mice (Fig. 48 A and B), but only similar mRNA levels of *IL6ST* (also known as

glycoprotein 130) and the STAT3 target gene *BIRC5* also known as *Survivin* (Fig. 48 C and D).

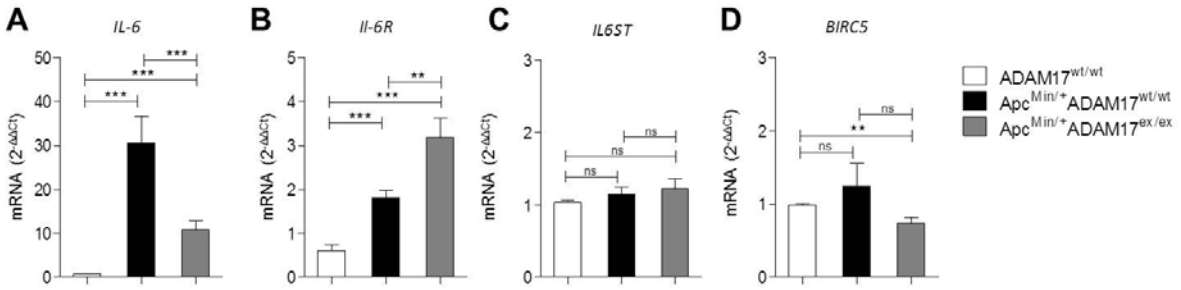

Fig. 48: qRT-PCR analysis of IL-6 pathway from Apc$^{Min/+}$ADAM17$^{wt/wt}$ mice and hypomorphic Apc$^{Min/+}$ADAM17$^{ex/ex}$ mice tissue.

26 tumor samples obtained from Apc$^{Min/+}$ADAM17$^{wt/wt}$ mice (n=7) and 10 tumor samples obtained from Apc$^{Min/+}$ADAM17$^{ex/ex}$ mice (n=4) were compared to three tissue samples from wildtype (n=1). Unpaired t test with Welch´s correction.

To analyze another pathway involved in the regulation of proliferation and apoptosis, the transcriptional coactivator YAP-1, corresponding to the Hippo signaling pathway, was investigated (Fig. 49 A-D). It was recently published that dysregulated YAP signaling contribute to epithelial cell proliferation along with aberrant cell differentiation and additional loss of APC leads to an upregulation and activation of YAP, Src family kinases, gp130 and STAT3 in colon carcinogenesis (Taniguchi et al., 2015, Taniguchi et al., 2017).

Apc$^{Min/+}$ADAM17$^{wt/wt}$ mice showed significantly increased mRNA levels of the proto-oncogene *YAP-1*, the serine/threonine kinase *LATS1* and the correlated target genes *Ctgf* (connective tissue growth factor) and *Cyr61* compared to ADAM17$^{wt/wt}$ mice. In contrast, Apc$^{Min/+}$ADAM17$^{ex/ex}$ mice showed a reduction of these mRNA transcripts. However, in Apc$^{Min/+}$ADAM17$^{ex/ex}$ mice significant decreased mRNA levels for *YAP-1*, *Ctgf* and *Cyr61* were measured compared to Apc$^{Min/+}$ADAM17$^{wt/wt}$ mice.

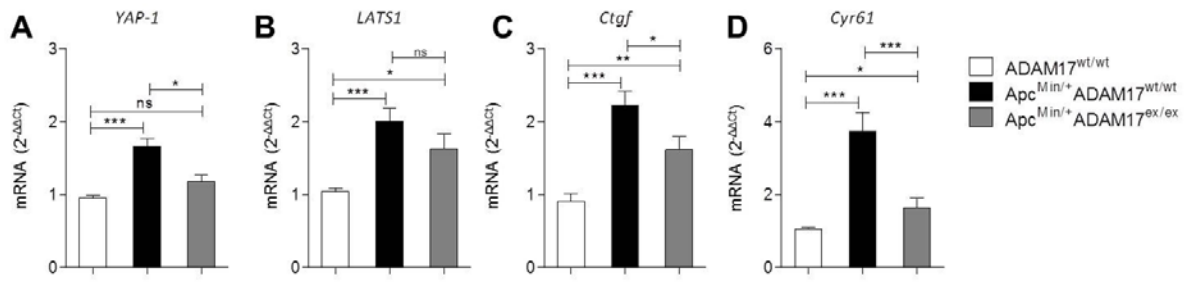

Fig. 49: qRT-PCR analysis of Hippo/YAP-pathway from $Apc^{Min/+}ADAM17^{wt/wt}$ mice and hypomorphic $Apc^{Min/+}ADAM17^{ex/ex}$ mice tissue.

26 tumor samples obtained from $Apc^{Min/+}ADAM17^{wt/wt}$ mice (n=7) and 10 tumor samples obtained from $Apc^{Min/+}ADAM17^{ex/ex}$ mice (n=4) were compared to three tissue samples from wildtype (n=1). Unpaired t test with Welch´s correction.

3.3.6 CHARACTERIZATION OF ORGANOIDS DERIVED FROM $APC^{MIN/+}ADAM17^{ex/ex}$ MICE

To address the question which cell type is mainly responsible for Amphiregulin expression and release within the small intestine, I established an *ex vivo* organoid culture system using intestinal epithelial cells (IEC) from $Apc^{Min/+}ADAM17^{ex/ex}$ mice and $Apc^{Min/+}ADAM17^{wt/wt}$ mice as well as unchallenged healthy hypomorphic $ADAM17^{ex/ex}$ mice and $ADAM17^{wt/wt}$ mice (Fig. 67; additional results). The advantage of *ex vivo* organoid cultures was to analyze intestinal epithelial cells beyond the intestinal niche and in the absence of their microenvironment.

Isolated crypts from indicated mouse strains were used to generate an *ex vivo* three-dimensional organoid culture system as described in subchapter 2.3. Primary organoids generated from $Apc^{Min/+}ADAM17^{ex/ex}$ mice and $Apc^{Min/+}ADAM17^{wt/wt}$ mice were counted and sized. The number of primary organoids received from $Apc^{Min/+}ADAM17^{wt/wt}$ mice were significantly increased compared to the number of hypomorphic $Apc^{Min/+}ADAM17^{ex/ex}$ organoids (Fig. 50 A). Interestingly, the determined size of hypomorphic $Apc^{Min/+}ADAM17^{ex/ex}$ organoids was slightly decreased in comparison to $Apc^{Min/+}ADAM17^{wt/wt}$ organoids (Fig. 50 B).

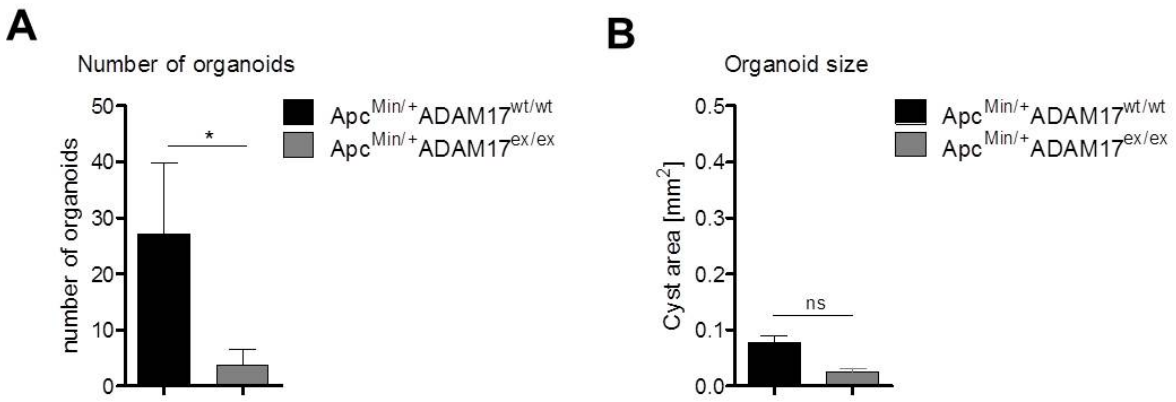

Fig. 50: Number and size of primary organoids from hypomorphic Apc$^{Min/+}$ADAM17$^{ex/ex}$ mice.

Primary organoids isolated from the small intestine of 24-week-old Apc$^{Min/+}$ADAM17$^{wt/wt}$ mice (n=6) and Apc$^{Min/+}$ADAM17$^{ex/ex}$ mice (n=9). (A) Number and (B) size of organoids formed 10 days after isolation. Mann Whitney test.

Microscopic characterization of established Apc$^{Min/+}$ organoids from both genotypes demonstrated different morphology compared to organoids from healthy unchallenged hypomorphic ADAM17$^{ex/ex}$ mice and ADAM17$^{wt/wt}$ mice due to insufficient cell differentiation (Fig. 51 A and B and Fig. 67 A and B; additional results). Constitutively active Wnt signaling in Apc$^{Min/+}$ organoids negatively affected cell lineage differentiation within the crypt-villus-unit which lead to spherically shaped organoids in both Apc$^{Min/+}$ genotypes without significant morphological differences.

Organoids established from healthy unchallenged hypomorphic ADAM17$^{ex/ex}$ mice and ADAM17$^{wt/wt}$ mice maintained under basal culture medium (BCM) culture conditions, proliferated and differentiated in a physiological manner and retained crypt-villus-units. These retained crypt-villus-units were identifiable by budded organoid structures (Fig. 51 C and D and Fig. 67 C and D; additional results). As expected, no differences regarding organoid shape or organoid size between healthy unchallenged hypomorphic ADAM17$^{ex/ex}$ mice and ADAM17$^{wt/wt}$ mice were detectable.

Further characterization via immunofluorescence analysis revealed lack of expression of Muc2 as goblet cell marker and MMP7 as Paneth cell marker in organoids originated from hypomorphic Apc$^{Min/+}$ADAM17$^{ex/ex}$ mice and Apc$^{Min/+}$ADAM17$^{wt/wt}$ mice (Fig. 51 C and D).

Accumulation of ß-Catenin thereupon lead to constitutively active Wnt signaling which in turn lead to a total loss of differentiated goblet cells and Paneth cells in both Apc$^{Min/+}$ organoids. Thereby, the impaired cell differentiation mediated by constitutively activated Wnt signaling was confirmed for both genotypes under *ex vivo* conditions.

In comparison to the previous observations, immunofluorescence experiments of organoids originated from healthy unchallenged hypomorphic ADAM17$^{ex/ex}$ mice and ADAM17$^{wt/wt}$ mice, confirmed physiological differentiation of specific intestinal cell types such as goblet cells and Paneth cells in mature organoid crypt-villus-units by positive Muc2 and MMP7 staining (Fig. 67 C and D; additional results).

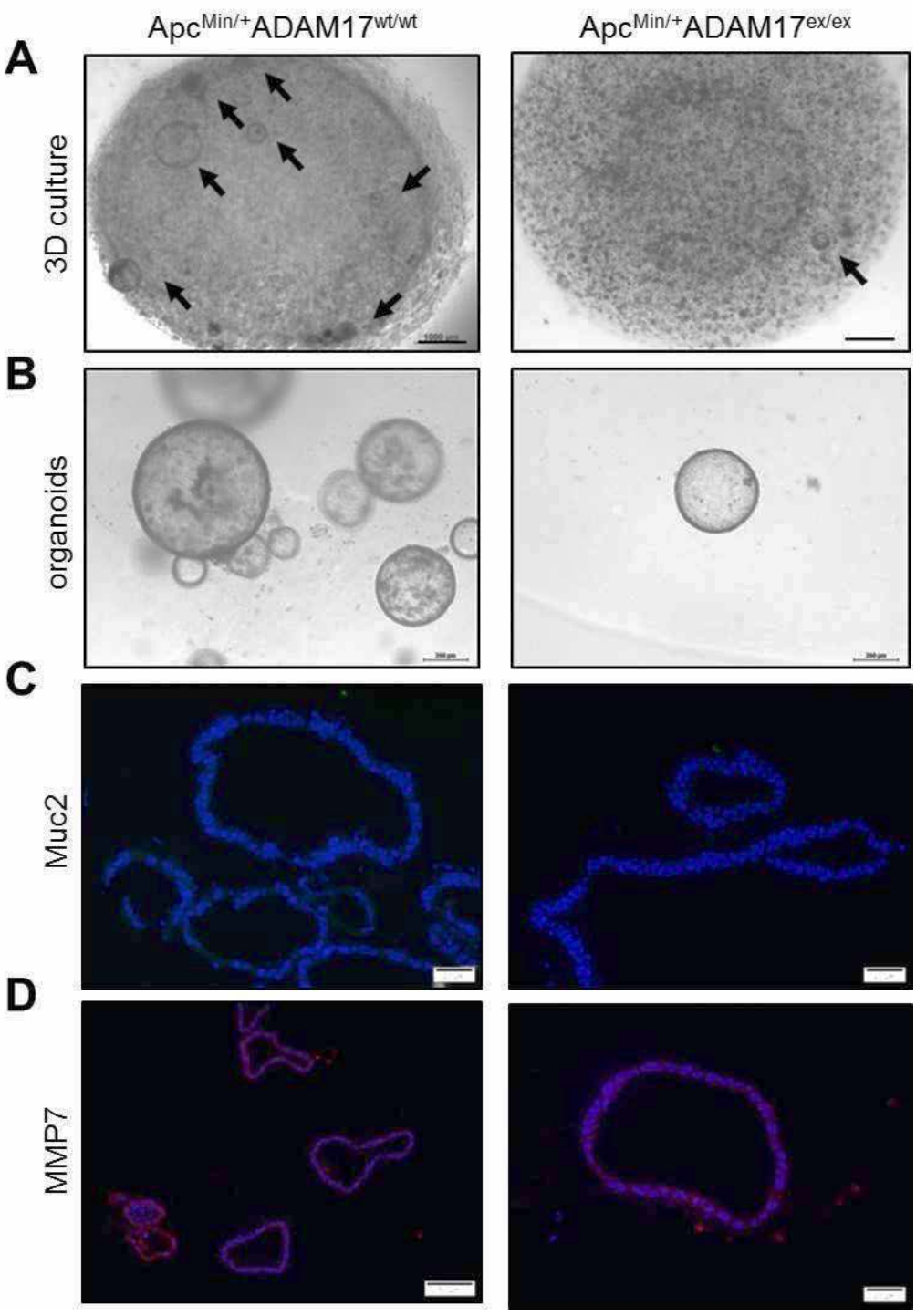

Fig. 51: Representative images of Apc$^{Min/+}$ADAM17$^{ex/ex}$ organoid cultures.

Representative images of (A) 3D organoid cultures, (B) 10 x magnification of single organoids. and immunofluorescence analysis of organoids stained for (C) Mucin 2 (Muc2) as goblet cell marker and (D) Matrix metalloproteinase 7 (MMP7) as marker for Paneth cells.

Due to constitutively activated Wnt signaling, organoid cultures derived from Apc$^{Min/+}$ADAM17$^{ex/ex}$ mice as well as Apc$^{Min/+}$ADAM17$^{wt/wt}$ mice formed adenomatous spherical structures independent of additional R-Spondin-1 or Wnt3a. After several passages, organoids from Apc$^{Min/+}$ADAM17$^{ex/ex}$ mice as well as Apc$^{Min/+}$ADAM17$^{wt/wt}$ mice

were still morphological comparable and kept their spherical shape and size as shown in Fig. 51 A and B and simplified in model of Fig. 52.

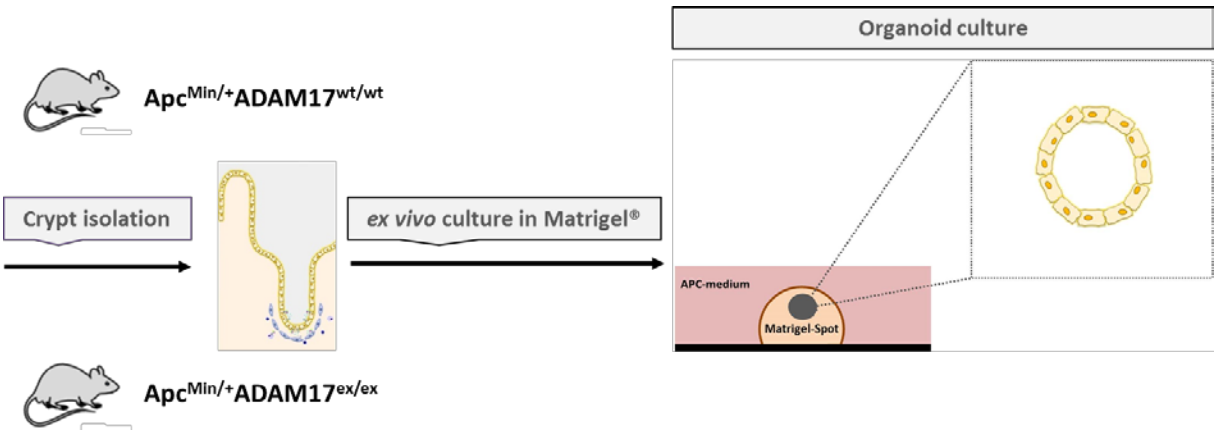

Fig. 52: Model of the generation of murine intestinal Apc$^{Min/+}$ organoids cultured in APC tumor medium.

Murine intestinal crypts from Apc$^{Min/+}$ADAM17$^{wt/wt}$ mice and hypomorphic Apc$^{Min/+}$ADAM17$^{ex/ex}$ mice were isolated and cultured *ex vivo* in Matrigel® GFR with APC tumor medium. Apc$^{Min/+}$ organoids showed characteristic spherical structures with intestinal lumen-like cavity. Adapted from (Schuijers and Clevers, 2012, Barker, 2014).

Organoids from ADAM17$^{ex/ex}$ mice and ADAM17$^{wt/wt}$ mice cultured in APC tumor medium were not able to proliferate and survive without the Wnt pathway supporting supplements R-Spondin-1 and Wnt3a (data not shown).

Regarding the characterization of derived organoids from hypomorphic Apc$^{Min/+}$ADAM17$^{ex/ex}$ mice and Apc$^{Min/+}$ADAM17$^{wt/wt}$ mice, the protein expression of ADAM17 was assessed by Western blot analysis (Fig. 53). In the interest of a basal characterization, ADAM17 protein expression in organoids from unchallenged healthy ADAM17$^{ex/ex}$ mice and ADAM17$^{wt/wt}$ mice was determined as well.

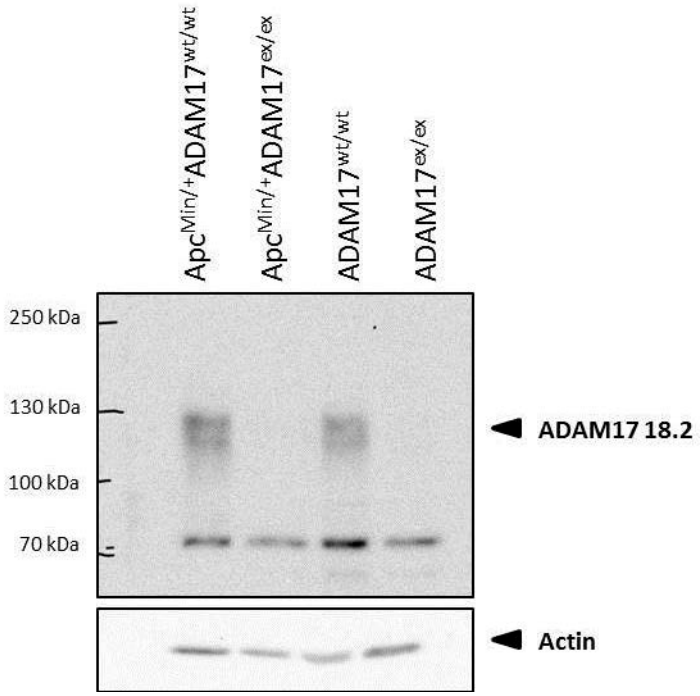

Fig. 53: ADAM17 protein expression in organoids.

Indicated organoids were lysed and 50 µg of total protein were analyzed. ADAM17 protein expression was assessed by Western blot analysis using a polyclonal anti-ADAM17 antibody (18.2).

As expected, the Western blot results revealed a lack of ADAM17 protein expression in $Apc^{Min/+}ADAM17^{ex/ex}$ or hypomorphic $ADAM17^{ex/ex}$ organoids. ADAM17 was detectable in lysates of $ADAM17^{wt/wt}$ organoids and $Apc^{Min/+}ADAM17^{wt/wt}$ organoids. The amount of ADAM17 protein in $Apc^{Min/+}ADAM17^{wt/wt}$ organoid lysates was slightly increased.

In line with these observations, the mRNA level of ADAM17 in $Apc^{Min/+}ADAM17^{wt/wt}$ organoids was significantly increased compared to unchallenged healthy $ADAM17^{wt/wt}$ organoids and $Apc^{Min/+}ADAM17^{ex/ex}$ organoids (Fig. 54).

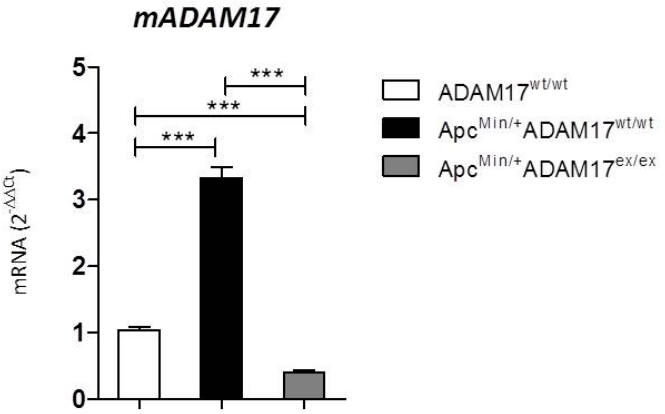

Fig. 54: qRT-PCR analysis of ADAM17 from Apc$^{Min/+}$ADAM17$^{wt/wt}$ and hypomorphic Apc$^{Min/+}$ADAM17$^{ex/ex}$ organoids.

Organoids obtained from Apc$^{Min/+}$ADAM17$^{wt/wt}$ mice and Apc$^{Min/+}$ADAM17$^{ex/ex}$ mice were compared to organoids from wildtype mice. Real-time PCR analysis of mRNA expression from ADAM17 in indicated organoids from four independent experiments. qRT PCR data were normalized to GAPDH. Unpaired t test with Welch´s correction.

For further characterization of Apc$^{Min/+}$ADAM17$^{ex/ex}$ or Apc$^{Min/+}$ADAM17$^{wt/wt}$ derived organoids, the transcriptional levels of mRNA encoding for EGFR was significantly increased in both Apc$^{Min/+}$ organoids (Fig. 55 A). In addition, analysis of mRNA encoding for AREG revealed significantly elevated levels in both Apc$^{Min/+}$ organoids by threefold (Fig. 55 B).

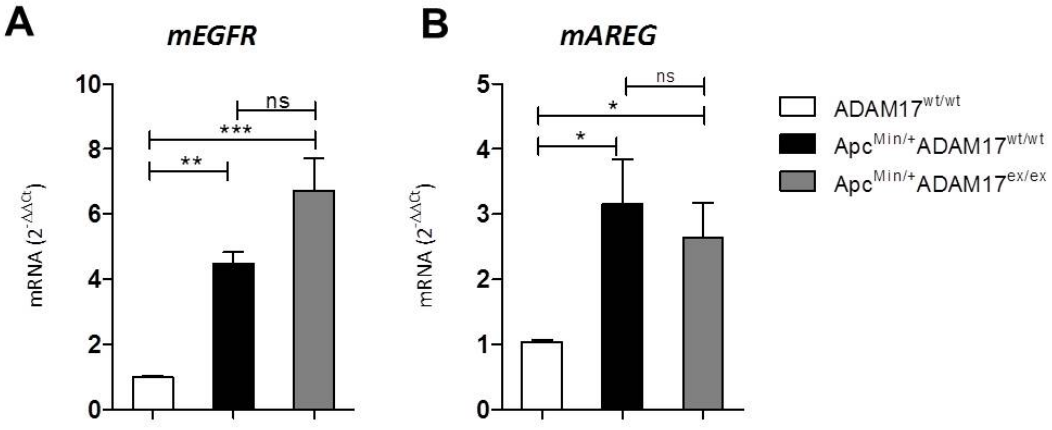

Fig. 55: qRT-PCR analysis of EGFR and AREG from Apc$^{Min/+}$ADAM17$^{wt/wt}$ and hypomorphic Apc$^{Min/+}$ADAM17$^{ex/ex}$ organoids.

Organoids obtained from Apc$^{Min/+}$ADAM17$^{wt/wt}$ mice and Apc$^{Min/+}$ADAM17$^{ex/ex}$ mice were compared to organoids from wildtype mice. Real-time PCR analysis of mRNA expression of (A) epidermal growth factor receptor (EGFR) and (B) Amphiregulin (AREG) in indicated organoids from four independent experiments. qRT-PCR data were normalized to GAPDH. Unpaired t test with Welch´s correction.

Because Wnt signaling plays a key role in the $Apc^{Min/+}$ model, selected target genes of the Wnt pathway were measured by quantitative real-time PCR in organoids. As expected, the amount of mRNA transcripts encoding for *c-Myc* and *Axin-2* in organoids originated from $Apc^{Min/+}ADAM17^{ex/ex}$ mice and $Apc^{Min/+}ADAM17^{wt/wt}$ mice was significantly elevated compared to $ADAM17^{wt/wt}$ organoids (Fig. 56). The mRNA levels for *Axin-2* was equally increased in both $Apc^{Min/+}$ organoids (Fig. 56 B). Interestingly, the mRNA transcripts encoding for *c-Myc* was increased by twofold in $Apc^{Min/+}ADAM17^{wt/wt}$ organoids in comparison to $Apc^{Min/+}ADAM17^{ex/ex}$ organoids (Fig. 56 A).

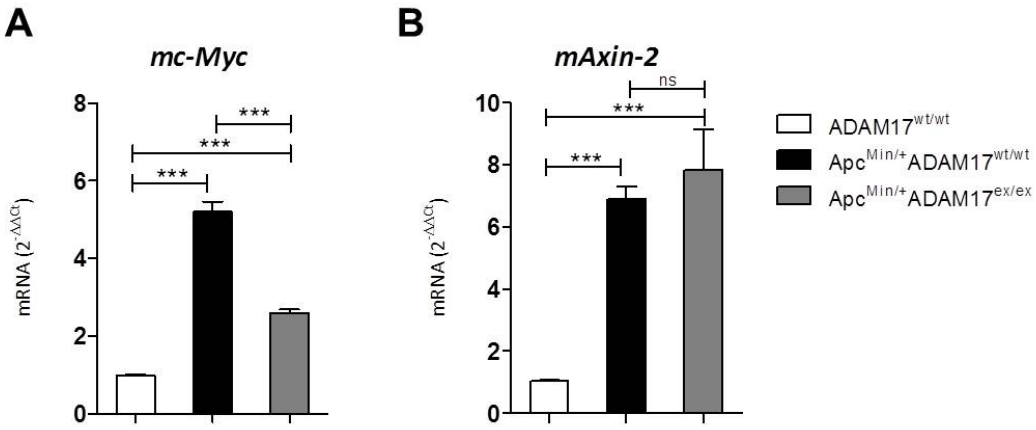

Fig. 56: qRT-PCR analysis of Wnt target genes from $Apc^{Min/+}ADAM17^{wt/wt}$ and hypomorphic $Apc^{Min/+}ADAM17^{ex/ex}$ organoids.

Organoids obtained from $Apc^{Min/+}ADAM17^{wt/wt}$ mice and $Apc^{Min/+}ADAM17^{ex/ex}$ mice were compared to organoids from wildtype mice. Real-time PCR analysis of mRNA expression of (A) c-Myc and (B) Axin-2 in indicated organoids from four independent experiments. qRT-PCR data were normalized to GAPDH. Unpaired t test with Welch´s correction.

Additionally, the mRNA profile of the IL-6 signaling pathway in $Apc^{Min/+}$ organoids was analyzed. Unfortunately, the mRNA level of Interleukin-6 (*IL-6*) could not be detected even after several repetitions (Fig. 57 A) in any specimen. Instead, the amount of mRNA encoding for the Interleukin-6 receptor (*IL-6R*) was significantly elevated in both $Apc^{Min/+}$ organoids compared to $ADAM17^{wt/wt}$ organoids. In $Apc^{Min/+}ADAM17^{ex/ex}$ organoids, the mRNA levels of *IL-6R* was reduced by one fifth (Fig. 57 B). The results for *IL6ST*, also known as *gp130* (glycoprotein 130), revealed more than a half-elevated mRNA levels in $Apc^{Min/+}ADAM17^{ex/ex}$ organoids compared to $Apc^{Min/+}ADAM17^{wt/wt}$ organoids (Fig. 57 C). However, the quantity of mRNA transcripts for the target gene *BIRC5*, also known as the inhibitor of apoptosis protein Survivin, was significantly increased only in $Apc^{Min/+}ADAM17^{wt/wt}$ organoids (Fig. 57 D). The number of *BIRC5* mRNA transcripts was similar in $Apc^{Min/+}ADAM17^{ex/ex}$ organoids and $ADAM17^{wt/wt}$ organoids.

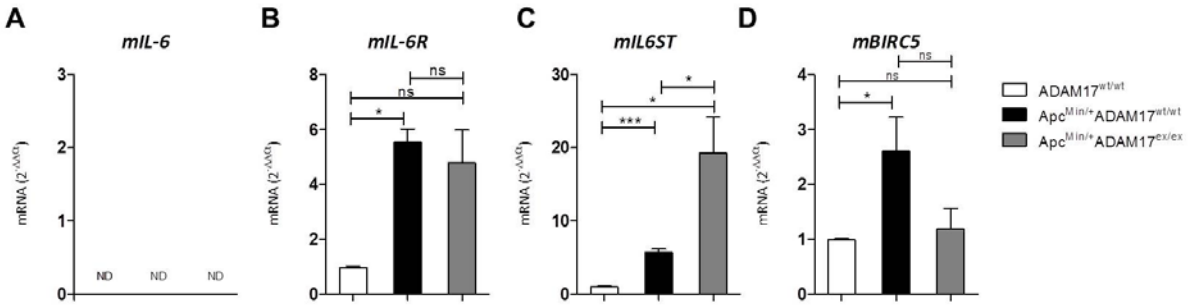

Fig. 57: qRT-PCR analysis of IL-6 pathway from Apc$^{Min/+}$ADAM17$^{wt/wt}$ and hypomorphic Apc$^{Min/+}$ADAM17$^{ex/ex}$ organoids.

Organoids obtained from Apc$^{Min/+}$ADAM17$^{wt/wt}$ mice and Apc$^{Min/+}$ADAM17$^{ex/ex}$ mice were compared to organoids from wildtype mice. Real-time PCR analysis of mRNA expression of (A) Interleukin-6 (IL-6), (B) Interleukin-6 receptor (IL-6R), (C) IL6ST (also known gp130) and (D) BIRC5 in indicated organoids from four independent experiments. qRT-PCR data were normalized to GAPDH. Unpaired t test with Welch´s correction.

The proto-oncogene *YAP-1* is known to play a key role during intestinal homeostasis, regeneration and cancer initiation (Gregorieff et al., 2015). Therefore, the mRNA signature for Hippo/YAP signaling pathway related target genes like *YAP-1* were tested via quantitative real-time PCR (Fig. 58). Organoids generated from Apc$^{Min/+}$ADAM17$^{wt/wt}$ mice and Apc$^{Min/+}$ADAM17$^{ex/ex}$ mice showed increased mRNA levels of *YAP-1*, the serine/threonine kinase *LATS1* and the linked target genes *Ctgf* and *Cyr61* compared to ADAM17$^{wt/wt}$ mice organoids. In both Apc$^{Min/+}$ organoids the levels of mRNA encoding for *YAP-1* and *LATS1* were comparable and showed a threefold increase compared to ADAM17$^{wt/wt}$ organoids (Fig. 58 A and B). The amount of *Ctgf* mRNA in Apc$^{Min/+}$ADAM17$^{ex/ex}$ organoids was half as much increased as in Apc$^{Min/+}$ADAM17$^{wt/wt}$ organoids. Such a significant difference was not observed in *Cyr61* mRNA levels (Fig. 58 C). However, in Apc$^{Min/+}$ADAM17$^{ex/ex}$ organoids the amount of *Cyr61* mRNA was slightly enhanced (Fig. 58 D).

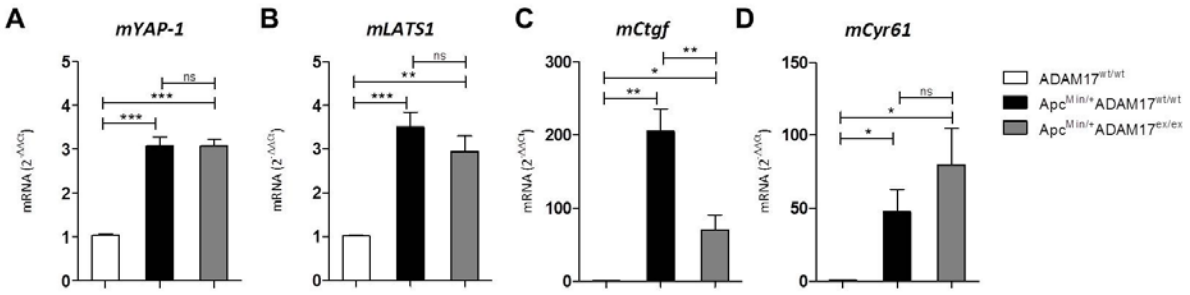

Fig. 58: qRT-PCR analysis of Hippo/YAP pathway from Apc$^{Min/+}$ADAM17$^{wt/wt}$ and hypomorphic Apc$^{Min/+}$ADAM17$^{ex/ex}$ mice organoids.

Organoids obtained from Apc$^{Min/+}$ADAM17$^{wt/wt}$ mice and Apc$^{Min/+}$ADAM17$^{ex/ex}$ mice were compared to organoids from wildtype mice. Real-time PCR analysis of mRNA expression of (A) YAP-1, (B) LATS1, (C) Ctgf and (D) Cyr61 in indicated organoids from four independent experiments. qRT-PCR data were normalized to GAPDH. Unpaired t test with Welch´s correction.

3.3.7 Organoids from Apc$^{Min/+}$ADAM17$^{ex/ex}$ mice show less Amphiregulin shedding

As observed *in vitro* in various human colorectal cancer cells (see subchapter 3.1), ADAM17 is able to cleave Amphiregulin. Indeed, a dependency between ADAM17 and soluble Amphiregulin was detected *ex vivo* in intestinal tissue by performing ELISA experiments from the supernatant of intestinal cultures as described in subchapter 2.5.2. The amount of soluble Amphiregulin in the supernatant of intestinal cultures from Apc$^{Min/+}$ADAM17$^{ex/ex}$ mice was reduced by half compared to the supernatant of intestinal cultures from Apc$^{Min/+}$ADAM17$^{wt/wt}$ mice (Fig. 59 A). Additionally, the influence of absent ADAM17 protein expression in Apc$^{Min/+}$ADAM17$^{ex/ex}$ mice regarding IL-6 and IL-6R release was investigated in intestinal cultures. As shown in Fig. 59 B and C, no differences in the amount of soluble IL-6 or IL-6R were detectable in both genotypes.

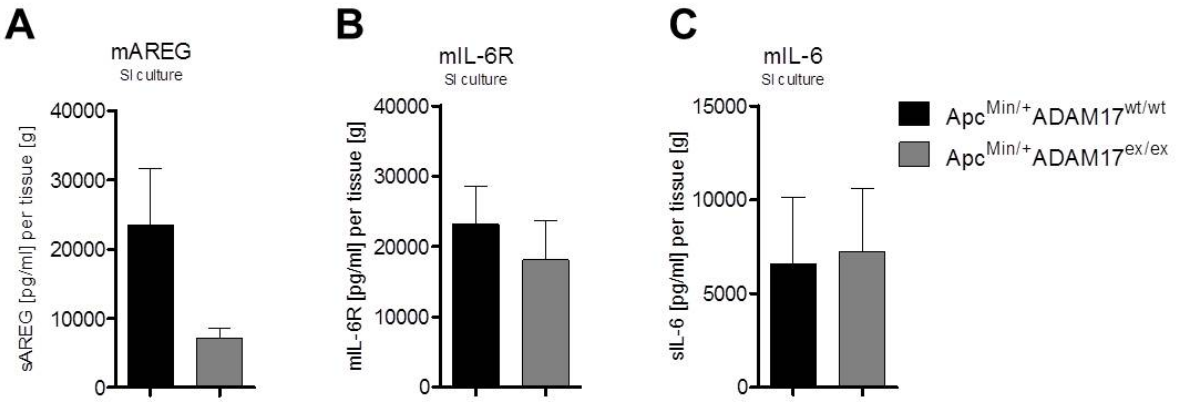

Fig. 59: Levels of soluble proteins in intestinal cultures from hypomorphic $Apc^{Min/+}ADAM17^{ex/ex}$ mice.

Three independent tissue pieces of each mouse were washed with PBS containing Pen/Strep and incubated in DMEM medium at 37 °C for 24 h (n=3-5 per group). Supernatants were harvested and measured by ELISA for soluble (A) Amphiregulin (AREG), (B) Interleukin-6 receptor (IL-6R) and (C) Interleukin-6 (IL-6). Unpaired t test with Welch´s correction.

Vice versa, the amount of membrane bound Amphiregulin in intestinal tissue lysates of $Apc^{Min/+}ADAM17^{ex/ex}$ mice was increased by twofold compared to intestinal tissue lysates of $Apc^{Min/+}ADAM17^{wt/wt}$ mice (Fig. 59 A). The results for IL-6R or IL-6 revealed no significant difference between the genotypes whereby IL-6 was not detectable in tissue lysates (Fig. 59 B and C).

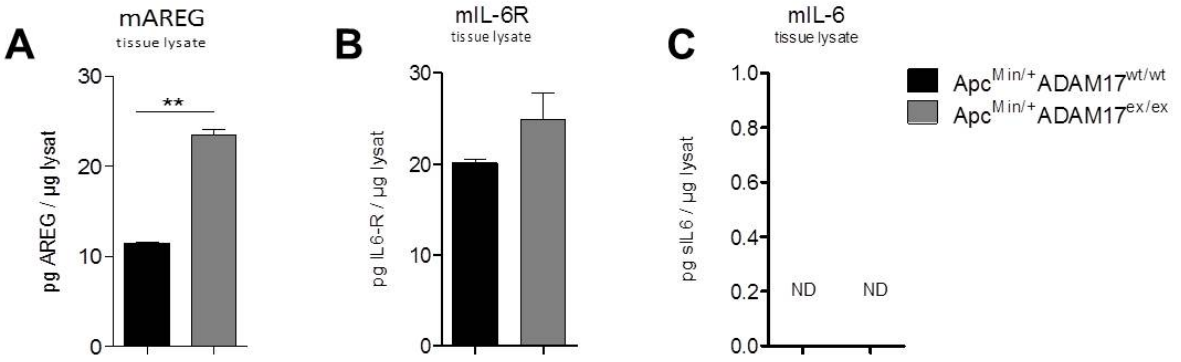

Fig. 60: Amount of proteins in tissue lysate from hypomorphic $Apc^{Min/+}ADAM17^{ex/ex}$ mice.

Tissue lysates from small intestine of $Apc^{Min/+}ADAM17^{wt/wt}$ mice (n=2) and $Apc^{Min/+}ADAM17^{ex/ex}$ mice (n=2) were measured by ELISA for (A) Amphiregulin (AREG), (B) Interleukin-6 receptor (IL-6R) and (C) Interleukin-6 (IL-6). Unpaired t test with Welch´s correction.

To confirm the previous observations in human colorectal cancer cells regarding ADAM17-mediated Amphiregulin shedding, the three-dimensional organoid culture system was utilized to analyze the role of ADAM17-dependent shedding in isolated intestinal epithelial cells from $Apc^{Min/+}$ mice.

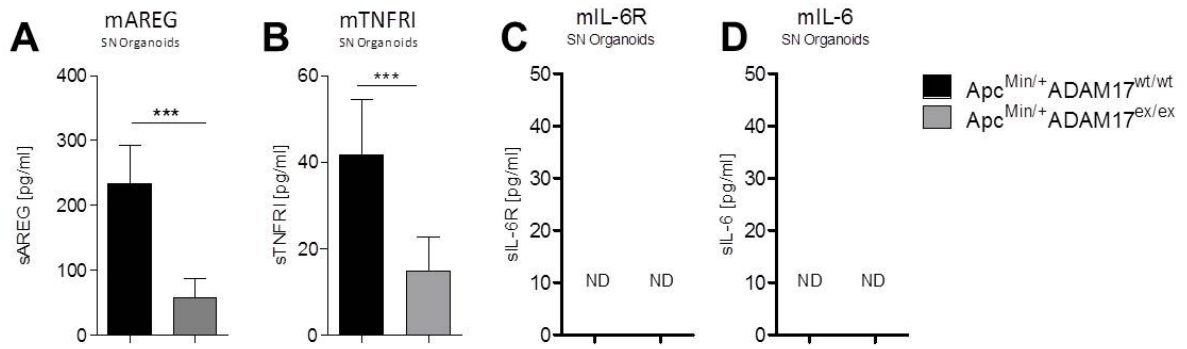

Fig. 61: Levels of soluble proteins in the supernatant of $Apc^{Min/+}$ organoid cultures.

Primary organoids isolated from the small intestine of 24-week-old $Apc^{Min/+}ADAM17^{wt/wt}$ mice (n=6) and $Apc^{Min/+}ADAM17^{ex/ex}$ mice (n=9). Supernatant of organoids formed 10 days after isolation measured by ELISA for soluble (A) Amphiregulin (AREG) (B) Tumor necrosis factor receptor I (TNFRI), (C) Interleukin-6 receptor (IL-6R) and (D) Interleukin-6 (IL-6). Mann Whitney test.

The quantity of soluble Amphiregulin in the supernatants of organoid cultures from $Apc^{Min/+}ADAM17^{ex/ex}$ mice were significantly reduced by two thirds compared to the supernatants of intestinal cultures from $Apc^{Min/+}ADAM17^{wt/wt}$ mice (Fig. 61 A). To verify that the observed effect was related to ADAM17, the amount of soluble TNFRI (Tumor necrosis factor receptor I), a known ADAM17 substrate (Reddy et al., 2000), was measured as well. As expected, the amount of shed TNFRI in the supernatants of organoid cultures from $Apc^{Min/+}ADAM17^{ex/ex}$ mice were significantly reduced compared to $Apc^{Min/+}ADAM17^{wt/wt}$ organoids (Fig. 61 B). Interestingly, neither shed IL-6R nor soluble IL-6 could be detected in the supernatants of organoid cultures from $Apc^{Min/+}$ mice (Fig. 61 C and D).

In the following experimental set up, organoid cultures from $Apc^{Min/+}$ mice were treated with protease inhibitors (Tab. 8) to assess the influence of ADAM17 activity on Amphiregulin shedding. To investigate the dependence of Amphiregulin shedding on ADAM17 inhibition both organoid cultures were treated with Marimastat (MM), a broad-spectrum matrix metalloprotease inhibitor, a selective inhibitor for ADAM10 (GI) and an ADAM10 and ADAM17 inhibitor (GW). To determine the amount of soluble Amphiregulin, the supernatants from organoids were harvested before (0 h) and after inhibitor treatment (72 h).

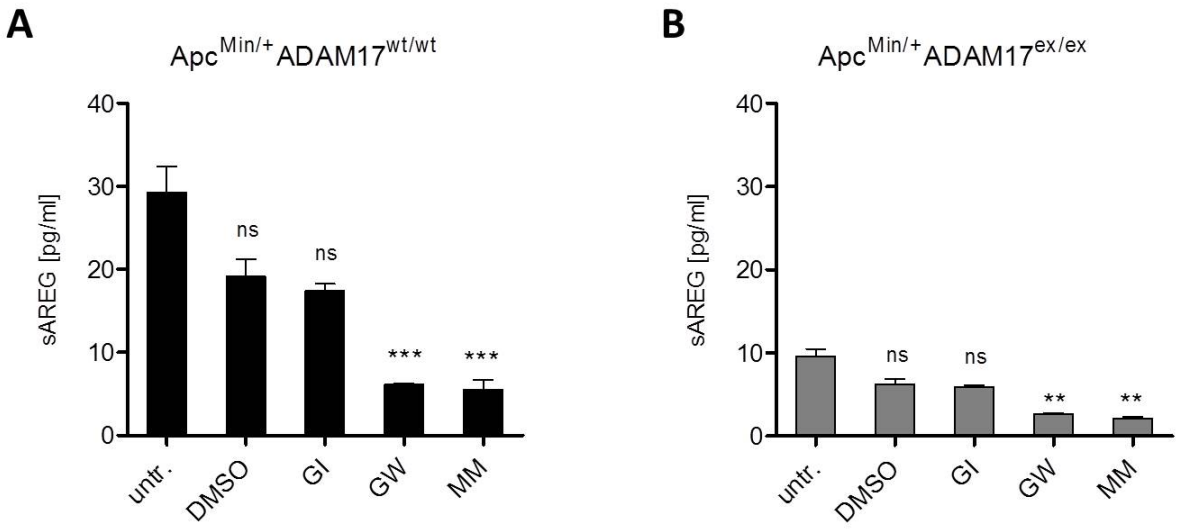

Fig. 62: Levels of soluble Amphiregulin in the supernatant of Apc$^{Min/+}$ organoid cultures after inhibitor treatment.

Organoids from (A) Apc$^{Min/+}$ADAM17$^{wt/wt}$ mice and (B) Apc$^{Min/+}$ADAM17$^{ex/ex}$ mice were cultured for 72 h in normal APC tumor medium (untr.) or mixed with DMSO for control as well as in the presence of GI (GI254023X, ADAM10-selective inhibitor, 30 µM), GW (GW280264X, ADAM10- and ADAM17-selective inhibitor, 30 µM) or MM (Marimastat, pan-metalloprotease inhibitor; 100 µM). Supernatants from organoids were measured by ELISA for soluble Amphiregulin. Values were normalized to organoid number per well. Kruskal-Wallis test.

The ELISA results in Fig. 62 showed that the ratio of soluble Amphiregulin in the DMSO treated controls versus untreated conditions among both Apc$^{Min/+}$ organoids was almost similar after 72 h. Compared to DMSO treated controls, the generation of soluble Amphiregulin was not affected by GI-mediated ADAM10 inhibition in both Apc$^{Min/+}$ organoids. However, the quantity of soluble Amphiregulin was drastically affected after 72 h GW inhibitor treatment. When ADAM17 was inhibited by GW, the amount of soluble Amphiregulin was markedly decreased by two-thirds in Apc$^{Min/+}$ADAM17$^{wt/wt}$ organoids (Fig. 62 A) as well as in Apc$^{Min/+}$ADAM17$^{ex/ex}$ organoids (Fig. 62 B). Marimastat treatment resulted in a decrease by two-thirds in both Apc$^{Min/+}$ organoids after 72 h as well. In summary, the generation of soluble Amphiregulin in organoid culture depends on ADAM17 activity.

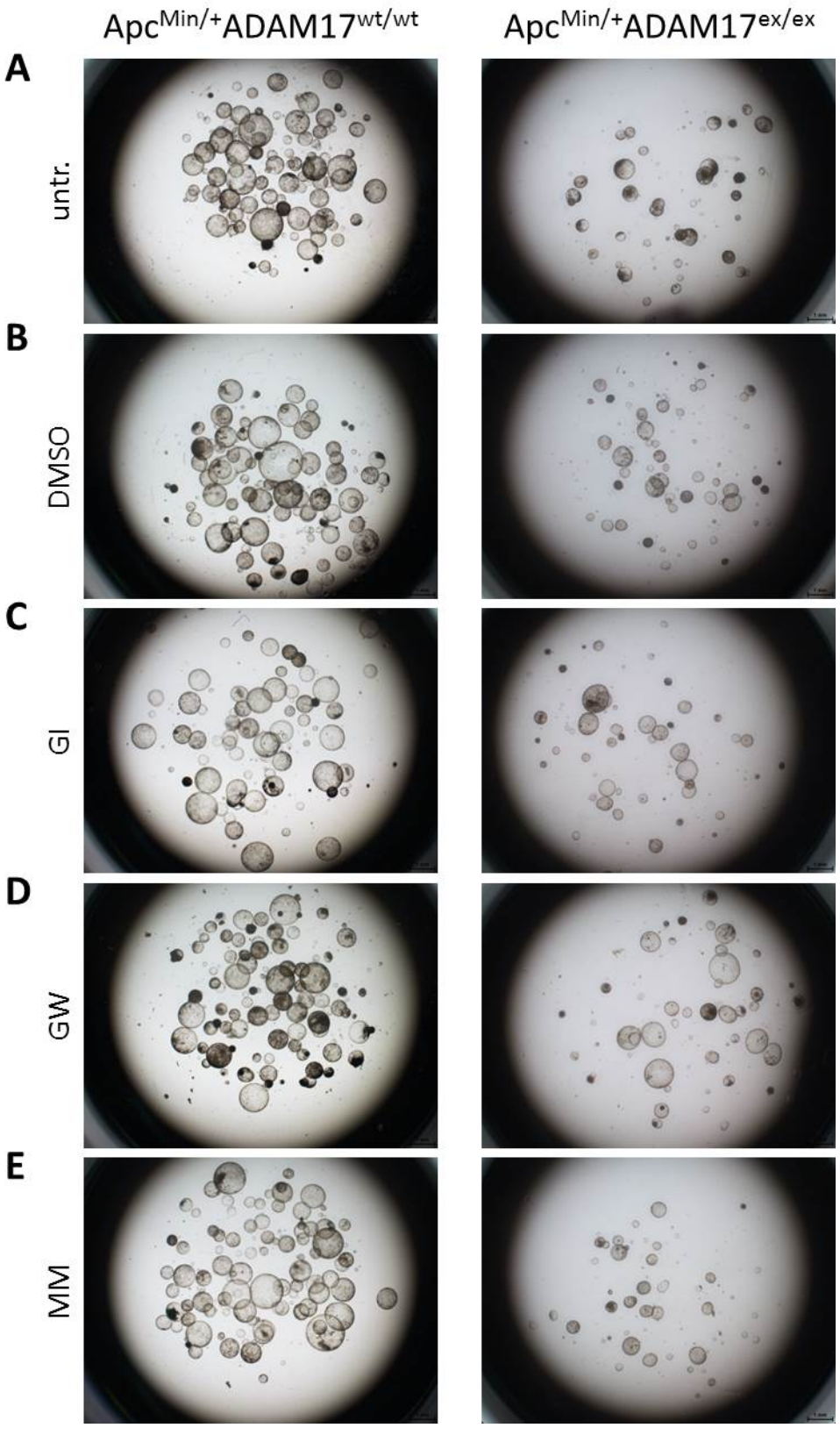

Fig. 63: Representative images of Apc$^{Min/+}$ organoid cultures after inhibitor treatment.

Organoids from Apc$^{Min/+}$ADAM17$^{wt/wt}$ mice and Apc$^{Min/+}$ADAM17$^{ex/ex}$ mice were cultured for 72 h in (A) normal APC tumor medium or mixed with (B) DMSO for control as well as in the presence of (C) GI (GI254023X, ADAM10-selective inhibitor, 30 µM), (D) GW (GW280264X, ADAM10- and ADAM17-selective inhibitor, 30 µM) or (E) MM (Marimastat, pan-metalloprotease inhibitor; 100 µM).

The inhibitor treatment did not cause changes to the morphology of treated organoids (Fig. 63 C-E) compared to controls (Fig. 63 A and B). $Apc^{Min/+}ADAM17^{wt/wt}$ organoids and hypomorphic $Apc^{Min/+}ADAM17^{ex/ex}$ organoids maintained their spherical shape and size during the whole experiment.

Ex vivo organoid cultures served as a system to test whether differentiated intestinal epithelial cells (IEC) or dedifferentiated IECs were indeed able to proliferate under special culture conditions. Organoids from both $Apc^{Min/+}$ mouse strains formed spheroids even in the absence of the Wnt signaling enhancers R-Spondin-1 and Wnt3a (Fig. 51 and 52). To investigate the importance of the EGFR signaling pathway in the $Apc^{Min/+}ADAM17^{ex/ex}$ organoid culture system, the established organoids were cultured in APC tumor medium without EGF (Tab. 7).

In order to assess the importance of EGFR ligands, organoid culture experiments were performed using APC tumor medium without EGF to assess the influence of Amphiregulin shedding on proliferation and maintenance of $Apc^{Min/+}$ organoids. Hypomorphic $Apc^{Min/+}ADAM17^{ex/ex}$ organoids and $Apc^{Min/+}ADAM17^{wt/wt}$ organoids were challenged with APC tumor medium lacking EGF to determine the plating efficiency and organoid size over two passages by microscopic examination.

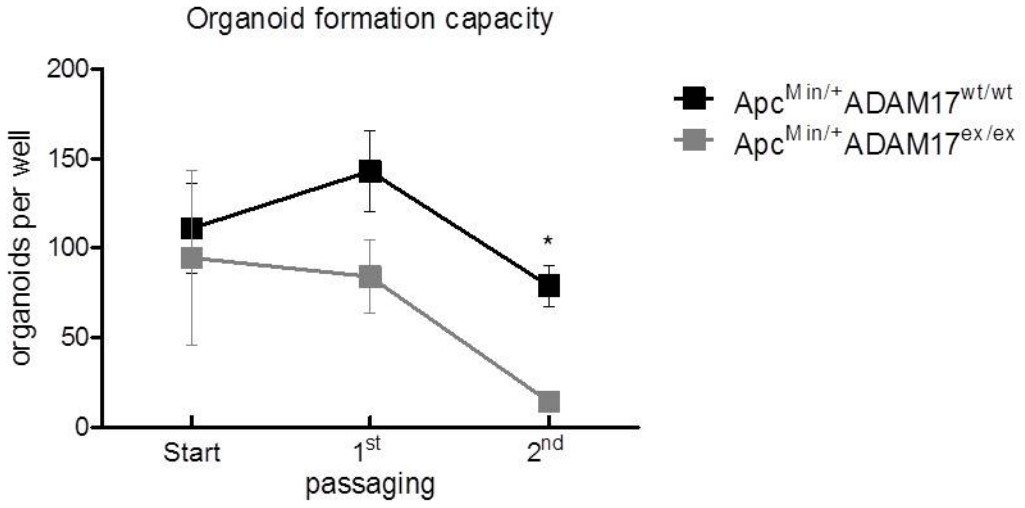

Fig. 64: Plating efficiency of $Apc^{Min/+}$ organoids without supplemented EGF.

Organoids from $Apc^{Min/+}ADAM17^{wt/wt}$ mice (n=3) and $Apc^{Min/+}ADAM17^{ex/ex}$ mice (n=1) were cultured in four independent wells of a 24 well plate in APC tumor medium without EGF over two passages. Each well was microscopically monitored and the number of organoids was counted. For passaging, one well was picked out, treated as described in subchapter 2.3.2 and plated in four independent wells in APC tumor medium without EGF. 2way ANOVA with Bonferroni posttest.

As depicted in Fig. 64, the organoid formation capacity measured by the number of organoids per well was significantly decreased in $Apc^{Min/+}ADAM17^{ex/ex}$ organoids after two passages compared to $Apc^{Min/+}ADAM17^{wt/wt}$ organoids.

Furthermore, the organoid size of both $Apc^{Min/+}$ organoid cultures was measured during the experiment. The withdrawal of EGF over two passages led to smaller organoids (Fig. 65).

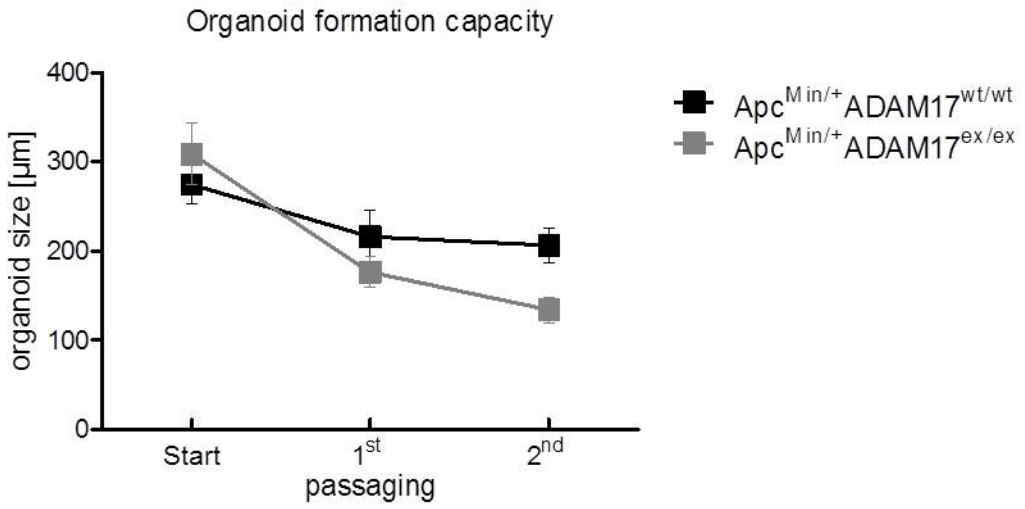

Fig. 65: Growth of $Apc^{Min/+}$ organoids without supplemented EGF.

Organoids from $Apc^{Min/+}ADAM17^{wt/wt}$ mice (n=3) and $Apc^{Min/+}ADAM17^{ex/ex}$ (n=1) mice were cultured in four independent wells of a 24 well plate in APC tumor medium without EGF over two passages. Each well was microscopically monitored and the size of organoids was measured. For passaging, one well was picked out, treated as described in subchapter 2.3.2 and plated in four independent wells in APC tumor medium without EGF. 2way ANOVA with Bonferroni posttest.

This effect was increased in hypomorphic $Apc^{Min/+}ADAM17^{ex/ex}$ organoids. Over the entire period no morphological changes were observed. In both $Apc^{Min/+}$ organoid cultures no changes in spherical shape and size was observed.

CHAPTER FOUR: DISCUSSION AND FUTURE PROSPECTS

Proliferation, apoptosis, regeneration and renewal within the intestine are important processes requiring the coordinated and orchestrated activation and inactivation of distinct signaling pathways. It is described that ADAM proteases, especially ADAM17, play a crucial role in the control of various signaling pathways due to irreversible proteolytic processing of membrane bound receptors or ligands. How this is regulated in detail, especially under pathological conditions, is a central question in current research.

Tumor initiation and progression are complex multistage processes, whereby it is most fundamental that a cell gains growth advantages towards other cells. For tumor initiation, development and progression, eight different but intertwined steps are required: self-efficacy regarding growth signals, insensitivity against antigrowth signals, ability to escape apoptosis, unlimited replicative potential, ability to implement angiogenesis, ability to invade surrounding tissue to metastasize, capability to modify metabolism and competence in evading immunological destruction. These capabilities are referred to as “The Hallmarks of cancer” (Hanahan and Weinberg, 2011, Hanahan and Weinberg, 2000).

The development of cancer is closely related to chronic inflammation and described in patients suffering from inflammatory bowel diseases (IBD) (McGuckin et al., 2009, Roda et al., 2010). Previous studies show a strong link between colorectal cancer development and IBD, as IBD patients bear an increased risk for the development of colorectal cancer but the underlying mechanism is still unknown (Itzkowitz and Harpaz, 2004, Gupta et al., 2007, Rutter et al., 2004). To grow in a chronically inflamed environment, cells must evolve the ability to escape immune recognition and suppress immune reactivity which is in accordance with the hallmark of cancer capabilities described previously (Cavallo et al., 2011). ADAM17 activation appears to play an important role in this interplay but the underlying mechanisms are poorly understood.

ADAM17 is expressed in all tissues, including the intestine (Fig. 18), and the lack of ADAM17 under healthy conditions has no influence on the development or morphology of both the small intestine and the colon (Fig. 66 A and B; additional results). In line with this observations, organoids generated from hypomorphic $ADAM17^{ex/ex}$ mice and $ADAM17^{wt/wt}$ mice showed no morphological differences (Fig. 67). Under normal physiological conditions, ADAM17 is not required for maintaining intestinal homeostasis. The normal physiological differentiation of secretory cells, such as Paneth cells and goblet cells, in the small intestine and colon of hypomorphic $ADAM17^{ex/ex}$ mice implies that proteolytic processing by ADAM17 is not essential for Notch signaling within the crypt-villus-unit (Tsai et

al., 2014). Even though ADAM17 is not decisive for physiological intestinal homeostasis, ADAM17 is essential for the protection and regeneration of the intestinal epithelium under pathophysiological conditions like DSS-induced colitis (Jones et al., 2015, Chalaris et al., 2010). This can be explained by ADAM17 acting as an upstream regulator of ErbB signaling via ErbB ligand shedding. ErbB ligand deficient mice, ErbB receptor deficient mice and hypomorphic ADAM17$^{ex/ex}$ mice suffer from severe DSS-colitis, while treatment with exogenous ErbB ligands protects against colitis development (Frey and Brent Polk, 2014, Zhang et al., 2012, Egger et al., 1997, Chalaris et al., 2010). It was shown that DSS-induced colitis leads to increased expression of the ADAM17 substrates Amphiregulin and Epiregulin (Fig. 70; additional results) due to activated TLR-mediated MyD88 signaling. In this context, ADAM17-mediated shedding of Amphiregulin and Epiregulin is necessary for ErbB signaling activation for intestinal epithelia regeneration (Brandl et al., 2010, Sahin et al., 2004).

Inflammation is linked clinically to cancer, but the underlying mechanisms are poorly understood. To evaluate the physiological relevance of ADAM17 in colitis-associated colorectal cancer, hypomorphic ADAM17$^{ex/ex}$ mice, which had drastically reduced ADAM17 protein levels in all tissues, were subjected to the AOM/DSS-model of inflammation-associated colorectal cancer. Mice were treated with DSS to induce chronic inflammation of the colon and injected with AOM to induce carcinogenesis. In line with the previous results from Chalaris et al., the drastically reduced ADAM17 protein expression in the hypomorphic ADAM17$^{ex/ex}$ mice resulted in severe inflammation of the colon (Fig. 24) and a significantly elevated clinical activity score as a consequence of the DSS-treatment (Fig. 22). Upon termination of the DSS-treatment, the intestinal epithelium of control mice started to regenerate in a physiological manner, which mainly involved proliferation of the intestinal epithelial cells thereby restoring normal intestinal epithelial barrier integrity. In addition concomitant parameters like occult blood, diarrhea, weight loss and thickened colon tissue (Fig. 19-21 and 24 B) improved in ADAM17$^{wt/wt}$ mice. This proliferative regeneration is driven by EGFR signaling, which in turn is impaired in hypomorphic ADAM17$^{ex/ex}$ mice (Chalaris et al., 2010). Due to impaired regeneration of the intestinal epithelium, as described in Chalaris et al., hypomorphic ADAM17$^{ex/ex}$ mice suffered from enhanced injury of the colon, clearly visible by traces of blood in the stool and rectal bleeding (Fig. 20) as well as thickened colon tissue and significantly shortened colon length (Fig. 24). Disturbed homeostasis and dysfunctional digestion was indicated by diarrhea (Fig. 21) and weight loss (Fig. 19) which resulted in significantly limited survival (Fig. 23) of hypomorphic ADAM17$^{ex/ex}$ mice during the experiments.

In the context of inflammatory bowel disease (IBD) and chronic inflammation it is well known that the intestinal microbiome plays an essential role in the pathogenesis of Crohn´s disease

(CD) and Ulcerative colitis (UC) due to enhanced proteolytic activity (Itzkowitz and Harpaz, 2004, Itzkowitz and Yio, 2004). An NIH program to study the human microbiome has started recently because the role of the microbiome is still on debate and requires more information (NIH HMP Working Group et al., 2009). Colitis severity induced by DSS-treatment in mice has also been shown to depend on the bacterial microflora (Kitajima et al., 2001). Interestingly, the microbiome of healthy unchallenged hypomorphic ADAM17$^{ex/ex}$ mice and ADAM17$^{wt/wt}$ mice revealed significant differences(Fig. 77; additional results). This could additionally contribute to the severe inflammation during DSS-induced colitis, apart from impaired EGFR signaling, in hypomorphic ADAM17$^{ex/ex}$ mice. Furthermore, clinical activity scores for each genotype were strongly influenced by the ratio of the genotypes co-housed in one cage as well as the distribution of littermates and non-littermates. According to these results, further research investigating the microbiome of AOM/DSS-treated hypomorphic ADAM17$^{ex/ex}$ mice and ADAM17$^{wt/wt}$ mice is warranted.

In line with the observed severe inflammation, hypomorphic ADAM17$^{ex/ex}$ mice showed increased infiltration of immune cells into neoplasia and the surrounding tissue after AOM/DSS-treatment (Fig. 25). The infiltration of neoplasia and the surrounding tissue by immune cells of the innate immune system and resulting tumor-associated inflammation is a well described observation, which paradoxically enhances tumor progression instead of preventing it (Dvorak, 1986). The inflammation process contributes to tumor progression by providing beneficial soluble components such as growth factors and cytokines to intensify proliferation as well as proteases such as matrix-metalloproteases to support invasion (Grivennikov et al., 2010). It has been established that neoplasia-infiltrating myeloid cells co-expressing the macrophage marker CD11b have an important function in inflammation-associated cancer (Qian and Pollard, 2010). Tumor development in the liver is linked to inflammation as well as colorectal cancer and it was described recently that EGFR-expressing macrophages had a tumor promoting role due to their IL-6 release (Lanaya et al., 2014).

In intestinal cultures of AOM/DSS-treated hypomorphic ADAM17$^{ex/ex}$ mice IL-6 was detectable, although without significant differences between genotypes (Fig. 71 A; additional results). This observation is in line with similar tumor numbers in AOM/DSS-treated mice of both genotypes (Fig. 27). Consistent with the assumption that macrophages are key modulators in inflammation-associated intestinal tumorigenesis, the increased amounts of the macrophage inflammatory protein-1 ß (MIP-1ß) in intestinal cultures of hypomorphic ADAM17$^{ex/ex}$ mice support the hypothesis of their tumor promoting role (Fig. 71 B; additional results). Importantly, it was shown that IL-6 signaling, in particular sIL-6R-mediated IL-6 trans-signaling, is involved in the transformation of M1 to M2 macrophages (Braune et al.,

2017, Mauer et al., 2014). M2 macrophages are associated with tumor promoting properties, while M1 macrophages are thought to be rather anti-tumorigenic (Biswas and Mantovani, 2010). As a result of the inflammatory response, increased IL-6 serum levels were detectable in DSS-treated mice in the recently published experiments of Srivatsa et al. in 2017. IL-6-signaling is involved in tumor growth and survival in colitis-associated colorectal cancer and plays a pro-tumorigenic role via Jak-dependent STAT3 signaling. Further, IL-6 signaling is involved in immune response due to IL-6 release from macrophages under inflammatory conditions underlined by enhanced BIRC5 expression in tumor bearing mice (Waldner and Neurath, 2014, Srivatsa et al., 2017). Mice subjected to DSS-induced colitis or AOM/DSS-induced colitis-associated colon cancer were protected against tumor development in case of a myeloid-specific knockout of the EGFR. Consequently, macrophages lacking EGFR signaling secreted less IL-6, which in turn led to diminished Jak-dependent STAT3 signaling in intestinal epithelial cells (Srivatsa et al., 2017, Hardbower et al., 2017). Due to impaired ADAM17-mediated ErbB ligand shedding and the pro-tumorigenic role of IL-6, it was assumed that hypomorphic ADAM17$^{ex/ex}$ mice should develop less neoplasia compared to ADAM17$^{wt/wt}$ mice during AOM/DSS-induced colitis. However, the number of tumors was not significantly altered between both genotypes (Fig. 27 A). Even though the number of low grade dysplasia was equal, the size of tumors in hypomorphic ADAM17$^{ex/ex}$ mice was surprisingly increased (Fig. 28). Furthermore, hypomorphic ADAM17$^{ex/ex}$ mice developed carcinoma, which did not appear in ADAM17$^{wt/wt}$ mice (Fig. 27 B). It was described that DSS-treatment induces an inflammatory response that promotes loss of heterozygosity (LOH) of APC, which contributes to driver mutations and progression of colon cancer development (Vogelstein and Kinzler, 1993, Yamada and Mori, 2006, Cooper et al., 2001).

An explanation for these unexpected findings could be the different inflammation score between both genotypes under basal conditions (Fig. 22 and 25). To circumvent the problem of an unequal baseline situation, a genetically predisposed cancer model without chemically induced chronic inflammation was investigated. To that end, hypomorphic ADAM17$^{ex/ex}$ mice were intercrossed with Apc$^{Min/+}$ mice.

Although Apc$^{Min/+}$ mice develop tumors predominantly within the small intestine, it is also a well-established mouse model to investigate colon carcinogenesis because it mimics APC mutations in human patients (Moser et al., 1990, Groden et al., 1991). No difference in the morphology of unaffected small intestinal tissue was observed between hypomorphic Apc$^{Min/+}$ADAM17$^{ex/ex}$ mice and Apc$^{Min/+}$ADAM17$^{wt/wt}$ mice. Both genotypes showed normal distribution of goblet cells along the crypt-villus-unit, regular localization of Paneth cells at the crypt bottom and physiological proliferation within the transit amplifying compartment and the

crypt bottom in unaffected tissue (Fig. 36, 37, 41). Furthermore, no difference in the inflammation score was observed between genotypes (Fig. 33 and 72; additional results). In line with this, organoids generated from hypomorphic $Apc^{Min/+}ADAM17^{ex/ex}$ mice and $Apc^{Min/+}ADAM17^{wt/wt}$ mice revealed no morphological differences (Fig. 51). As expected, hypomorphic $Apc^{Min/+}ADAM17^{ex/ex}$ mice showed a drastically reduced ADAM17 protein expression compared to $Apc^{Min/+}ADAM17^{wt/wt}$ mice which was also observed in the *ex vivo* organoid cultures (Fig. 29 and 53).

Diminished ADAM17 expression in hypomorphic $Apc^{Min/+}ADAM17^{ex/ex}$ mice led to a significantly reduced number of neoplasia and accordingly a significantly reduced number of initially generated organoids (Fig. 30 B, 32 and 50). In addition, reduced ADAM17 activity led to protection against high grade dysplasia and carcinoma development in $Apc^{Min/+}$ mice (Fig. 34). The considerable differences in proliferation among the two $Apc^{Min/+}$ mouse strains were in line with the reduced tumor progression from low grade dysplasia to carcinoma in hypomorphic $Apc^{Min/+}ADAM17^{ex/ex}$ mice (Fig. 41, 42). Interestingly, no differences in the size of low grade dysplasia or tumor distribution along the small intestine were observed between genotypes (Fig. 30 C, 31 and 35).

The contrasting results concerning negligible ADAM17 activity in hypomorphic mice and carcinoma formation in the AOM/DSS-model and the $Apc^{Min/+}$ model seemed to be influenced by severe inflammation. Under inflammatory conditions, the lack of ADAM17 in hypomorphic $ADAM17^{ex/ex}$ mice promoted carcinoma formation due to a still inconclusive mechanism (Fig. 27). Vice versa, in a genetically predisposed situation, without additional inflammatory trigger, the lack of ADAM17 protected against carcinoma development (Fig. 34). To reveal the mechanism behind the protective role of reduced ADAM17 activity under non-inflammatory conditions, *in vitro* analysis of epithelial cells from human colorectal cancers as well as *ex vivo* experiments with organoids were carried out and analysis of neoplasia from $Apc^{Min/+}$ mice.

Intriguingly, mRNA levels of the ErbB receptor EGFR and the ErbB ligand Amphiregulin were significantly upregulated in epithelial human colorectal cancer cells, organoids and neoplasia of both $Apc^{Min/+}$ mouse strains (Fig. 13, 43, 44 and 55). Moreover, enhanced protein expression of ADAM17 and EGFR in intestinal epithelial cells were observed *in vitro* in various human colorectal cancer cell lines and *ex vivo* in organoids of hypomorphic $Apc^{Min/+}ADAM17^{ex/ex}$ mice and $Apc^{Min/+}ADAM17^{wt/wt}$ control mice (Fig. 15, 16 and 53). Analysis of intestinal cultures and small intestinal tissue of hypomorphic $Apc^{Min/+}ADAM17^{ex/ex}$ mice and $Apc^{Min/+}ADAM17^{wt/wt}$ mice confirmed Amphiregulin protein expression in both genotypes (Fig. 59 A and 60 B). Amphiregulin is a reported substrate of ADAM17 and these first

examinations might point to a connection between ADAM17 activity and Amphiregulin shedding (Sahin and Blobel, 2007).

However, analysis of whole small intestinal tissue does not allow any conclusions regarding the Amphiregulin-expressing cell type, because besides the intestinal epithelial layer, the lamina propria including various immune cells and myofibroblasts together with muscle cells is present in whole intestinal tissue lysates. To extend the results obtained from human intestinal epithelial colorectal cancer cells to the murine model, *ex vivo* organoid cultures were established (Fig. 10 and 52). *Ex vivo* organoids allow the investigation of intestinal epithelial cells detached from the microenvironment. Strikingly, organoids from hypomorphic $Apc^{Min/+}ADAM17^{ex/ex}$ mice revealed significantly decreased shedding of Amphiregulin compared to $Apc^{Min/+}ADAM17^{wt/wt}$ organoids showing regular ADAM17 activity (Fig. 61 A). These observations were connected directly to ADAM17 activity, since native shedding of a second ADAM17 substrate as well as pharmacological ADAM17 inhibition confirmed the involvement of ADAM17. Specifically, shedding of the well-known ADAM17 substrate TNFRI was significantly diminished in organoids of hypomorphic $Apc^{Min/+}ADAM17^{ex/ex}$ mice (Fig. 61 B). Pharmacological inhibition of ADAM17 activity by GW and Marimastat treatment led to significantly reduced Amphiregulin shedding in intestinal epithelia cells *ex vivo* in organoids and *in vitro* in human colorectal cancer cells (Fig. 17, 62 and 68; additional results). The results are in accordance with a recent report showing that pharmacological inhibition of ADAM17 resulted in reduced numbers of intestinal tumors in $Apc^{Min/+}$ mice due to dysregulated ErbB signaling (Mustafi et al., 2017).

To assess the physiological relevance of ADAM17-mediated Amphiregulin shedding, organoids from hypomorphic $Apc^{Min/+}ADAM17^{ex/ex}$ mice and $Apc^{Min/+}ADAM17^{wt/wt}$ control mice were cultured without supplemented EGF. It was shown, that exogenous EGF is essential for the proliferation of organoid cultures *in vitro* and is able to stimulate crypt proliferation *in vivo* (Frey and Brent Polk, 2014). Only $Apc^{Min/+}ADAM17^{wt/wt}$ organoids were able to maintain proliferation and replaiting efficiency for further passages. Due to diminished Amphiregulin shedding, the replaiting efficiency of hypomorphic $Apc^{Min/+}ADAM17^{ex/ex}$ organoids was impaired (Fig. 64 and 65). These results indicate that growth stimuli such as EGF or Amphiregulin comprise the capability to create a self-sufficient growth niche *ex vivo* in organoid culture systems and confirm that the ADAM17-mediated Amphiregulin shedding occurred on intestinal epithelial cells and played a physiological role to maintain proliferation. An explanation for the observed effect is the EGFR signaling redundancy due to the variety of redundant EGFR ligands (Fig. 5). Both Amphiregulin and EGF can activate the EGFR and Amphiregulin is bona fide substrate of ADAM17 (Sahin and Blobel, 2007). The overlapping functions of Amphiregulin and EGF stimulating the EGFR signaling pathway explains the

replaiting efficiency of $Apc^{Min/+}ADAM17^{wt/wt}$ organoids in contrast of $Apc^{Min/+}ADAM17^{ex/ex}$ organoids by ADAM17-mediated Amphiregulin shedding.

To clarify which signaling pathway contributes to the observed effects *ex vivo* in organoids and *in vivo* in hypomorphic $Apc^{Min/+}ADAM17^{ex/ex}$ mice, the Notch, the Wnt, the Hippo/YAP and the STAT3 signaling pathways were further investigated.

In vitro experiments investigating the inhibition of ADAM17 in autocrine ErbB signaling-depended colorectal cancer cell lines showed reduced proliferation, increased apoptosis and diminished MAPK pathway activation, underlining the contribution of ADAM17-dependent ErbB signaling in colon cancer development (Dong et al., 1999, Merchant et al., 2008).

To maintain physiological homeostasis and cell differentiation within the intestine, an accurate regulation of the Notch signaling pathway is required. During tumorigenesis, components of the Notch pathway are dysregulated, leading to an upregulation of Notch target genes (Noah and Shroyer, 2013, Nakamura et al., 2007). ADAM17-dependent cleavage of the Notch ligand JAG-1 from endothelia cells induced non-canonical Notch signaling in colorectal cancer microenvironment thereby supporting tumor development (Lu et al., 2013). Therefore it was interesting to see whether Notch target genes are transcriptionally altered in intestinal tissue from $Apc^{Min/+}$ mice compared to control wildtype mice. $Apc^{Min/+}$ mice displayed increased transcription of Notch target genes in whole intestinal tissue compared to wildtype which is consistent with the altered morphology and cell differentiation shown in Fig. 36 and 37. In whole intestinal tissue of hypomorphic $Apc^{Min/+}ADAM17^{ex/ex}$ mice, transcription levels tended to be lower than in $Apc^{Min/+}ADAM17^{wt/wt}$ mice, which was confirmed by RNA-Sequencing results. However, RNA-Sequencing of tumors revealed no significant difference regarding the Notch signaling pathway between both $Apc^{Min/+}$ mouse strains (Tab. 26-29; additional results). These results imply that Notch signaling is upregulated in both $Apc^{Min/+}$ mouse strains and is not altered in tumors of hypomorphic $Apc^{Min/+}ADAM17^{ex/ex}$ mice compared to $Apc^{Min/+}ADAM17^{wt/wt}$ mice.

Besides the mentioned signaling pathways the c-Met pathway was analyzed as well, as it was shown that upregulation of c-Met and HGF contributes to cancer progression in the intestine (Di Renzo et al., 1995). However, transcriptional levels of neither *c-Met* nor *HGF* itself were significantly elevated, nor did target genes of the pathway showed significant dysregulation in RNA-Sequencing experiments (Fig. 46 and Tab. 26-29; additional results). Consequently, ADAM17-mediated regulation of the c-Met/HGF pathway does not contribute predominantly to the observed phenotype (Chalupsky et al., 2013).

It can be assumed that additional signaling pathways are involved in colon cancer initiation, development and progression in the investigated $Apc^{Min/+}$ mouse model. Upregulation of mRNAs coding for *YAP-1* and the corresponding target genes *Ctgf* and *Cyr61* suggests that the Hippo/YAP signaling pathway may be involved in dysregulation of proliferation and apoptosis. The mRNA levels of these genes were significantly decreased in hypomorphic $Apc^{Min/+}ADAM17^{ex/ex}$ mice, which could contribute to the lack of high grade dysplasia and carcinoma in this mouse strain (Fig. 49). However, it still remains unclear whether YAP-1 promotes tumorigenesis directly or rather indirectly by alteration of the microenvironment and intestinal niche to promote tumor development (Steinhardt et al., 2008). An influence of the microenvironment and intestinal niche on proliferation of intestinal epithelial cells could be excluded in organoid cultures as described above. Interestingly, analysis of organoids from hypomorphic $Apc^{Min/+}ADAM17^{ex/ex}$ mice revealed altered transcriptional levels of the target genes *Ctgf* and *Cyr61* (Fig. 58). In this context, it is worth mentioning that downstream signaling events *ex vivo* in organoids are very vulnerable to variations in culture conditions, such as ingredients and stiffness of Matrigel®. Matrigel® is a solubilized basement membrane matrix extracted from the Engelbreth-Holm-Swarm (EHS) mouse sarcoma with natural variances. Furthermore, it was recently published that the stiffness of Matrigel® influences downstream signaling, especially YAP signaling, so activation of YAP signaling had to be assessed by additional techniques (Gjorevski et al., 2016). Determination of the cellular localization of YAP-1 by IHC as well as the phosphorylation status of YAP-1 could clarify the activation of YAP signaling in the future.

A current publication implicates that loss of APC leads to an upregulation of gp130, YAP-1 and STAT3 in colon carcinogenesis (Taniguchi et al., 2017). In the intestine of both $Apc^{Min/+}$ mouse strains, upregulation of *YAP-1* was found, while transcriptional levels of *gp130* were comparable (Fig. 49 A and 48 C). Surprisingly, the transcriptional levels of *BIRC5* (also known as Survivin), a well-known STAT3 target gene, were significantly downregulated in the intestines and organoids (Fig. 48 D and 57 D). It has previously been published that BIRC5 is upregulated in various cancers including breast cancer (Boidot et al., 2008). In this work, activation of STAT3 signaling was confirmed on protein level by IHC staining of small intestinal tissue from hypomorphic $Apc^{Min/+}ADAM17^{ex/ex}$ mice. STAT3 is localized in the cytoplasm and upon activation, the dimerized and phosphorylated protein translocates into the nucleus including the transcription of target genes such as *BIRC5*. STAT3 immunohistochemistry revealed that a translocation, or in other words activation, of STAT3 was completely missing in hypomorphic $Apc^{Min/+}ADAM17^{ex/ex}$ mice, even in unaffected tissue (Fig. 39).

Following the loss of the remaining, non-mutated *Apc* allele, $Apc^{Min/+}$ mice exhibit constitutively activated Wnt signaling leading to cytoplasmic accumulation of ß-Catenin, as shown in Fig. 4. Accumulated ß-Catenin within the cytoplasm confirmed constitutively activated Wnt signaling in both $Apc^{Min/+}$ mouse strains (Fig. 38). No difference in terms of cytosolic ß-Catenin between both genotypes was observed (Fig. 73; additional results). In line with this result, target genes of the Wnt signaling pathway were significantly upregulated in hypomorphic $Apc^{Min/+}ADAM17^{ex/ex}$ mice and $Apc^{Min/+}ADAM17^{wt/wt}$ mice as well as organoids, but not significantly altered between both $Apc^{Min/+}$ mouse strains, except *c-Myc* and *Sox9* (Fig. 47 and 56). The transcription factor *Sox9* was significantly upregulated in hypomorphic $Apc^{Min/+}ADAM17^{ex/ex}$ mice (Fig. 47 E). Previous studies indicate that Sox3, Sox9 and Sox17 have an inhibitory effect on ß-Catenin-dependent promoters, which could lead to decreased transcription of ß-Catenin-TCF/LEF induced genes in hypomorphic $Apc^{Min/+}ADAM17^{ex/ex}$ mice (Akiyama et al., 2004, Zorn et al., 1999). Further it was shown that Paneth cell differentiation depends on Sox9 (Feng et al., 2013). Surprisingly, the direct Wnt target gene *c-Myc* was significantly downregulated in intestinal tissue and organoids from hypomorphic $Apc^{Min/+}ADAM17^{ex/ex}$ mice (Fig. 47 A and 56 A) (He et al., 1998, Fodde, 2002). In support of this, RNA-Sequencing of tumors and surrounding intestinal tissue suggested that the Wnt signaling pathway was downregulated in hypomorphic $Apc^{Min/+}ADAM17^{ex/ex}$ mice (Tab. 26-29; additional results). To gain further insight into downregulation of the Wnt signaling in hypomorphic $Apc^{Min/+}ADAM17^{ex/ex}$ mice, deeper analysis of the RNA-Sequencing results using more sophisticated bioinformatics tools is necessary.

It has been published that c-Myc is involved in the crosstalk between Wnt-dependent and Wnt-independent signaling pathways such as STAT3 downstream signaling (Hanada et al., 2006, Rigby et al., 2007, Sansom et al., 2007, Kaiser et al., 2007, Amos-Landgraf et al., 2007). The important role of c-Myc as a key regulator and mediator during colon cancer was demonstrated by deletion of c-Myc to rescue Apc-deficiency (Sansom et al., 2007). Consistent with this, c-Myc is downregulated in hypomorphic $Apc^{Min/+}ADAM17^{ex/ex}$ mice, although other Wnt target genes are not altered. In addition, STAT3 activation is absent in hypomorphic $Apc^{Min/+}ADAM17^{ex/ex}$ mice. Taken together, these results may indicate that a crosstalk between Wnt-dependent and Wnt-independent signaling pathways in hypomorphic $Apc^{Min/+}ADAM17^{ex/ex}$ mice plays a crucial role during cancer development as well.

This assumption could be a conceivable explanation for the reduced tumor burden in hypomorphic $Apc^{Min/+}ADAM17^{ex/ex}$ mice, as it was published that dysregulated STAT3 signaling is a prerequisite for the development of solid tumors in colon cancer (Corvinus et al., 2005) (Silva, 2004). STAT3 target genes, such as *BIRC5*, are involved in the inhibition of apoptosis and cell cycle regulation and interestingly, *c-Myc* also represents a STAT3 target

gene (Quesnelle et al., 2007). Based on the lack of STAT3 activation and reduced mRNA levels of *BIRC5* and *c-Myc* in hypomorphic $Apc^{Min/+}ADAM17^{ex/ex}$ mice, it is plausible that ADAM17-activity influences STAT3 signaling via EGFR signaling independent of Janus kinases (JAK) (Andl et al., 2004, Darnell et al., 1994). It has been published previously that Amphiregulin-dependent EGFR activation leads to JAK-independent induction of STAT3 signaling. STAT3 can interact directly through its SH2 domain or indirectly through SRC proteins with phosphorylated EGFR to forward downstream signaling (David et al., 1996). The oncogenic role of EGFR and Amphiregulin is closely linked to the regulation of ErbB downstream signaling. In head and neck cancer as well as esophageal cancer, upregulation of the ErbB ligand TGF-α, the ErbB receptor EGFR and STAT3 is an early event during tumorigenesis and autocrine signaling of the ErbB ligand through the EGFR receptor leading to constitutive activation of STAT3 and tumor progression (Song and Grandis, 2000).

Reduced ADAM17-activity *in vitro*, *ex vivo* and *in vivo* resulted in diminished Amphiregulin shedding, EGFR activation as well as STAT3 downstream signaling and finally led to protection against carcinoma development. Additionally, it has been reported that Amphiregulin-induced EGFR activation increases MMP2 and MMP9 expression, which could contribute to tumor progression from dysplasia to carcinoma due to altered extracellular matrix composition and support cell invasion, a typical hallmark of cancer (Kondapaka et al., 1997). In this context it would be worthy to study if the development of carcinoma is time- and age-dependent. All $Apc^{Min/+}$ mice used in this work were scarified at the age of six months and it would be interesting to analyze neoplasia from $Apc^{Min/+}$ mice older than six months for tumor staging.

Intestinal epithelial cells in organoid cultures of both genotypes express STAT3 proteins at comparable levels, however, the amount of phosphorylated STAT3 is slightly enhanced in $Apc^{Min/+}ADAM17^{wt/wt}$ organoids compared to hypomorphic organoids, which were shown to exhibit negligible ADAM17-activity and reduced Amphiregulin shedding (Fig. 74; additional results). This observation can be translated to the presented results regarding autocrine or paracrine signaling of the ErbB ligand Amphiregulin through the EGFR receptor in intestinal epithelial cells. In epithelial tissues, EGFR signaling can be activated by ErbB ligands either in an autocrine or paracrine manner (Harris et al., 2003). In the paracrine mode the soluble ligand is released by one cell and acts on adjacent cells or on cells in the close proximity. In autocrine EGFR signaling ErbB ligand binds to the ErbB receptor on the same cell they were produced.

However, it is unlikely that ADAM17-mediated Amphiregulin shedding and subsequent EGFR activation as well as STAT3 downstream signaling is involved in each step of colon carcinogenesis and represent the sole driving force behind tumorigenesis (Fig. 3). Moreover,

$Apc^{Min/+}$ mice crossed with IL-$6^{-/-}$ knockout mice showed a reduced tumor burden as well as $Apc^{Min/+}$ mice crossed with sgp130Fc-tg mice (Tracy Putoczki, Matthias Ernst, unpublished data). The sgp130Fc-tg mice overexpress the soluble gp130Fc protein as a transgene, which blocks IL-6 trans-signaling without affecting IL-6 classic signaling, under the control of a liver specific promoter (Jostock et al., 2001, Rabe et al., 2008). Nevertheless, EGFR signaling plays a crucial role in promoting proliferation and forwarding growth signals for tumor initiation, development and progression, even in the $Apc^{Min/+}$ mouse model, shown by Roberts et al. in 2002. In that study $Apc^{Min/+}$ mice were crossed to hypomorphic EGFR mice, which possess 90 % reduced kinase activity resulting in reduced tumor burden in hypomorphic $Apc^{Min/+}Egfr^{wa2}$ mice. The observations of Roberts et al. are in accordance with the results observed in hypomorphic $Apc^{Min/+}ADAM17^{ex/ex}$ mice shown in this thesis (Luetteke et al., 1994, Roberts et al., 2002).

Analysis of cell type specific ADAM17-deficient mice is required to assess the source of participating cells in ADAM17-dependent ErbB signaling during tumor initiation as well as progression. This could be investigated with the help of $Apc^{Min/+}ADAM17^{flox/flox}$villin $cre^{+/-}$ mice, to investigate the influence of ADAM17-deletion in intestinal epithelial cells, $Apc^{Min/+}ADAM17^{flox/flox}$LysM $cre^{+/-}$ mice, to assess the influence of ADAM17-deletion in myeloid cells or $Apc^{Min/+}ADAM17^{flox/flox}$Myh11-eGFP $cre^{+/-}$ mice, with a deletion of ADAM17 only in myofibroblasts. Recent studies revealed tumor-associated fibroblast as the main source of Epiregulin during colitis-associated colorectal cancer, with Epiregulin being a well-known ADAM17 substrate (Neufert et al., 2013). To assess the overall survival of Apc mutant mice in this context, $Apc^{flox/flox}EGFR^{flox/flox}$villin $cre^{ER(T2)}$ mice, $Apc^{flox/flox}ADAM17^{flox/flox}$villin $cre^{ER(T2)}$ mice and $Apc^{flox/flox}$villin $cre^{ER(T2)}$ mice will be worth analyze. These mice develop tumors within 30 days due to Tamoxifen-induced *Apc* deletion.

The presented results indicate that several signaling pathways and cell types are involved in tumor development. In this thesis, multiple signaling pathways were connected successfully to tumorigenesis. Crosstalk between different signaling pathways could be established as an important key factor in tumorigenesis. However, involvement of multiple signaling pathways did not allow the precise identification of individual contribution to the observed phenotype. The result presented in this thesis may serve as an essential basis for further research in this field.

The relevance of ADAM17 as a potential link in the ADAM17-AREG-EGFR axis during colon cancer development appears to be important as well as the contribution of IL-6 trans-signaling. However, clinical use of ADAM17 inhibitors is currently not an option due to the complex substrate spectrum of ADAM17 (Scheller et al., 2011). The development of sophisticated ADAM17 inhibitors for clinical use is a central task of current research. The

application of EGFR inhibitors in colon cancer therapy is restricted as well because EGFR downstream signaling mutations in for example KRAS or BRAF abrogate the therapeutic effect of EGFR blocking antibodies such as cetuximab (Van Emburgh et al., 2014, Arteaga and Engelman, 2014). In order to overcome these clinical problems, a novel therapeutic strategy for the treatment of colon carcinogenesis could be the application of sgp130Fc (Olamkicept), an inhibitory protein, which interacts specifically with the soluble IL-6R to prevent IL-6 trans-signaling mediated colon carcinogenesis (Jostock et al., 2001, Rose-John, 2017).

APPENDIX

A) ADDITIONAL RESULTS

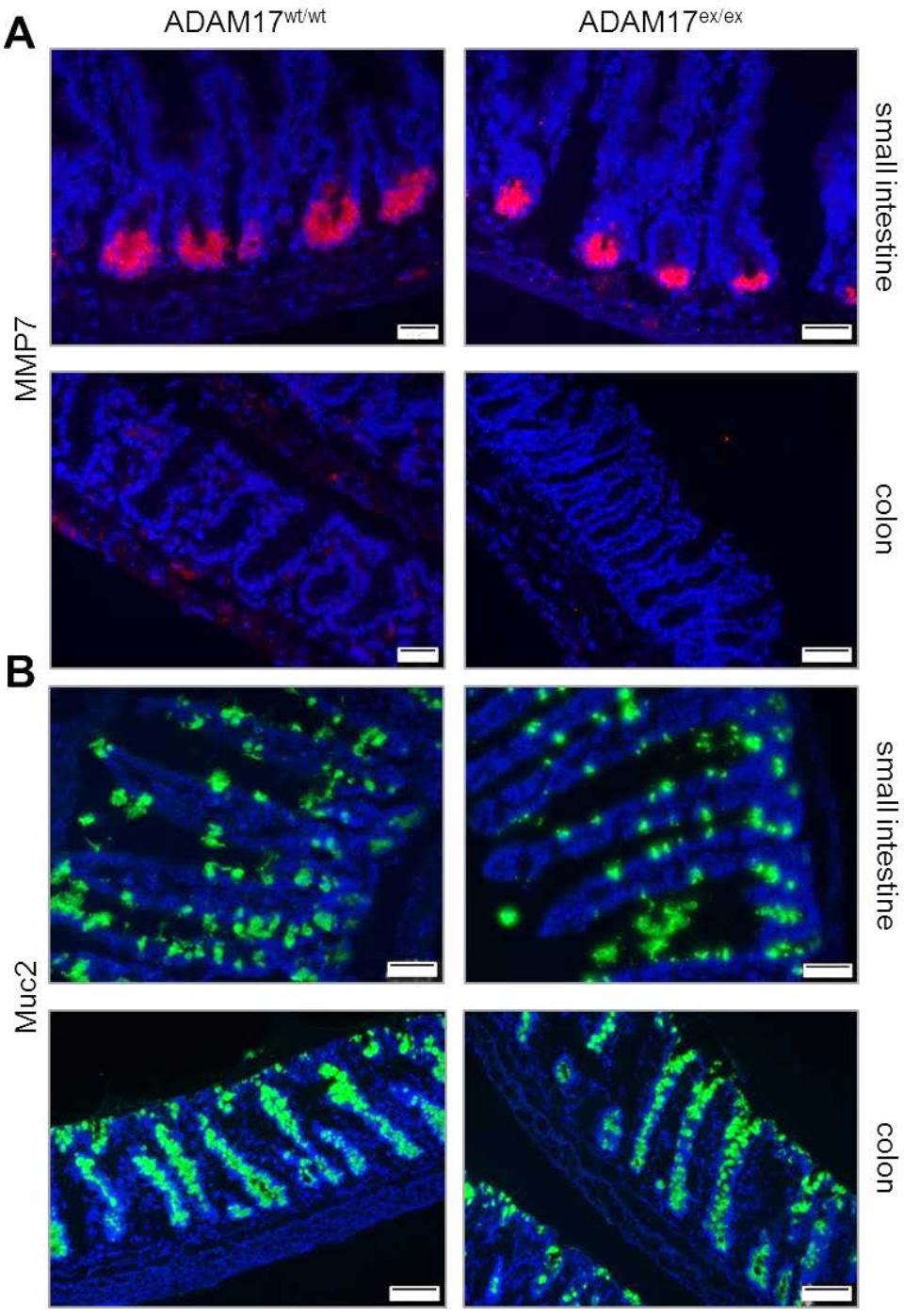

Fig. 66: Representative images of tissue from unchallenged ADAM17$^{wt/wt}$ and hypomorphic ADAM17$^{ex/ex}$ mice.

Small intestine and colon tissue from 24-week-old ADAM17$^{wt/wt}$ (n=1) and ADAM17$^{ex/ex}$ (n=1) mice were used for histological analysis. Representative images of (A) Matrix metalloproteinase 7 (MMP7) as Paneth cell marker and (B) Mucin 2 (Muc2) as marker for goblet cells showed no difference in morphology or differentiation for indicated cell types within the intestine.

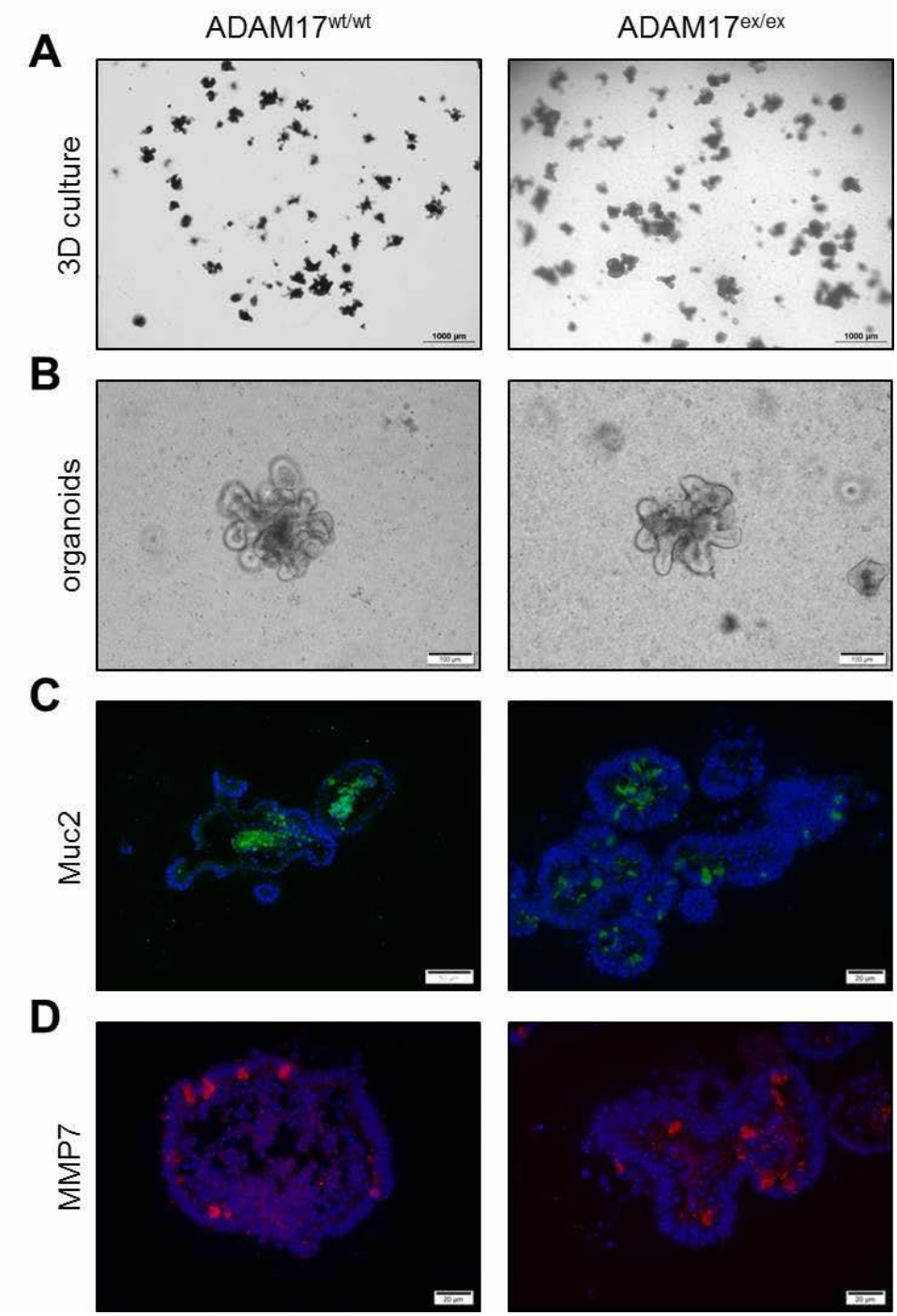

Fig. 67: Representative images of organoids from ADAM17$^{wt/wt}$ mice and hypomorphic ADAM17$^{ex/ex}$ mice.

Primary organoids isolated from the small intestine of 24-week-old ADAM17$^{wt/wt}$ (n=4) and ADAM17$^{ex/ex}$ (n=4) mice. (A) Representative images of 3D organoid culture per well and (B) magnification of single organoids with characteristic structures. Immunofluorescence analysis of organoids stained for (C) Mucin 2 (Muc2) as goblet cell marker and (D) Matrix metalloproteinase 7 (MMP7) as marker for Paneth cells showed no difference in morphology or differentiation for indicated cell types.

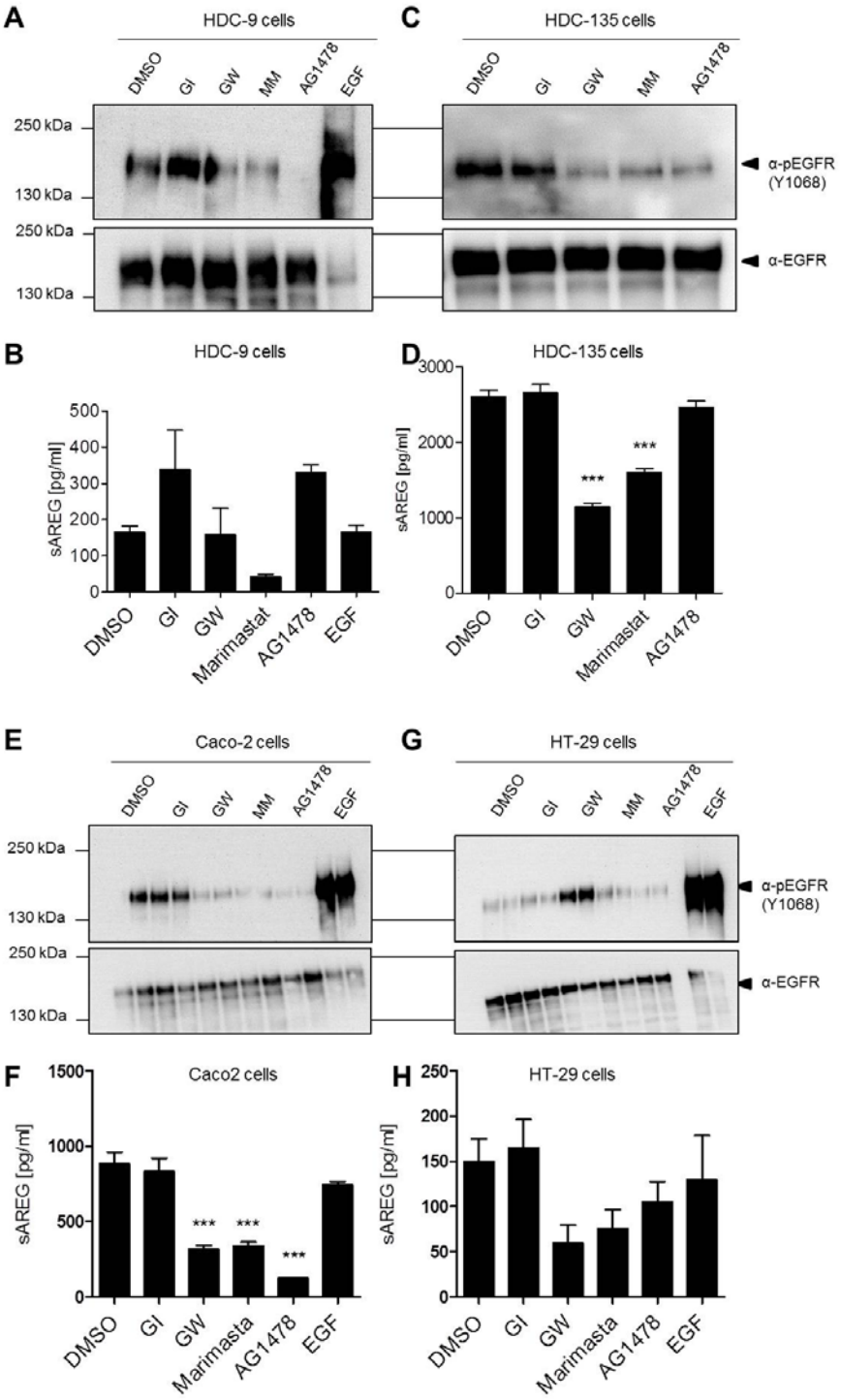

Fig. 68: Inhibition of ADAM17 leads to decreased Amphiregulin shedding in human colorectal cancer cells.

Indicated cell lines were seeded at a density of 3.0 x 10^6 cells and starved for 24 h in presence or absence of the pan-metalloprotease inhibitor MM (Marimastat, 10 µM), the metalloprotease inhibitors GI (GI254023X, ADAM10-selective, 3 µM) and GW (GW280264X, ADAM10- and ADAM17-selective, 3 µM) or the EGFR and ErbB2 kinase inhibitor AG1478 (10 µM). EGF (100 ng/ml) stimulated cells served as positive control. (A, C, E, G) Tyrosine-phosphorylated EGFR was assessed by Western blot analysis using a monoclonal anti-pEGFR Tyr1068 (#3777) antibody and EGFR was assessed by Western blot analysis using a anti-EGFR (#4267) antibody. (B, D, F, H) Soluble Amphiregulin was measured by ELISA in the conditioned media of indicated cell lines.

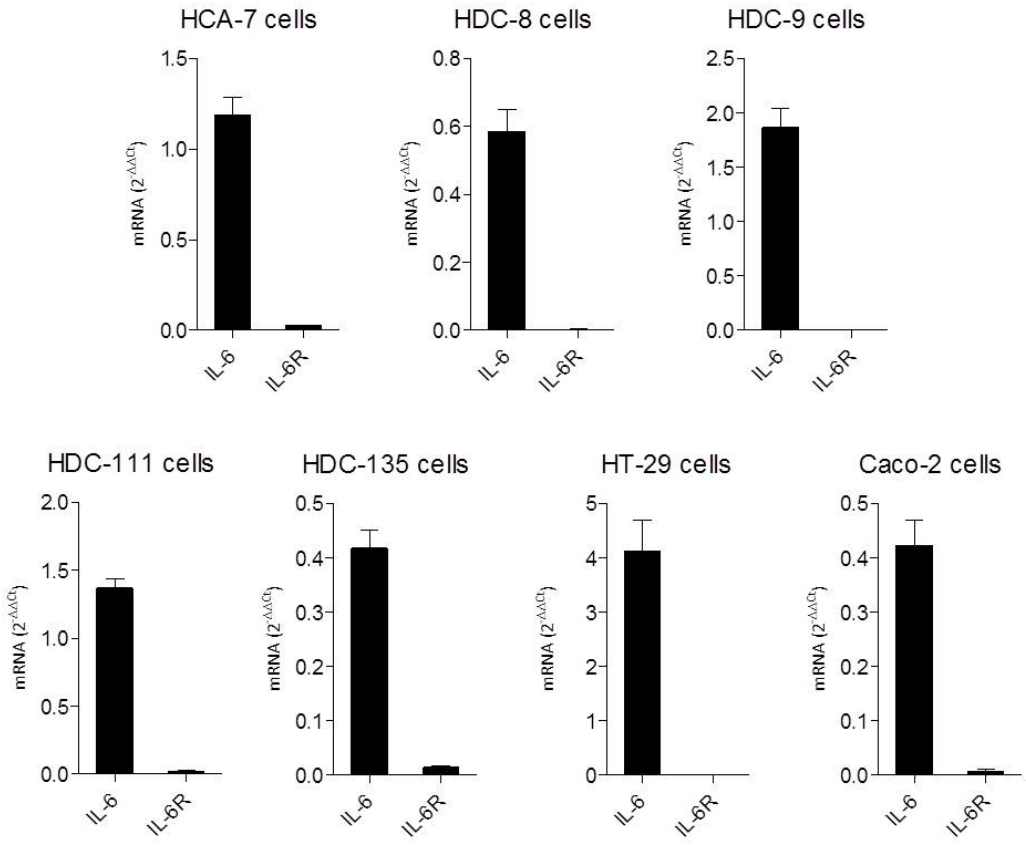

Fig. 69: qRT-PCR analysis of IL-6 and IL-6R in human CRC cells.

qRT-PCR analysis revealed elevated amounts of IL-6 and IL-6R in indicated human colorectal cancer cells. qRT-PCR data were normalized to GAPDH.

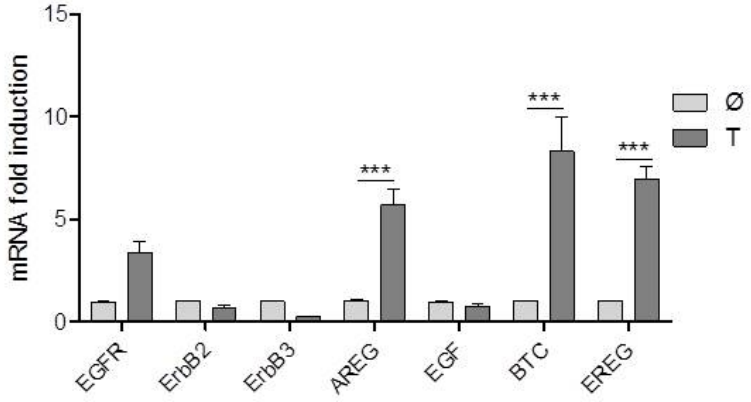

Fig. 70: qRT-PCR analysis of epidermal growth factor receptors and corresponding ligands in colon tissue from AOM/DSS-treated ADAM17$^{wt/wt}$ mice.

mRNA expression of EGF receptors and selected EGFR ligands of distal colonic tumor (T) and non-tumor (Ø) tissue from wildtype mice collected on day 90 of the CAC model.

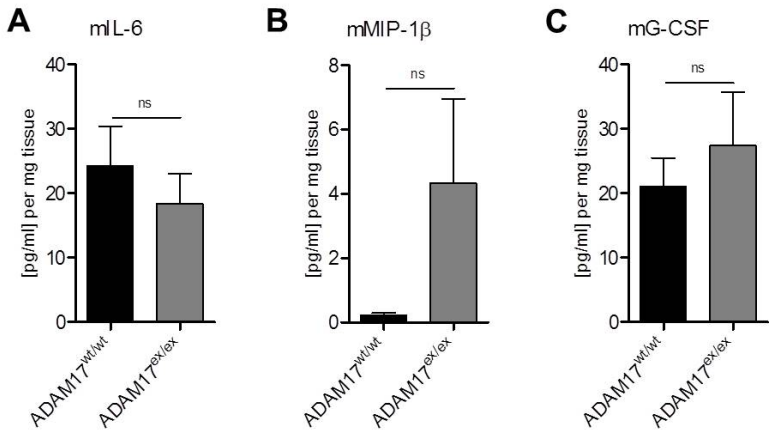

Fig. 71: Levels of soluble proteins in colon cultures from AOM/DSS-treated hypomorphic ADAM17$^{ex/ex}$ mice.

Tissue pieces from the colon of each mouse were washed with PBS containing Pen/Strep and incubated in DMEM medium at 37°C for 24 h. Supernatants were harvested and measured by ELISA for (A) soluble IL-6, (B) MIP-1ß and (C) G-CSF. ADAM17$^{wt/wt}$ (n=13) and ADAM17$^{ex/ex}$ (n=8). Mann-Whitney test.

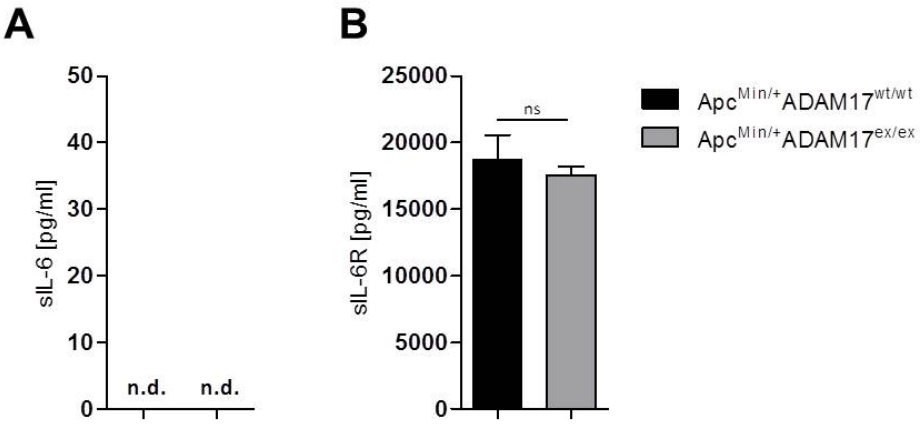

Fig. 72: Serum levels of sIL-6 and sIL-6R in hypomorphic Apc$^{Min/+}$ADAM17$^{ex/ex}$ mice.

Serum samples from 6-month-old mice were analyzed for (A) IL-6 and (B) soluble IL-6R. Apc$^{Min/+}$ADAM17$^{wt/wt}$ (n=4) and Apc$^{Min/+}$ADAM17$^{ex/ex}$ (n=4). Mann-Whitney test.

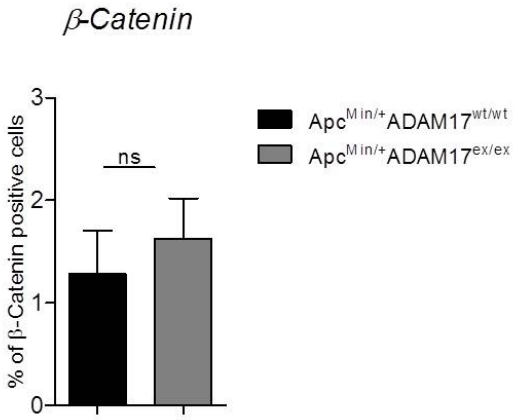

Fig. 73: Quantification of ß-Catenin stained tissue from hypomorphic Apc$^{Min/+}$ADAM17$^{wt/wt}$ mice and Apc$^{Min/+}$ADAM17$^{ex/ex}$ mice.

Small intestine from 24-week-old Apc$^{Min/+}$ADAM17$^{wt/wt}$ mice and Apc$^{Min/+}$ADAM17$^{ex/ex}$ mice was used in IHC for analysis (Fig. 37) of ß-Catenin positive cell proliferation. Quantification of ß-Catenin positive signals by ImageJ. Apc$^{Min/+}$ADAM17$^{wt/wt}$ mice (n=8) and Apc$^{Min/+}$ADAM17$^{ex/ex}$ mice (n=6). Mann-Whitney test.

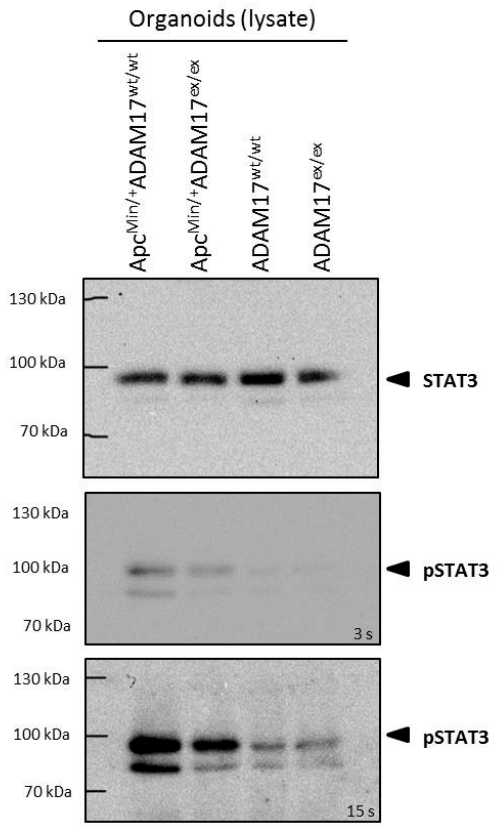

Fig. 74: STAT3 and pSTAT3 protein expression in organoids.

Indicated organoids were lysed and 50 µg of total protein were analyzed. Protein expression was assessed by Western blot analysis using a anti-STAT3 antibody (#9139) and pSTAT3 antibody (#9145).

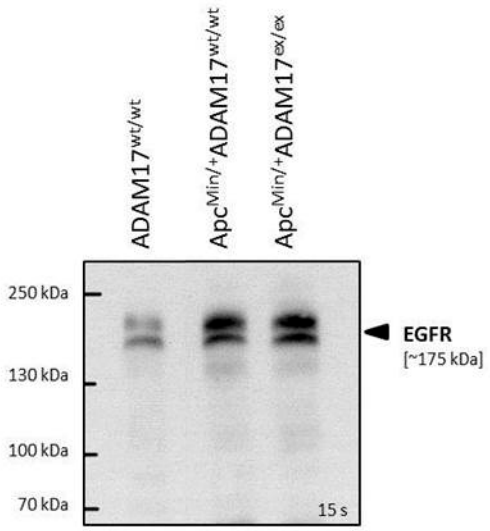

Fig. 75: EGFR protein expression in organoids.

Indicated organoids were lysed and 50 µg of total protein were analyzed. Protein expression was assessed by Western blot analysis using a anti-EGFR antibody (#52894).

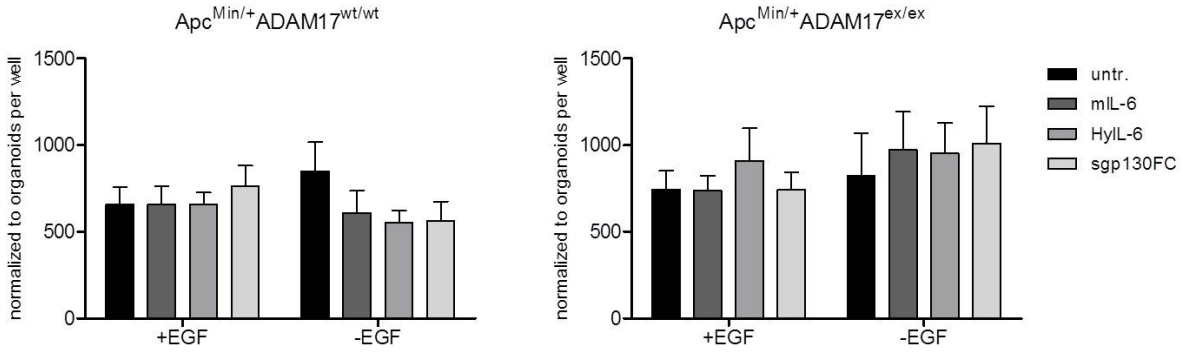

Fig. 76: Cell viability assay from organoids of hypomorphic Apc$^{Min/+}$ADAM17$^{ex/ex}$ mice.

Organoids were cultured in APC tumor medium with and without EGF and supplemented as indicated in Tab. 7 with recombinant proteins. The cell viability assays were performed as described in subchapter 2.3.6 in three independent experiments (n=3). 2way ANOVA with Bonferroni posttest $p > 0.05$.

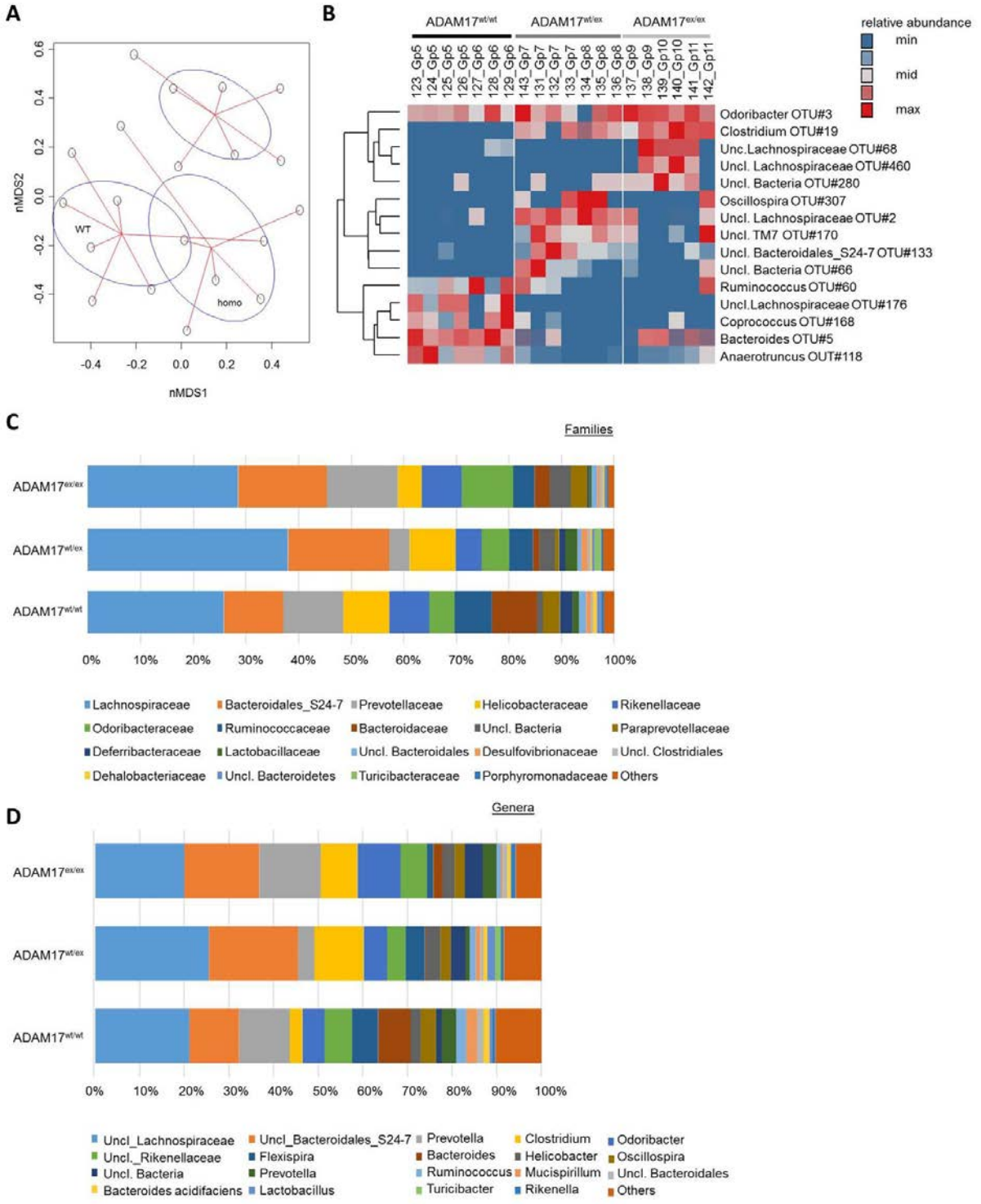

Fig. 77: Microbiome analysis of unchallenged ADAM17$^{wt/wt}$ mice, ADAM17$^{wt/ex}$ mice and hypomorphic ADAM17$^{ex/ex}$ mice.

Each genotype of mice was co-housed separately for four weeks and feces were collected. (A) Multidimensional scaling revealed distinct clustering between genotypes, (B) Operational taxonomic unit (OUT) abundance, (C-D) Significant changes in family and genera level between genotypes. Analysis in cooperation with Ateequr Rehman from the Institute of Clinical Molecular Biology (IKMB) Kiel. ADAM17$^{wt/wt}$ mice (n=10), ADAM17$^{wt/ex}$ mice (n=10) h ypomorphic ADAM17$^{ex/ex}$ mice (n=12)

Tab. 25: RNA-Sequencing: Significant downregulated pathways in intestinal neoplasia of hypomorphic $Apc^{Min/+}ADAM17^{ex/ex}$ mice.

	KEGG pathway_id_name	p.geo-mean	stat. mean	p.val	q.val	set. size	exp1
1	mmu04512 ECM-receptor interaction	0,0000	-6,0653	0,0000	0,0000	86	0,0000
2	mmu04510 Focal adhesion	0,0000	-4,8670	0,0000	0,0001	199	0,0000
3	mmu04340 Hedgehog signaling pathway	0,0002	-3,6835	0,0002	0,0101	54	0,0002
4	mmu04974 Protein digestion and absorption	0,0004	-3,4378	0,0004	0,0130	77	0,0004
5	mmu04916 Melanogenesis	0,0004	-3,3978	0,0004	0,0130	97	0,0004
6	mmu04310 Wnt signaling pathway	0,0005	-3,3429	0,0005	0,0130	146	0,0005
7	mmu04360 Axon guidance	0,0020	-2,9108	0,0020	0,0461	128	0,0020
8	mmu04742 Taste transduction	0,0032	-2,7782	0,0032	0,0654	60	0,0032
9	mmu00590 Arachidonic acid metabolism	0,0045	-2,6486	0,0045	0,0820	87	0,0045
10	mmu04530 Tight junction	0,0062	-2,5189	0,0062	0,1014	134	0,0062
11	mmu04972 Pancreatic secretion	0,0076	-2,4509	0,0076	0,1136	100	0,0076
12	mmu00072 Synthesis and degradation of ketone bodies	0,0230	-2,1515	0,0230	0,2721	10	0,0230
13	mmu04350 TGF-beta signaling pathway	0,0241	-1,9898	0,0241	0,2721	83	0,0241
14	mmu00910 Nitrogen metabolism	0,0247	-2,0266	0,0247	0,2721	23	0,0247
15	mmu04975 Fat digestion and absorption	0,0260	-1,9767	0,0260	0,2721	45	0,0260
16	mmu00900 Terpenoid backbone biosynthesis	0,0296	-2,0010	0,0296	0,2721	14	0,0296
17	mmu04520 Adherens junction	0,0316	-1,8719	0,0316	0,2721	73	0,0316
18	mmu00564 Glycerophospholipid metabolism	0,0326	-1,8579	0,0326	0,2721	80	0,0326
19	mmu00592 alpha-Linolenic acid metabolism	0,0334	-1,9106	0,0334	0,2721	20	0,0334
20	mmu00565 Ether lipid metabolism	0,0340	-1,8614	0,0340	0,2721	36	0,0340
21	mmu04540 Gap junction	0,0348	-1,8258	0,0348	0,2721	84	0,0348
22	mmu00480 Glutathione metabolism	0,0380	-1,7926	0,0380	0,2835	51	0,0380
23	mmu04610 Complement and coagulation cascades	0,0491	-1,6676	0,0491	0,3500	75	0,0491

Tab. 26: RNA-Sequencing: Significant upregulated pathways in intestinal neoplasia of hypomorphic $Apc^{Min/+}ADAM17^{ex/ex}$ mice.

	KEGG pathway_ID_name	p.geo-mean	stat. mean	p.val	q.val	Set .size	exp1
1	mmu04672 Intestinal immune network for IgA production	0,0000	4,8569	0,0000	0,0005	42	0,0000
2	mmu03030 DNA replication	0,0000	4,6479	0,0000	0,0009	35	0,0000
3	mmu04660 T cell receptor signaling pathway	0,0000	4,1747	0,0000	0,0012	107	0,0000
4	mmu04650 Natural killer cell mediated cytotoxicity	0,0001	3,8547	0,0001	0,0032	107	0,0001
5	mmu04662 B cell receptor signaling pathway	0,0001	3,7522	0,0001	0,0042	73	0,0001
6	mmu03430 Mismatch repair	0,0002	3,9999	0,0002	0,0047	22	0,0002
7	mmu03440 Homologous recombination	0,0003	3,7265	0,0003	0,0070	27	0,0003
8	mmu03040 Spliceosome	0,0006	3,3036	0,0006	0,0123	116	0,0006
9	mmu03013 RNA transport	0,0007	3,2433	0,0007	0,0125	149	0,0007
10	mmu04612 Antigen processing and presentation	0,0010	3,1388	0,0010	0,0171	68	0,0010
11	mmu04110 Cell cycle	0,0012	3,0766	0,0012	0,0175	121	0,0012
12	mmu03410 Base excision repair	0,0014	3,1152	0,0014	0,0197	31	0,0014
13	mmu03018 RNA degradation	0,0025	2,8743	0,0025	0,0320	66	0,0025
14	mmu03420 Nucleotide excision repair	0,0033	2,8064	0,0033	0,0391	42	0,0033
15	mmu04622 RIG-I-like receptor signaling pathway	0,0052	2,6127	0,0052	0,0570	65	0,0052
16	mmu04380 Osteoclast differentiation	0,0065	2,5062	0,0065	0,0662	115	0,0065
17	mmu03008 Ribosome biogenesis in eukaryotes	0,0072	2,4891	0,0072	0,0693	73	0,0072
18	mmu04620 Toll-like receptor signaling pathway	0,0079	2,4370	0,0079	0,0716	97	0,0079
19	mmu04120 Ubiquitin mediated proteolysis	0,0111	2,3069	0,0111	0,0956	132	0,0111
20	mmu04666 Fc gamma R-mediated phagocytosis	0,0200	2,0697	0,0200	0,1640	86	0,0200
21	mmu00830 Retinol metabolism	0,0213	2,0477	0,0213	0,1660	72	0,0213
22	mmu04070 Phosphatidylinositol signaling system	0,0260	1,9597	0,0260	0,1940	75	0,0260
23	mmu03015 mRNA surveillance pathway	0,0398	1,7659	0,0398	0,2813	82	0,0398

24	mmu04722 Neurotrophin signaling pathway	0,0412	1,7445	0,0412	0,2813	126	0,0412
25	mmu03450 Non-homologous end-joining	0,0462	1,7998	0,0462	0,2944	12	0,0462
26	mmu04210 Apoptosis	0,0476	1,6789	0,0476	0,2944	84	0,0476
27	mmu00983 Drug metabolism - other enzymes	0,0485	1,6748	0,0485	0,2944	54	0,0485

Tab. 27: RNA-Sequencing: Significant downregulated pathways in intestinal tissue of hypomorphic $Apc^{Min/+}ADAM17^{ex/ex}$ mice.

	KEGG pathway_id_name	p.geo-mean	stat. mean	p.val	q.val	set. size	exp1
1	mmu04510 Focal adhesion	0,0000	-6,4102	0,0000	0,0000	199	0,0000
2	mmu04512 ECM-receptor interaction	0,0000	-4,8539	0,0000	0,0001	86	0,0000
3	mmu04810 Regulation of actin cytoskeleton	0,0000	-4,1894	0,0000	0,0009	212	0,0000
4	mmu04010 MAPK signaling pathway	0,0003	-3,4946	0,0003	0,0093	265	0,0003
5	mmu04145 Phagosome	0,0003	-3,4490	0,0003	0,0093	156	0,0003
6	mmu04310 Wnt signaling pathway	0,0003	-3,4360	0,0003	0,0093	146	0,0003
7	mmu04380 Osteoclast differentiation	0,0005	-3,3212	0,0005	0,0111	115	0,0005
8	mmu04360 Axon guidance	0,0005	-3,3072	0,0005	0,0111	128	0,0005
9	mmu04670 Leukocyte transendothelial migration	0,0015	-2,9910	0,0015	0,0281	118	0,0015
10	mmu04270 Vascular smooth muscle contraction	0,0019	-2,9311	0,0019	0,0295	116	0,0019
11	mmu04350 TGF-beta signaling pathway	0,0020	-2,9239	0,0020	0,0295	83	0,0020
12	mmu04630 Jak-STAT signaling pathway	0,0028	-2,7894	0,0028	0,0385	147	0,0028
13	mmu04664 Fc epsilon RI signaling pathway	0,0040	-2,6913	0,0040	0,0499	78	0,0040
14	mmu04062 Chemokine signaling pathway	0,0046	-2,6229	0,0046	0,0532	173	0,0046
15	mmu04520 Adherens junction	0,0051	-2,6016	0,0051	0,0532	73	0,0051
16	mmu04540 Gap junction	0,0052	-2,5923	0,0052	0,0532	84	0,0052
17	mmu04640 Hematopoietic cell lineage	0,0061	-2,5367	0,0061	0,0586	81	0,0061

18	mmu04144 Endocytosis	0,0073	-2,4523	0,0073	0,0666	207	0,0073
19	mmu04610 Complement and coagulation cascades	0,0098	-2,3650	0,0098	0,0847	75	0,0098
20	mmu00565 Ether lipid metabolism	0,0111	-2,3381	0,0111	0,0876	36	0,0111
21	mmu04370 VEGF signaling pathway	0,0119	-2,2829	0,0119	0,0876	75	0,0119
22	mmu04340 Hedgehog signaling pathway	0,0120	-2,2892	0,0120	0,0876	54	0,0120
23	mmu04660 T cell receptor signaling pathway	0,0126	-2,2571	0,0126	0,0876	107	0,0126
24	mmu04530 Tight junction	0,0128	-2,2444	0,0128	0,0876	134	0,0128
25	mmu04916 Melanogenesis	0,0178	-2,1162	0,0178	0,1169	97	0,0178
26	mmu04742 Taste transduction	0,0255	-1,9729	0,0255	0,1609	60	0,0255
27	mmu04514 Cell adhesion molecules (CAMs)	0,0291	-1,9021	0,0291	0,1756	139	0,0291
28	mmu00900 Terpenoid backbone biosynthesis	0,0300	-1,9743	0,0300	0,1756	14	0,0300
29	mmu04330 Notch signaling pathway	0,0336	-1,8518	0,0336	0,1902	49	0,0336
30	mmu04912 GnRH signaling pathway	0,0401	-1,7597	0,0401	0,2163	95	0,0401
31	mmu03040 Spliceosome	0,0416	-1,7425	0,0416	0,2163	116	0,0416
32	mmu04666 Fc gamma R-mediated phagocytosis	0,0429	-1,7277	0,0429	0,2163	86	0,0429
33	mmu04620 Toll-like receptor signaling pathway	0,0435	-1,7201	0,0435	0,2163	97	0,0435

Tab. 28: RNA-Sequencing: Significant upregulated pathways in intestinal tissue of hypomorphic Apc$^{Min/+}$ADAM17$^{ex/ex}$ mice.

	KEGG pathway_id_name	p.geo-mean	stat. mean	p.val	q.val	set. size	exp1
1	mmu00980 Metabolism of xenobiotics by cytochrome P450	0,0000	4,8972	0,0000	0,0003	72	0,0000
2	mmu00982 Drug metabolism - cytochrome P450	0,0000	4,6953	0,0000	0,0003	82	0,0000
3	mmu00830 Retinol metabolism	0,0000	4,5705	0,0000	0,0003	72	0,0000
4	mmu00983 Drug metabolism - other enzymes	0,0000	4,2423	0,0000	0,0010	54	0,0000
5	mmu00020 Citrate cycle (TCA cycle)	0,0000	4,3168	0,0000	0,0011	31	0,0000
6	mmu04146 Peroxisome	0,0005	3,3648	0,0005	0,0134	78	0,0005

7	mmu00071 Fatty acid metabolism	0,0016	3,0316	0,0016	0,0375	46	0,0016
8	mmu00280 Valine, leucine and isoleucine degradation	0,0031	2,8033	0,0031	0,0631	48	0,0031
9	mmu00040 Pentose and glucuronate interconversions	0,0056	2,6241	0,0056	0,1026	29	0,0056
10	mmu00140 Steroid hormone biosynthesis	0,0097	2,3870	0,0097	0,1458	50	0,0097
11	mmu00630 Glyoxylate and dicarboxylate metabolism	0,0102	2,4253	0,0102	0,1458	19	0,0102
12	mmu00640 Propanoate metabolism	0,0112	2,3493	0,0112	0,1458	31	0,0112
13	mmu00500 Starch and sucrose metabolism	0,0116	2,3190	0,0116	0,1458	42	0,0116
14	mmu00053 Ascorbate and aldarate metabolism	0,0175	2,1854	0,0175	0,1931	23	0,0175
15	mmu04977 Vitamin digestion and absorption	0,0177	2,1731	0,0177	0,1931	24	0,0177
16	mmu00190 Oxidative phosphorylation	0,0214	2,0379	0,0214	0,2191	127	0,0214
17	mmu03060 Protein export	0,0233	2,0710	0,0233	0,2248	21	0,0233
18	mmu04142 Lysosome	0,0294	1,8981	0,0294	0,2683	120	0,0294
19	mmu00510 N-Glycan biosynthesis	0,0311	1,8911	0,0311	0,2685	50	0,0311
20	mmu00860 Porphyrin and chlorophyll metabolism	0,0353	1,8401	0,0353	0,2898	37	0,0353
21	mmu00450 Selenocompound metabolism	0,0425	1,7771	0,0425	0,3308	17	0,0425
22	mmu04141 Protein processing in endoplasmic reticulum	0,0444	1,7069	0,0444	0,3308	161	0,0444
23	mmu00380 Tryptophan metabolism	0,0464	1,7021	0,0464	0,3308	43	0,0464

B) MOUSE STRAINS

ADAM17$^{flox/flox}$ BALB/C MICE

During this thesis, the commercial available Adam17$^{tm1.2Bbl}$/J mice (Jackson Laboratory; #009597), homozygous with a loxP site and frt site upstream of exon 2 and a second loxP site downstream of exon 2 of the Adam17 gene, were backcrossed (< N10) to BALB/c mice (Charles River; #028).

The floxed *ADAM17* allele was characterized by ADAM17$^{flox/flox}$ Genotyping-PCR (Tab. 29)

Tab. 29: Layout ADAM17$^{flox/flox}$ Genotyping-PCR.

1x mix ADAM17$^{flox/flox}$ PCR	
10x Puffer DreamTaq	2.0 µl
dNTP-Mix [10 mM]	1.0 µl
$MgCl_2$ [25 mM]	1.0 µl
Primer 9041 [1:10]	2.0 µl
Primer 9218 [1:10]	2.0 µl
Primer 9219 [1:10]	2.0 µl
DreamTaq Polymerase	0.1 µl
H_2O	8.9 µl
gDNA	2.0 µl
	20.0 µl

temperature [°C]	**time [sek]**	**cycles**
94	180	1 x
94	30	35 x
58	30	
72	30	
72	600	1 x
4	∞	

Primer A17ff_9218: 5´-TGG GGA AGC AAA GTT GTA GG-3´ (common)
Primer A17ff_9219: 5´-TCT CTG GAC CCC TTC TTC CT-3´ (wildtype)
Primer A17ff_9041: 5´- CTT CGT ATA ATG TAT GCT ATA CG-3´ (mutant)

The ADAM17 wildtype allele was visualized via agarose gel electrophoresis by a PCR product of 218 bp while the heterozygous ADAM17$^{flox/+}$ was determined by PCR products of 120 bp and 218 bp and the homozygous ADAM17$^{flox/flox}$ by a PCR product of 120 bp (Fig. 77).

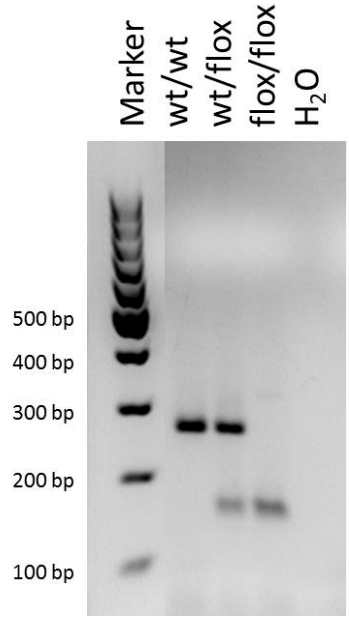

Fig. 78: Genotyping-PCR for ADAM17$^{flox/flox}$ mice.

DNA extracted from tail biopsies was used for PCR. 6x DNA loading dye was added to the samples. Up next, separation via agarose gel electrophoresis with 2 % agarose in 0.5 % TBE buffer including ethidium bromide was performed. The PCR from homozygous ADAM17$^{flox/flox}$ mice showed a result at a size of 120 bp, from heterozygous ADAM17$^{wt/flox}$ mice a size of 120 bp and 218 bp and from wildtype ADAM17$^{wt/wt}$ mice a size of 218 bp.

ADAM17$^{flox/flox}$ VILLIN CRE$^{+/-}$ MICE

During this doctoral thesis, a conditional knockout mice, so-called ADAM17$^{flox/flox}$ villin cre$^{+/}$ mice, with a tissue specific deletion of ADAM17 in intestinal epithelial cells of the small intestine and colon was generated additionally. The commercially available B6.SJL-Tg(Vil-cre)997Gum/J mice (Jackson Laboratory; #004586), heterozygous for a transgene containing the coding domain of cre recombinase driven by the murine villin 1 promoter, were crossbred with the commercially available Adam17$^{tm1.2Bbl}$/J mice (Jackson Laboratory; #009597), homozygous with a loxP site and frt site upstream of exon 2 and a second loxP site downstream of exon 2 of the Adam17 gene. Both strains were backcrossed to C57BL/6J. This results in excision of exon 2 of the *Adam17* gene which leads to the lack of ADAM17 protein expression in intestinal epithelial cells. Intestinal epithelial cell-specific ADAM17-deficiency does not induce any obvious phenotype and mice were bred normally at a usual Mendelian ratio.

The floxed *ADAM17* allele was characterized by ADAM17$^{flox/flox}$ Genotyping-PCR (Tab. 29) and visualized via agarose gel electrophoresis at a size of 120 bp (Fig. 78 A). The heterozygous villin cre$^{+/-}$ allele was characterized by villin cre$^{+/-}$ Genotyping-PCR (Tab. 30) via agarose gel electrophoresis by a PCR product of 1,000 bp (Fig. 78 B). The villin cre$^{+/-}$ Genotyping-PCR cannot distinguish homozygous from heterozygous transgenic mice.

Tab. 30: Layout villin cre$^{+/-}$ Genotyping-PCR.

1x mix villin cre$^{+/-}$ PCR	
10x Puffer DreamTaq	2.0 µl
dNTP-Mix [10 mM]	1.0 µl
Primer vc_for [1:10]	1.0 µl
Primer vc_rev [1:10]	1.0 µl
DreamTaq-Polymerase	0.1 µl
H_2O	12.9 µl
gDNA	2.0 µl
	20.0 µl

temperature [°C]	time [sek]	cycles
94	180	1 x
94	30	35 x
62	60	
72	90	
72	600	1 x
4	∞	

Primer vc_for: 5-´GTG TGG GAC AGA GAA CAA ACC-3´

Primer vc_rev: 5-´ACA TCT TCA GGT TCT GCG GG-3´

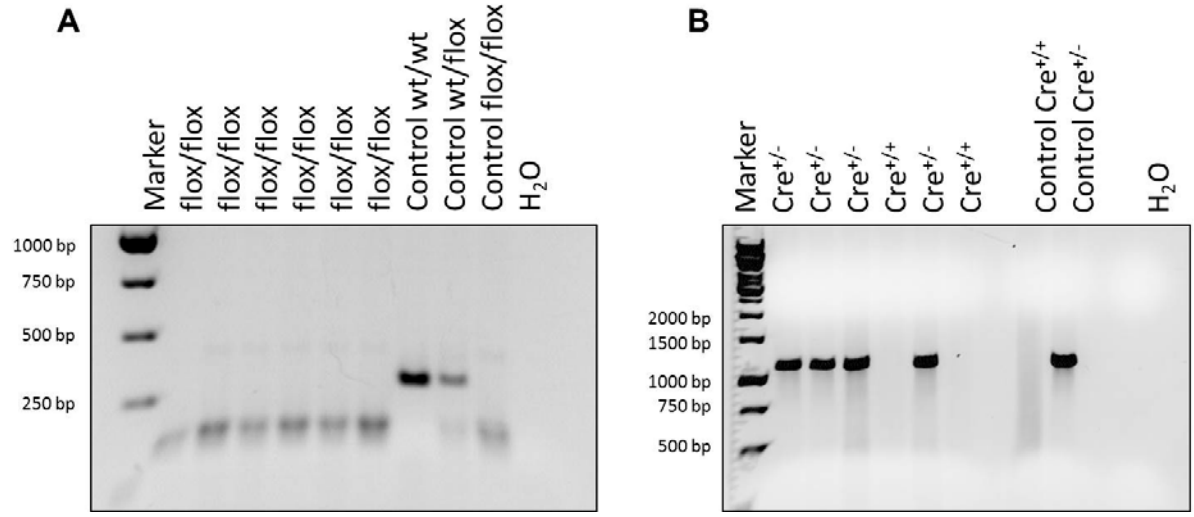

Fig. 79: Genotyping-PCR for ADAM17$^{flox/flox}$ villin cre$^{+/-}$ mice.

DNA extracted from tail biopsies was used for PCR. 6x DNA loading dye was added to the samples. Up next, separation via agarose gel electrophoresis with 2 % agarose in 0.5 % TBE buffer including ethidium bromide was performed. The PCR from homozygous ADAM17$^{flox/flox}$ mice showed a result at a size of 120 bp. The PCR product from heterozygous villin cre$^{+/-}$ mice has a size of 1,000 bp.

To confirm the successful deletion of full length ADAM17 within intestinal epithelial cells, isolated crypts (see subchapter 2.3.1) from ADAM17$^{flox/flox}$ villin cre$^{+/-}$ mice were checked for ADAM17 protein expression (Fig. 79).

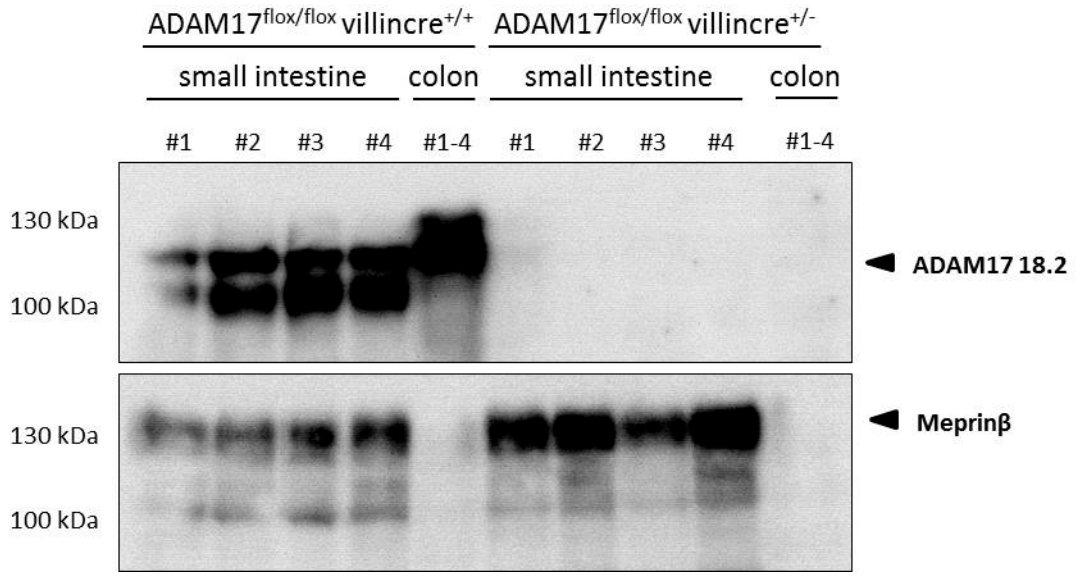

Fig. 80: Western blot of isolated crypts from ADAM17$^{flox/flox}$villin cre$^{+/-}$ mice.

Crypts of indicated mice were isolated, lysed and concentrated via Concanavalin A precipitation. Western blot analysis for ADAM17 revealed normal levels of ADAM17 protein in ADAM17$^{flox/flox}$villin cre$^{+/+}$ mice (n=4). ADAM17 was not detectable in crypts isolated from ADAM17$^{flox/flox}$villin cre$^{+/-}$ (n=4) mice, which lack ADAM17 in the intestinal epithelium. Meprinß serves as loading control.

The intestinal epithelial cells from conditional ADAM17$^{flox/flox}$ villin cre$^{+/-}$ knockout mice showed a lack of ADAM17 expression, whereas control ADAM17$^{flox/flox}$ villin cre$^{+/+}$ mice still expressed ADAM17 protein. Both mice display Meprinß protein expression as loading control.

REFERENCES

ADRAIN, C., ZETTL, M., CHRISTOVA, Y., TAYLOR, N. & FREEMAN, M. 2012. Tumor necrosis factor signaling requires iRhom2 to promote trafficking and activation of TACE. *Science,* 335**,** 225-228.

AKIYAMA, H., LYONS, J. P., MORI-AKIYAMA, Y., YANG, X., ZHANG, R., ZHANG, Z., DENG, J. M., TAKETO, M. M., NAKAMURA, T., BEHRINGER, R. R., MCCREA, P. D. & DE CROMBRUGGHE, B. 2004. Interactions between Sox9 and beta-catenin control chondrocyte differentiation. *Genes Dev,* 18**,** 1072-87.

AMOS-LANDGRAF, J. M., KWONG, L. N., KENDZIORSKI, C. M., REICHELDERFER, M., TORREALBA, J., WEICHERT, J., HAAG, J. D., CHEN, K.-S., WALLER, J. L., GOULD, M. N. & DOVE, W. F. 2007. A target-selected Apc-mutant rat kindred enhances the modeling of familial human colon cancer. *Proc Natl Acad Sci U S A,* 104**,** 4036-4041.

ANDL, C. D., MIZUSHIMA, T., OYAMA, K., BOWSER, M., NAKAGAWA, H. & RUSTGI, A. K. 2004. EGFR-induced cell migration is mediated predominantly by the JAK-STAT pathway in primary esophageal keratinocytes. *Am J Physiol Gastrointest Liver Physiol,* 287**,** G1227-37.

ARIAS, A. M., BROWN, A. M. & BRENNAN, K. 1999. Wnt signalling: pathway or network? *Curr Opin Genet Dev,* 9**,** 447-454.

ARTEAGA, C. L. & ENGELMAN, J. A. 2014. ERBB receptors: from oncogene discovery to basic science to mechanism-based cancer therapeutics. *Cancer Cell,* 25**,** 282-303.

BARKER, N. 2014. Adult intestinal stem cells: critical drivers of epithelial homeostasis and regeneration. *Nat Rev Mol Cell Biol,* 15**,** 19-33.

BARKER, N., VAN ES, J. H., KUIPERS, J., KUJALA, P., VAN DEN BORN, M., COZIJNSEN, M., HAEGEBARTH, A., KORVING, J., BEGTHEL, H., PETERS, P. J. & CLEVERS, H. 2007. Identification of stem cells in small intestine and colon by marker gene Lgr5. *Nature,* 449**,** 1003-1007.

BATLLE, E., HENDERSON, J. T., BEGHTEL, H., VAN DEN BORN, M. M., SANCHO, E., HULS, G., MEELDIJK, J., ROBERTSON, J., VAN DE WETERING, M., PAWSON, T. & CLEVERS, H. 2002. Beta-catenin and TCF mediate cell positioning in the intestinal epithelium by controlling the expression of EphB/ephrinB. *Cell,* 111**,** 251-263.

BATZER, A. G., ROTIN, D., UREÑA, J. M., SKOLNIK, E. Y. & SCHLESSINGER, J. 1994. Hierarchy of binding sites for Grb2 and Shc on the epidermal growth factor receptor. *Mol Cell Biol,* 14**,** 5192-5201.

BEN-ZE'EV, A. & GEIGER, B. 1998. Differential molecular interactions of beta-catenin and plakoglobin in adhesion, signaling and cancer. *Curr Opin Cell Biol,* 10**,** 629-639.

BIENZ, M. & CLEVERS, H. 2000. Linking colorectal cancer to Wnt signaling. *Cell,* 103**,** 311-320.

BISWAS, S. K. & MANTOVANI, A. 2010. Macrophage plasticity and interaction with lymphocyte subsets: cancer as a paradigm. *Nat Immunol,* 11**,** 889-96.

BJERKNES, M. & CHENG, H. 1981. The stem cell zone of the small intestinal epithelium. I. Evidence from paneth cells in the adult mouse. *Am J Anat,* 160**,** 51-63.

BLACHE, P., VAN DE WETERING, M., DULUC, I., DOMON, C., BERTA, P., FREUND, J. N., CLEVERS, H. & JAY, P. 2004. SOX9 is an intestine crypt transcription factor, is regulated by the Wnt pathway, and represses the CDX2 and MUC2 genes. *J Cell Biol,* 166**,** 37-47.

BLACK, R. A., RAUCH, C. T., KOZLOSKY, C. J., PESCHON, J. J., SLACK, J. L., WOLFSON, M. F., CASTNER, B. J., STOCKING, K. L., REDDY, P., SRINIVASAN, S., NELSON, N., BOIANI, N., SCHOOLEY, K. A., GERHART, M., DAVIS, R., FITZNER, J. N., JOHNSON, R. S., PAXTON, R. J., MARCH, C. J. & CERRETTI, D. P. 1997. A metalloproteinase disintegrin that releases tumour-necrosis factor-alpha from cells. *Nature,* 385**,** 729-733.

BLANCHOT-JOSSIC, F., JARRY, A., MASSON, D., BACH-NGOHOU, K., PAINEAU, J., DENIS, M. G., LABOISSE, C. L. & MOSNIER, J.-F. F. 2005. Up-regulated expression of ADAM17 in human colon carcinoma: co-expression with EGFR in neoplastic and endothelial cells. *J Pathol,* 207**,** 156-163.

BLOBEL, C. P. 2005. ADAMs: key components in EGFR signalling and development. *Nat Rev Mol Cell Biol,* 6**,** 32-43.

BLOBEL, C. P., CARPENTER, G. & FREEMAN, M. 2009. The role of protease activity in ErbB biology. *Exp Cell Res,* 315**,** 671-682.

BOIDOT, R., VEGRAN, F., JACOB, D., CHEVRIER, S., GANGNEUX, N., TABOUREAU, J., OUDIN, C., RAINVILLE, V., MERCIER, L. & LIZARD-NACOL, S. 2008. The expression of BIRC5 is correlated with loss of specific chromosomal regions in breast carcinomas. *Genes Chromosomes Cancer,* 47**,** 299-308.

BOIVIN, G. P., WASHINGTON, K., YANG, K., WARD, J. M., PRETLOW, T. P., RUSSELL, R., BESSELSEN, D. G., GODFREY, V. L., DOETSCHMAN, T., DOVE, W. F., PITOT, H. C., HALBERG, R. B., ITZKOWITZ, S. H., GRODEN, J. & COFFEY, R. J. 2003. Pathology of mouse models of intestinal cancer: Consensus report and recommendations. *Gastroenterology,* 124**,** 762-777.

BOON, E. M., VAN DER NEUT, R., VAN DE WETERING, M., CLEVERS, H. & PALS, S. T. 2002. Wnt signaling regulates expression of the receptor tyrosine kinase met in colorectal cancer. *Cancer Res,* 62**,** 5126-8.

BOS, J. L. 1989. ras oncogenes in human cancer: a review. *Cancer Res,* 49**,** 4682-4689.

BOZKULAK, E. & WEINMASTER, G. 2009. Selective Use of ADAM10 and ADAM17 in Activation of Notch1 Signaling. *Mol Cell Biol,* 29**,** 5679-5695.

BRABLETZ, T., JUNG, A., DAG, S., HLUBEK, F. & KIRCHNER, T. 1999. beta-catenin regulates the expression of the matrix metalloproteinase-7 in human colorectal cancer. *Am J Pathol,* 155**,** 1033-8.

BRANDL, K., SUN, L., NEPPL, C., SIGGS, O. M., LE GALL, S. M., TOMISATO, W., LI, X., DU, X., MAENNEL, D. N., BLOBEL, C. P. & BEUTLER, B. 2010. MyD88 signaling in nonhematopoietic cells protects mice against induced colitis by regulating specific EGF receptor ligands. *Proc Natl Acad Sci U S A,* 107**,** 19967-72.

BRAUNE, J., WEYER, U., HOBUSCH, C., MAUER, J., BRUNING, J. C., BECHMANN, I. & GERICKE, M. 2017. IL-6 Regulates M2 Polarization and Local Proliferation of Adipose Tissue Macrophages in Obesity. *J Immunol,* 198**,** 2927-2934.

BREW, K. & NAGASE, H. 2010. The tissue inhibitors of metalloproteinases (TIMPs): an ancient family with structural and functional diversity. *Biochim Biophys Acta,* 1803**,** 55-71.

BRITTAN, M. & WRIGHT, N. A. 2004. Stem cell in gastrointestinal structure and neoplastic development. *Gut,* 53**,** 899-910.

BROU, C., LOGEAT, F., GUPTA, N., BESSIA, C., LEBAIL, O., DOEDENS, J. R., CUMANO, A., ROUX, P., BLACK, R. A. & ISRAEL, A. 2000. A novel proteolytic cleavage involved in Notch signaling: the role of the disintegrin-metalloprotease TACE. *Mol Cell,* 5**,** 207-16.

BROWN, C. L., MEISE, K. S., PLOWMAN, G. D., COFFEY, R. J. & DEMPSEY, P. J. 1998. Cell surface ectodomain cleavage of human amphiregulin precursor is sensitive to a metalloprotease inhibitor. Release of a predominant N-glycosylated 43-kDa soluble form. *J Biol Chem,* 273**,** 17258-68.

CAVALLO, F., DE GIOVANNI, C., NANNI, P., FORNI, G. & LOLLINI, P.-L. L. 2011. 2011: the immune hallmarks of cancer. *Cancer Immunol Immunother,* 60**,** 319-326.

CHALARIS, A., ADAM, N., SINA, C., ROSENSTIEL, P., LEHMANN-KOCH, J., SCHIRMACHER, P., HARTMANN, D., CICHY, J., GAVRILOVA, O., SCHREIBER, S., JOSTOCK, T., MATTHEWS, V., HÄSLER, R., BECKER, C., NEURATH, M. F., REIS, K., SAFTIG, P., SCHELLER, J. & ROSE-JOHN, S. 2010. Critical role of the disintegrin metalloprotease ADAM17 for intestinal inflammation and regeneration in mice. *J Exp Med,* 207**,** 1617-1624.

CHALUPSKY, K., KANCHEV, I., ZBODAKOVA, O., BURYOVA, H., JIROUSKOVA, M., KORINEK, V., GREGOR, M. & SEDLACEK, R. 2013. ADAM10/17-dependent release of soluble c-Met correlates with hepatocellular damage. *Folia Biol (Praha),* 59**,** 76-86.

CHAPPELL, V. L., LE, L. X., LAGRONE, L. & MILESKI, W. J. 2000. Stat proteins play a role in tumor necrosis factor alpha gene expression. *Shock,* 14**,** 400-2; discussion 402-3.

CHENG, H. & LEBLOND, C. P. 1974. Origin, differentiation and renewal of the four main epithelial cell types in the mouse small intestine I. Columnar cell. *Am J Anat,* 141**,** 461-79.

CHEUNG, A. F., CARTER, A. M., KOSTOVA, K. K., WOODRUFF, J. F., CROWLEY, D., BRONSON, R. T., HAIGIS, K. M. & JACKS, T. 2009. Complete deletion of Apc results in severe polyposis in mice. *Oncogene,* 29**,** 1857-1864.

CHOI, H. J. & HAN, J. S. 2012. Overexpression of phospholipase D enhances Bcl-2 expression by activating STAT3 through independent activation of ERK and p38MAPK in HeLa cells. *Biochim Biophys Acta,* 1823**,** 1082-91.

CLEVERS, H. 2006. Wnt/beta-catenin signaling in development and disease. *Cell,* 127**,** 469-480.

CLEVERS, H. 2013. The intestinal crypt, a prototype stem cell compartment. *Cell,* 154**,** 274-284.

COHEN, S. 1962. Isolation of a mouse submaxillary gland protein accelerating incisor eruption and eyelid opening in the new-born animal. *J Biol Chem,* 237**,** 1555-1562.

COLNOT, S., NIWA-KAWAKITA, M., HAMARD, G., GODARD, C., LE PLENIER, S., HOUBRON, C., ROMAGNOLO, B., BERREBI, D., GIOVANNINI, M. & PERRET, C. 2004. Colorectal cancers in a new mouse model of familial adenomatous polyposis: influence of genetic and environmental modifiers. *Lab Invest,* 84**,** 1619-1630.

COOK, P. W., PITTELKOW, M. R., KEEBLE, W. W., GRAVES-DEAL, R., COFFEY, R. J., JR. & SHIPLEY, G. D. 1992. Amphiregulin messenger RNA is elevated in psoriatic epidermis and gastrointestinal carcinomas. *Cancer Res,* 52**,** 3224-7.

COOPER, H. S., EVERLEY, L., CHANG, W. C., PFEIFFER, G., LEE, B., MURTHY, S. & CLAPPER, M. L. 2001. The role of mutant Apc in the development of dysplasia and cancer in the mouse model of dextran sulfate sodium-induced colitis. *Gastroenterology,* 121**,** 1407-16.

CORVINUS, F. M., ORTH, C., MORIGGL, R., TSAREVA, S. A., WAGNER, S., PFITZNER, E. B., BAUS, D., KAUFMANN, R., HUBER, L. A., ZATLOUKAL, K., BEUG, H., OHLSCHLÄGER, P., SCHÜTZ, A., HALBHUBER, K.-J. J. & FRIEDRICH, K. 2005. Persistent STAT3 activation in colon cancer is associated with enhanced cell proliferation and tumor growth. *Neoplasia,* 7**,** 545-555.

DANIELSEN, A. J. & MAIHLE, N. J. 2002. The EGF/ErbB receptor family and apoptosis. *Growth factors,* 20**,** 1-15.

DARNELL, J. E., KERR, I. M. & STARK, G. R. 1994. Jak-STAT pathways and transcriptional activation in response to IFNs and other extracellular signaling proteins. *Science,* 264**,** 1415-1421.

DATTA, S. R., DUDEK, H., TAO, X., MASTERS, S., FU, H., GOTOH, Y. & GREENBERG, M. E. 1997. Akt phosphorylation of BAD couples survival signals to the cell-intrinsic death machinery. *Cell,* 91**,** 231-241.

DAVID, M., WONG, L., FLAVELL, R., THOMPSON, S. A., WELLS, A., LARNER, A. C. & JOHNSON, G. R. 1996. STAT activation by epidermal growth factor (EGF) and amphiregulin. Requirement for the EGF receptor kinase but not for tyrosine phosphorylation sites or JAK1. *J Biol Chem,* 271**,** 9185-9188.

DELKER, D. A., MCKNIGHT, S. J. & ROSENBERG, D. W. 1998. The role of alcohol dehydrogenase in the metabolism of the colon carcinogen methylazoxymethanol. *Toxicol Sci,* 45**,** 66-71.

DI RENZO, M. F., OLIVERO, M., GIACOMINI, A., PORTE, H., CHASTRE, E., MIROSSAY, L., NORDLINGER, B., BRETTI, S., BOTTARDI, S. & GIORDANO, S. 1995. Overexpression and amplification of the met/HGF receptor gene during the progression of colorectal cancer. *Clin Cancer Res,* 1**,** 147-154.

DONG, J., OPRESKO, L. K., DEMPSEY, P. J., LAUFFENBURGER, D. A., COFFEY, R. J. & WILEY, H. S. 1999. Metalloprotease-mediated ligand release regulates autocrine signaling through the epidermal growth factor receptor. *Proc Natl Acad Sci U S A,* 96**,** 6235-6240.

DOWNWARD, J., YARDEN, Y., MAYES, E., SCRACE, G., TOTTY, N., STOCKWELL, P., ULLRICH, A., SCHLESSINGER, J. & WATERFIELD, M. D. 1984. Close similarity of epidermal growth factor receptor and v-erb-B oncogene protein sequences. *Nature,* 307**,** 521-527.

DU, Y. C., OSHIMA, H., OGUMA, K., KITAMURA, T., ITADANI, H., FUJIMURA, T., PIAO, Y. S., YOSHIMOTO, T., MINAMOTO, T., KOTANI, H., TAKETO, M. M. & OSHIMA, M. 2009. Induction and down-regulation of Sox17 and its possible roles during the course of gastrointestinal tumorigenesis. *Gastroenterology,* 137**,** 1346-57.

DUFFY, M. J., MCKIERNAN, E., O'DONOVAN, N. & MCGOWAN, P. M. 2009. Role of ADAMs in cancer formation and progression. *Clin Cancer Res,* 15**,** 1140-1144.

DVORAK, H. F. 1986. Tumors: wounds that do not heal. Similarities between tumor stroma generation and wound healing. *N Engl J Med,* 315**,** 1650-9.

EDWARDS, D. R., HANDSLEY, M. M. & PENNINGTON, C. J. 2008. The ADAM metalloproteinases. *Mol Aspects Med,* 29**,** 258-289.

EGGER, B., PROCACCINO, F., LAKSHMANAN, J., REINSHAGEN, M., HOFFMANN, P., PATEL, A., REUBEN, W., GNANAKKAN, S., LIU, L., BARAJAS, L. & EYSSELEIN, V. E. 1997. Mice lacking transforming growth factor alpha have an increased susceptibility to dextran sulfate-induced colitis. *Gastroenterology,* 113**,** 825-32.

ENDRES, K., ANDERS, A., KOJRO, E., GILBERT, S., FAHRENHOLZ, F. & POSTINA, R. 2003. Tumor necrosis factor-alpha converting enzyme is processed by proprotein-convertases to its mature form which is degraded upon phorbol ester stimulation. *Eur J Biochem,* 270**,** 2386-2393.

ERICKSON, S. L., O'SHEA, K. S., GHABOOSI, N., LOVERRO, L., FRANTZ, G., BAUER, M., LU, L. H. & MOORE, M. W. 1997. ErbB3 is required for normal cerebellar and cardiac development: a comparison with ErbB2-and heregulin-deficient mice. *Development,* 124**,** 4999-5011.

FEARON, E. R., CHO, K. R., NIGRO, J. M., KERN, S. E., SIMONS, J. W., RUPPERT, J. M., HAMILTON, S. R., PREISINGER, A. C., THOMAS, G. & KINZLER, K. W. 1990. Identification of a chromosome 18q gene that is altered in colorectal cancers. *Science,* 247**,** 49-56.

FEARON, E. R. & VOGELSTEIN, B. 1990. A genetic model for colorectal tumorigenesis. *Cell,* 61**,** 759-767.

FENG, Y., SENTANI, K., WIESE, A., SANDS, E., GREEN, M., BOMMER, G. T., CHO, K. R. & FEARON, E. R. 2013. Sox9 induction, ectopic Paneth cells, and mitotic spindle axis defects in mouse colon adenomatous epithelium arising from conditional biallelic Apc inactivation. *Am J Pathol,* 183**,** 493-503.

FEVR, T., ROBINE, S., LOUVARD, D. & HUELSKEN, J. 2007. Wnt/beta-catenin is essential for intestinal homeostasis and maintenance of intestinal stem cells. *Mol Cell Biol,* 27**,** 7551-7559.

FODDE, R. 2002. The APC gene in colorectal cancer. *Eur J Cancer,* 38**,** 867-871.

FODDE, R., EDELMANN, W., YANG, K., VAN LEEUWEN, C., CARLSON, C., RENAULT, B., BREUKEL, C., ALT, E., LIPKIN, M. & KHAN, P. M. 1994. A targeted chain-termination mutation in the mouse Apc gene results in multiple intestinal tumors. *Proc Natl Acad Sci U S A,* 91**,** 8969-8973.

FODDE, R., KUIPERS, J., ROSENBERG, C., SMITS, R., KIELMAN, M., GASPAR, C., VAN ES, J. H., BREUKEL, C., WIEGANT, J., GILES, R. H. & CLEVERS, H. 2001a. Mutations in the APC tumour suppressor gene cause chromosomal instability. *Nat Cell Biol,* 3**,** 433-438.

FODDE, R., SMITS, R. & CLEVERS, H. 2001b. APC, signal transduction and genetic instability in colorectal cancer. *Nat Rev Cancer,* 1**,** 55-67.

FOLGOSA, L., ZELLNER, H. B., EL SHIKH, M. E. & CONRAD, D. H. 2013. Disturbed follicular architecture in B cell A disintegrin and metalloproteinase (ADAM)10 knockouts is mediated by compensatory increases in ADAM17 and TNF-α shedding. *J Immunol,* 191**,** 5951-5958.

FRANKE, T. F., KAPLAN, D. R., CANTLEY, L. C. & TOKER, A. 1997. Direct regulation of the Akt proto-oncogene product by phosphatidylinositol-3,4-bisphosphate. *Science,* 275**,** 665-668.

FREY, M. R. & BRENT POLK, D. 2014. ErbB receptors and their growth factor ligands in pediatric intestinal inflammation. *Pediatr Res,* 75**,** 127-132.

FUNAYAMA, N., FAGOTTO, F., MCCREA, P. & GUMBINER, B. M. 1995. Embryonic axis induction by the armadillo repeat domain of beta-catenin: evidence for intracellular signaling. *J Cell Biol,* 128**,** 959-968.

GARRETT, T. P., MCKERN, N. M., LOU, M., ELLEMAN, T. C., ADAMS, T. E., LOVRECZ, G. O., KOFLER, M., JORISSEN, R. N., NICE, E. C., BURGESS, A. W. & WARD, C. W. 2003. The crystal structure of a truncated ErbB2 ectodomain reveals an active conformation, poised to interact with other ErbB receptors. *Mol Cell,* 11**,** 495-505.

GASSMANN, M., CASAGRANDA, F., ORIOLI, D., SIMON, H., LAI, C., KLEIN, R. & LEMKE, G. 1995. Aberrant neural and cardiac development in mice lacking the ErbB4 neuregulin receptor. *Nature,* 378**,** 390-394.

GILMORE, A. P. 2005. Anoikis. *Cell Death Differ,* 12 Suppl 2**,** 1473-1477.

GJOREVSKI, N., SACHS, N., MANFRIN, A., GIGER, S., BRAGINA, M. E., ORDONEZ-MORAN, P., CLEVERS, H. & LUTOLF, M. P. 2016. Designer matrices for intestinal stem cell and organoid culture. *Nature,* 539**,** 560-564.

GRAUS-PORTA, D., BEERLI, R. R., DALY, J. M. & HYNES, N. E. 1997. ErbB-2, the preferred heterodimerization partner of all ErbB receptors, is a mediator of lateral signaling. *EMBO J,* 16**,** 1647-1655.

GREGORIEFF, A., LIU, Y., INANLOU, M. R., KHOMCHUK, Y. & WRANA, J. L. 2015. Yap-dependent reprogramming of Lgr5+ stem cells drives intestinal regeneration and cancer. *Nature,* 526**,** 715-718.

GRITSKO, T., WILLIAMS, A., TURKSON, J., KANEKO, S., BOWMAN, T., HUANG, M., NAM, S., EWEIS, I., DIAZ, N., SULLIVAN, D., YODER, S., ENKEMANN, S., ESCHRICH, S., LEE, J. H., BEAM, C. A., CHENG, J., MINTON, S., MURO-CACHO, C. A. & JOVE, R. 2006. Persistent activation of stat3 signaling induces survivin gene expression and confers resistance to apoptosis in human breast cancer cells. *Clin Cancer Res,* 12**,** 11-9.

GRIVENNIKOV, S., KARIN, E., TERZIC, J., MUCIDA, D., YU, G. Y., VALLABHAPURAPU, S., SCHELLER, J., ROSE-JOHN, S., CHEROUTRE, H., ECKMANN, L. & KARIN, M. 2009. IL-6 and Stat3 are required for survival of intestinal epithelial cells and development of colitis-associated cancer. *Cancer Cell,* 15**,** 103-13.

GRIVENNIKOV, S. I., GRETEN, F. R. & KARIN, M. 2010. Immunity, inflammation, and cancer. *Cell,* 140**,** 883-99.

GRODEN, J., THLIVERIS, A., SAMOWITZ, W., CARLSON, M., GELBERT, L., ALBERTSEN, H., JOSLYN, G., STEVENS, J., SPIRIO, L. & ROBERTSON, M. 1991. Identification and characterization of the familial adenomatous polyposis coli gene. *Cell,* 66**,** 589-600.

GUPTA, R. B., HARPAZ, N., ITZKOWITZ, S., HOSSAIN, S., MATULA, S., KORNBLUTH, A., BODIAN, C. & ULLMAN, T. 2007. Histologic inflammation is a risk factor for progression to colorectal neoplasia in ulcerative colitis: a cohort study. *Gastroenterology,* 133**,** 1099.

GUY, P. M., PLATKO, J. V., CANTLEY, L. C., CERIONE, R. A. & CARRAWAY, K. L. 1994. Insect cell-expressed p180erbB3 possesses an impaired tyrosine kinase activity. *Proc Natl Acad Sci U S A,* 91**,** 8132-8136.

HANADA, T., KOBAYASHI, T., CHINEN, T., SAEKI, K., TAKAKI, H., KOGA, K., MINODA, Y., SANADA, T., YOSHIOKA, T., MIMATA, H., KATO, S. & YOSHIMURA, A. 2006. IFNgamma-dependent, spontaneous development of colorectal carcinomas in SOCS1-deficient mice. *J Exp Med,* 203**,** 1391-1397.

HANAHAN, D. & WEINBERG, R. A. 2000. The Hallmarks of Cancer. *Cell,* 100**,** 57-70.

HANAHAN, D. & WEINBERG, R. A. 2011. Hallmarks of Cancer: The Next Generation. *Cell,* 144**,** 646-674.

HARARI, D., TZAHAR, E., ROMANO, J., SHELLY, M., PIERCE, J. H., ANDREWS, G. C. & YARDEN, Y. 1999. Neuregulin-4: a novel growth factor that acts through the ErbB-4 receptor tyrosine kinase. *Oncogene,* 18**,** 2681-2689.

HARDBOWER, D. M., COBURN, L. A., ASIM, M., SINGH, K., SIERRA, J. C., BARRY, D. P., GOBERT, A. P., PIAZUELO, M. B., WASHINGTON, M. K. & WILSON, K. T. 2017. EGFR-mediated macrophage activation promotes colitis-associated tumorigenesis. *Oncogene,* 36**,** 3807-3819.

HARRIS, R. C., CHUNG, E. & COFFEY, R. J. 2003. EGF receptor ligands. *Exp Cell Res,* 284**,** 2-13.

HE, T. C., SPARKS, A. B., RAGO, C., HERMEKING, H., ZAWEL, L., DA COSTA, L. T., MORIN, P. J., VOGELSTEIN, B. & KINZLER, K. W. 1998. Identification of c-MYC as a target of the APC pathway. *Science,* 281**,** 1509-12.

HEATH, J. P. 1996. Epithelial cell migration in the intestine. *Cell Biol Int,* 20**,** 139-146.

HEYER, J., YANG, K., LIPKIN, M., EDELMANN, W. & KUCHERLAPATI, R. 1999. Mouse models for colorectal cancer. *Oncogene,* 18**,** 5325-5333.

HIGGINBOTHAM, J. N., DEMORY BECKLER, M., GEPHART, J. D., FRANKLIN, J. L., BOGATCHEVA, G., KREMERS, G.-J. J., PISTON, D. W., AYERS, G. D., MCCONNELL, R. E., TYSKA, M. J. & COFFEY, R. J. 2011. Amphiregulin exosomes increase cancer cell invasion. *Curr Biol,* 21**,** 779-786.

HINKLE, C. L., SUNNARBORG, S. W., LOISELLE, D., PARKER, C. E., STEVENSON, M., RUSSELL, W. E. & LEE, D. C. 2004. Selective roles for tumor necrosis factor alpha-converting enzyme/ADAM17 in the shedding of the epidermal growth factor receptor ligand family: the juxtamembrane stalk determines cleavage efficiency. *J Biol Chem,* 279**,** 24179-24188.

HOOPER, N. M., KARRAN, E. H. & TURNER, A. J. 1997. Membrane protein secretases. *Biochem J,* 321 (Pt 2)**,** 265-79.

HUANG, M. Y., CHANG, H. J., CHUNG, F. Y., YANG, M. J., YANG, Y. H., WANG, J. Y. & LIN, S. R. 2010. MMP13 is a potential prognostic marker for colorectal cancer. *Oncol Rep,* 24**,** 1241-7.

HUBBARD, S. R., MOHAMMADI, M. & SCHLESSINGER, J. 1998. Autoregulatory mechanisms in protein-tyrosine kinases. *J Biol Chem,* 273**,** 11987-11990.

HUNG, W. & ELLIOTT, B. 2001. Co-operative effect of c-Src tyrosine kinase and Stat3 in activation of hepatocyte growth factor expression in mammary carcinoma cells. *J Biol Chem,* 276**,** 12395-403.

HURSTING, S. D., SLAGA, T. J., FISCHER, S. M., DIGIOVANNI, J. & PHANG, J. M. 1999. Mechanism-based cancer prevention approaches: targets, examples, and the use of transgenic mice. *J Natl Cancer Inst,* 91**,** 215-225.

ITZKOWITZ, S. H. & HARPAZ, N. 2004. Diagnosis and management of dysplasia in patients with inflammatory bowel diseases. *Gastroenterology,* 126**,** 1634-1648.

ITZKOWITZ, S. H. & YIO, X. 2004. Inflammation and cancer IV. Colorectal cancer in inflammatory bowel disease: the role of inflammation. *Am J Physiol Gastrointest Liver Physiol,* 287**,** G7-17.

JACKSON, L. F., QIU, T. H., SUNNARBORG, S. W., CHANG, A., ZHANG, C., PATTERSON, C. & LEE, D. C. 2003. Defective valvulogenesis in HB-EGF and TACE-null mice is associated with aberrant BMP signaling. *EMBO J,* 22**,** 2704-2716.

JOHNSON, G. R. & WONG, L. 1994. Heparan sulfate is essential to amphiregulin-induced mitogenic signaling by the epidermal growth factor receptor. *J Biol Chem,* 269**,** 27149-27154.

JONES, J. C., RUSTAGI, S. & DEMPSEY, P. J. 2015. ADAM Proteases and Gastrointestinal Function. *Annu Rev Physiol,* 78**,** 243-76.

JORISSEN, R. N., WALKER, F., POULIOT, N., GARRETT, T. P. J., WARD, C. W. & BURGESS, A. W. 2003. Epidermal growth factor receptor: mechanisms of activation and signalling. *Exp Cell Res,* 284**,** 31-53.

JOSTOCK, T., MULLBERG, J., OZBEK, S., ATREYA, R., BLINN, G., VOLTZ, N., FISCHER, M., NEURATH, M. F. & ROSE-JOHN, S. 2001. Soluble gp130 is the natural inhibitor of soluble interleukin-6 receptor transsignaling responses. *Eur J Biochem,* 268**,** 160-7.

KAISER, S., PARK, Y.-K. K., FRANKLIN, J. L., HALBERG, R. B., YU, M., JESSEN, W. J., FREUDENBERG, J., CHEN, X., HAIGIS, K., JEGGA, A. G., KONG, S., SAKTHIVEL, B., XU, H., REICHLING, T., AZHAR, M., BOIVIN, G. P., ROBERTS, R. B., BISSAHOYO, A. C., GONZALES, F., BLOOM, G. C., ESCHRICH, S., CARTER, S. L., ARONOW, J. E., KLEIMEYER, J., KLEIMEYER, M., RAMASWAMY, V., SETTLE, S. H., BOONE, B., LEVY, S., GRAFF, J. M., DOETSCHMAN, T., GRODEN, J., DOVE, W. F., THREADGILL, D. W., YEATMAN, T. J., COFFEY, R. J. & ARONOW, B. J. 2007. Transcriptional recapitulation and subversion of embryonic colon development by mouse colon tumor models and human colon cancer. *Genome Biol,* 8**,** R131.

KENNY, P. A. & BISSELL, M. J. 2007. Targeting TACE-dependent EGFR ligand shedding in breast cancer. *J Clin Invest,* 117**,** 337-345.

KHOKHA, R., MURTHY, A. & WEISS, A. 2013. Metalloproteinases and their natural inhibitors in inflammation and immunity. *Nat Rev Immunol,* 13**,** 649-665.

KIMELMAN, D. & XU, W. 2006. beta-catenin destruction complex: insights and questions from a structural perspective. *Oncogene,* 25**,** 7482-7491.

KING, L. E., CARPENTER, G. & COHEN, S. 1980. Characterization by electrophoresis of epidermal growth factor stimulated phosphorylation using A-431 membranes. *Biochemistry,* 19**,** 1524-1528.

KINJYO, I., INOUE, H., HAMANO, S., FUKUYAMA, S., YOSHIMURA, T., KOGA, K., TAKAKI, H., HIMENO, K., TAKAESU, G., KOBAYASHI, T. & YOSHIMURA, A. 2006. Loss of SOCS3 in T helper cells resulted in reduced immune responses and hyperproduction of interleukin 10 and transforming growth factor-beta 1. *J Exp Med,* 203**,** 1021-31.

KINZLER , N. M., SU LK, VOGELSTEIN B, BRYAN TM, LEVY DB, SMITH KJ, PREISINGER AC, HEDGE P, MCKECHNIE D, ET AL. 1991. Identification of FAP locus genes from chromosome 5q21. *Science,* 253**,** 661-5.

KITAJIMA, S., MORIMOTO, M., SAGARA, E., SHIMIZU, C. & IKEDA, Y. 2001. Dextran sodium sulfate-induced colitis in germ-free IQI/Jic mice. *Exp Anim,* 50**,** 387-95.

KIUCHI, N., NAKAJIMA, K., ICHIBA, M., FUKADA, T., NARIMATSU, M., MIZUNO, K., HIBI, M. & HIRANO, T. 1999. STAT3 is required for the gp130-mediated full activation of the c-myc gene. *J Exp Med,* 189**,** 63-73.

KNUDSON, A. G., HETHCOTE, H. W. & BROWN, B. W. 1975. Mutation and childhood cancer: a probabilistic model for the incidence of retinoblastoma. *Proc Natl Acad Sci U S A,* 72**,** 5116-5120.

KONDAPAKA, S. B., FRIDMAN, R. & REDDY, K. B. 1997. Epidermal growth factor and amphiregulin up-regulate matrix metalloproteinase-9 (MMP-9) in human breast cancer cells. *Int J Cancer,* 70**,** 722-726.

KORINEK, V., BARKER, N., MOERER, P., VAN DONSELAAR, E., HULS, G., PETERS, P. J. & CLEVERS, H. 1998. Depletion of epithelial stem-cell compartments in the small intestine of mice lacking Tcf-4. *Nat Genet,* 19**,** 379-383.

LAKEN, S. J., PAPADOPOULOS, N., PETERSEN, G. M., GRUBER, S. B., HAMILTON, S. R., GIARDIELLO, F. M., BRENSINGER, J. D., VOGELSTEIN, B. & KINZLER, K. W. 1999. Analysis of masked mutations in familial adenomatous polyposis. *Proc Natl Acad Sci U S A,* 96**,** 2322-2326.

LANAYA, H., NATARAJAN, A., KOMPOSCH, K., LI, L., AMBERG, N., CHEN, L., WCULEK, S. K., HAMMER, M., ZENZ, R., PECK-RADOSAVLJEVIC, M., SIEGHART, W., TRAUNER, M., WANG, H. & SIBILIA, M. 2014. EGFR has a tumour-promoting role in liver macrophages during hepatocellular carcinoma formation. *Nat Cell Biol,* 16**,** 972-81.

LEE, J. S., ISHIMOTO, A. & YANAGAWA, S. 1999. Characterization of mouse dishevelled (Dvl) proteins in Wnt/Wingless signaling pathway. *J Biol Chem,* 274**,** 21464-21470.

LEE, K. F., SIMON, H., CHEN, H., BATES, B., HUNG, M. C. & HAUSER, C. 1995. Requirement for neuregulin receptor erbB2 in neural and cardiac development. *Nature,* 378**,** 394-398.

LESLIE, K., LANG, C., DEVGAN, G., AZARE, J., BERISHAJ, M., GERALD, W., KIM, Y. B., PAZ, K., DARNELL, J. E., ALBANESE, C., SAKAMAKI, T., PESTELL, R. & BROMBERG, J. 2006. Cyclin D1 is transcriptionally regulated by and required for transformation by activated signal transducer and activator of transcription 3. *Cancer Res,* 66**,** 2544-52.

LI, L. & CLEVERS, H. 2010. Coexistence of Quiescent and Active Adult Stem Cells in Mammals. *Science,* 327**,** 542-545.

LÓPEZ-OTÍN, C. & MATRISIAN, L. M. 2007. Emerging roles of proteases in tumour suppression. *Nat Rev Cancer,* 7**,** 800-808.

LORENZEN, I., LOKAU, J., DÜSTERHÖFT, S., TRAD, A., GARBERS, C., SCHELLER, J., ROSE-JOHN, S. & GRÖTZINGER, J. 2012. The membrane-proximal domain of A Disintegrin and Metalloprotease 17 (ADAM17) is responsible for recognition of the interleukin-6 receptor and interleukin-1 receptor II. *FEBS Lett,* 586**,** 1093-1100.

LU, J., YE, X., FAN, F., XIA, L., BHATTACHARYA, R., BELLISTER, S., TOZZI, F., SCEUSI, E., ZHOU, Y., TACHIBANA, I., MARU, D. M., HAWKE, D. H., RAK, J., MANI, S. A., ZWEIDLER-MCKAY, P. & ELLIS, L. M. 2013. Endothelial cells promote the colorectal cancer stem cell phenotype through a soluble form of Jagged-1. *Cancer Cell,* 23**,** 171-185.

LUETTEKE, N. C., PHILLIPS, H. K., QIU, T. H., COPELAND, N. G., EARP, H. S., JENKINS, N. A. & LEE, D. C. 1994. The mouse waved-2 phenotype results from a point mutation in the EGF receptor tyrosine kinase. *Genes Dev,* 8**,** 399-413.

LUETTEKE, N. C., QIU, T. H., FENTON, S. E., TROYER, K. L., RIEDEL, R. F., CHANG, A. & LEE, D. C. 1999. Targeted inactivation of the EGF and amphiregulin genes reveals distinct roles for EGF receptor ligands in mouse mammary gland development. *Development,* 126**,** 2739-2750.

LUONGO, C., MOSER, A. R., GLEDHILL, S. & DOVE, W. F. 1994. Loss of Apc+ in intestinal adenomas from Min mice. *Cancer Res,* 54**,** 5947-5952.

MARSHALL, C. J. 1994. MAP kinase kinase kinase, MAP kinase kinase and MAP kinase. *Curr Opin Genet Dev,* 4**,** 82-89.

MARSHMAN, E., BOOTH, C. & POTTEN, C. S. 2002. The intestinal epithelial stem cell. *Bioessays,* 24**,** 91-98.

MAUER, J., CHAURASIA, B., GOLDAU, J., VOGT, M. C., RUUD, J., NGUYEN, K. D., THEURICH, S., HAUSEN, A. C., SCHMITZ, J., BRONNEKE, H. S., ESTEVEZ, E., ALLEN, T. L., MESAROS, A., PARTRIDGE, L., FEBBRAIO, M. A., CHAWLA, A., WUNDERLICH, F. T. & BRUNING, J. C. 2014. Signaling by IL-6 promotes alternative activation of macrophages to limit endotoxemia and obesity-associated resistance to insulin. *Nat Immunol,* 15**,** 423-30.

MAY, P. & MAY, E. 1999. Twenty years of p53 research: structural and functional aspects of the p53 protein. *Oncogene,* 18**,** 7621-7636.

MCGOWAN, P. M., MCKIERNAN, E., BOLSTER, F., RYAN, B. M., HILL, A. D., MCDERMOTT, E. W., EVOY, D., O'HIGGINS, N., CROWN, J. & DUFFY, M. J. 2008. ADAM-17 predicts adverse outcome in patients with breast cancer. *Ann Oncol,* 19**,** 1075-1081.

MCGUCKIN, M. A., ERI, R., SIMMS, L. A., FLORIN, T. & RADFORD SMITH, G. 2009. Intestinal barrier dysfunction in inflammatory bowel diseases. *Inflamm Bowel Dis,* 15**,** 100-113.

MERCHANT, N. B., VOSKRESENSKY, I., ROGERS, C. M., LAFLEUR, B., DEMPSEY, P. J., GRAVES-DEAL, R., REVETTA, F., FOUTCH, C. A., ROTHENBERG, M. L., WASHINGTON, M. K. & COFFEY, R. J. 2008. TACE/ADAM-17: A Component of the Epidermal Growth Factor Receptor Axis and a Promising Therapeutic Target in Colorectal Cancer. *Clin Cancer Res,* 14**,** 1182-1191.

MIETTINEN, P. J., BERGER, J. E., MENESES, J., PHUNG, Y., PEDERSEN, R. A., WERB, Z. & DERYNCK, R. 1995. Epithelial immaturity and multiorgan failure in mice lacking epidermal growth factor receptor. *Nature,* 376**,** 337-341.

MIWA, N., FURUSE, M., TSUKITA, S., NIIKAWA, N., NAKAMURA, Y. & FURUKAWA, Y. 2001. Involvement of claudin-1 in the beta-catenin/Tcf signaling pathway and its frequent upregulation in human colorectal cancers. *Oncol Res,* 12**,** 469-76.

MOOLENBEEK, C. & RUITENBERG, E. J. 1981. The "Swiss roll": a simple technique for histological studies of the rodent intestine. *Lab Anim,* 15**,** 57-59.

MORIN, P. J., SPARKS, A. B., KORINEK, V., BARKER, N., CLEVERS, H., VOGELSTEIN, B. & KINZLER, K. W. 1997. Activation of beta-catenin-Tcf signaling in colon cancer by mutations in beta-catenin or APC. *Science,* 275**,** 1787-90.

MOSER, A. R., PITOT, H. C. & DOVE, W. F. 1990. A Dominant Mutation That Predispose to Multiple Intestinal Neoplasia in the Mouse. *Science* 247**,** 322-324.

MOSS, M. L., JIN, S. L., MILLA, M. E., BICKETT, D. M., BURKHART, W., CARTER, H. L., CHEN, W. J., CLAY, W. C., DIDSBURY, J. R., HASSLER, D., HOFFMAN, C. R., KOST, T. A., LAMBERT, M. H., LEESNITZER, M. A., MCCAULEY, P., MCGEEHAN, G., MITCHELL, J., MOYER, M., PAHEL, G., ROCQUE, W., OVERTON, L. K., SCHOENEN, F., SEATON, T., SU, J. L. & BECHERER, J. D. 1997. Cloning of a disintegrin metalloproteinase that processes precursor tumour-necrosis factor-alpha. *Nature,* 385**,** 733-736.

MOWAT, A. M. & AGACE, W. W. 2014. Regional specialization within the intestinal immune system. *Nat Rev Immunol,* 14**,** 667-85.

MURPHY, G. 2008. The ADAMs: signalling scissors in the tumour microenvironment. *Nat Rev Cancer,* 8**,** 929-941.

MURTHY, A., SHAO, Y. W., NARALA, S. R., MOLYNEUX, S. D., ZUNIGA-PFLUCKER, J. C. & KHOKHA, R. 2012. Notch activation by the metalloproteinase ADAM17 regulates myeloproliferation and atopic barrier immunity by suppressing epithelial cytokine synthesis. *Immunity,* 36**,** 105-19.

MURUMKAR, P. R., DASGUPTA, S., CHANDANI, S. R., GIRIDHAR, R. & YADAV, M. R. 2010. Novel TACE inhibitors in drug discovery: a review of patented compounds. *Expert Opin Ther Pat,* 20**,** 31-57.

MUSTAFI, R., DOUGHERTY, U., MUSTAFI, D., AYALOGLU-BUTUN, F., FLETCHER, M., ADHIKARI, S., SADIQ, F., MECKEL, K., HAIDER, H. I., KHALIL, A., PEKOW, J., KONDA, V., JOSEPH, L., HART, J., FICHERA, A., LI, Y. C. & BISSONNETTE, M. 2017. ADAM17 is a Tumor Promoter and Therapeutic Target in Western Diet-associated Colon Cancer. *Clin Cancer Res,* 23**,** 549-561.

NAKAGAWA, M., NABESHIMA, K. & ASANO, S. 2009. Upregulated expression of ADAM17 in gastrointestinal stromal tumors: coexpression with EGFR and EGFR ligands. *Cancer Sci,* 100**,** 654-62.

NAKAMURA, T., TSUCHIYA, K. & WATANABE, M. 2007. Crosstalk between Wnt and Notch signaling in intestinal epithelial cell fate decision. *J Gastroenterol,* 42**,** 705-10.

NÄTHKE, I. S. 2004. The adenomatous polyposis coli protein: the Achilles heel of the gut epithelium. *Annu Rev Cell Dev Biol,* 20**,** 337-366.

NEUFERT, C., BECKER, C. & NEURATH, M. F. 2007. An inducible mouse model of colon carcinogenesis for the analysis of sporadic and inflammation-driven tumor progression. *Nat Protoc,* 2**,** 1998-2004.

NEUFERT, C., BECKER, C., TÜRECI, Ö., WALDNER, M. J., BACKERT, I., FLOH, K., ATREYA, I., LEPPKES, M., JEFREMOW, A., VIETH, M., SCHNEIDER-STOCK, R., KLINGER, P., GRETEN, F. R., THREADGILL, D. W., SAHIN, U. & NEURATH, M. F. 2013. Tumor fibroblast-derived epiregulin promotes growth of colitis-associated neoplasms through ERK. *J Clin Invest,* 123**,** 1428-1443.

NIH HMP WORKING GROUP, PETERSON, J., GARGES, S., GIOVANNI, M., MCINNES, P., WANG, L., SCHLOSS, J. A., BONAZZI, V., MCEWEN, J. E., WETTERSTRAND, K. A., DEAL, C., BAKER, C. C., DI FRANCESCO, V., HOWCROFT, T. K., KARP, R. W., LUNSFORD, R. D., WELLINGTON, C. R., BELACHEW, T., WRIGHT, M., GIBLIN, C., DAVID, H., MILLS, M., SALOMON, R., MULLINS, C., AKOLKAR, B., BEGG, L., DAVIS, C., GRANDISON, L., HUMBLE, M., KHALSA, J., LITTLE, A. R., PEAVY, H., PONTZER, C., PORTNOY, M., SAYRE, M. H., STARKE-REED, P., ZAKHARI, S., READ, J., WATSON, B. & GUYER, M. 2009. The NIH Human Microbiome Project. *Genome Res,* 19**,** 2317-2323.

NOAH, T. K. & SHROYER, N. F. 2013. Notch in the intestine: regulation of homeostasis and pathogenesis. *Annu Rev Physiol,* 75**,** 263-288.

OHTSU, H., DEMPSEY, P. J. & EGUCHI, S. 2006. ADAMs as mediators of EGF receptor transactivation by G protein-coupled receptors. *Am J Physiol Cell Physiol,* 291.

OLAYIOYE, M. A., NEVE, R. M., LANE, H. A. & HYNES, N. E. 2000. The ErbB signaling network: receptor heterodimerization in development and cancer. *EMBO J,* 19**,** 3159-3167.

OSHIMA, M., OSHIMA, H., KITAGAWA, K., KOBAYASHI, M., ITAKURA, C. & TAKETO, M. 1995. Loss of Apc heterozygosity and abnormal tissue building in nascent intestinal polyps in mice carrying a truncated Apc gene. *Proc Natl Acad Sci U S A,* 92**,** 4482-4486.

PAWSON, T. & GISH, G. D. 1992. SH2 and SH3 domains: from structure to function. *Cell,* 71**,** 359-362.

PESCHON, J. J., SLACK, J. L., REDDY, P., STOCKING, K. L., SUNNARBORG, S. W., LEE, D. C., RUSSELL, W. E., CASTNER, B. J., JOHNSON, R. S., FITZNER, J. N., BOYCE, R. W., NELSON, N., KOZLOSKY, C. J., WOLFSON, M. F., RAUCH, C. T., CERRETTI, D. P., PAXTON, R. J., MARCH, C. J. & BLACK, R. A. 1998. An essential role for ectodomain shedding in mammalian development. *Science* 282**,** 1281-1284.

PLOWMAN, G. D., GREEN, J. M., MCDONALD, V. L., NEUBAUER, M. G., DISTECHE, C. M., TODARO, G. J. & SHOYAB, M. 1990a. The amphiregulin gene encodes a novel epidermal growth factor-related protein with tumor-inhibitory activity. *Mol Cell Biol,* 10**,** 1969-1981.

PLOWMAN, G. D., WHITNEY, G. S., NEUBAUER, M. G., GREEN, J. M., MCDONALD, V. L., TODARO, G. J. & SHOYAB, M. 1990b. Molecular cloning and expression of an additional epidermal growth factor receptor-related gene. *Proc Natl Acad Sci U S A,* 87**,** 4905-4909.

POLAKIS, P. 2000. Wnt signaling and cancer. *Genes Dev,* 14**,** 1837-1851.

POWELL, S. M., ZILZ, N., BEAZER-BARCLAY, Y., BRYAN, T. M., HAMILTON, S. R., THIBODEAU, S. N., VOGELSTEIN, B. & KINZLER, K. W. 1992. APC mutations occur early during colorectal tumorigenesis. *Nature,* 359**,** 235-237.

PRENZEL, N., ZWICK, E., DAUB, H., LESERER, M., ABRAHAM, R., WALLASCH, C. & ULLRICH, A. 1999. EGF receptor transactivation by G-protein-coupled receptors requires metalloproteinase cleavage of proHB-EGF. *Nature,* 402**,** 884-8.

QIAN, B. Z. & POLLARD, J. W. 2010. Macrophage diversity enhances tumor progression and metastasis. *Cell,* 141**,** 39-51.

QUESADA, C. F., KIMATA, H., MORI, M., NISHIMURA, M., TSUNEYOSHI, T. & BABA, S. 1998. Piroxicam and acarbose as chemopreventive agents for spontaneous intestinal adenomas in APC gene 1309 knockout mice. *Jpn J Cancer Res,* 89**,** 392-396.

QUESNELLE, K. M., BOEHM, A. L. & GRANDIS, J. R. 2007. STAT-mediated EGFR signaling in cancer. *J Cell Biochem,* 102**,** 311-319.

RABE, B., CHALARIS, A., MAY, U., WAETZIG, G. H., SEEGERT, D., WILLIAMS, A. S., JONES, S. A., ROSE-JOHN, S. & SCHELLER, J. 2008. Transgenic blockade of interleukin 6 transsignaling abrogates inflammation. *Blood,* 111**,** 1021-8.

RADTKE, F. & CLEVERS, H. 2005. Self-Renewal and Cancer of the Gut: Two Sides of a Coin. *Science,* 307**,** 1904-1909.

REDDY, P., SLACK, J. L., DAVIS, R., CERRETTI, D. P., KOZLOSKY, C. J., BLANTON, R. A., SHOWS, D., PESCHON, J. J. & BLACK, R. A. 2000. Functional analysis of the domain structure of tumor necrosis factor-alpha converting enzyme. *J Biol Chem,* 275**,** 14608-14614.

REISS, K. & SAFTIG, P. 2009. The "a disintegrin and metalloprotease" (ADAM) family of sheddases: physiological and cellular functions. *Semin Cell Dev Biol,* 20**,** 126-137.

REYA, T. & CLEVERS, H. 2005. Wnt signalling in stem cells and cancer. *Nature,* 434**,** 843-850.

RIESE, D. J. & STERN, D. F. 1998. Specificity within the EGF family/ErbB receptor family signaling network. *Bioessays,* 20**,** 41-48.

RIGBY, R. J., SIMMONS, J. G., GREENHALGH, C. J., ALEXANDER, W. S. & LUND, P. K. 2007. Suppressor of cytokine signaling 3 (SOCS3) limits damage-induced crypt hyper-proliferation and inflammation-associated tumorigenesis in the colon. *Oncogene,* 26**,** 4833-4841.

RIVERA, S., KHRESTCHATISKY, M., KACZMAREK, L., ROSENBERG, G. A. & JAWORSKI, D. M. 2010. Metzincin proteases and their inhibitors: foes or friends in nervous system physiology? *J Neurosci,* 30**,** 15337-15357.

ROBANUS-MAANDAG, E. C., KOELINK, P. J., BREUKEL, C., SALVATORI, D. C., JAGMOHAN-CHANGUR, S. C., BOSCH, C. A., VERSPAGET, H. W., DEVILEE, P., FODDE, R. & SMITS, R. 2010. A new conditional Apc-mutant mouse model for colorectal cancer. *Carcinogenesis,* 31**,** 946-952.

ROBERTS, R. B., MIN, L., WASHINGTON, K. M., OLSEN, S. J., SETTLE, S. H., COFFEY, R. J. & THREADGILL, D. W. 2002. Importance of epidermal growth factor receptor signaling in establishment of adenomas and maintenance of carcinomas during intestinal tumorigenesis. *Proc Natl Acad Sci U S A,* 99**,** 1521-1526.

RODA, G., SARTINI, A., ZAMBON, E., CALAFIORE, A., MAROCCHI, M., CAPONI, A., BELLUZZI, A. & RODA, E. 2010. Intestinal epithelial cells in inflammatory bowel diseases. *World J Gastroenterol,* 16**,** 4264-4271.

RODILLA, V., VILLANUEVA, A., OBRADOR-HEVIA, A., ROBERT-MORENO, A., FERNANDEZ-MAJADA, V., GRILLI, A., LOPEZ-BIGAS, N., BELLORA, N., ALBA, M. M., TORRES, F., DUNACH, M., SANJUAN, X., GONZALEZ, S., GRIDLEY, T., CAPELLA, G., BIGAS, A. & ESPINOSA, L. 2009. Jagged1 is the pathological link between Wnt and Notch pathways in colorectal cancer. *Proc Natl Acad Sci U S A,* 106**,** 6315-20.

ROGHANI, M., BECHERER, J. D., MOSS, M. L., ATHERTON, R. E., ERDJUMENT-BROMAGE, H., ARRIBAS, J., BLACKBURN, R. K., WESKAMP, G., TEMPST, P. & BLOBEL, C. P. 1999. Metalloprotease-disintegrin MDC9: intracellular maturation and catalytic activity. *J Biol Chem,* 274**,** 3531-3540.

ROSE-JOHN, S. 2017. The soluble Interleukin 6 receptor: Advanced therapeutic options in inflammation. *Clin Pharmacol Ther*.

ROSENBERG, D. W., GIARDINA, C. & TANAKA, T. 2009. Mouse models for the study of colon carcinogenesis. *Carcinogenesis,* 30**,** 183-196.

ROTIN, D., MARGOLIS, B., MOHAMMADI, M., DALY, R. J., DAUM, G., LI, N., FISCHER, E. H., BURGESS, W. H., ULLRICH, A. & SCHLESSINGER, J. 1992. SH2 domains prevent tyrosine dephosphorylation of the EGF receptor: identification of Tyr992 as the high-affinity binding site for SH2 domains of phospholipase C gamma. *EMBO J,* 11**,** 559-567.

RUTTER, M., SAUNDERS, B., WILKINSON, K., RUMBLES, S., SCHOFIELD, G., KAMM, M., WILLIAMS, C., PRICE, A., TALBOT, I. & FORBES, A. 2004. Severity of inflammation is a risk factor for colorectal neoplasia in ulcerative colitis. *Gastroenterology,* 126**,** 451-459.

SAHIN, U. & BLOBEL, C. P. 2007. Ectodomain shedding of the EGF-receptor ligand epigen is mediated by ADAM17. *FEBS Lett,* 581**,** 41-44.

SAHIN, U., WESKAMP, G., KELLY, K., ZHOU, H.-M. M., HIGASHIYAMA, S., PESCHON, J., HARTMANN, D., SAFTIG, P. & BLOBEL, C. P. 2004. Distinct roles for ADAM10 and ADAM17 in ectodomain shedding of six EGFR ligands. *J Cell Biol,* 164**,** 769-779.

SANSOM, O. J., MENIEL, V. S., MUNCAN, V., PHESSE, T. J., WILKINS, J. A., REED, K. R., VASS, J. K., ATHINEOS, D., CLEVERS, H. & CLARKE, A. R. 2007. Myc deletion rescues Apc deficiency in the small intestine. *Nature,* 446**,** 676-679.

SANSOM, O. J., REED, K. R., HAYES, A. J., IRELAND, H., BRINKMANN, H., NEWTON, I. P., BATLLE, E., SIMON-ASSMANN, P., CLEVERS, H., NATHKE, I. S., CLARKE, A. R. & WINTON, D. J. 2004. Loss of Apc in vivo immediately perturbs Wnt signaling, differentiation, and migration. *Genes Dev,* 18**,** 1385-1390.

SASAI, H., MASAKI, M. & WAKITANI, K. 2000. Suppression of polypogenesis in a new mouse strain with a truncated Apc(Delta474) by a novel COX-2 inhibitor, JTE-522. *Carcinogenesis,* 21**,** 953-958.

SATO, T., VRIES, R. G., SNIPPERT, H. J., VAN DE WETERING, M., BARKER, N., STANGE, D. E., VAN ES, J. H., ABO, A., KUJALA, P., PETERS, P. J. & CLEVERS, H. 2009. Single Lgr5 stem cells build crypt–villus structures in vitro without a mesenchymal niche. *Nature,* 459**,** 262-265.

SCHELLER, J., CHALARIS, A., GARBERS, C. & ROSE-JOHN, S. 2011. ADAM17: a molecular switch to control inflammation and tissue regeneration. *Trends Immunol,* 32**,** 380-387.

SCHLONDORFF, J., BECHERER, J. D. & BLOBEL, C. P. 2000. Intracellular maturation and localization of the tumour necrosis factor alpha convertase (TACE). *Biochem J,* 347 Pt 1**,** 131-8.

SCHUIJERS, J. & CLEVERS, H. 2012. Adult mammalian stem cells: the role of Wnt, Lgr5 and R spondins. *EMBO J,* 31**,** 2685-2696.

SCHWARZ, J., SCHMIDT, S., WILL, O., KOUDELKA, T., KÖHLER, K., BOSS, M., RABE, B., THOLEY, A., SCHELLER, J., SCHMIDT-ARRAS, D., SCHWAKE, M., ROSE-JOHN, S. & CHALARIS, A. 2014. Polo-like kinase 2, a novel ADAM17 signaling component, regulates tumor necrosis factor α ectodomain shedding. *J Biol Chem,* 289**,** 3080-3093.

SCOVILLE, D. H., SATO, T., HE, X. C. & LI, L. 2008. Current view: intestinal stem cells and signaling. *Gastroenterology,* 134**,** 849-864.

SEBASTIAN, S., SETTLEMAN, J., RESHKIN, S. J., AZZARITI, A., BELLIZZI, A. & PARADISO, A. 2006. The complexity of targeting EGFR signalling in cancer: from expression to turnover. *Biochim Biophys Acta,* 1766**,** 120-139.

SHIBATA, H., TOYAMA, K., SHIOYA, H., ITO, M., HIROTA, M., HASEGAWA, S., MATSUMOTO, H., TAKANO, H., AKIYAMA, T., TOYOSHIMA, K., KANAMARU, R., KANEGAE, Y., SAITO, I., NAKAMURA, Y., SHIBA, K. & NODA, T. 1997. Rapid colorectal adenoma formation initiated by conditional targeting of the Apc gene. *Science,* 278**,** 120-123.

SHOYAB, M., MCDONALD, V. L., BRADLEY, J. G. & TODARO, G. J. 1988. Amphiregulin: a bifunctional growth-modulating glycoprotein produced by the phorbol 12-myristate 13-acetate-treated human breast adenocarcinoma cell line MCF-7. *Proc Natl Acad Sci U S A,* 85**,** 6528-6532.

SIBILIA, M. & WAGNER, E. F. 1995. Strain-dependent epithelial defects in mice lacking the EGF receptor. *Science,* 269**,** 234-238.

SILVA, C. M. 2004. Role of STATs as downstream signal transducers in Src family kinase-mediated tumorigenesis. *Oncogene,* 23**,** 8017-8023.

SINGH, B. & COFFEY, R. J. 2014. Trafficking of epidermal growth factor receptor ligands in polarized epithelial cells. *Annu Rev Physiol,* 76**,** 275-300.

SONG, J. I. & GRANDIS, J. R. 2000. STAT signaling in head and neck cancer. *Oncogene,* 19**,** 2489-2495.

SONG, Y., QIAN, L., SONG, S., CHEN, L., ZHANG, Y., YUAN, G., ZHANG, H., XIA, Q., HU, M., YU, M., SHI, M., JIANG, Z. & GUO, N. 2008. Fra-1 and Stat3 synergistically regulate activation of human MMP-9 gene. *Mol Immunol,* 45**,** 137-43.

SOOND, S. M., EVERSON, B., RICHES, D. W. & MURPHY, G. 2005. ERK-mediated phosphorylation of Thr735 in TNFalpha-converting enzyme and its potential role in TACE protein trafficking. *J Cell Sci,* 118**,** 2371-2380.

SRIVATSA, S., PAUL, M. C., CARDONE, C., HOLCMANN, M., AMBERG, N., PATHRIA, P., DIAMANTI, M. A., LINDER, M., TIMELTHALER, G., DIENES, H. P., KENNER, L., WRBA, F., PRAGER, G. W., ROSE-JOHN, S., EFERL, R., LIGUORI, G., BOTTI, G., MARTINELLI, E., GRETEN, F. R., CIARDIELLO, F. & SIBILIA, M. 2017. EGFR in Tumor-Associated Myeloid Cells Promotes Development of Colorectal Cancer in Mice and Associates With Outcomes of Patients. *Gastroenterology,* 153**,** 178-190 e10.

STEINHARDT, A. A., GAYYED, M. F., KLEIN, A. P., DONG, J., MAITRA, A., PAN, D., MONTGOMERY, E. A. & ANDERS, R. A. 2008. Expression of Yes-associated protein in common solid tumors. *Hum Pathol,* 39**,** 1582-1589.

STERN, D. F. 2003. ErbBs in mammary development. *Exp Cell Res,* 284**,** 89-98.

STÖCKER, W., GRAMS, F., REINEMER, P., BODE, W., BAUMANN, U., GOMIS RÜTH, F. X. & MCKAY, D. B. 1995. The metzincins — Topological and sequential relations between the astacins, adamalysins, serralysins, and matrixins (collagenases) define a super family of zinc peptidases. *Protein Sci,* 4**,** 823-840.

STOVER, D. R., BECKER, M., LIEBETANZ, J. & LYDON, N. B. 1995. Src phosphorylation of the epidermal growth factor receptor at novel sites mediates receptor interaction with Src and P85 alpha. *J Biol Chem,* 270**,** 15591-15597.

SU, L. K., KINZLER, K. W., VOGELSTEIN, B., PREISINGER, A. C., MOSER, A. R., LUONGO, C., GOULD, K. A. & DOVE, W. F. 1992. Multiple intestinal neoplasia caused by a mutation in the murine homolog of the APC gene. *Science,* 256**,** 668-670.

SUHARDJA, A. & HOFFMAN, H. 2003. Role of growth factors and their receptors in proliferation of microvascular endothelial cells. *Microsc Res Tech,* 60**,** 70-75.

SUNNARBORG, S. W., HINKLE, C. L., STEVENSON, M., RUSSELL, W. E., RASKA, C. S., PESCHON, J. J., CASTNER, B. J., GERHART, M. J., PAXTON, R. J., BLACK, R. A. & LEE, D. C. 2002. Tumor necrosis factor-alpha converting enzyme (TACE) regulates epidermal growth factor receptor ligand availability. *J Biol Chem,* 277**,** 12838-12845.

SUZUKI, R., KOHNO, H., SUGIE, S., NAKAGAMA, H. & TANAKA, T. 2006. Strain differences in the susceptibility to azoxymethane and dextran sodium sulfate-induced colon carcinogenesis in mice. *Carcinogenesis,* 27**,** 162-169.

TAKEDA, S. 2009. Three-dimensional domain architecture of the ADAM family proteinases. *Semin Cell Dev Biol,* 20**,** 146-152.

TANAKA, T., KOHNO, H., SUZUKI, R., YAMADA, Y., SUGIE, S. & MORI, H. 2003. A novel inflammation-related mouse colon carcinogenesis model induced by azoxymethane and dextran sodium sulfate. *Cancer Sci,* 94**,** 965-973.

TANIGUCHI, K., MOROISHI, T., DE JONG, P. R., KRAWCZYK, M., GREBBIN, B. M., LUO, H., XU, R. H., GOLOB-SCHWARZL, N., SCHWEIGER, C., WANG, K., DI CARO, G., FENG, Y., FEARON, E. R., RAZ, E., KENNER, L., FARIN, H. F., GUAN, K. L., HAYBAECK, J., DATZ, C., ZHANG, K. & KARIN, M. 2017. YAP-IL-6ST autoregulatory loop activated on APC loss controls colonic tumorigenesis. *Proc Natl Acad Sci U S A,* 114**,** 1643-1648.

TANIGUCHI, K., WU, L. W., GRIVENNIKOV, S. I., DE JONG, P. R., LIAN, I., YU, F. X., WANG, K., HO, S. B., BOLAND, B. S., CHANG, J. T., SANDBORN, W. J., HARDIMAN, G., RAZ, E., MAEHARA, Y., YOSHIMURA, A., ZUCMAN-ROSSI, J., GUAN, K. L. & KARIN, M. 2015. A gp130-Src-YAP module links inflammation to epithelial regeneration. *Nature,* 519**,** 57-62.

THREADGILL, D. W., DLUGOSZ, A. A., HANSEN, L. A., TENNENBAUM, T., LICHTI, U., YEE, D., LAMANTIA, C., MOURTON, T., HERRUP, K. & HARRIS, R. C. 1995. Targeted disruption of mouse EGF receptor: effect of genetic background on mutant phenotype. *Science,* 269**,** 230-234.

TSAI, Y. H., VANDUSSEN, K. L., SAWEY, E. T., WADE, A. W., KASPER, C., RAKSHIT, S., BHATT, R. G., STOECK, A., MAILLARD, I., CRAWFORD, H. C., SAMUELSON, L. C. & DEMPSEY, P. J. 2014. ADAM10 regulates Notch function in intestinal stem cells of mice. *Gastroenterology,* 147**,** 822-834 e13.

ULLRICH, A., COUSSENS, L., HAYFLICK, J. S., DULL, T. J., GRAY, A., TAM, A. W., LEE, J., YARDEN, Y., LIBERMANN, T. A. & SCHLESSINGER, J. 1984. Human epidermal growth factor receptor cDNA sequence and aberrant expression of the amplified gene in A431 epidermoid carcinoma cells. *Nature,* 309**,** 418-425.

VAN DE WETERING, M., SANCHO, E., VERWEIJ, C., DE LAU, W., OVING, I., HURLSTONE, A., VAN DER HORN, K., BATLLE, E., COUDREUSE, D., HARAMIS, A. P., TJON-PON-FONG, M., MOERER, P., VAN DEN BORN, M., SOETE, G., PALS, S., EILERS, M., MEDEMA, R. & CLEVERS, H. 2002. The beta-catenin/TCF-4 complex imposes a crypt progenitor phenotype on colorectal cancer cells. *Cell,* 111**,** 241-250.

VAN DER FLIER, L. G. & CLEVERS, H. 2009. Stem Cells, Self-Renewal, and Differentiation in the Intestinal Epithelium. *Annu Rev Physiol,* 71**,** 241-260.

VAN EMBURGH, B. O., SARTORE-BIANCHI, A., DI NICOLANTONIO, F., SIENA, S. & BARDELLI, A. 2014. Acquired resistance to EGFR-targeted therapies in colorectal cancer. *Mol Oncol,* 8**,** 1084-94.

VANDUSSEN, K. L., CARULLI, A. J., KEELEY, T. M., PATEL, S. R., PUTHOFF, B. J., MAGNESS, S. T., TRAN, I. T., MAILLARD, I., SIEBEL, C., KOLTERUD, Å., GROSSE, A. S., GUMUCIO, D. L., ERNST, S. A., TSAI, Y.-H., DEMPSEY, P. J. & SAMUELSON, L. C. 2012. Notch signaling modulates proliferation and differentiation of intestinal crypt base columnar stem cells. *Development,* 139**,** 488-497.

VOGELSTEIN, B. & KINZLER, K. W. 1993. The multistep nature of cancer. *Trends Genet,* 9**,** 138-141.

WALDNER, M. J. & NEURATH, M. F. 2014. Master regulator of intestinal disease: IL-6 in chronic inflammation and cancer development. *Semin Immunol,* 26**,** 75-79.

WANG, T., NIU, G., KORTYLEWSKI, M., BURDELYA, L., SHAIN, K., ZHANG, S., BHATTACHARYA, R., GABRILOVICH, D., HELLER, R., COPPOLA, D., DALTON, W., JOVE, R., PARDOLL, D. & YU, H. 2004. Regulation of the innate and adaptive immune responses by Stat-3 signaling in tumor cells. *Nat Med,* 10**,** 48-54.

WEHKAMP, J. & STANGE, E. F. 2006. Paneth cells and the innate immune response. *Curr Opin Gastroenterol,* 22**,** 644-650.

WEISS, A. & SCHLESSINGER, J. 1998. Switching signals on or off by receptor dimerization. *Cell,* 94**,** 277-280.

WILLERT, K. & NUSSE, R. 1998. Beta-catenin: a key mediator of Wnt signaling. *Curr Opin Genet Dev,* 8**,** 95-102.

WIRTZ, S., NEUFERT, C., WEIGMANN, B. & NEURATH, M. F. 2007. Chemically induced mouse models of intestinal inflammation. *Nat Protoc,* 2**,** 541-546.

WONG, L., DEB, T. B., THOMPSON, S. A., WELLS, A. & JOHNSON, G. R. 1999. A differential requirement for the COOH-terminal region of the epidermal growth factor (EGF) receptor in amphiregulin and EGF mitogenic signaling. *J Biol Chem,* 274**,** 8900-8909.

WRIGHT, N. A. 2000. Epithelial stem cell repertoire in the gut: clues to the origin of cell lineages, proliferative units and cancer. *Int J Exp Pathol,* 81**,** 117-143.

XIE, T. X., WEI, D., LIU, M., GAO, A. C., ALI-OSMAN, F., SAWAYA, R. & HUANG, S. 2004. Stat3 activation regulates the expression of matrix metalloproteinase-2 and tumor invasion and metastasis. *Oncogene,* 23**,** 3550-60.

YAMADA, Y., HATA, K., HIROSE, Y., HARA, A., SUGIE, S., KUNO, T., YOSHIMI, N., TANAKA, T. & MORI, H. 2002. Microadenomatous lesions involving loss of Apc heterozygosity in the colon of adult Apc(Min/+) mice. *Cancer Res,* 62**,** 6367-6370.

YAMADA, Y. & MORI, H. 2006. Multistep carcinogenesis of the colon in Apc(Min/+) mouse. *Cancer Sci,* 98**,** 6-10.

YAN, D., WIESMANN, M., ROHAN, M., CHAN, V., JEFFERSON, A. B., GUO, L., SAKAMOTO, D., CAOTHIEN, R. H., FULLER, J. H., REINHARD, C., GARCIA, P. D., RANDAZZO, F. M., ESCOBEDO, J., FANTL, W. J. & WILLIAMS, L. T. 2001. Elevated expression of axin2 and hnkd mRNA provides evidence that Wnt/beta -catenin signaling is activated in human colon tumors. *Proc Natl Acad Sci U S A,* 98**,** 14973-8.

YAN, I., SCHWARZ, J., LÜCKE, K., SCHUMACHER, N., SCHUMACHER, V., SCHMIDT, S., RABE, B., SAFTIG, P., DONNERS, M., ROSE-JOHN, S., MITTRÜCKER, H.-W. W. & CHALARIS, A. 2016. ADAM17 controls IL-6 signaling by cleavage of the murine IL-6Rα from the cell surface of leukocytes during inflammatory responses. *J Leukoc Biol,* 99**,** 749-760.

YARDEN, Y. & SLIWKOWSKI, M. X. 2001. Untangling the ErbB signalling network. *Nat Rev Mol Cell Biol,* 2**,** 127-137.

YODA, M., KIMURA, T., TOHMONDA, T., MORIOKA, H., MATSUMOTO, M., OKADA, Y., TOYAMA, Y. & HORIUCHI, K. 2013. Systemic overexpression of TNFα-converting enzyme does not lead to enhanced shedding activity in vivo. *PloS one,* 8**,** e54412.

ZACZEK, A., BRANDT, B. & BIELAWSKI, K. P. 2005. The diverse signaling network of EGFR, HER2, HER3 and HER4 tyrosine kinase receptors and the consequences for therapeutic approaches. *Histol Histopathol,* 20**,** 1005-1015.

ZHANG, D., SLIWKOWSKI, M. X., MARK, M., FRANTZ, G., AKITA, R., SUN, Y., HILLAN, K., CROWLEY, C., BRUSH, J. & GODOWSKI, P. J. 1997. Neuregulin-3 (NRG3): a novel neural tissue-enriched protein that binds and activates ErbB4. *Proc Natl Acad Sci U S A,* 94**,** 9562-9567.

ZHANG, T., OTEVREL, T., GAO, Z., GAO, Z., EHRLICH, S. M., FIELDS, J. Z. & BOMAN, B. M. 2001. Evidence that APC regulates survivin expression: a possible mechanism contributing to the stem cell origin of colon cancer. *Cancer Res,* 61**,** 8664-7.

ZHANG, Y., DUBÉ, P. E., WASHINGTON, M. K., YAN, F. & POLK, D. B. 2012. ErbB2 and ErbB3 regulate recovery from dextran sulfate sodium-induced colitis by promoting mouse colon epithelial cell survival. *Lab Invest,* 92**,** 437-450.

ZLOBEC, I., VUONG, T., HAYASHI, S., HAEGERT, D., TORNILLO, L., TERRACCIANO, L., LUGLI, A. & JASS, J. 2007. A simple and reproducible scoring system for EGFR in colorectal cancer: application to prognosis and prediction of response to preoperative brachytherapy. *Br J Cancer,* 96**,** 793-800.

ZORN, A. M., BARISH, G. D., WILLIAMS, B. O., LAVENDER, P., KLYMKOWSKY, M. W. & VARMUS, H. E. 1999. Regulation of Wnt signaling by Sox proteins: XSox17 alpha/beta and XSox3 physically interact with beta-catenin. *Mol Cell,* 4**,** 487-98.

LIST OF TABLES

LIST OF FIGURES

LIST OF PUBLICATIONS

ADAM17 is required for EGFR induced colon cancer induction via IL-6 trans-signaling.

Schmidt S, Schwarz J, Schumacher N, Roos S, Kenner L, Chalaris A, Sibilia M, Garbers C, Rosenstiel P, Arnold P, Zunke F, Westermann J, Dempsey J. P, Putoczki T, Rose-John S.

In preparation

Circulating Soluble IL-6R but Not ADAM17 Activation Drives Mononuclear Cell Migration in Tissue Inflammation.

Schumacher N, **Schmidt S**, Schwarz J, Dohr D, Lokau J, Scheller J, Garbers C, Chalaris A, Rose-John S, Rabe B.

J Immunol. 2016 Nov 1;197(9):3705-3715.

Mechanistic insights into a TIMP3-sensitive pathway constitutively engaged in the regulation of cerebral hemodynamics.

Capone C, Dabertrand F, Baron-Menguy C, Chalaris A, Ghezali L, Domenga-Denier V, **Schmidt S**, Huneau C, Rose-John S, Nelson MT, Joutel A.

Elife. 2016 Aug 1;5. pii: e17536.

ADAM17 controls IL-6 signaling by cleavage of the murine IL-6Rα from the cell surface of leukocytes during inflammatory responses.

Yan I, Schwarz J, Lücke K, Schumacher N, Schumacher V, **Schmidt S**, Rabe B, Saftig P, Donners M, Rose-John S, Mittrücker HW, Chalaris A.

J Leukoc Biol. 2016 May;99(5):749-60.

Polo-like kinase 2, a novel ADAM17 signaling component, regulates tumor necrosis factor α ectodomain shedding.

Schwarz J, **Schmidt S**, Will O, Koudelka T, Köhler K, Boss M, Rabe B, Tholey A, Scheller J, Schmidt-Arras D, Schwake M, Rose-John S, Chalaris A.

J Biol Chem. 2014 Jan 31;289(5):3080-93.

Short-term TNFα shedding is independent of cytoplasmic phosphorylation or furin cleavage of ADAM17.

Schwarz J, Broder C, Helmstetter A, **Schmidt S**, Yan I, Müller M, Schmidt-Arras D, Becker-Pauly C, Koch-Nolte F, Mittrücker HW, Rabe B, Rose-John S, Chalaris A.

Biochim Biophys Acta. 2013 Dec;1833(12):3355-67.

CONFERENCES

08/2016 2. SFB Symposium “Protease World in Health & Disease”; Kiel, Germany

- Poster

09/2015 IRTG summer school “Proteolysis & Pathophysiology”; Kiel, Germany

- Talk

02/2015 32. Winter School on Proteinases and their Inhibitors; Tiers, Italy

- Talk

10/2014 Annual CSD-Retreat; Breckenridge, Colorado, USA

- Poster

05/2014 International Cytokine and Interferone Society (ICIS) Interleukin 6: Biology-Pathophysiology-Therapy; Kiel, Germany

- Poster

FELLOWSHIP

09-12/2014 IRTG Fellowship sponsored by Collaborative Research Centre 877 Proteolysis as a Regulatory Event in Pathophysiology

- Research stay at the group of Dr. Peter J. Dempsey from the University of Colorado Medical School, Aurora, Colorado, USA.
- Study 3D organoid culture

DANKSAGUNG

Mein größter Dank geht an Prof. Dr. Stefan Rose-John, der es mir ermöglicht hat unter hervorragender wissenschaftlicher Anleitung und Betreuung in einem produktiven Arbeitsumfeld meine Doktorarbeit am Biochemischen Institut im Rahmen des SFB 877 anzufertigen.

Besonders danken möchte ich meiner ehemaligen Arbeitsgruppenleiterin Dr. Athena Chalaris für das interessant gewählte Thema und die großartige Betreuung. Sie war stets Ansprechpartnerin bei Fragen und Problemen und hat mich die gesamte Zeit über motiviert und unterstützt.

This work would not have been possible without the contribution of many other people, whom I would like to thank: Conny Brindley, Rebecca Tucker and especially Assoc. Prof. Dr. Peter J. Dempsey from the University of Colorado Medical School, Aurora, (USA), who gave me the opportunity to visit his research group. I´m really grateful to him for sharing his knowledge and experiences, the great working atmosphere in his lab, for many fruitful discussions and for supporting me all the way.

Ferner möchte ich mich bei allen weiteren Kooperationspartner bedanken, die an diesem Projekt mitgewirkt haben: Dr. Simone Roos und Prof. Dr. Lukas Kenner von der Veterinärmedizinischen Universität Wien danke ich vielmals für ergebnisreiche Zusammenarbeit und Durchführung der pathologischen Begutachtungen. Vom IKMB Kiel möchte ich Dr. Maren Falk-Paulsen, Sabine Kock, Dr. Ateequr Rehman, Dr. Robert Häsler und Prof. Dr. Philip Rosenstiel für die Unterstützung und Zusammenarbeit im Rahmen der RNA-Sequenzierung und Mikrobiomanalyse danken. Den Anatomischen Instituten der Universität Lübeck und Kiel, insbesondere Prof. Dr. Jürgen Westermann und Dr. Philipp Arnold, danke ich für die Anfertigung Azan-gefärbter Paraffinschnitte in Kiel und die Möglichkeit Laser-Mikrodissektions-Experimente in Lübeck durchzuführen.

Bei (Jun.-) Prof. Dr. Björn Rabe, PD Dr. Christoph Garbers und Dr. Dirk Schmidt-Arras und möchte ich mich für die hilfreichen Ratschläge und Gespräche danken und dafür, dass sie sich stets Zeit genommen haben, um mir wertvolle Tipps zu geben und weiter zu helfen. Vielen herzlichen Dank!

Insbesondere möchte ich meinen ehemaligen Arbeitsgruppemitgliedern Jeanette, Neele, Melanie, Kaja, Dana, Nina, Britta, Christian und meinen lieben Kollegen Rielana, Frederike, Anna und Petra für die gemeinsame Zeit danken! Ihr habt mir nicht nur jederzeit hilfsbereit zur Seite gestanden, sondern mit eurer freundschaftlichen Art auch für eine wunderbare

Arbeitsatmosphäre gesorgt und dazu beigetragen das sich Freundschaften entwickelt haben, die ich nicht mehr missen möchte. Darüber hinaus geht mein Dank noch an Miryam, die mit mir gemeinsam über viele Jahre die Organisation des Thermo-Freezers im Institut übernommen hat.

Des Weiteren möchte ich mich auch bei Marika Eschke, dem gesamten VHH-Team, Sarah Vieten und Prof. Dr. Schultheiß für die Unterstützung bei allen Tierstallangelegenheiten danken.

Ganz besonders bedanken möchte ich mich auch bei meinen lieben Freunden, meiner Familie und meinem Partner. Ihr habt mir über die gesamte Zeit immer zur Seite gestanden und mich unterstützt. Sich bei jedem einzelnen von euch fabelhaften Leuten namentlich zu bedanken würde den Rahmen sprengen, aber jeder von euch, der dies liest, möge sich auf ganz persönliche Art und Weise von mir angesprochen fühlen.

Ihr seid die Größten! Danke für alles!